

ATHEROSCLEROTIC PLAQUE BIOCHEMISTRY

AND MARS SPECTRAL IMAGING

---

A thesis submitted in partial fulfilment of the requirements for the Degree

of Doctor of Philosophy in Biochemistry

in the School of Biological Sciences, University of Canterbury

by H. M. Prebble

2018

---

## Abstract

This thesis reports on the use of neopterin and 7,8-dihydroneopterin as biomarkers of inflammation in advanced atherosclerosis and the use of spectral CT imaging to assess the features and morphology of vulnerable atherosclerotic plaque. New non-invasive imaging modalities are being explored as current methods for the diagnosis of cardiovascular disease cannot be used for subclinical atherosclerosis. Specifically, non-invasive tools are required to assess plaque vulnerability, the main cause of stroke or heart attack. Neopterin has shown promise as biomarker for cardiovascular disease, with both prognostic and diagnostic capabilities. However, despite its known utility as a marker, little is understood about how the neopterin measured in blood plasma or serum relates to the underlying condition and how it relates to plaque vulnerability. Furthermore, it is generally unknown how the parent compound 7,8-dihydroneopterin becomes oxidised in biological systems.

In this thesis, live excised carotid plaques from symptomatic patients provided a unique experimental system to test the effects of oxidants and inflammatory stimulants on the inflammatory biomarkers neopterin and 7,8-dihydroneopterin. Activating macrophages in the plaque produced a response that is inversely proportional to the volume of calcification in the tissue. The antioxidant and radical scavenging properties 7,8-dihydroneopterin were explored using a key oxidant, superoxide. Neopterin was found to be a central product of the complex reaction. Baseline 7,8-dihydroneopterin and neopterin values in plaque compared to plasma demonstrated that the plasma values do not necessarily reflect the antioxidant capacity or inflammatory status of the plaque tissue. However, there appears to be good correlation between immune cell activity in plaque and plasma lactate values. Calcification, haemorrhage, and lipid cores were identified using MARS spectral CT. Development of a low-density lipoprotein- based nanoparticle for the identification of macrophages within in plaque had limited success, with more work needed to improve the uptake in a cell model before use in a tissue sample.

The results of this thesis demonstrate that spectral imaging has the capability to assess features of plaque vulnerability such as calcium deposition, lipid pools and intraplaque haemorrhage. This has the potential to improve patient diagnosis if this can be translated to

human use. Furthermore, 7,8-dihydroneopterin and neopterin are modulated by changes in oxidant levels and immunological stimulation in atherosclerotic tissue, improving support for the case for adding these markers to panel of biomarkers for cardiovascular disease. Further research into how plasma levels of both compounds relative to in situ plaque production impacts patient outcomes would provide insight into the role of antioxidant capacity in plaque vulnerability and atherosclerosis.



Deputy Vice-Chancellor's Office  
Postgraduate Office

### Co-Authorship Form

This form is to accompany the submission of any thesis that contains research reported in co-authored work that has been published, accepted for publication, or submitted for publication. A copy of this form should be included for each co-authored work that is included in the thesis. Completed forms should be included at the front (after the thesis abstract) of each copy of the thesis submitted for examination and library deposit.

Please indicate the chapter/section/pages of this thesis that are extracted from co-authored work and provide details of the publication or submission from the extract comes:

*Chapter 4 is extracted from Prebble, H., Cross, S., Marks, E., Healy, J. L., Searle, E., Aamir, R., Butler, A., Roake, J., Hock, B., Anderson, N., & Giese, S. P. (2018). Induced macrophage activation in live excised atherosclerotic plaque. Immunobiology. Advance online publication. doi: 10.1016/j.imbio.2018.03.002*

Please detail the nature and extent (%) of contribution by the candidate:

*I contributed to the design of the study, carried out experiments, analysis of the results and wrote the manuscript. My contribution was 75%.*

#### Certification by Co-authors:

If there is more than one co-author then a single co-author can sign on behalf of all

The undersigned certifies that:

- The above statement correctly reflects the nature and extent of the PhD candidate's contribution to this co-authored work
- In cases where the candidate was the lead author of the co-authored work he or she wrote the text

Name: A/Prof Steven Giese Signature:  Date: 30 May 2018

Date: 30 May

## Acknowledgements

I'd like to thank my supervisors, Steven, Anthony and Barry, for their efforts in getting this project to the end. I would also like to thank my family, especially Freddie, Oliver and Isobel, for their on-going support. Sean, Nina, Maria, Greg, Anthony, Anurup: I am going to miss doing science and hanging out with all of you. To the MARS team, thanks for the Wednesday seminars and feeling like I'm part of a group that's working towards a bigger goal.

## Scientific Contribution

### Peer-reviewed publications

**Prebble, H.**, Cross, S., Marks, E., Healy, J. L., Searle, E., Aamir, R., Butler, A., Roake, J., Hock, B., Anderson, N., & Giese, S. P. (2018). Induced macrophage activation in live excised atherosclerotic plaque. *Immunobiology*. Advance online publication. doi: 10.1016/j.imbio.2018.03.002

*This paper establishes the differential response of stimulated plaques compared with stimulated macrophage and PBMC tissue cultures. It also addresses the intraplaque variation in neopterin and 7,8-dihydroneopterin release by investigating plaque morphology using MARS-CT. I contributed to the study design, collected all the cell data, performed the data analysis and prepared the manuscript. Cross, and Marks contributed plaque experiments. Healy, Searle, and Aamir contributed to the imaging aspects of the paper. Roake was involved in the organisation and collection of the plaques and general study design. Hock, Anderson and Giese also contributed to the study design. This is the first paper to measure macrophage and PBMC activation in live stimulated plaque and to attempt to explain the variation seen across the plaque by studying the calcium content.*

### Peer-reviewed publications (in draft)

Baxter-Parker, G., **Prebble, H.**, Cross, S., Steyn, N., Othman, M. I., Cousins, A., and Giese, S.P. (2018) 7,8-Dihydroneopterin can be oxidized to neopterin by superoxide: evidence from cellular, ex vivo atherosclerotic plaque, enzymatic and radiolytic systems.

*This paper will show that neopterin is a product of the reaction between superoxide and 7,8-dihydroneopterin. I contributed to this paper by performing the xanthine oxidase and plaque experiments, analysing the data related to these experiments, and I am preparing the manuscript in conjunction with Baxter-Parker. Baxter-Parker is contributing significant data from radiolysis experiments and cell experiments. Cross contributed to the plaque experiments. Steyn and Othman have conducted cell experiments. Cousins and Giese contributed to the study design. This is the first paper to show that superoxide is able to oxidize 7,8-dihydroneopterin to neopterin and will discuss the ramifications of this in terms of atherosclerotic plaque.*

### Scientific Meeting Proceedings (oral abstracts)

**Hannah Prebble**, Sean Cross, Edward Marks, Vicky White, Justin Roake, Steven Giese. (2016) Activation of immune cells in live carotid plaque. *The New Zealand Medical Journal* Vol 129 No 1439, Proceedings of the Scientific Meetings of the Health Research Society of Canterbury 2016.

*This talk explained why plaque culture is a useful tool and showed that using several cytokines and mitogens it is possible to achieve activation of the immune cells within excised tissue. I contributed by collecting the stimulated plaque data and analysing it. I also prepared the talk. This talk was significant as it presented the first time plaque had been stimulated indirectly via T-cells as opposed to directly through the macrophages.*

### **Grants and Awards**

Named investigator on the National Heart Foundation Grant in Aid “Spectral CT imaging of low-density lipoprotein labelled with iodine and gold atoms”

*I co-authored this grant with Dr Raja Aamir, a Post-Doctoral Fellow at the University of Otago. I wrote the sections related to the biological aspects and researched the methods to produce I-LDL and Au-LDL. Dr Aamir wrote the sections relating to the use of spectral-CT to image the iodine and gold atoms. This study is significant as it tests the ability of the MARS-CT to produce clinical level images using common contrast agents in a targeted delivery system.*

PhD scholarship

University of Canterbury School of Biological Sciences Travel award

Health Research Society Canterbury Grand Round Oral Presentation Award

Callaghan Innovation Summer Experience Grant

### **Invited talks**

**Prebble, H. M.,** Cross, S., Aamir, R., Anderson, N.G., White, V., Roake, J.A., Healy, J., Giesege, S.P. (2016). Imaging vulnerable plaques: recent advances in spectral CT. Australian Atherosclerosis Society SCOLAR webinar, November 2016.

*In this webinar, I gave an overview of the issues around obtaining a clear diagnosis of atherosclerosis. I contributed to this talk by collecting the plaque data, carrying out the spectral scanning and material decomposition and prepared the presentation. This is the first webinar that has been given on the subject of plaque imaging to the AAS.*

**Prebble, H. M.,** Cross, S., Aamir, R., Anderson, N.G., White, V., Roake, J.A., Healy, J., Giesege, S.P. (2016). Macrophage activation in excised human carotid plaque. QMB Heart, Nelson, New Zealand, August 2016.

*I was invited to talk on our recent findings in measuring macrophage activation in live plaque. The talk presented a case study of a single plaque. I contributed by carrying*

*out the data analysis and spectral scanning of the plaque. This talk was significant as it showed the first material decomposition of a plaque that had been cultured for 5 days.*

### **Oral Presentations**

Steven P. Giesege, **Hannah Prebble**, Emily Searle, Anthony Butler. Spectral X-ray imaging of atherosclerotic plaque by MARS-scanning. International Symposium of Atherosclerosis, Toronto, Canada, June 2018 (*abstract accepted for oral presentation*). To be presented by A/Prof Steven Giesege.

**Hannah Prebble**. Understanding vulnerable plaque using MARS CT. MD Anderson Cancer Centre, Houston, TX, USA, April 2018, Johns Hopkins University, Baltimore, MD, USA, April 2018, and Emory University, Atlanta, GA, USA, April 2018.

Aamir Raja (Presented by **Hannah Prebble**). MARS Spectral CT Imaging: A New Paradigm to Influence Future Medical Care. MD Anderson Cancer Centre, Houston, TX, USA, April 2018, Johns Hopkins University, Baltimore, MD, USA, April 2018, and Emory University, Atlanta, GA, USA, April 2018.

**Hannah Prebble**. MARS CT: a novel approach to an old problem. University of Melbourne. October 2017.

**Hannah Prebble**. Neopterin and 7,8-Dihydroneopterin Production in Live Plaque Culture. Continuing Medical Education, Christchurch Hospital, New Zealand, May 2016.

**Hannah Prebble**. Live carotid plaque tissue: Understanding the role of macrophages. Annual Biology Conference, Christchurch, New Zealand, October 2016.

Giesege SP, Roake JA, Chen A, Katouah H, Cross SP, Othman MI, **Prebble H**. 7,8-Dihydroneopterin oxidation to neopterin in macrophages and atherosclerotic plaques. 35th International Winter-Workshop Clinical, Chemical and Biochemical Aspects of Pteridines and Related Topics, Innsbruck, Austria, February 2016. (Presented by Associate Professor Giesege on behalf of the group)

Steven Giesege, Sean Cross, Shane Reeves, Izani Othman, **Hannah Prebble**, Tejraj Janmale, Alpha Chen, Justin Roake. Is plasma neopterin the product of intracellular oxidant scavenging by 7,8-dihydroneopterin? The Society of Free Radical Research Australasia and Japan 7th Joint Meeting, Christchurch, New Zealand, December 2015. (Presented by Associate Professor Giesege on behalf of the group)

### **Poster Presentations**

**Hannah Prebble**, Emily Searle, Raja Aamir, Nigel Anderson, Anthony Butler and Steven P. Giesege.. Labelling Low Density Lipoprotein with Gold Nanoparticles or Iodine Prevents Uptake in U937 cells. Society for Biomaterials, Atlanta, GA, USA, April 2018



**Hannah Prebble**, Sean Cross, Edward Marks, Joe Healy, Raja Aamir, Nigel Anderson, Justin Roake, Vicky White, Anthony Butler and Steven Giese. Activation of T Cells and Macrophages in Live Carotid Plaque. Australian Atherosclerosis Society Meeting, Hobart, Australia, December 2016. (Presented by Joe Healy on behalf of the group)

**Hannah Prebble**, Sean Cross, Edward Marks, Joe Healy, Raja Aamir, Nigel Anderson, Justin Roake, Vicky White, Anthony Butler and Steven Giese. Activation of T Cells and Macrophages in Live Carotid Plaque. Health Research Society Canterbury Poster Presentation Evening, October 2016

### **Student Supervision**

A group of four BCHM381 students (Oscar Graham, Qituo Ding, Leighton Inglis, Lolohea Ofa) undertaking a project, “Measuring the superoxide mediated production of neopterin using fluorometry”, 2016.

Harshil Gulati. Callaghan Innovation summer student 2017-2018

### **Mentoring**

Anurup Balpande, Masters Candidate, 2017.

Maria Ghodsian, PhD candidate, 2017.

## TABLE OF CONTENTS

Abstract.....	i
Acknowledgements.....	iv
Scientific Contribution.....	v
Peer-reviewed publications.....	v
Peer-reviewed publications (in draft).....	v
Scientific Meeting Proceedings (oral abstracts).....	v
Grants and Awards.....	vi
Invited talks.....	vi
Oral Presentations.....	vii
Poster Presentations.....	vii
Student Supervision.....	viii
Mentoring.....	viii
TABLE OF CONTENTS.....	1
TABLE OF FIGURES.....	5
1 Introduction.....	10
1.1 Overview.....	10
1.2 Background.....	11
1.3 Cardiovascular Disease and Atherosclerosis.....	11
1.4 Health Burden of Atherosclerosis in New Zealand.....	12
1.5 Current Methods for Detection and Diagnosis.....	12
1.5.1 Risk based assessment.....	13
1.5.2 Non-invasive assessment.....	13
1.5.3 Invasive assessment.....	15
1.6 Inflammation.....	16
1.6.1 Background.....	16
1.6.2 Key contributors to inflammation in atherosclerosis.....	16
1.6.3 Macrophage based mechanisms inflammation in atherosclerosis.....	18
1.7 Biomarkers of Atherosclerosis.....	20
1.8 Neopterin and 7,8-Dihydroneopterin.....	21
1.9 Imaging of Atherosclerosis.....	24
1.10 Summary.....	25
1.11 Research Aims and Significance.....	27
Long term goal.....	27
Medium term goal.....	27

PhD goals .....	27
1.12 Thesis Outline.....	28
1.13 Major scientific findings.....	30
2 Methods and Materials .....	31
2.1 Materials.....	31
2.2 Preparation of General Solutions and Buffers.....	33
2.3 Methods.....	34
3 Macrophage activation in live excised atherosclerotic plaque .....	42
3.1 Introduction .....	42
3.2 Methods in brief .....	44
3.3 Results .....	45
3.3.1 7,8-Dihydroneopterin and neopterin formation in unstimulated plaque .....	45
3.3.2 Direct activation of plaque macrophages by interferon- $\gamma$ in cultured plaque .....	47
3.3.3 Direct activation of macrophages by interferon- $\gamma$ in cell culture.....	49
3.3.4 Indirect stimulation of macrophages in cultured plaque with PMA .....	49
3.3.5 Stimulation of macrophages and PBMCs in cell culture with PMA.....	50
3.3.6 Indirect stimulation of plaque with PHA .....	52
3.3.7 Indirect stimulation of macrophages and PBMCs in cell culture with PHA.....	52
3.3.8 Plaque calcium quantification by spectral imaging .....	54
3.4 Discussion .....	56
3.5 Conclusion.....	57
4 Relationship between 7,8-dihydroneopterin and neopterin in the presence of superoxide 58	
4.1 Introduction .....	58
4.1.1 Measuring neopterin formation by superoxide in a xanthine oxidase system .....	59
4.2 Methods in brief .....	62
4.3 Results .....	63
4.3.1 Superoxide induced loss of 7,8-dihydroneopterin and generation of neopterin.....	63
4.3.2 Measurement of 7,8-dihydroneopterin superoxide scavenging ability .....	65
4.3.3 Competition between 7,8-dihydroneopterin and superoxide dismutase .....	71
4.3.4 Initial reactions of 7,8-dihydroneopterin with superoxide .....	75
4.3.5 Potential other products of the reaction between superoxide and 7,8-dihydroneopterin 79	
4.4 Discussion .....	82
4.5 Conclusion.....	86
5 Effect of oxidant modulation on 7,8-dihydroneopterin and neopterin generation in biological systems.....	87

5.1	Introduction .....	87
5.2	Methods in brief .....	89
5.3	Results .....	90
5.3.1	Reducing superoxide production by inhibiting NADPH oxidase in plaque .....	90
5.3.2	Experiments with interferon-gamma and ABAH .....	94
5.3.3	Removing superoxide in plaque culture directly using PEG-SOD .....	97
5.3.4	Increasing the oxidant production in plaque by adding oxidized LDL.....	99
5.3.5	Increasing and inhibiting oxidants in macrophages .....	104
5.4	Discussion .....	108
5.4.1	Plaque Culture.....	110
5.5	Conclusion.....	112
6	Plaque baseline production of 7,8-dihydroneopterin and neopterin: correlation to plasma markers.....	113
6.1	Introduction .....	113
6.2	Methods in brief .....	114
6.3	Results .....	115
6.3.1	Variation in whole plaque and plaque section weight.....	115
6.3.2	Variation in total neopterin and neopterin in media and plasma between individuals	116
6.3.3	Relationship between neopterin, 7,8-dihydroneopterin and total neopterin .....	120
6.3.4	Correlation between plasma and plaque values of neopterin, total neopterin, and 7,8-dihydroneopterin .....	122
6.3.5	Correlation of blood and plaque lactate values to plaque total neopterin and neopterin values	124
6.4	Discussion .....	127
6.5	Conclusion.....	128
7	Developing imaging procedures for assessing plaque vulnerability .....	129
7.1	Introduction .....	129
7.1.1	Principles of spectral CT for quantitative material assessment.....	130
7.1.2	Separating iron from calcium in spectral CT .....	130
7.2	Methods in brief .....	131
7.2.1	MARS spectral scanning protocols.....	131
7.2.2	Method developed for calculating plaque volume by using ImageJ .....	132
<b>7.2.3</b>	Calculating plaque calcium volume by using ImageJ .....	132
7.3	Results and Discussion.....	133
7.3.1	Identification of calcium as a marker of plaque vulnerability .....	133
7.3.2	Investigation of inconsistent plaque lipid values in material decomposition.....	134
7.3.3	Imaging intraplaque haemorrhage.....	140

7.4	Conclusion.....	153
8	Imaging of nanoparticle probes targeting macrophages.....	154
8.1	Introduction.....	154
8.2	Methods in brief.....	155
8.3	Results.....	158
8.3.1	Non-functionalized gold nanoparticle uptake in macrophages.....	158
8.3.2	Modified LDL as a probe for macrophage like cells.....	160
8.4	Discussion.....	162
8.5	Conclusion.....	163
9	General Discussion and Future Directions.....	164
9.1	Biomarkers of inflammation.....	164
9.2	Future of MARS imaging.....	165
9.3	Conclusion.....	165
9.4	Summary.....	166
	References.....	167
	Appendix A.....	183
	Appendix B.....	193
	.....	193

## TABLE OF FIGURES

Figure 1.1 Chemical structures of neopterin (left) and 7,8-dihydroneopterin (right) .....	22
Figure 2.1 Example of a plaque cut into sections and placed in individual culture dishes. ....	36
Figure 2.2 The MARS small bore spectral scanner for small animal imaging.....	40
Figure 3.1 Production of total neopterin and neopterin in media from an unstimulated plaque. .....	46
Figure 3.2 Media total neopterin and neopterin from plaque stimulated with 500 U/mL of interferon- $\gamma$ .....	47
Figure 3.3 Production of total neopterin and neopterin in media from plaque, macrophages, and PBMC culture stimulated with 500 U/mL of interferon- $\gamma$ . ....	48
Figure 3.4 Media total neopterin and neopterin from plaque stimulated with 5 $\mu$ M PMA. ....	50
Figure 3.5 Production of total neopterin and neopterin in media from plaque, macrophages, and PBMC culture stimulated with 5 $\mu$ M PMA. ....	51
Figure 3.6 Production of total neopterin and neopterin in media from plaque, macrophages, and PBMC culture stimulated with 50 ng/mL PHA. ....	52
Figure 3.7 Production of total neopterin and neopterin in media from plaque, macrophages, and PBMC culture stimulated with 50 ng/mL PHA. ....	53
Figure 3.8 MARS imaging of plaque tissue.....	55
Figure 4.1 Loss of 7,8-dihydroneopterin and gain of neopterin at different initial concentrations of 7,8-dihydroneopterin after 60 minutes of incubation with 1.67 mU/mL xanthine oxidase.....	64
Figure 4.2 NBT assay of superoxide production with increasing concentrations of 7,8- dihydroneopterin in the presence of 1.67 mU of xanthine oxidase. ....	66
Figure 4.3 Effect of increasing concentrations of xanthine oxidase enzyme on loss of 7,8- dihydroneopterin and gain of neopterin. ....	68
Figure 4.4 Loss of 7,8-dihydroneopterin and gain of neopterin over time in the presence of increasing concentrations of xanthine oxidase enzyme. ....	70
Figure 4.5 Effect of increasing concentrations of SOD on loss of 7,8-dihydroneopterin and gain of neopterin in the presence of 1.67 mU/mL of xanthine oxidase for 60 minutes.....	72
Figure 4.6 Effect of SOD on loss of 7,8-dihydroneopterin and gain of neopterin in the presence or absence of the enzyme substrate with 1.67 mU/mL of xanthine oxidase for 30 minutes. ....	74

Figure 4.7 Effect of 33 U/mL of CAT and 100 U of SOD on 10 $\mu$ M of 7,8-dihydroneopterin in the presence of 1.67 mU/mL of xanthine oxidase for 15 minutes. ....	76
Figure 4.8 Effect of 33 U/mL of CAT and 33 U/mL of SOD on 100 $\mu$ M of 7,8-dihydroneopterin in the presence of 1.67 mU/mL of xanthine oxidase for 15 minutes. ....	78
Figure 4.9 Chromatograms of 7,8-dihydroneopterin and neopterin detection via SCX method. ....	81
Figure 6.10 Hypothesised reaction mechanisms of 7,8-dihydroneopterin with superoxide....	83
Figure 5.1 Apocynin and diapocynin molecules.....	87
Figure 5.2 Effect of 100 $\mu$ M of apocynin before or after stimulation using 5 $\mu$ M of PMA on total neopterin and neopterin production in plaque. ....	92
Figure 5.3 Effect of 100 $\mu$ M of apocynin (a and b) before IFN- $\gamma$ (500 U/mL) stimulation on total neopterin and neopterin production in plaque. ....	93
Figure 5.4 Effect of IFN- $\gamma$ (500 U/mL) stimulation on total neopterin and neopterin production in plaque. (a) and (b) show the total neopterin and neopterin measured in the media from a plaque obtained from a 56-year-old, non-smoking, diabetic male. The plaque was cultured for 3 days with IFN- $\gamma$ after the initial media only day. ....	95
Figure 5.5 Effect of 1 mM of ABAH (a and b) before IFN- $\gamma$ (500 U/mL) stimulation on total neopterin and neopterin production in plaque. ....	96
Figure 5.6 Effect of 5 $\mu$ M of PMA and PEG-SOD (50 U/mL) on total neopterin (a and b), neopterin (c and d) and lactate (e and f) production in plaque. ....	98
Figure 5.7 Effect of 5 $\mu$ M of PMA and OxLDL (2 mg/mL) on total neopterin (a and b), neopterin (c and d) and lactate (e and f) production in plaque. ....	101
Figure 5.8 Combined plaque sections after incubation with 5 $\mu$ M of PMA with or without OxLDL (2 mg/mL) on neopterin (a) and total neopterin (b) .....	102
Figure 5.9 Effect of OxLDL (2 mg/mL) and nLDL (2 mg/mL) on total neopterin (a), neopterin (b) and lactate (c) production in plaque. ....	103
Figure 5.10 Effect of 2mg/mL of oxLDL and 50 U/mL of PEG-SOD on intracellular and extracellular total neopterin and neopterin on HMDM cells in the absence of exogenous 7,8-dihydroneopterin. ....	105
Figure 5.11 Effect of 2 mg/mL of oxLDL and 50 U/mL of PEG-SOD on intracellular and extracellular total neopterin and neopterin on HMDM cells in the presence of exogenous 7,8-dihydroneopterin (200 $\mu$ M). ....	106

Figure 5.12 Light microscopy of HMDM cells after 24 hours culture. a) represents HMDMs that were treated with 78NP only, b) had both 78NP and oxLDL, c) had 78NP, oxLDL, and PEG-SOD, and d) had 78NP and PEG-SOD. ....	107
Figure 5.13 Chemical structures of PMA and ABAH .....	108
Figure 3.1 Mean and Standard Deviation of Total Plaque Weight from Cultured Plaques...	116
Figure 3.2 Mean and Standard Deviation of Baseline Total Neopterin and Neopterin produced in all cultured plaque sections. ....	117
Figure 3.3 Mean and Standard Deviation of Baseline Neopterin and Total Neopterin produced in all cultured plaques. ....	118
Figure 3.4 Mean and Standard Deviation of Neopterin and Total Neopterin in patient plasma samples.....	119
Figure 6.5 Correlation of (a) plaque neopterin to plasma neopterin, (b) plaque total neopterin to plasma total neopterin, and (c) plaque 7,8-dihydroneopterin to plasma 7,8-dihydroneopterin. ....	123
Figure 6.6 Correlation of (a) plaque total neopterin to plasma neopterin and (b) plaque neopterin to plasma total neopterin.....	124
Figure 6.7 Correlation of blood lactate to plaque total neopterin (a), neopterin (b) and 7,8-dihydroneopterin (c).....	125
Figure 6.8 Correlation of Blood Lactate to Plaque Lactate. ....	126
Figure 6.9 Correlation of plaque lactate to plaque (a) total neopterin and (b) neopterin. ....	126
Figure 7.1 Image of a thrombus taken by traditional CT. Image reproduced from Roshal (2016). Permission has been sought from the publisher. ....	131
Figure 7.2 Spectral signal and k-edge of calcium and iron. Images reproduced from Hubbell and Seltzer (1995). Permission has been sought from the publisher. ....	131
Figure 7.3 MARS images of plaque sections 5 (top) and 4 (bottom) of plaque 120 displaying two different types of calcification from within a single plaque. ....	133
Figure 7.4 Photograph (left) and MARS image (right) of Plaque 82. ....	135
Figure 7.5 Photograph (left) and MARS image (right) of Plaque 115 .....	135
Figure 7.6 Photograph (centre) and MARS image (left and right) of Plaque 118.....	136
Figure 7.7 Photograph (first and third image) and MARS image (second and fourth image) of Plaque 136.....	136
Figure 7.8 Photograph of Plaque 82 unstained (left) or stained with oil red o (right).....	137
Figure 7.9 Photograph of Plaque 136 stained with oil red o (left) or unstained (right).....	138



Figure 7.10 Evidence of neovascularization and intraplaque haemorrhage in plaque sections	141
Figure 7.11 Plaque 158 with suspected intraplaque haemorrhage	141
Figure 7.12 Ferric Nitrate signal in blood clots	141
Figure 7.13 Misidentification of materials	143
Figure 7.14 Photographs of Plaque 158, back view, front view, sagittal slice view	145
Figure 7.15 3D visualisation of plaque 158 from MARS Vision of the whole plaque (left), magic lens to show intraplaque haemorrhage (centre, blue), and with photo of the interior of the bifurcation overlain (right)	146
Figure 7.16 MARS image of plaque bifurcation (a), photograph of plaque bifurcation (b), close up of MARS image of plaque bifurcation (c) and with magic lens for iron (d)	147
Figure 7.17 Axial slices (a-d) showing the progression of an ulceration in plaque 158 in four separate slices	148
Figure 7.18 Axial, coronal and sagittal slices from plaque 158	150
Figure 7.19 Photograph of Plaque 158 cut in half	152
Figure 7.20 Axial 3D MARS image of plaque 158	152
Figure 8.1 Iodine measurement by spectral CT of pellets of n-LDL and I-LDL. The iodine concentration was measured by selecting five regions of interest each of the same size within the pellet. Error bars are SD	156
Figure 8.2 ACN precipitated pellets of I-LDL, Au-LDL and n-LDL (left to right)	156
Figure 8.3 Macrophages with 10 % Human Serum and Gold Nanoparticles prior to (top) and after (bottom) 24 hour incubation	158
Figure 8.4 Macrophages without Human Serum and Gold Nanoparticles prior to (top) and after (bottom) 24 hour incubation	159
Figure 8.5 Photo of layout of vials (left) and MARS image (right) of macrophages with non-functionalized gold nanoparticles	160
Figure 8.6 PMA-treated U937 cells before (left) and after (right) 24 hours incubation with n-LDL	161
Figure 8.7 PMA- treated U937 cells before (left) and after (right) 24 hours incubation with Au-LDL	161
Figure 8.8 PMA-treated U937 cells before (left) and after (right) 24 hours incubation with I-LDL	161

Figure 8.9 MARS images of U937 cells incubated with modified LDL without (left) and with (right) lipid channel.....	162
---	-----

TABLE OF TABLES

Table 3.1 Average weight per plaque section from all cultured plaques.....	115
Table 3.2 Patient data arranged by plasma 7,8-dihydroneopterin level.....	121
Table 3.3 Patient data arranged by plaque 7,8-dihydroneopterin level .....	121
Table 6.1 Theoretical and measured values for superoxide production using 1.67 mU/mL of xanthine oxidase.....	67
Table 7.1 Plaque volume and total volume of calcification in a selection of plaques .....	134
Table 7.2 Measurements from the phantom used to calibrate the MD for the previous images. ....	139

# 1 Introduction

## 1.1 Overview

The development of tools to assess subclinical cardiovascular disease is essential to improving the health outcomes for millions of people. At present identifying subclinical or asymptomatic atherosclerosis in patients is problematic and often not attempted due to the invasive nature of the tests required. Instead, subclinical patients are treated based on a risk score. Undetected atherosclerosis is a concern, as cardiovascular disease is the cause of approximately 33% of deaths each year in New Zealand (Heart Foundation New Zealand), and can also have serious impact on patients' quality of life.

The aim of this thesis is to explore aspects relating to the diagnosis and detection of subclinical atherosclerosis using excised carotid plaque tissue from symptomatic patients. This thesis examines the link between neopterin, a known marker of cardiovascular disease, and the plaque tissue. This is achieved through a combination of biochemical assessments and spectral imaging of plaque tissue. In addition, this thesis broadens the understanding of the biomarker neopterin by examining the oxidative effect of superoxide on the parent compound, 7,8-dihydroneopterin. This research explores potential imaging targets in advanced atherosclerotic tissue using spectral CT, which may lead to developments in the detection of subclinical atherosclerosis.

## 1.2 Background

Despite there being extraordinary breadth and depth to the literature relating to atherosclerosis, the disease is still not well understood. Here, the scope of this review is to establish the relevance of atherosclerosis in the New Zealand setting, to briefly explore the current methods of diagnosis and detection and their limitations, assess the role of inflammation as this specifically relates to macrophages in atherosclerotic plaque, and to examine potential biomarkers related to inflammation in atherosclerosis and new imaging modalities for detection of the disease.

## 1.3 Cardiovascular Disease and Atherosclerosis

Cardiovascular disease is the broad term given to the various inter-related pathologies that affect the heart and arteries (P. M. Ridker & Antman, 1999). Pathologies encompassed by this term include myocardial infarction, ischemic stroke, heart failure, and arrhythmia (Dhamoon, Sciacca, Rundek, Sacco, & Elkind, 2006). Atherosclerosis is one of the underlying processes that cause the conditions related to cardiovascular disease. It is the formation of plaque in the artery wall which eventually produces the symptoms of cardiovascular disease, e.g. high blood pressure, narrowing or stenosis of the artery (Narasimhulu et al., 2016).

Plaques form from an early age, beginning as fatty streaks due to an accumulation of lipid-rich material (Gu & Zhang, 2015). Monocytes, a macrophage precursor cell, infiltrate the arterial wall in early atherosclerosis (Ulrich, Heine, Gerhart, Kohler, & Girndt, 2008; Xu et al., 2015; Yamashita et al., 2000). Once resident, macrophages promote inflammation through the generation of oxidants and the release of inflammatory cytokines (Biessen & Wouters, 2017). Macrophages continue the progression of an atherosclerotic lesion by taking up toxic oxidized low-density lipoprotein (oxLDL) in an uncontrolled manner, causing foam cell formation and eventual cell necrosis (Howell et al., 2011; Kavurma, Rayner, & Karunakaran, 2017). The subsequent release of lipids from dying macrophages promotes the formation of a lipid or necrotic core in the arterial wall (Otsuka et al., 2015; Silvestre-Roig et al., 2014; I. Tabas, 2009).

The build-up of plaque inside the artery wall, which is predominately composed of oxidized lipids and calcification (Rodriguez-Palomares & Masip, 2016), causes a narrowing of the lumen (He, Zhang, Shi, Chen, & Gao, 2013), decreasing blood flow and increasing blood pressure. The necrotic core is separated from the blood by a thin fibrous cap. Over time,

resident macrophages may release matrix metalloproteinases degrading the fibrous cap (Kong et al., 2005), making the plaque prone to rupture (Gao & Long, 2008; Gupta et al., 2013). Plaque rupture opens the contents of the necrotic core to the blood clotting factors triggering thrombosis (Owens & Mackman, 2012). The thrombi can then break away from the site of plaque rupture and obstruct small vessels (Nakanishi & Homma, 2016). These infarcts typically occur in the brain or heart and often result in death (Psychogios et al., 2015).

#### 1.4 Health Burden of Atherosclerosis in New Zealand

Approximately one third of mortality worldwide is attributed to cardiovascular diseases (Moran et al., 2014; Mozaffarian et al., 2016). In New Zealand, 33% of deaths annually are due to cardiovascular disease and 1 in 20 adults are currently living with the disease (National Heart Foundation website accessed 22 Nov 2017). A 2009 Ministry of Health report puts the combined cost of coronary heart disease and ischemic attacks at \$621 million. This figure includes both the direct medical costs and the estimated loss of productivity to the economy (Ministry of Health, 2009). It is clear from the literature that cardiovascular disease presents a health, economic and social burden to New Zealand.

Since the introduction of statins, a class of lipid lowering drugs, in the late 1980's (Endo, 2017), the prevalence of cardiovascular diseases has reduced. This has coincided with a reduction in the number of people who smoke and exposure to second-hand smoke, a key risk factor for developing cardiovascular disease. Although the overall prevalence has reduced, Maori and Pacific Islanders remain at a higher risk of developing cardiovascular disease (Feigin et al., 2006). There is also now significant concern about the growing effect of conditions such as obesity and diabetes, which are also thought to contribute to the risk of developing atherosclerosis (Alberti et al., 2009). Despite significant research into the underlying mechanisms of cardiovascular disease, it is still not well understood why some will develop the disease and others will not. Therefore it is important, in both the New Zealand setting and globally, to address the issue of diagnosis and detection using contemporary techniques such as imaging and biomarkers.

#### 1.5 Current Methods for Detection and Diagnosis

At present detection and diagnosis of confirmed cardiovascular disease does not typically occur until after an initial event. Early intervention strategies are generally based on a patient's modified Framingham risk score, which is determined by age, sex, smoking status, diabetic

status, history of cardiovascular disease, blood pressure, and lipid status (Lloyd-Jones et al., 2000).

### 1.5.1 Risk based assessment

The Framingham Risk Assessment was based on a long term population study of the residents of Framingham, Massachusetts (Wilson et al., 1998). This study was fundamental to the current understanding of cardiovascular disease as it showed the predictive value of cholesterol (Natarajan et al., 2003). The initial risk assessment (1998 and 2002) was only able to predict the 10-year risk of coronary heart disease (CHD), but the updated 2008 model now includes heart failure, stroke and transient ischemic attacks (TIAs) (Pencina, D'Agostino, Larson, Massaro, & Vasan, 2009). The 2008 Framingham Risk Score is the current modality for assessing patients in New Zealand (Ministry of Health). In order to include the higher risk in patients of Maori and Pacific Island descent (Feigin et al., 2006; Macmahon et al., 1995), an extra 5% is added to these patients' scores. The Framingham Risk Score separates people into categories: low risk (< 10% of CHD), intermediate risk (10-20%), and high risk (>20%). Those who are determined to be clinically at risk (>20%) are treated with aspirin, a beta-blocker, a statin and then are followed up every 6 months. Common criticisms of the Framingham Risk Score include that it is based on a United States only population and that it overestimates risk in a low-risk population and underestimates it in a high-risk population (Bove et al., 2011; Moss, Williams, Newby, & Nicol, 2017). Whilst risk profiling works well on a population level, it does not necessarily apply well at the individual level. It is quite possible for a patient with little to no risk factors to experience an adverse event, and conversely it is possible for someone with many risk factors to never develop any symptoms. In many medical fields, including the area of cardiovascular medicine, there is currently a move towards personalized medicine, where the diagnosis and treatment plan is tailored to the individual (Favalli, Serio, Giuliani, & Arbustini, 2017; Loscalzo, 2012). However, in order for this approach to be successful, the clinician needs access to accurate diagnostic information. As will be outlined in the following sections, the task of gaining an accurate diagnosis of cardiovascular disease either via non-invasive or invasive methods can be difficult.

### 1.5.2 Non-invasive assessment

There are a number of non-invasive assessment techniques available which provide clinicians with both functional and anatomical information relating to cardiovascular disease. Non-

invasive assessments are not recommended as a screening tool in low risk patients due to a high chance of a false positive result (Aroney, 2012). In patients who are at high risk of cardiovascular disease or have displayed symptoms, then non-invasive assessments are the first option for diagnosis and treatment. Outlined here are some of the most common procedures.

#### *Stress electrocardiogram (ECG)*

An ECG monitors the electrical activity of the heart using electrodes. In the case of a stress test, this takes place while a patient is active, or can be artificially stressed using specific drugs. Whilst this technique is fast and relatively safe, it has a low specificity (72%) and sensitivity (67%) (Mohamed, 2007), and is not appropriate for all patients e.g. endurance athletes.

#### *Stress echocardiogram*

During a stress echocardiogram, blood pressure and heart rate are monitored while the patient is exercising. The procedure also involves an ultrasound of the heart to determine blood flow. As with any ultrasound technique, there are limitations related to user expertise in obtaining accurate measurements. Despite this limitation, echocardiogram has been found to have good prognostic and diagnostic value (Konety et al., 2016).

#### *Carotid artery ultrasound*

This procedure is often used to assess patients who are at risk of stroke for treatment, for example whether placing a stent or carrying out a removal of the plaque is appropriate (Halliday et al., 2004; Stein et al., 2008). The ultrasound measures blood flow and narrowing of the artery, which is calculated as the percentage of stenosis (Bots, Hofman, & Grobbee, 1997; M. P. Spencer & Reid, 1979).

#### *Cardiac CT*

A cardiac CT is used to detect calcium in the coronary arteries in addition to blockages (Budoff et al., 2006). This procedure often involves administering beta-blockers to slow the heart rate, and a contrast agent to improve visualization of the arteries. A calcium score is calculated based on the Hounsfield Units measured (Criqui et al., 2014). A score over 10 indicates coronary artery disease (CAD) is present, and a score over 400 indicates extensive CAD. There is some debate about the prognostic value of this information and how to use this information to tailor patient treatment is uncertain (Detrano et al., 1999; Shaw, Raggi, Schisterman, Berman, &

Callister, 2003; Ulzheimer & Kalender, 2003). There is a growing use of this technique to rule out cardiovascular disease

### *Cardiac MRI*

A cardiac MRI allows clinicians to assess the anatomy and function of the heart using magnetic resonance (Chung, 2002; Fisher, Steinberg, & Rogers, 1987). The benefit of this over CT is that there is no radiation involved; however, it is much more difficult to obtain high-quality images using this technique, as any motion will distort the image.

### 1.5.3 Invasive assessment

Invasive assessments are typically carried out on patients showing secondary symptoms of cardiovascular disease (e.g. shortness of breath). Invasive assessments provide a more accurate diagnosis of level of disease burden and aid the correct treatment choice. However, this increased accuracy gained from choosing an invasive assessment over non-invasive, also means an increased risk of an adverse event for the patient undergoing the procedure.

### *Angiogram*

An angiogram involves the threading of a catheter into the patient's artery, where a dye is then injected and monitored via x-ray. The x-ray will show if any blood vessels are narrowed or blocked. For a long time the technique was considered the gold standard for diagnosing cardiovascular disease, however, with improvements in imaging modalities there may be a shift away from this high risk invasive technique.

### *Intravascular ultrasound (IVUS)*

IVUS is similar to an angiogram in that a catheter is used, but instead of releasing a dye, the catheter contains an ultrasound transducer. IVUS is used to measure plaque burden and stenosis of the artery.

### *Fractional flow reserve (FFR)*

This technique measures pressure differences across an artery caused by narrowing. To do this, a catheter is inserted with a specially designed transducer which is able to measure pressure, flow and temperature. This technique can be used to tell if a narrowing of an artery is functionally relevant or not.



Current invasive and non-invasive assessments provide anatomical and functional information about cardiovascular disease and aid clinicians in risk stratification. However, one particular area that is not covered by any of these assessments is the risk of plaque rupture, which is a key event in cardiovascular disease.

## 1.6 Inflammation

### 1.6.1 Background

The current assessment and treatment of cardiovascular disease is heavily weighted towards lipid status. Since the early 1990's, there have been indications that there may be an inflammatory component to atherosclerosis. The discovery of involvement of inflammatory cells and cytokines started a shift in thinking away from atherosclerosis simply being a cholesterol storage disorder. Until recently, the hypothesis that inflammation has a significant role in the progression of atherosclerosis was untested in humans. A review by S Antonopoulos, Margaritis, Lee, Channon, and Antoniades (2012) highlights some of the early evidence from clinical trials with statins of an anti-inflammatory effect occurring which was separate to the lipid-lowering mechanism. However, these trials (e.g. LIPID, JUPITER, and PRINCE) did not confirm that the reduction in primary end points was independent of the lipid-lowering effect of the statins. In 2017, the CANTOS trial came to an end. This trial, along with the CIRT trial which finishes in late 2018, was designed specifically to test the inflammation hypothesis. The study found a significant reduction in the primary end point (non-fatal myocardial infarction, non-fatal stroke or cardiovascular death) in patients who received a 150 mg dose of canakinumab every 3 months over a 48 month period compared with the placebo (Paul M Ridker et al., 2017). Canakinumab was specifically selected as it has no lipid-lowering capabilities, but instead inhibits interleukin-1 $\beta$ . The patients in this trial were selected for continuing to have high levels of inflammation as determined by high sensitivity C-reactive protein of 2 mg/L or greater despite receiving statins and lipid-lowering therapy. This evidence that targeting inflammation reduces the risk of a cardiovascular event is further evidence as to why diagnosis of cardiovascular disease needs to move beyond the risk factors identified in the Framingham Risk Score alone.

### 1.6.2 Key contributors to inflammation in atherosclerosis

From early on, it was suspected that monocyte and leukocyte recruitment contributed to the development of atherosclerotic plaque (Herbin et al., 2016). Whilst there is still some debate

as to the initiating mechanism of atherosclerosis (Stocker and Keaney Jr (2004) provide an eloquent overview of the oxidative modification, response-to-injury, and response-to-retention hypotheses), in all cases it is thought that recruitment of monocytes and T cells is a key step in plaque progression. It has since been established that there are different subsets of circulating monocytes, classical (CD14<sup>++</sup> CD16<sup>-</sup>), non-classical (CD14<sup>+</sup>CD16<sup>++</sup>) and intermediate (CD14<sup>++</sup>CD16<sup>+</sup>), which have different pro-inflammatory and anti-inflammatory properties. In humans, an increase in CD16<sup>+</sup> monocytes appears to be associated with plaque vulnerability (Imanishi et al., 2010). A recent study with mice found that increasing circulating monocytes by giving a constant very low dose of LPS increased the progression of atherosclerosis by priming the monocytes towards an inflammatory state (Geng et al., 2016).

More recently, resident macrophage proliferation has been found to contribute to inflammation and destabilize atherosclerotic plaque. Proliferation of the resident macrophages maintains the local macrophage population in tissue (Hashimoto et al., 2013; Jenkins et al., 2011) and in advanced atherosclerotic plaque (Robbins et al., 2013). In *ApoE*<sup>-/-</sup> mice, inhibiting macrophage proliferation using simvastatin suppressed atherosclerotic plaque inflammation (Tang et al., 2015).

It is now understood that macrophages in the plaque are not homogeneous. Macrophage phenotypes were initially classed into two broad categories. M1 macrophages were defined as macrophages with classical activation, analogous to Th1 T cells. M2 macrophages were those polarized towards alternative activation, or an anti-inflammatory state. It was thought that M1 macrophages contributed to plaque progression and M2 were involved in plaque regression (Mantovani, Sica, & Locati, 2005). However, initial classifications were determined based on cell culture. Several more macrophage phenotypes have now been identified in atherosclerotic plaque tissue. These include M(hb), Mox, M4 among others (Chinetti-Gbaguidi, Colin, & Staels, 2015; Erbel et al., 2015; Kadl et al., 2010). Each has properties that define it from other subsets. For example, Mox macrophages are the result of exposure to oxidized phospholipids, and can be differentiated from others by their increased expression of heme oxygenase 1 (Marques, Negre-Salvayre, Costa, & Canonne-Hergaux, 2016). Studies looking at the distribution of macrophage phenotypes within atherosclerotic plaque have found that both M1 and M2 markers are increasingly expressed in advanced plaque (Johnson & Newby, 2009; Ira Tabas, 2010), and that certain areas of the plaque such as the plaque shoulder have greater numbers of M1 macrophages (Stöger et al., 2012). Ira Tabas and Bornfeldt (2016) provide a

particularly in-depth review of changes in macrophage polarization and phenotype that occur during the different stages of plaque development. Interestingly, cell culture studies have found that it is M2 macrophages that accumulate oxLDL rather than M1, due to a higher expression of CD36 (Van Tits, Stienstra, Van Lent, Netea, & Stalenhoef, 2011). After accumulating oxLDL, the M2 cells challenged with LPS produced pro-inflammatory cytokines at levels that matched M1 cells.

Efferocytosis was previously thought of as purely the removal of dead or dying cells, however, there is now a wider understanding of how efferocytosis, and conversely, defective efferocytosis affects the ongoing immune response (Elliott, Koster, & Murphy, 2017). Defective efferocytosis prevents the appropriate reverse cholesterol transport pathways from operating which encourages foam cell formation (Kojima et al., 2014). Impaired efferocytosis of apoptotic cells leads to secondary necrosis which results in a build-up of dead cells, which in atherosclerosis, go on to form the necrotic core (Thorp, 2010). In addition to the accumulation of dead cells, there is an increase in TNF- $\alpha$  and IL-6, which promote on-going inflammation. Apoptotic cells release a number of chemokines which attract macrophages to the site of inflammation. It has recently been found that nuclear receptors including PPAR- $\gamma$  enhance transcription of phagocytosis related genes (Chinetti-Gbaguidi et al., 2011; Noelia et al., 2009) particularly those relating to phosphatidylserine binding receptors including CD36, suggesting a link between efferocytosis and immune signalling, although the mechanism of nuclear receptor enhancement in the presence of apoptotic cells is not understood.

### 1.6.3 Macrophage based mechanisms inflammation in atherosclerosis

Inflammation in atherosclerosis is mediated by a number of cytokines, pathways and cell signalling molecules. Here, three of the relevant processes are explored in more detail. A full account of the various processes occurring can be found in Galkina and Ley (2009).

#### *Signalling via interferon- $\gamma$*

Interferon- $\gamma$  has been found to have a pro-atherogenic affect in mouse models via the activation of the JAK/STAT pathway. The JAK/STAT pathway is a signalling cascade which has been implicated in a variety of inflammatory pathologies. Binding of a ligand at the cell surface triggers the phosphorylation of various proteins in the cascade, eventually resulting in DNA transcription. N. Li et al. (2010) found that incubating human monocyte-like THP-1 cells with interferon- $\gamma$  increases STAT1 phosphorylation. This effect was reliant on ERK1/2 signalling.

Furthermore, it was found that interferon- $\gamma$  increased the uptake of acetylated or oxidized LDL, again an ERK1/2 dependent mechanism. ERK1/2 is a component of the MAPK/ERK pathway, a separate cell signalling cascade which also induces gene transcription. Typically, binding of epidermal growth factor (EGF) to its receptor (EGFR) at the cell surface triggers the pathway. Defects in this pathway are thought to contribute to uncontrolled cell growth.

### *NLRP3 inflammasome*

Inflammasomes are complexes that form in the cytoplasm of macrophages in response to danger or pattern recognition signals (DAMPs and PAMPs). Assembly of the NLRP3 inflammasome, which is specific for sterile (non-bacterial) inflammation results in the cleavage of pro-interleukin-1 $\beta$  via caspase-1 to the mature interleukin-1 $\beta$ . Interleukin-1 contributes to atherosclerosis through actions such as monocyte recruitment (via MCP-1) and induction of IL-6 secretion (Ben-Sasson et al., 2009). Loss of function studies with IL-1 have shown that atherogenesis is lessened in mice (Alexander et al., 2012). In humans, blocking IL-1 reduced CRP release after acute coronary syndrome (Crossman et al., 2008). Initially thought to be only activated by cholesterol crystals in atherosclerosis (Düwell et al., 2010), it is now known that this also is mediated by oxLDL via CD36 (Sheedy et al., 2013). Reactive oxygen species (ROS) including superoxide generated by NADPH oxidase are thought to contribute to the priming of the NLRP3 inflammasome in atherosclerosis (Martinon, 2010).

### *ROS generation via NADPH oxidase*

NADPH oxidase (NOX) is an enzyme complex which facilitates the transfer of electrons, usually resulting in the formation of superoxide or in some cases hydrogen peroxide (Abo et al., 1991). NOX is a membrane bound protein which exists in various isoforms. It is usually composed of six subunits: Rho-GTPase, gp91phox, p22phox (NOX 1,2,3,4 only), p40phox, p47phox, and p67phox. Isoforms include phagocytic oxidase which can be activated by NF- $\kappa$ B (Byrne et al., 2003), NOX 1, 2, 3 and 4 which have a similar morphology to each other (Bedard & Krause, 2007). NOX 2 is the main isoform in phagocytic cell such as macrophages. NOX 3 has been found to be constitutively active in cells, whereas NOX 1 and 4 can be upregulated by PMA (Ueno, Takeya, Miyano, Kikuchi, & Sumimoto, 2005). NOX 5 has a calcium binding domain and is involved in the phosphorylation of c-abl, a kinase involved in cell differentiation, division, and stress response (Bánfi et al., 2004). DUOX 1 and 2 are also regulated by calcium binding. DUOXs contain an additional extracellular domain and produce hydrogen peroxide in preference to superoxide (Lambeth, Kawahara, Diebold, & Medicine,

2007). There are several peptide-based inhibitors of NOX (for example, GP91ds-tat) as well as small molecule inhibitors (e.g. VAS compounds, apocynin, GKT inhibitors, DPI) (Altenhöfer et al., 2015). NOX inhibitor design is now focussing on inhibiting specific isoforms, rather than non-selective inhibition like that achieved by apocynin and DPI.

Superoxide is converted to other products including hypochlorous acid, hydroxyl radicals and hydrogen peroxide. In healthy cells, ROS remain in homeostasis due to cellular mechanisms to remove ROS. However, in inflammatory conditions the flux of ROS exceeds the cellular capability for removal and leads to the activation of a number of inflammatory pathways. The NF- $\kappa$ B pathway is one pathway which influences the transcription of a number of genes related to stress response. Another is the MAPK/ERK pathway detailed above. ROS also activate the Nrf2 pathway which promotes the translation of enzymes that remove cellular ROS such as glutathione synthetase and peroxiredoxin. Inhibition of NOX has been shown to reduce atherosclerotic lesions and vascular ROS in ApoE<sup>-/-</sup> mice (Di Marco et al., 2014). Interestingly, ApoE<sup>-/-</sup> overexpressing superoxide dismutase (SOD), an enzyme which dismutates superoxide to hydrogen peroxide, still developed lesions, whereas ApoE<sup>-/-</sup> overexpressing either catalase, an enzyme that converts hydrogen peroxide to water and oxygen, or both catalase and SOD, did not go on to develop atherosclerotic lesions.

Hydrogen peroxide may be contributing to the lesion development through a soluble fms-like tyrosine kinase-1 (sFLT-1) signalling pathway (H. Li, Gu, Zhang, Lewis, & Wang, 2005). Hydrogen peroxide has been found to induce the expression of sFLT-1 via activation of apoptosis signal-regulating kinase 1 (ASK1) (Agarwal et al., 2012). sFLT-1 a protein found carried in the bloodstream. Under normal circumstances, sFLT-1 reduces vascularization by binding free vascular endothelial growth factor (VEGF). In an overabundance, it can cause impaired angiogenesis which leads to endothelial dysfunction, promoting lesion development. It is also possible that hydrogen peroxide may be participating in a Fenton reaction which could promote the oxidation of LDL to oxLDL (Agil, Fuller, & Jialal, 1995; Formanowicz, Radom, Rybarczyk, & Formanowicz, 2018; S. P. Giese, Crone, Flavall, & Amit, 2008).

## 1.7 Biomarkers of Atherosclerosis

As the understanding of the underlying mechanisms of atherosclerosis has improved, there has been significant progress towards identifying novel markers of the disease. Yet, even with the progress that has been achieved, no marker has yet shown enough value to be included in the

standard risk assessment. An ideal biomarker would be a metabolite that was robust, non-invasive, specific, sensitive, and most importantly, clinically relevant.

CRP is often highlighted as the most promising biomarker of atherosclerosis (Kaski et al., 2008; Skopec et al., 2016) and certainly there is a wealth of data related to CRP. It is produced in the liver and at sites of inflammation. It has been shown to be an independent predictor of cardiovascular risk in healthy men (the MRFIT trial), and has been found when used in conjunction with the Framingham Risk Assessment to provide more accurate risk stratification (Rifai & Ridker, 2001). However, CRP has low specificity as it is also increasing during infection and other types of chronic inflammation. This tends to be a common drawback of any inflammatory biomarker. Other promising biomarkers include TNF- $\alpha$  (Signorelli et al., 2016), IL-6 (Gostner & Fuchs, 2016), MDA-LDL (Haller, Lindner, & Lammerhofer, 2015), sFLT (Boyaud & Inguibert, 2011; Gruson, Hermans, Ferracin, Ahn, & Rousseau, 2016), matrix metalloproteinases (Halade, Jin, & Lindsey, 2013; Konstantino et al., 2009; Olson et al., 2008), serum myeloperoxidase (Chen, Shi, Liang, Liang, & Fu, 2011; Scharnagl et al., 2014; Wang et al., 2017) and PTX3 (Fornai et al., 2016; Hollan et al., 2010). It is interesting to note that although development of a non-invasive biomarker has been a research focus for several decades now, there remains a lot of work to get a biomarker to the stage of clinical acceptance.

In conjunction with the markers above, neopterin has also been put forward as a potential biomarker (De Rosa et al., 2011; Firoz et al., 2015; Schnabel et al., 2010; Videm, Wiseth, Gunnes, Madsen, & Garred, 2007; Zhang et al., 2016; Zuo et al., 2016). To date, over 200 clinical studies have been conducted measuring neopterin in relation to major adverse cardiac events (MACE) or comparing healthy populations to those with symptomatic cardiovascular disease. A large proportion of these studies found that neopterin had predictive value in assess risk of cardiovascular events. Yet despite significant evidence of the prognostic and diagnostic value of neopterin, there has been little movement in the past decade towards acceptance of neopterin as a biomarker of atherosclerosis.

### 1.8 Neopterin and 7,8-Dihydroneopterin

Neopterin is produced by human macrophages in response to immune activation. Neopterin production is predominately induced by interferon- $\gamma$  but also to a lesser extent by IL-10, LPS and PHA (Christoph Huber et al., 1984). In vitro experiments have found that in macrophages neopterin production peaks 48 hours after stimulation (Burrowes, 2012). Neopterin production ranges depending on level of stimulation with reported values of 20 pmol/mL after 72 hours

for  $2.5 \times 10^5$  macrophages (Christoph Huber et al., 1984) through to  $2.5 \mu\text{mol/L}$  in plaque tissue (Steven P Giese et al., 2009). In sepsis patients, it has been found that if neopterin continues to be produced in increasing quantities for longer than three days, there is a higher likelihood of patient mortality (Adamik, Kübler-Kielb, Golebiowska, Gamian, & Kübler, 2000). Interestingly, the biological function of neopterin is largely uncharacterized. 7,8-Dihydroneopterin, the parent compound to neopterin, is synthesized from GTP via an enzyme known as GTP cyclohydrolase I (GTPCH-I) (Niederwieser et al., 1984).

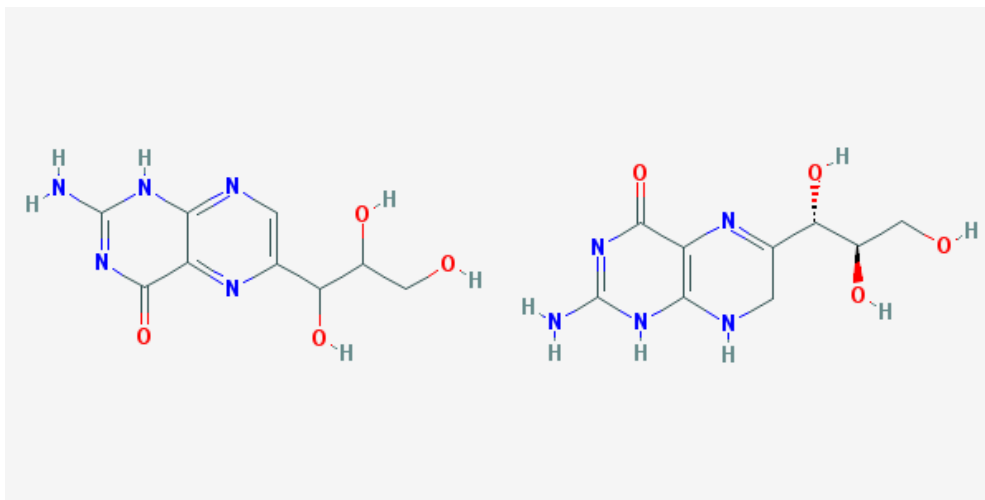


Figure 1.1 Chemical structures of neopterin (left) and 7,8-dihydroneopterin (right)

Previously, this research group has shown that atherosclerotic plaque is a source of 7,8-dihydroneopterin and neopterin in patients with symptomatic atherosclerosis (T. Janmale et al., 2015). In most cells, 7,8-dihydroneopterin is funnelled down the folate biosynthesis pathway. Macrophages lack significant quantities of the enzyme 6-pyruvoyltetrahydropterin synthase which controls this flux into the folate pathway, so compared to other cell types macrophages produce an excess of 7,8-dihydroneopterin (B Widner, Enzinger, Laich, Wirleitner, & Fuchs, 2002). Oxidation of 7,8-dihydroneopterin produces neopterin, among other compounds (e.g. xanthopterin) (Dantola, Thomas, Braun, Oliveros, & Lorente, 2007; B. Widner, Mayr, Wirleitner, & Fuchs, 2000). In the literature, this oxidation step is often ignored, and researchers tend to refer to neopterin as the product of GTPCH-I in macrophages. However, it is known from research undertaken in this laboratory and others that a substantial amount of the 7,8-dihydroneopterin produced by macrophages is never converted to neopterin. To say neopterin is a measure of immune activation in macrophages is false, neopterin is a measure of the combined effects of immune activation and oxidation, whereas 7,8-dihydroneopterin alone provides a true measure of immune activation. Despite the fact there have been a substantial

number of studies relating to the use of neopterin as a biomarker, not a single clinical study has measured 7,8-dihydroneopterin.

7,8-Dihydroneopterin in addition to being a marker of immune activation has been found to have several interesting properties in *in vitro* cell culture studies. It has been found to have a protective effect against oxLDL cytotoxicity in human macrophages (Shchepetkina, Hock, Miller, Kennedy, & Giese, 2017). 7,8-dihydroneopterin has also been shown to reduce uptake of cholesterol and oxysterols in human macrophages pre-treated before the addition of oxLDL (Davies, 2015). It is thought this effect may be mediated by the downregulation of CD36, a key cell surface scavenger receptor for oxLDL. Whereas incubation with oxLDL increases CD36, 7,8-dihydroneopterin has been shown to downregulate the expression of this protein. At present, a number of pathways are being studied to analyse how 7,8-dihydroneopterin is able to induce this downregulation. Initial indications are that PPAR- $\gamma$  and ERK1/2 are likely to be involved (Yeandle, 2017). However, the specific mechanism of action on this pathway is yet to be resolved.

7,8-Dihydroneopterin also acts as a chain breaking, peroxy radical scavenging antioxidant (S. P. Giese, Reibnegger, Wachter, & Esterbauer, 1995). K. Oettl, Dikalov, Freisleben, Mlekusch, and Reibnegger (1997) reported that 7,8-dihydroneopterin reduced radical scavenging by DMPO by up to 90%. They found that the rate constants for the reaction of 7,8-dihydroneopterin with superoxide and peroxy radicals were  $10^3\text{M}^{-1}\text{s}^{-1}$  and  $10^7\text{M}^{-1}\text{s}^{-1}$  respectively. Early studies in cells found that micromolar concentrations of 7,8-dihydroneopterin were able to inhibit red blood cell lysis mediated by AAPH (a radical generator), hydrogen peroxide and hypochlorite (S. Giese, Duggan, & Gebicki, 2000). More recently, 7,8-dihydroneopterin has been shown to protect cells against oxLDL-mediated glutathione loss and GAPDH inactivation (S. P. Giese, Amit, Yang, Shchepetkina, & Katouah, 2010). Following on from this work, it has been hypothesized that 7,8-dihydroneopterin may be scavenging superoxide radicals generated by NADPH oxidase. It is thought that the neopterin which is being generated by atherosclerotic plaque may be a result of this scavenging.

As outlined earlier, oxidation and generation of ROS are key components driving inflammation. With it becoming clearer that inflammation contributes to the development and progression of atherosclerosis, it makes sense to try to develop biomarkers that will capture



specific targets such as a patient's antioxidant capacity (7,8-dihydroneopterin), level of macrophage activation (total neopterin), and level of oxidative stress (neopterin).

### 1.9 Imaging of Atherosclerosis

Whilst biomarkers of inflammation would provide a quick and easy test, any inflammatory biomarker will always require ruling out other sources of inflammation such as infection. It is likely that if a biomarker is adopted it will become part of a toolbox of tests that a clinician has available. Part of the problem for diagnosing cardiovascular disease at present is that current assessments of cardiovascular disease have low sensitivity or have a relatively high risk of adverse effects. To address this problem, new imaging modalities are being investigated.

One of these imaging modalities is spectral photon counting computed tomography (CT). Spectral CT is already used in a number of preclinical applications ranging from measuring pore size in titanium scaffolds to identifying breast cancer cells using targeted nanoparticles (Rajendran et al., 2014; Roeder et al., 2017). It has been identified as an innovative technique that may allow the diagnosis of early plaque development in the carotid artery (Galaska et al., 2016). This technique has recently been used for vascular imaging of the head and neck in asymptomatic patients (Symons et al., 2017) which gave high image quality and lower noise with fewer artefacts than conventional single energy CT. The MARS Bioimaging group based at the University of Canterbury has developed a commercial preclinical spectral CT scanner which produces images comparable to current histological techniques (Anderson & Butler, 2014). In addition to providing a 3D reconstruction of the scanned object, the MARS scanner uses a proprietary algorithm to identify and quantify up to six materials within the object. Depending on the material, the sensitivity is as low as 1 mg/mL. The ability of spectral CT to identify materials within an image means that it provides the user with significantly more information than traditional CT. Information is captured from each photon by a highly sensitive read out chip, which means the dose required is roughly 1/5<sup>th</sup> of that used in standard CT methods. As a sensitive, low dose non-invasive technique, spectral CT shows promise as a diagnostic tool, in addition to its use for preclinical studies.

Imaging and quantification of calcification within excised plaque has previously been shown to be possible using MARS spectral CT. (Zainon et al., 2014; Zainon et al., 2012). As discussed earlier, increased calcification in the coronary arteries has been linked to a higher risk of adverse events. However, the level of calcification in a carotid artery is not routinely captured.

Understanding more about plaque morphology and calcification is essential, as this is a key aspect of atherosclerosis that cannot be replicated by tissue culture experiments. It is suspected that the morphology of the plaque tissue may influence immune activation, and therefore is likely to have relevance to the development of biomarkers.

The number and distribution of inflammatory cells within plaque tissue is of particular interest to researchers trying to understand plaque vulnerability. Spectral CT cannot identify macrophages directly as the individual cells are below the spatial resolution of the scanner and their composition (predominately water and lipid) is the same as any cell that makes up the soft tissue. However, spectral CT is particularly adept at measuring materials with a high atomic number. These are commonly referred to as high-z materials. These materials produce a distinctive spectral signal. These materials tend to be the heavier metal atoms e.g. gold. It is hypothesized that macrophages in plaque tissue could be identified by spectral CT using gold nanoparticle labelling.

Whilst imaging of atherosclerotic plaque using spectral CT is still in its infancy, there is some evidence that this technique can be used to distinguish features relevant to plaque vulnerability (Cormode et al., 2010; Zainon et al., 2012). Key features of atherosclerotic plaques which have been identified as having a role in plaque vulnerability include the necrotic core, fibrous cap, microcalcification, and intraplaque hemorrhage. Using a non-invasive method to measure and monitor the features may improve detection of aspects such as silent infarction in asymptomatic carotid atherosclerosis (Brott et al., 1994). In addition, a better understanding of how these features contribute to plaque vulnerability may lead to a reduction in unnecessary carotid endarterectomy surgery. This surgery introduced in 1954 used to prevent strokes. At present, the absolute risk reduction for patients undergoing the surgery is 13.1% over 2 years for those with symptomatic stenosis greater than 70% (Barnett & Collaborators, 1998). Feasby and Barnett (2007), among others, have identified the need for better assessment tools for selection for this surgery.

## 1.10 Summary

Despite atherosclerosis being a leading cause of mortality, the current tools available for assessment and diagnosis are limited. At present, the lack of understanding of the underlying mechanisms of the disease has prevented the development of a sensitive yet specific biomarker for cardiovascular disease. Importantly however, new non-invasive imaging techniques may prove crucial to understanding and assessing the risks associated with plaque vulnerability.

Furthermore, the combination of a biomarker of inflammation and improved imaging may provide clinicians with the tools they need to accurately assess patient risk.

## 1.11 Research Aims and Significance

Below are the overall objectives of the Free Radical Research Group at the University of Canterbury and how this thesis fits within those goals.

### Long term goal

To identify a robust panel of biomarkers that correlate with increased risk of atherosclerosis and develop screening tools to assess whether patients require carotid endarterectomy surgery.

*Statistical calculations from large group studies have shown up to 65 patients need to undergo an endarterectomy surgery to prevent a single stroke (Barnett, 2004). Development of appropriate screening tools and biomarkers to identify vulnerable plaque (plaque likely to rupture) would prevent many unnecessary surgeries reducing the cost to the health system and reducing risk to the individual patient.*

### Medium term goal

Explore neopterin as a biomarker for atherosclerosis and to identify markers of vulnerable plaque using MARS CT.

*Neopterin is known to be elevated in patients with cardiovascular disease and has been shown to a predictor of adverse outcomes. If neopterin could be used as a measure of atherosclerosis it would provide an inexpensive assay monitoring tool. Identification of vulnerable plaque using non-invasive imaging modalities would allow monitoring of disease progression and the effectiveness of treatment.*

### PhD goals

The specific aim of this thesis is to investigate the inflammatory response of macrophages within excised atherosclerotic plaque and the relation of the clinical biomarker neopterin, and its parent compound, 7,8-dihydroneopterin, to the morphology of the plaque.

- Investigate the relationship between plaque morphology and its biochemical response, particularly release of neopterin and 7,8-dihydroneopterin, to stimuli.

*Neopterin and 7,8-dihydroneopterin production is not consistent across the length of the plaque (T. Janmale et al., 2015). By exploring the material composition of the plaque (lipid,*

*calcium, water, macrophage content) we are hoping to gain a better understanding of why this variation occurs and what the biological significance of this might be.*

- To develop techniques in conjunction with others that will identify macrophages and regions of interest within the plaque.

*Macrophages are key target within the plaque as they are known to contribute to the oxidative stress by producing ROS, they take up oxLDL and form foam cells, and lately have been implicated in leaving micro-calcium deposits in the plaque. Identifying regions that are rich in active macrophages may help broaden the understanding of the disease progression. Could neopterin be used as a tool to assess plaque vulnerability?*

- To explore the role of superoxide, a reactive oxygen species produced by NADPH oxidase in macrophages, in the oxidation of 7,8-dihydroneopterin to neopterin.

*7,8-dihydroneopterin is known to be a strong antioxidant and radical scavenger, but its interactions with superoxide, a key oxidant in plaque generated by NADPH oxidase, have not previously been explored.*

## 1.12 Thesis Outline

A note on the format of this thesis:

This thesis borrows some of the formatting style from a typical medical physics thesis. This research covered a number of research areas which had different methodologies and goals but ultimately all contribute to the same broader goal. For this reason, the thesis is split into a number of small chapters, with a general discussion tying them together.

**Chapter 2** covers the general methods used in the experimental sections of the thesis in detail, including the development of an HPLC assay system to measure the superoxide generated oxidation of 7,8-dihydroneopterin, modifications to improve the SCX based detection system for neopterin in plasma and cell culture samples, and advancement of the existing plaque culture system.

**Chapter 3** assesses the activation of macrophages within excised plaque tissue, and examines this in relation to plaque morphology, specifically calcium. This is the first evidence that plaque

morphology modulates the inflammatory response in plaque. In addition, this is the first evidence that macrophages are able to produce total neopterin in response to PMA.

This chapter forms the basis for the paper “Induced macrophage activation in atherosclerotic plaque” which has been accepted for publication by the journal Immunobiology.

**Chapter 4** explores the formation of neopterin with superoxide to further understand the relationship between 7,8-dihydroneopterin and neopterin. This is the first time that it has been shown that neopterin is a product of the reaction between 7,8-dihydroneopterin and superoxide. This work is part of a paper titled “7,8-Dihydroneopterin can be oxidized to neopterin by superoxide: evidence from cellular, *ex vivo* atherosclerotic plaque, enzymatic and radiolytic systems” which is being drafted at present.

**Chapter 5** examines the biological significance of oxidants in plaque in relation to total neopterin and neopterin output. This chapter shows that modulating the oxidant levels in the plaque using various inhibitors and stimulants has a direct effect on the level of neopterin produced relative to total neopterin.

**Chapter 6** studies the relationship between plaque biomarkers, total neopterin, neopterin and lactate, and plasma levels of these markers. This is the first time this relationship between plaque biochemistry and the measurable markers has been examined. In addition, the finding in this chapter that plaque total neopterin is correlated to plasma lactate levels, is original.

**Chapter 7** assesses various tools associated with spectral imaging of plaques.

**Chapter 8** examines the use of functionalized and non-functionalized gold nanoparticles as a marker of macrophages. In addition, a protocol for identifying intraplaque hemorrhage, a key marker of plaque vulnerability, is developed. The identification of intraplaque hemorrhage is a completely novel technique for spectral CT. This chapter also addresses the improvement of lipid measurement in plaque.

This chapter forms the basis for a poster was presented at the Society for Biomaterials conference in Atlanta, Georgia in April 2018.

**Chapter 9** summarizes the findings of this thesis and looks at the future directions of this work.

### 1.13 Major scientific findings

1. Neopterin is generated from superoxide induced oxidation of 7,8-dihydroneopterin. The 7,8-dihydroneopterin appears to outcompete superoxide dismutase for the superoxide radicals. This is significant as it suggests HOCl-mediated oxidation of 7,8-dihydroneopterin may not be the sole source of neopterin in macrophages.
2. Plaque total neopterin output (macrophage activation) is correlated to plasma lactate values, which are known to be associated with the degree of carotid atherosclerosis present, and inversely correlated to calcium volume. This is significant as this is a first step towards being able to relate macrophage activity in vulnerable tissue to plasma markers which would help to improve clinical assessment of atherosclerosis.
3. Oxidant production in ex-vivo plaque tissue can be induced through the addition of either oxLDL or nLDL. This is significant as being able to modulate oxidants in tissue ex-vivo provides a complex cell system to test questions related to the progression/regression of atherosclerosis.
4. MARS imaging of plaque tissue produces high quality images with excellent differentiation of key hallmarks of plaque vulnerability, including lipid pools within the necrotic core and microcalcification, which are highly consistent with visual inspection of the tissue. This is significant as this means MARS imaging is now at a standard where it can be used to accurately quantify plaque vulnerability.
5. Intraplaque haemorrhage can be identified and differentiated from calcification in ex-vivo plaque tissue. This is significant as iron and calcium cannot be distinguished using traditional CT methods, and it provides a further tool to assess plaque vulnerability.

## 2 Methods and Materials

### 2.1 Materials

All reagents were a minimum of analytical grade. All solutions were prepared using nanopure water (Millipore Milli-Q, MA, USA).

7,8-Dihydroneopterin	Schricks Laboratory, Switzerland
Accutase	Invitrogen, Life Technologies, New Zealand
Acetic acid	Scharlau Chemie S.A., Spain
Acetonitrile	J. T. Baker, NJ, USA
Ammonium Chloride (NH <sub>4</sub> Cl)	May & Baker Ltd, Dagenham, England
Ammonium Phosphate	Sigma-Aldrich Co. LLC, New Zealand
Apocynin	Sigma Chemical Co., MO, USA
Ascorbic acid	Sigma Chemical Co., MO, USA
BCA protein determination kit	Pierce, IL, USA
Canola Oil	Sunfield, NZ
Chelex-100 resin	Bio-Rad Laboratories, California, USA
Cholesterol reagent	Roche Diagnostics, USA
Copper Chloride	Sigma Chemical Co., MO, USA
Dimethyl sulphoxide (DMSO)	BDH Lab Supplies Ltd, Poole, England
Dipotassium phosphate	Scharlau Chemie, Italy
Ethanol	BDH Lab Supplies Ltd, Poole, England
Ethylene-diamine-tetra-acetic acid (EDTA)	Sigma-Aldrich Co. LLC, New Zealand
Gold nanoparticles	Otago School of Medicine, Christchurch, NZ
Granulocyte-macrophage colony-stimulating factor (GM-CSF)	Bayer Healthcare Pharma. LLC, Seattle, USA
Hydrochloric acid (HCl)	BDH Lab Supplies, Poole, England
Interferon-gamma (IFN-g)	Sigma Chemical Co., MO, USA
Iodine (I)	BDH Lab Supplies Ltd, Poole, England
Iodine Chloride	Sigma Chemical Co., MO, USA
Isopropanol	BDH Lab Supplies Ltd, Poole, England
Lactate kit	Roche Diagnostics, USA
Lymphoprep	Axis-Shield PoC AS, Oslo, Norway



Methanol	Merck, Darmstadt, Germany
Neopterin	Schircks Laboratory, Switzerland
Oil Red O	Sigma Chemical Co., MO, USA
Penicillin/ Streptomycin	Invitrogen, Life Technologies, New Zealand
Phorbol-12-myristate-13-acetate	Sigma Chemical Co., MO, USA
Phosphoric acid	Sigma-Aldrich Co. LLC, New Zealand
Phytohemagglutinin	Sigma Chemical Co., MO, USA
Potassium bicarbonate (KHCO <sub>3</sub> )	May & Baker Ltd, Dagenham, England
Potassium Iodide (KI)	May & Baker Ltd, Dagenham, England
Roswell Park Memorial Institute 1640 (RPMI 1640)	Sigma-Aldrich Co. LLC, New Zealand
Sodium bicarbonate (NaHCO <sub>3</sub> )	May & Baker Ltd, Dagenham, England
Sodium chloride (NaCl)	BDH Lab Supplies Ltd, Poole, England
Sodium dihydrogen orthophosphate (NaH <sub>2</sub> PO <sub>4</sub> )	Merck, Darmstadt, Germany
Sodium hydroxide (NaOH)	Merck, Darmstadt, Germany
Sodium hypochlorite (NaOCl)	Clorogene Supplies, Petone, New Zealand
Trichloroacetic acid	Merck, Darmstadt, Germany
Xanthine	Sigma Chemical Co., MO, USA
Xanthine Oxidase	Sigma Chemical Co., MO, USA

## 2.2 Preparation of General Solutions and Buffers

### **7,8-Dihydroneopterin solution**

7,8-Dihydroneopterin was prepared fresh prior to each experiment and shielded from light. Generally, a 2mM stock solution was prepared by sonicating 7,8-dihydroneopterin in ice cold RPMI 1640 (for cell culture experiments) or in phosphate buffer. If prepared for cell culture the stock solution was filter-sterilised via a 0.22 um filter membrane (Satorius AG, Goettingen, Germany).

### **HPLC Mobile Phase**

Ammonium phosphate buffer was prepared by dissolving 5.28g of ammonium phosphate in 1900 mL of nanopure water and adjusting the pH to 2.5 with 10 M phosphoric acid. The volume was then adjusted to 2000 mL using nanopure water. The solution was passed through a 0.45um filter and sonicated to degas. The final concentration of the stock solution was 20 mM which was mixed online to achieve the desired concentration.

### **NBT solution**

4-Nitro blue tetrazolium chloride (NBT) was prepared by dissolving 0.1832 g of NBT powder in 100 ml 50 mM Phosphate Buffer (described below).

### **Oil Red O stock solutions**

Oil red O powder (300 mg) was dissolved in 100 mL of isopropanol. A working solution was prepared by diluting at 6 parts of Oil Red O stock solution to 4 parts nanopure water. The working solution was left to stand for 10 minutes and then filtered through a 0.45um Whitman filter prior to immediate use.

A 1 M concentrated citrate solution was prepared by dissolving 1.92 g of citric acid in 10mL of deionized water. This was then further diluted at a 1:4 ratio in deionized water and stored at 4 degrees Celsius.

### **Phosphate Buffer for NBT and Xanthine Oxidase Assays**

A 216 mM potassium phosphate buffer of pH 7.8 was made by dissolving 4.93 g of potassium phosphate dibasic into 90mL of water. The pH was adjusted to 7.8 and the volume topped up to 100 mL.

## 2.3 Methods

All cell work was conducted under sterile conditions in a Class II Laminar Flow Hood.

### **Blood Collection**

Blood was collected from haemochromatosis patients at NZ Blood, Christchurch under ethics approval CTY/98/07/069 granted by the Upper South (B) Regional Ethics Committee. Blood for monocyte or macrophage preparation was obtained in bags with the anticoagulant citrate-phosphate-dextrose-adenine (CPDA-1). Blood for serum preparation was obtained in anticoagulant-free dry bags.

### **Preparation of Human Serum**

Blood in dry bags was allowed to clot overnight in the fridge. The serum was then collected from the bags using a cannula and syringe into 50 mL centrifuge tubes. The tubes were spun for 15 minutes at 500g and the supernatant was extracted. The serum was stored at -80C.

### **Isolation of Monocytes and PBMCs**

Blood from an autologous bag containing an anticoagulant (CPDA-1) was centrifuged in 50 mL tubes for 30 minutes at 1000 g, slow acceleration, slow deceleration, room temperature. The resulting buffy coat, a white layer of immune cells that sits between the plasma and the red blood cells, was transferred to new tubes (maximum 15 mL per tube). The buffy coat was diluted with PBS (35 mL), and lymphoprep (15 mL) was underlaid. The tubes were centrifuged for 30 minutes as described above. A thick band forms about the middle of the tube which is the PBMC layer. This was carefully collected, avoiding the red blood cells, and placed in new tubes. The tubes were topped up with PBS (35 mL) and spun for 15 minutes, 500 g, fast deceleration. The resulting cell pellet was washed a total of 3 times using PBS. After washing, cells were resuspended in warm RPMI-1640 (serum-free) for counting. Cells were diluted to  $5 \times 10^6$  cells/mL. In the case of PBMCs, the medium was adjusted to contain 10% human serum and the cells were immediately plated into 24-well plates. For monocytes and macrophages, the cells remained in serum-free medium and were transferred to 6 well suspension plates for culture in a 5% CO<sup>2</sup> incubator for 40 hours. After 40 hours, the monocyte cells were carefully collected, without disturbing the platelets and T cells that had adhered to the bottom of the plate. The cells were pelleted by centrifuge as described above and resuspended at  $5 \times 10^6$  cells/mL in RPMI 1640 with 10% human serum. The monocytes were then plated into 24-well

plates. Monocytes that were being differentiated into HMDM cells were supplemented with 2  $\mu\text{L}/\text{mL}$  of GM-CSF at the time of plating.

### **Cell culture**

All cells were cultured in RPMI-1640 with 10% human serum and antibiotics (pen/strep). The media were changed every 3 days. Monocyte and PBMC cells were used within one week of plating. HMDM cells were cultured for 2-3 weeks to develop a “lawn” of mature macrophages.

### **BCA protein assay**

The BCA assay (Smith et al., 1985) monitors a two-step reaction of protein with copper ions to form a purple complex which is monitored at 562 nm. This assay was carried out following the manufacturer’s instructions. Briefly, standards were prepared by diluting 2 mg/mL BSA into a range of concentrations (5-250  $\mu\text{g}/\text{mL}$ ). Protein from cell samples was diluted 1/5 to ensure measurements were within the linear range. It is important to note that whilst the assay should be used in the linear range, the standards form a curve not a straight line. This should be calculated using a quadratic equation to avoid error. The working reagent was prepared at 50 parts Reagent A to 1 part Reagent B. Sample (50  $\mu\text{L}$ ) and the working reagent (1 mL) were added together to a test tube and mixed well. This solution was heated at 60C for 30 minutes. The tubes were cooled in ice to stop the reaction and then read at 562 nm.

### **Plaque culture**

Freshly excised carotid plaque tissue was obtained from consenting patients undergoing endarterectomy at Christchurch Hospital (ethics approval CTY/01/04/036 granted by the New Zealand Upper South B Ethics Committee). Plaques were transported to the laboratory on ice. Sections were cut approximately 3 mm thick and weighed (example in Figure 2.1). These were cultured in individual centre-well organ culture dishes (BD Falcon, NJ, USA) in 2 mL of RPMI-1640 containing penicillin (100 U/mL) and streptomycin (100 g/mL), supplemented with 10% human serum. Human serum was prepared from whole blood and stored at  $-80^{\circ}\text{C}$  until required. Sectioned plaques were incubated for 24 h prior to any experimental treatment. The media were changed every 24 h and the media was collected for lactate measurement and HPLC analysis of neopterin and total neopterin.

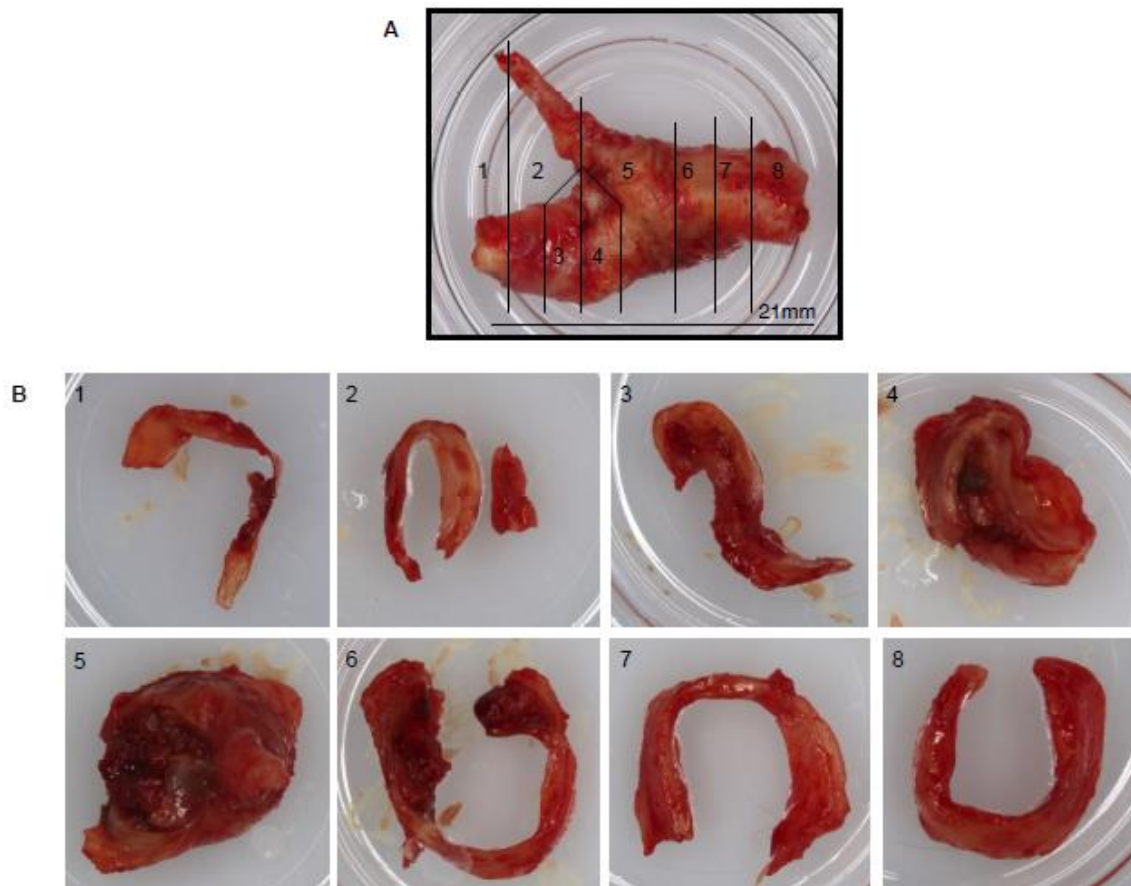


**Figure 2.1 Example of a plaque cut into sections and placed in individual culture dishes.**

Plaque sections were in general cut to be 2-3 mm in width, however, heavy calcification such as in section 5 at times prevented even cutting.

### **Lactate assay**

Media lactate concentrations were determined using an enzymatic based absorbance assay in the form of a commercial kit (Lactate Assay Kit from Roche Diagnostics NZ Ltd, Auckland, NZ) and the assay was performed following the manufacturer's specifications.

### **HPLC assay**

Neopterin, 7,8-dihydroneopterin and total neopterin concentrations were determined by isocratic HPLC using Phenomenex™ SCX column on a Shimadzu 20A HPLC (Flavall, Crone, Moore, & Gieseg, 2008). For direct measurement of 7,8-dihydroneopterin, ultraviolet and visible light were measured using a Photodiode Array (PDA) detector. For neopterin and total neopterin, a fluorescence detector was used. In supernatant or plasma samples, media proteins were removed by acetonitrile precipitation (Flavall et al., 2008). 7,8-dihydroneopterin is

difficult to detect in biological samples in its native form so it was first oxidized to neopterin using acidic iodide, and then measured as total neopterin. The concentration of ammonium phosphate was modified depending on sample type (plasma vs media) to achieve clean separation of peaks on the chromatograms. For media samples, separation of peaks was achieved at 10 mM ammonium phosphate, whereas 1 mM ammonium phosphate was acceptable for plasma samples. Lowering the ammonium phosphate concentration increased peak heights but this occurred in the same manner in both the samples and external controls.

In the case of the the xanthine oxidase assay, the solution was transferred directly to HPLC vials, and the rack temperature was increased to 25 degrees Celsius from the standard 4 degrees to allow the reaction to be carried out directly in the HPLC. Samples were prepared just prior to the relevant injection time to ensure timepoints were as accurate as possible. The samples were run in the absence of ACN. The 7,8-dihydroneopterin concentration was measured directly using absorbance detection at 254nm. The small contamination of neopterin (~3%) in the samples from the outset was controlled for by taking a sample at time 0 to use to measure the change in 7,8-dihydroneopterin and neopterin. In addition, an enzyme free sample was also measured to monitor the lability of 7,8-dihydroneopterin at 25 degrees Celsius.

### **Oil Red O staining**

This method is based on the method described by Culling, Allison, and Barr (2014). Briefly, tissue sections were placed in 60% isopropanol for 10 minutes before blotting. Sections were then stained with fresh filtered Oil Red O for 10 minutes. The tissue was blotted again, and then washed with 60 % isopropanol for 2 minutes. Finally, sections were rinsed with water, blotted dry and then photographed.

### **Xanthine Oxidase Superoxide Generation**

This is based on the method by Fridovich (1970). A 1.08 mM (increased from 0.108 mM in most methods) xanthine solution was prepared by dissolving xanthine in a small amount of concentrated KOH. Once the xanthine dissolved this was topped with deionized water to 90 mL and the pH was adjusted to 7.8. The volume was then finally adjusted to 100 mL.

A reaction buffer was created by mixing 23 mL of H<sub>2</sub>O with 25 mL of phosphate buffer. To this 1mL of 4 mg/mL EDTA solution was added and 50 mL of the xanthine solution described above. If cytochrome c was being used 1 mL of a 14.6 mg/mL (1.1 mM) cytochrome c solution was added at this time, otherwise this was replaced with 1 mL of water.

The reaction was carried out in test tubes initially using a total reaction volume of 3 mL. This was made up of 100 uL of diluted xanthine oxidase enzyme solution, 100 uL of diluted SOD enzyme solution, 100 uL of 7,8-dihydroneopterin solution (made up at a 30x final concentration stock solution in phosphate buffer) and was topped up to 3 mL using the reaction buffer. The xanthine oxidase enzyme solution was always added last to begin the reaction.

If the reaction was being carried out in the HPLC, the test tubes would be quickly mixed, and 1.8 mL of the reaction solution transferred to an HPLC vial, just prior to the needle injection.

### **Cytochrome c Assay for Measuring Superoxide generation**

This is based on the method by McCord and Fridovich (1968). The cytochrome c assay to measure superoxide generation could only be carried out in the absence of 7,8-dihydroneopterin as this reacts directly with cytochrome c. The reaction buffer was prepared as detailed above for the xanthine oxidase assay. Xanthine oxidase was added last to begin the reaction. The reaction was monitored using continuous spectroscopic detection at 550 nm. To assess the amount of superoxide generated, the slope of the reaction was calculated, and an extinction coefficient of  $21.1 \times 10^3 \text{ M/cm}$  was used to calculate the change in cytochrome c.

### **NBT Assay for Measuring Superoxide Generation**

The superoxide radicals were estimated by the spectrophotometric measurement at 560 nm of the reaction product of NBT (Beauchamp & Fridovich, 1971). The reaction mixture contained 50 mM potassium phosphate buffer (pH 7.8), 0.5 mM xanthine, 5 mU xanthine oxidase, 100  $\mu\text{M}$  NBT, and various concentrations of 7,8-dihydroneopterin.

### **Preparation of LDL**

Plasma was obtained from healthy donors under ethics approval CTY/98/07/069 granted by the Upper South (B) Regional Ethics Committee. LDL was isolated from donor plasma using a centrifugation gradient separation method as described by S. P. Giese and Esterbauer (1994). Briefly, human plasma was thawed and centrifuged at 4,700 rpm for 10 minutes at 4°C. After placing in a beaker on ice, the plasma density was adjusted to 1.24 g/mL by the gradual addition of 11.4 g of solid potassium bromide (KBr). Next, 8 mL of 1 mg/mL EDTA (pH 7.4) was added to each ultracentrifugation tubes (OptiSeal™, Beckman Coulter, USA). The density adjusted plasma (3.8 mL per tube) was then underlain. A Beckman Near Vertical (NVTi-65) rotor was used to centrifuge the tubes at 60,000 rpm for 2 hours at 10°C using slow acceleration/deceleration in Optima™ L-90K Preparative Ultracentrifuge (Beckman Coulter

Inc., Fullerton, California). Isolated LDL was washed with phosphate buffered saline (PBS) using an Amicon Ultra-15 membrane filter centrifugation tubes (Millipore, USA) at 3000 g, 4°C for 30 minutes, and repeated twice. LDL concentration was adjusted to 10 mg (LDL total mass) per mL, which was determined using a total cholesterol assay kit (Roche Diagnostics, Germany), assuming the total cholesterol accounts for 31.69% of the LDL particle (MW 2500kDa).

### **Oxidation of LDL**

Oxidation of LDL was performed using the method modified from Gerry, Satchell, and Leake (2008). This is the standard method for producing oxLDL in this laboratory. Briefly, Concentrated LDL at 10 mg/mL (total mass) was mixed with 0.5 mM copper chloride and placed into a dialysis tube.

The LDL-containing dialysis tubing was suspended using a microtube at one end and a weighted clip at the other in a large glass bottle. The bottle contained 1 L of PBS per 10 mg of LDL protein and copper chloride at a final concentration of 0.5 mM. The LDL was dialysed for 24 hours at 37°C in an orbital shaker (Bioline, Edwards Instrument Company, Australia). Upon complete oxidation the solution became colourless. The oxLDL was then washed twice at 4°C for two hours and finally overnight in 1 L of PBS, containing a quarter teaspoon of washed Chelex-100 to remove excess copper ions. OxLDL was filter-sterilised through a 0.22 µm syringe filter and stored at 4°C prior to use.

### **MARS Spectral CT**

The MARS spectral scanner (V6.0 MARS Bioimaging Ltd, Christchurch, New Zealand) was used to image phantoms, cell samples and carotid specimens (**Figure 2.2**). Spectral CT operates in the same manner as traditional CT except that the detector measures the energy of the incoming photon, rather than just recording that a photon arrived. The energy of the photon provides information about the material that the photon travelled through before arriving at the detector. The data obtained from the scanner includes a reconstruction of the object with an image from each energy bin for each slice, and a material decomposition which uses the energy information to assign each voxel to a material. These material maps are then available as separate layers which can be viewed together or separately in 2D or 3D using the MARS vision software.



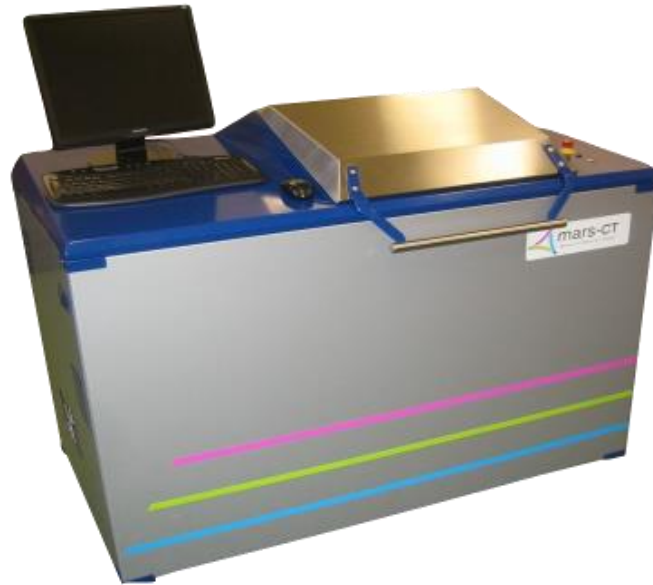


**Figure 2.2 The MARS small bore spectral scanner for small animal imaging**

### **Preparation of phantoms**

A phantom is a calibration tool designed to mimic the intended sample. All phantoms used in the MARS spectral contain at a minimum samples of lipid (canola oil) and water, as these are integral to the material decomposition algorithm. A number of phantoms were used for these studies depending on the purpose of the experiment. For plaque scans, the phantom contained, in addition to lipid and water, hydroxyapatite at 0, 100, 200 and 400 mg/mL. For cell work the phantoms contained iodine (9, 18 mg/mL) and gold (4, 8 mg/mL). Identifying intraplaque hemorrhage used hydroxyapatite (0, 50, 100 mg/mL) and ferric nitrate (50, 100, 200 mg/mL).

### **Preparation and scanning of samples**

For scanning samples containing iodine and gold, MARS scanning was carried out using the “Factory A1 Protocol” with 2 mm aluminium filtration. The samples were scanned using a tube voltage of 118 kVp, a tube current of 13  $\mu$ A, and an exposure time of 300 ms per position. Four energy bins were used, these in the range 18 – 29.9 keV, 29.9 – 44.9 keV, 44.9-77.9 keV, and 77.9 keV <. This energy range expresses the k-edge of iodine at approximately 33.2 keV and captures the increase in attenuation of gold in the higher energy band, as gold has a k-edge at approximately 80.7 keV. Plaques scanned for lipid, soft tissue and calcium were imaged using 2mm Aluminium filtration with energy bands beginning at 18, 30, 40, 50 and 60 keV, tube voltage 118 kVp, tube current 13  $\mu$ A and exposure time of 200ms per position. When

attempting to identify intraplaque haemorrhage, thresholds were set a 20, 28, 36 and 44keV with a tube voltage of 80kVp, a tube current of 55  $\mu$ A and 100ms exposure time per position.

### **Image Analysis**

Image analysis was carried using a combination of ImageJ and MARS Vision (Mars Bioimaging Ltd, Christchurch, New Zealand).

### **Statistical Analysis**

Prism 8.0 (GraphPad Software, CA, USA) was used to analyse the data. All statistical analysis was carried out using Prism software (GraphPad Software Inc, USA). A repeated measures one-way analysis of variance (ANOVA) was performed on all plaque data, using each section as a replicate. A repeated measures one-way ANOVA was performed on cell culture data. Plaque results are from individual plaques unless stated otherwise and each plaque is from a separate patient. Cell culture results are mean  $\pm$  SEM of three independent experiments. Significance is indicated as \*,  $p < 0.05$ ; \*\*,  $p < 0.01$ ; \*\*\*,  $p < 0.001$ .

### 3 Macrophage activation in live excised atherosclerotic plaque

In this chapter, I carried out two of the plaque experiments, one was conducted by Ed Marks, and another by Sean Cross. I carried out all cell culture experiments, and the plaque scanning (with some guidance from Joe Healy and Aamir Raja). I prepared the associated manuscript.

The results from this chapter have been disseminated as a paper entitled “Induced macrophage activation in live excised atherosclerotic plaque”.

#### 3.1 Introduction

To date, most research into the role of neopterin in inflammatory conditions has made use of isolated cultures of macrophages or peripheral blood mononuclear cells (PBMC), however, this approach does not allow for the investigation of the more complex interactions between array of cell types (smooth muscle cells, macrophages, monocytes, T cells) and cytokines within the plaque tissue (Hsu, Lim, Tintut, & Demer, 2016; Wolf, Zirlik, & Ley, 2015). In this chapter, this disadvantage of mono layer cultures is overcome by activating resident macrophages in live carotid plaque tissue samples from carotid endarterectomy patients.

Three different known macrophage stimulants were used to activate plaque in this chapter, interferon- $\gamma$ , PMA and PHA and compared activation within the plaque tissue with traditional monolayer cultures in the presence and absence of T cells. Interferon- $\gamma$  directly induces the production of 7,8-dihydroneopterin in macrophages via the enzyme GTP cyclohydrolase I (GTPCH-I), while PMA and PHA are known to activate T cells, which produce interferon- $\gamma$  in response (CF, 1986; Gostner et al., 2015; C. Huber et al., 1984; A. Lindsay et al., 2015). PMA and PHA are capable of indirectly increasing 7,8-dihydroneopterin. As 7,8-dihydroneopterin and its oxidation product neopterin are of low molecular weight, they easily diffuse out of the plaque into the blood stream or tissue culture media and can be measured as serum markers of macrophage activity and oxidation (S. P. Giese et al., 2008).

Typically, in clinical settings only serum neopterin levels are analysed. In this study, both neopterin and 7,8-dihydroneopterin are measured. Neopterin can be measured directly and 7,8-dihydroneopterin indirectly by oxidizing to neopterin. In a sample that has undergone this laboratory oxidation, the measured value is referred to as ‘total neopterin’ as the value given contains both the laboratory oxidized 7,8-dihydroneopterin and any biologically produced neopterin (A. Lindsay, Janmale, Draper, & Giese, 2014; A. Lindsay, Othman, Prebble, Davies, & Giese, 2016). The concentration of 7,8-dihydroneopterin alone can be inferred by

subtracting the known neopterin value which was measured in the non-oxidized sample. The advantage to analysing both total neopterin and neopterin is that the amount of oxidation (as neopterin) and the level of macrophage activation (as total neopterin) occurring in the tissue is measured.

### 3.2 Methods in brief

This chapter examines the inflammatory and oxidative state of plaques from the carotid arteries of four individual patients. The plaques were prepared and cultured as described in Chapter 2.

Neopterin levels in the media were determined by isocratic HPLC using Phenomenex™ SCX column on a Shimadzu 20A HPLC with fluorescence detection of the eluting neopterin as previously described. Media proteins were removed by acetonitrile precipitation. Due to the non-fluorescent nature of 7,8-dihydroneopterin, this was first oxidized to neopterin using acidic iodide, and then measured as total neopterin.

Media lactate concentrations were determined using a lactate assay as described in Chapter 2.

Primary cultures of human PBMC (a mixture of lymphocytes and monocytes) and HMDM cells were isolated from fresh whole blood donated under ethics approval CTY/98/07/069 and cultured as described in Chapter 2.

Fourteen plaque sections from two plaques were scanned using a MARS spectral scanner (MARS Bioimaging Ltd, New Zealand) using a 2mm Aluminium filter at 30, 40, 50 and 60 keV and material decomposition carried out using MARS Vision software (Butler et al.; Zainon et al.) Image J was used for additional image analysis.

All statistical analysis was carried out using Prism software (GraphPad Software Inc, USA). A repeated measures one-way analysis of variance (ANOVA) was performed on all plaque data, using each section as a replicate. A repeated measures one-way ANOVA was performed on cell culture data. Plaque results are from individual plaques unless stated otherwise and each plaque is from a separate patient. Cell culture results are mean  $\pm$  SEM of three independent experiments. Significance is indicated as \*,  $p < 0.05$ ; \*\*,  $p < 0.01$ ; \*\*\*,  $p < 0.001$ .

### 3.3 Results

#### 3.3.1 7,8-Dihydroneopterin and neopterin formation in unstimulated plaque

Unstimulated plaque in tissue culture is viable and produces both 7,8-dihydroneopterin (measured as total neopterin) and neopterin. The plaque was obtained from a 49-year-old male ex-smoker who presented with a stroke, retinal ischaemia, and familial hypercholesterolaemia and cut into sections before being cultured. The mean total neopterin produced by the plaque between 48 and 72 h was  $0.34 \pm 0.08$  nmol/g and the mean neopterin was  $0.23 \pm 0.05$  nmol/g. The incubation of unstimulated plaque for 72 h resulted in a significant decrease ( $-0.27$  nmol/g,  $p = 0.027$ ) in total neopterin at 48 h, but then no further change (Figure 3.1a). Mean neopterin did not significantly decrease ( $-0.05$  nmol/g,  $p = 0.012$ ) until 72 hours (b). Neither mean neopterin nor total neopterin increased at any point, which is consistent with the plaque being unstimulated.

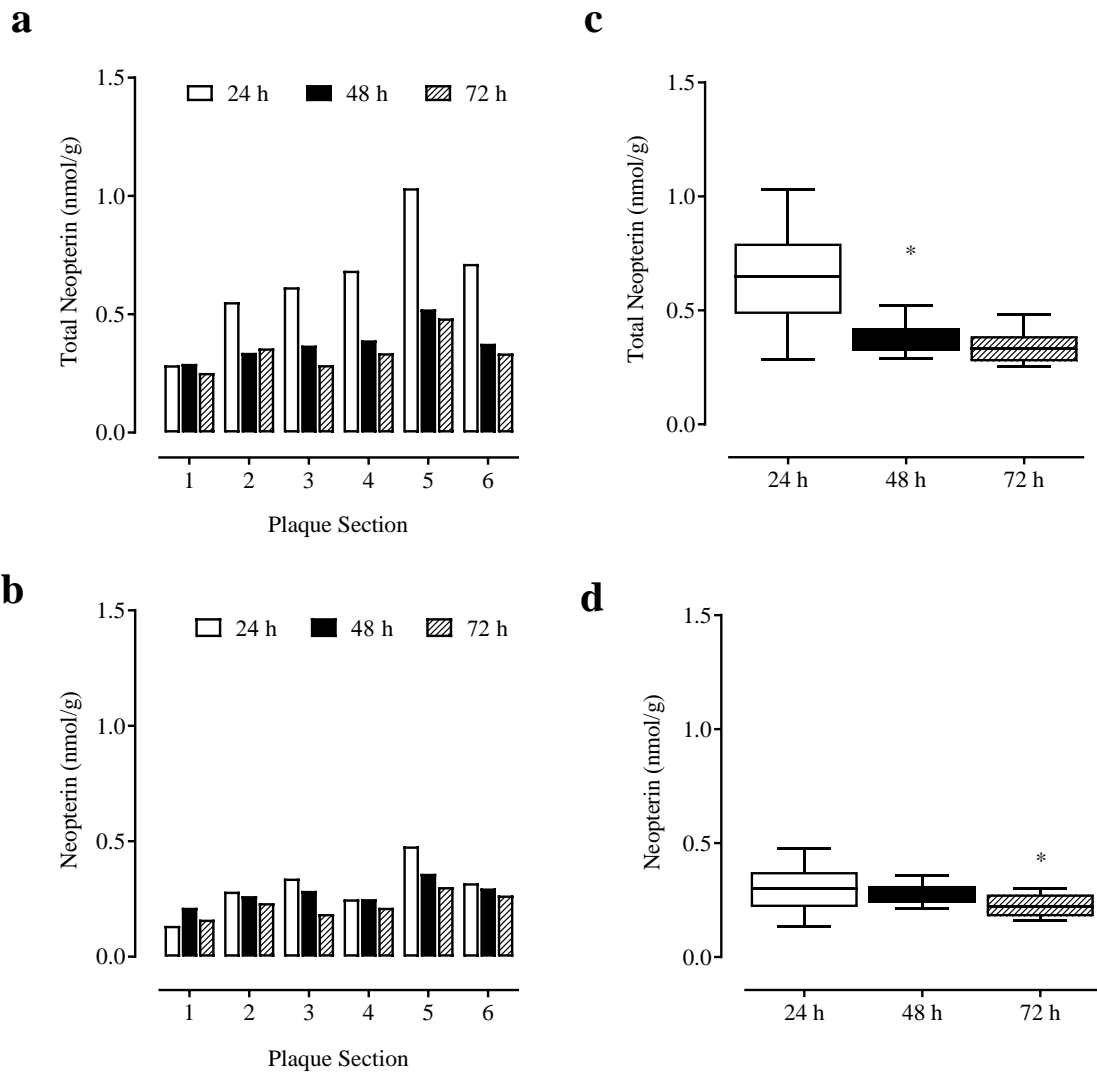


**Figure 3.1 Production of total neopterin and neopterin in media from an unstimulated plaque.** The plaque was retrieved from a 49-year-old male ex-smoker who presented with a stroke, retinal ischaemia, and familial hypercholesterolaemia. Ultrasound of the artery determined 60–69% stenosis. The plaque was incubated in RPMI-1640, supplemented with 10% human serum for a total of 72 h (N=1). (a) shows the total neopterin produced, as measured by HPLC at each media change. (b) shows the neopterin for the same time periods. Plaque total neopterin and neopterin concentrations for each section are given in nmol/g of plaque. (c) and (d) compare the mean and range of plaque total neopterin and neopterin at each time point. A repeated measures one-way ANOVA was conducted. Significance is indicated as compared to the previous 24 h period: \*\*\* indicates  $p < 0.05$ .

### 3.3.2 Direct activation of plaque macrophages by interferon- $\gamma$ in cultured plaque

Interferon- $\gamma$ , generated *in vitro* by T helper-1-type (Th-1) cells, is a key stimulator of the macrophage inflammatory response (C. Huber et al., 1984). A single addition of interferon- $\gamma$  (500 U/mL) to a plaque obtained from an 82-year-old male non-smoker who presented with a transient ischaemic attack and right upper limb weakness caused a sustained rise in total neopterin and neopterin (Figure 3.2 a and b, also Figure 3.3). The initial levels of total neopterin before the addition of the interferon- $\gamma$  ranged from 0.48 nmol/g to 4.28 nmol/g, suggesting this patient had higher levels of baseline inflammation in their plaque tissue, compared to the plaque analysed in , which ranged from 0.28 nmol/g to 1.03 nmol/g. The neopterin was less than 0.44 nmol/g for all 8 sections prior to interferon- $\gamma$  addition. For all sections, there was a significant rise in both the mean total neopterin following interferon- $\gamma$  addition, which increased by 4.89 nmol/g ( $p = 0.003$ ) and neopterin (2.82 nmol/g  $p = 0.037$ ) over the 72 h. The magnitude of rise was different for each section, with some sections responding slowly to the interferon- $\gamma$  stimulation (, sections 5–7). This demonstrates that along the length of the plaque there are marked differences in inflammatory activity as well as differing levels of oxidative stress. The high levels of lactate released from the plaques confirmed that the plaques remained metabolically active during the entire incubation. The lactate levels ranged from 121.7  $\mu\text{mol/g/24 h}$  to 318.4  $\mu\text{mol/g/24 h}$ .

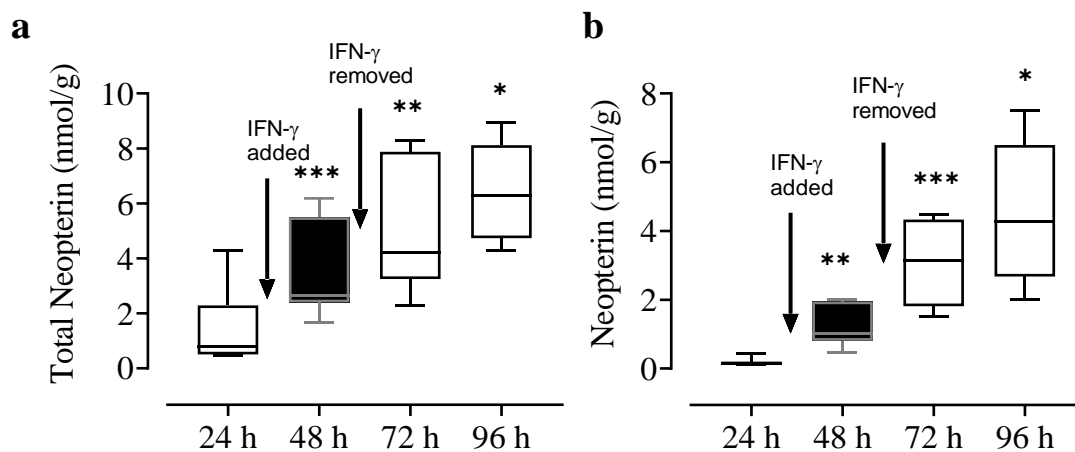


**Figure 3.2 Media total neopterin and neopterin from plaque stimulated with 500 U/mL of interferon- $\gamma$ .** Interferon- $\gamma$  stimulation of the plaque or cells occurred in a single dose after an initial 24 h of media with 10% human serum. Subsequent media changes at 48 h and 72 h contained RPMI-1640 with 10% human serum only. (a) and (b) show the total neopterin and neopterin measured in the interferon- $\gamma$  treated plaque (N=1) obtained from an 82-year-old male non-smoker who presented with a transient ischaemic attack and right upper limb weakness; 80–95% stenosis of the artery was determined by ultrasound. The plaque tissue exhibited moderate levels of calcification. Repeated measures one-way ANOVA was carried out. Significance is indicated as compared to the previous 24 h period: \*\* indicates  $p < 0.01$ ; \*\*\*,  $p < 0.001$ .



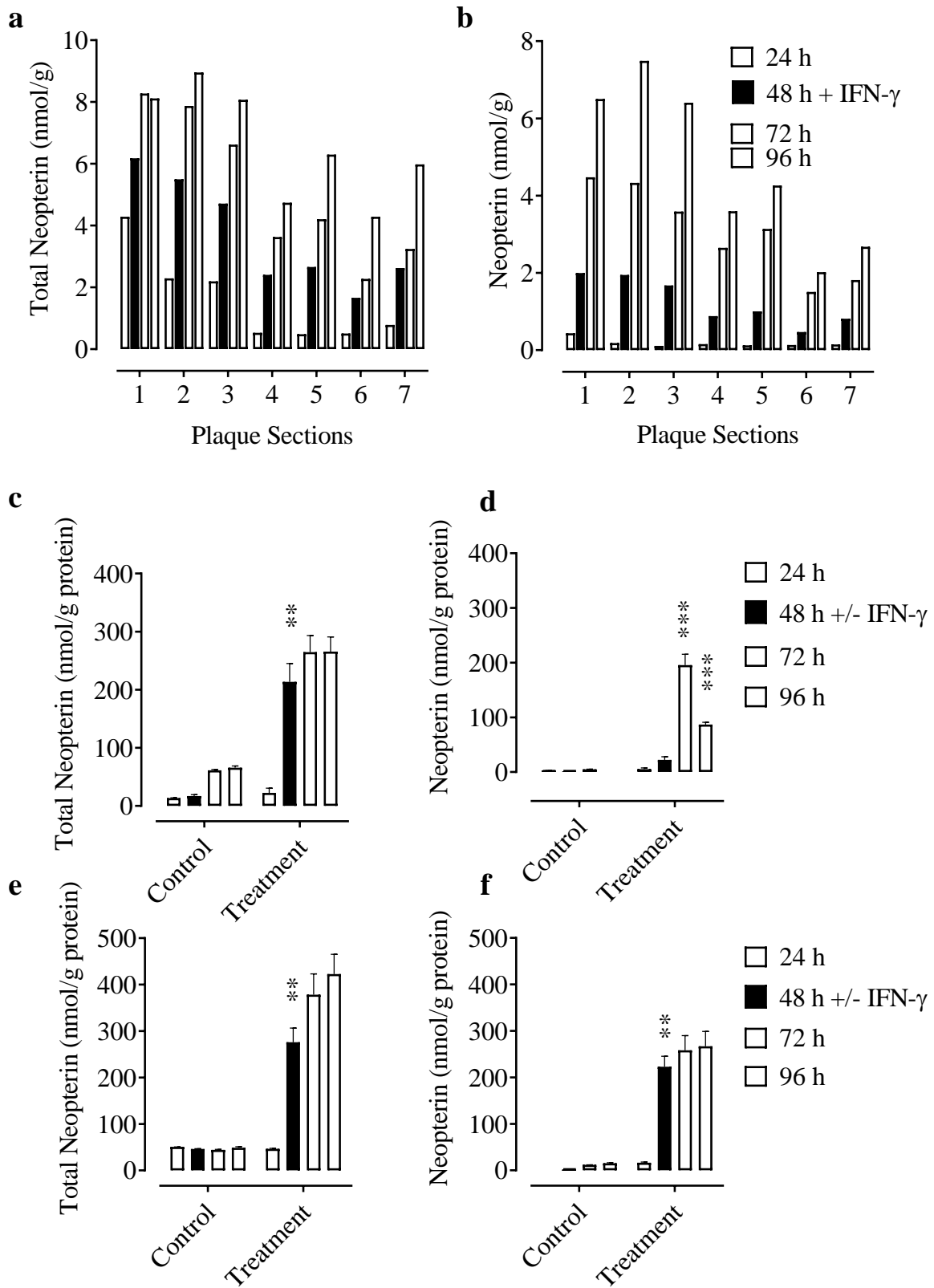


**Figure 3.3** Production of total neopterin and neopterin in media from plaque, macrophages, and PBMC culture stimulated with 500 U/mL of interferon- $\gamma$ .

Interferon- $\gamma$  stimulation of the plaque or cells occurred in a single dose after 24 h. Subsequent media changes contained RPMI-1640 with 10% human serum only. (a) and (b) show the total neopterin and neopterin measured in the interferon- $\gamma$  treated plaque (N=1) obtained from an 82-year-old male non-smoker who presented with a transient ischaemic attack and right upper limb weakness; 80–95% stenosis of the artery was determined by ultrasound. The plaque tissue exhibited moderate levels of calcification. Unrelated human HMDM and PBMCs were analysed. Total neopterin and neopterin were also measured in a HMDM culture (c) and (d), and in a PBMC culture (e) and (f) (N=3). Error bars represent SEM. Repeated measures one-way ANOVAs were carried out on each dataset. Significance is indicated as compared to the previous 24 h period: \*\* indicates  $p < 0.01$ ; \*\*\*,  $p < 0.001$ .

### 3.3.3 Direct activation of macrophages by interferon- $\gamma$ in cell culture

To better understand the dynamic behaviour of neopterin-releasing cells within the plaque, we examined cultured HMDM and PBMC prepared from donated blood supplied by the blood bank. The interferon- $\gamma$  activation of the HMDM cells produced a significant 29-fold increase in total neopterin ( $p = 0.004$ ) after 24 h (Figure 3.3c). The level remained around 200 nmol/g cell protein for the whole 72 h period. However, there was no significant neopterin formation until 48 h after adding interferon- $\gamma$  (Figure 3.3d). The level of neopterin then decreased in the following 24 h, indicating a decrease in oxidant production. Interferon- $\gamma$  stimulation of the PBMC caused a total neopterin rise that was larger than that seen with HMDM (Figure 3.3e). In contrast, the neopterin rose immediately and stayed elevated for the whole 72 h of incubation which was like that seen in the plaque stimulated with interferon- $\gamma$ .

### 3.3.4 Indirect stimulation of macrophages in cultured plaque with PMA

Both PHA and PMA stimulation of T cells has been shown to cause the release of interferon- $\gamma$  which is capable of inducing macrophages to produce 7,8-dihydroneopterin (C. Huber et al., 1984). A plaque obtained from a 65-year-old male non-smoker who was suffering from dysphasia and amaurosis fugax was sectioned (shown in Figure 2.1), and after a 24 h washout period was stimulated with PMA. In the first three sections (1–3) of the plaque there was a substantial rise in total neopterin within 24 h, and the level continued to rise in the following 24 h period (Figure 3.5a). Sections 4, 7, and 8 only showed a rise after the second dose of PMA. However, the overall mean change in total neopterin across the plaque was not significant due to the wide variation between sections ( $3.06 \pm 1.54$  nmol/g,  $p = 0.073$ ). The level of oxidation in the plaque measured by neopterin was low compared to the output of total neopterin (Figure 3.5b c.f. Figure 3.5 a). The rise in mean neopterin over 72 hours ( $4.78 \pm 1.99$  nmol/g) was significant ( $p = 0.037$ ).

### 3.3.5 Stimulation of macrophages and PBMCs in cell culture with PMA

With HMDM cells, total neopterin significantly increased with the addition of PMA after both 24 and 48 h of stimulation (Figure 3.5c). The PMA was given twice as it is likely to take longer than 24 hours to reach maximal activation if the process is being driven from a gene transcription level. The PMA was removed for the last 24 h incubation and replaced with interferon- $\gamma$  to test whether stimulation had been successful, which generated a small but significant increase. The same treatment with PBMC showed a similar trend of increasing total neopterin by the PMA, but twice the level seen with the interferon- $\gamma$ . The presence of the T cells appears to have greatly enhanced the generation of 7,8-dihydroneopterin from the monocytes.

The time course of 7,8-dihydroneopterin oxidation to neopterin with PMA-stimulated HMDM cells was very like that seen with interferon- $\gamma$ , with an initial delay of 24 h in the rise of neopterin levels (Figure 3.5d). With PBMC, the presence of the PMA has abolished the delay in the oxidation of 7,8-dihydroneopterin, starting strongly after 24 h, but with a small decrease in the following 24 h (Figure 3.5f). The replacement of the PMA with interferon- $\gamma$  in the HMDM cells showed a decrease in oxidation or neopterin formation of 34%, but with PBMC the decrease was not significant.

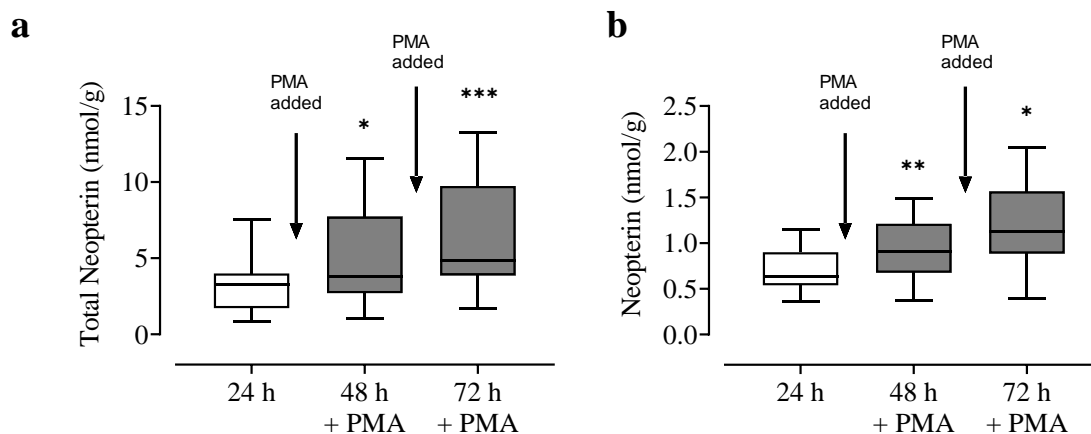


**Figure 3.4 Media total neopterin and neopterin from plaque stimulated with 5  $\mu$ M PMA.**

The plaque (a) and (b) and cells were treated with PMA for 2 d following an initial media-only day (N=1). The plaque was obtained from a 65-year-old male non-smoker who was suffering from dysphasia and amaurosis fugax. Stenosis of the artery was reported as 80–99%. In the HMDM (c) and (d) and PBMC (e) and (f) experiments (N=3), 500 U/mL of interferon- $\gamma$  was added on the final day. Error bars represent SEM. Significance is indicated as compare d to the previous 24 h period: \* indicates  $p < 0.05$ ; \*\*,  $p < 0.01$ ; \*\*\*,  $p < 0.001$ .

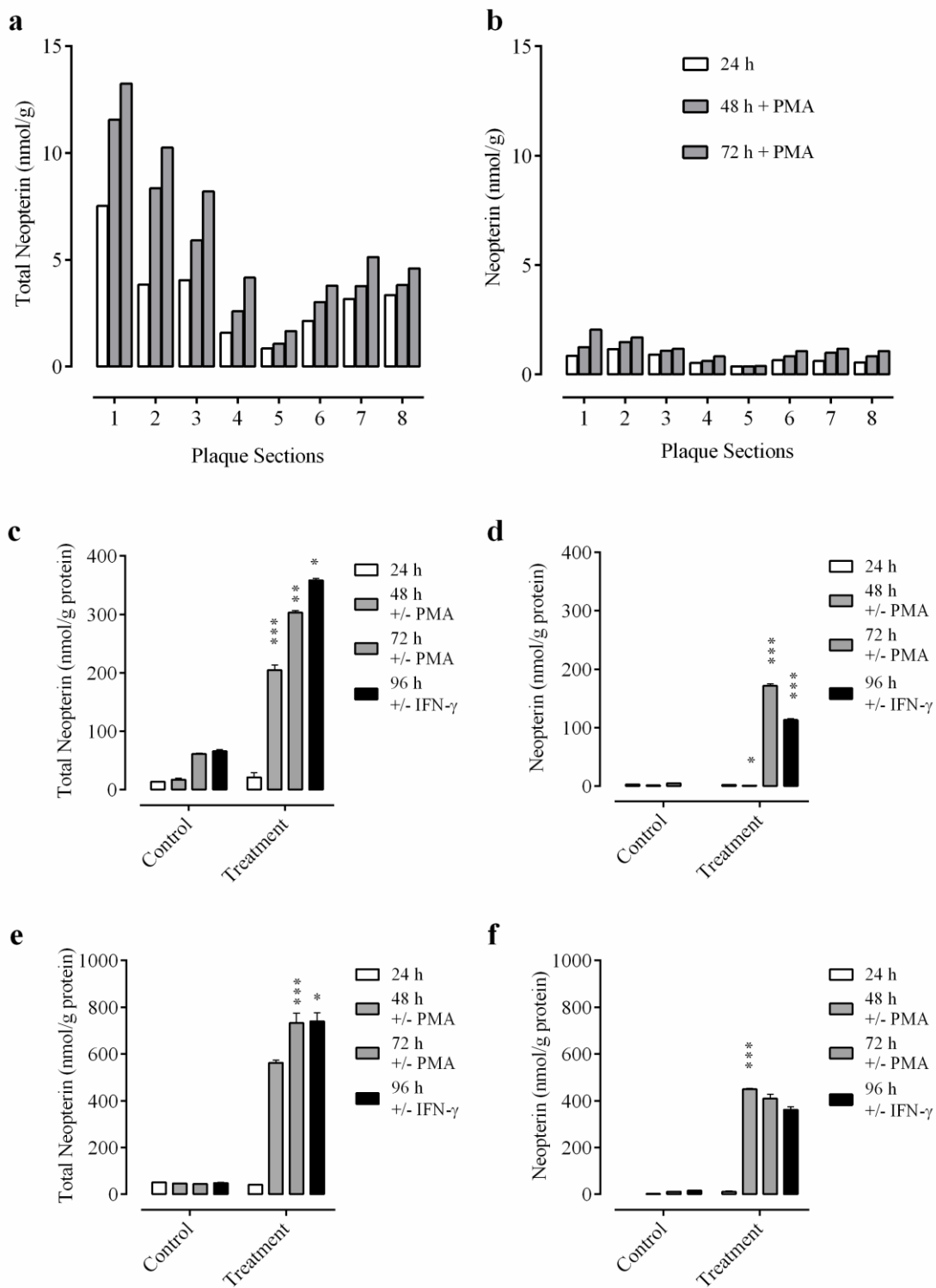


**Figure 3.5 Production of total neopterin and neopterin in media from plaque, macrophages, and PBMC culture stimulated with 5  $\mu$ M PMA.**

The plaque (a) and (b) and cells were treated with PMA for 2 d following an initial media-only day (N=1). The plaque was obtained from a 65-year-old male non-smoker who was suffering from dysphasia and amaurosis fugax. Stenosis of the artery was reported as 80–99%. In the HMDM (c) and (d) and PBMC (e) and (f) experiments (N=3), 500 U/mL of interferon- $\gamma$  was added on the final day. Error bars represent SEM.

Significance is indicated as compare d to the previous 24 h period: \* indicates  $p < 0.05$ ; \*\*,  $p < 0.01$ ; \*\*\*,  $p < 0.001$ .

### 3.3.6 Indirect stimulation of plaque with PHA

Addition of PHA to a plaque obtained from a 77-year-old male non-smoker who was suffering from dysarthria and TIAs caused an increase in both mean total neopterin (5.28 nmol/g,  $p < 0.0001$ ) and neopterin (2.95 nmol/g,  $p < 0.0001$ ) by 72 hours (Figure 3.7a and b). The addition of interferon- $\gamma$  for the final 24 hours resulted in a further rise in both mean total neopterin (1.3 nmol/g,  $p < 0.0001$ ) and neopterin (1.0 nmol/g,  $p < 0.0001$ ).

### 3.3.7 Indirect stimulation of macrophages and PBMCs in cell culture with PHA

In tissue culture, addition of PHA to HMDM cells produced a significant increase in mean total neopterin at 72 hours (162.8 nmol/g,  $p < 0.0001$ ) and a further rise with the introduction of interferon- $\gamma$  (92.85 nmol/g,  $p = 0.0021$ ), like that seen in the plaque (Figure 3.7c). Neopterin also rose significantly in the first 72 hours (130.1 nmol/g,  $p < 0.0001$ ), however, unlike the plaque, neopterin fell upon stimulation with interferon- $\gamma$  (-73.71 nmol/g,  $p < 0.0001$ ) (Figure 3.7d). In PBMCs both total neopterin and neopterin increased significantly by 72 hours (20.86 nmol/g,  $p < 0.0001$  and 11.73 nmol/g,  $p = 0.005$  respectively) (Figure 3.7e and f). Addition of interferon- $\gamma$  caused a significant rise in total neopterin (31.74 nmol/g,  $p < 0.0001$ ) but not in neopterin.

The increase in total neopterin in both PBMC and some sections of the plaque tissue is suggestive of an interaction between T cells and macrophages within atherosclerotic plaque.

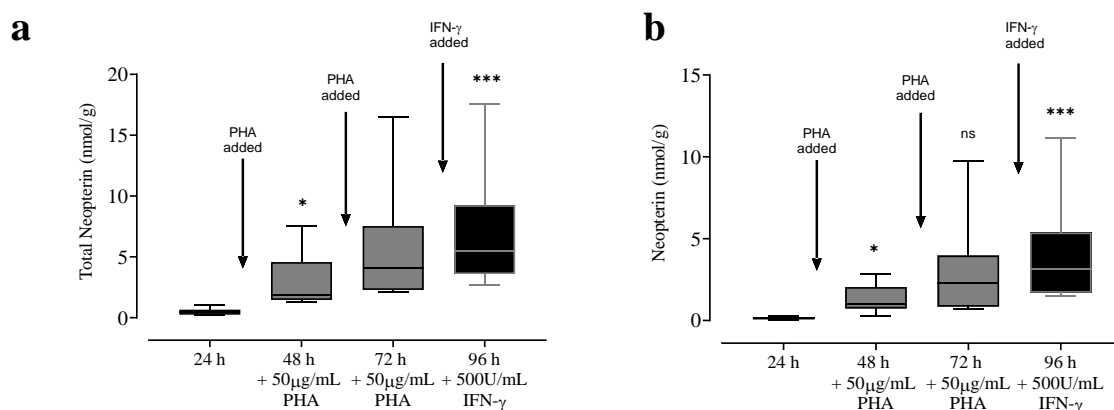


**Figure 3.6 Production of total neopterin and neopterin in media from plaque, macrophages, and PBMC culture stimulated with 50 ng/mL PHA.**

The plaque (a) and (b) was treated with PHA for 2 d following an initial media-only day, 500 U/mL of interferon- $\gamma$  was added on the final day (N=1). The plaque was obtained from a 77-year-old male non-smoker who was suffering from dysarthria and TIAs. Stenosis of the artery was reported as 80–95%. Significance is indicated as compared to the previous 24 h period: \* indicates  $p < 0.05$ ; \*\*,  $p < 0.01$ ; \*\*\*,  $p < 0.001$ .

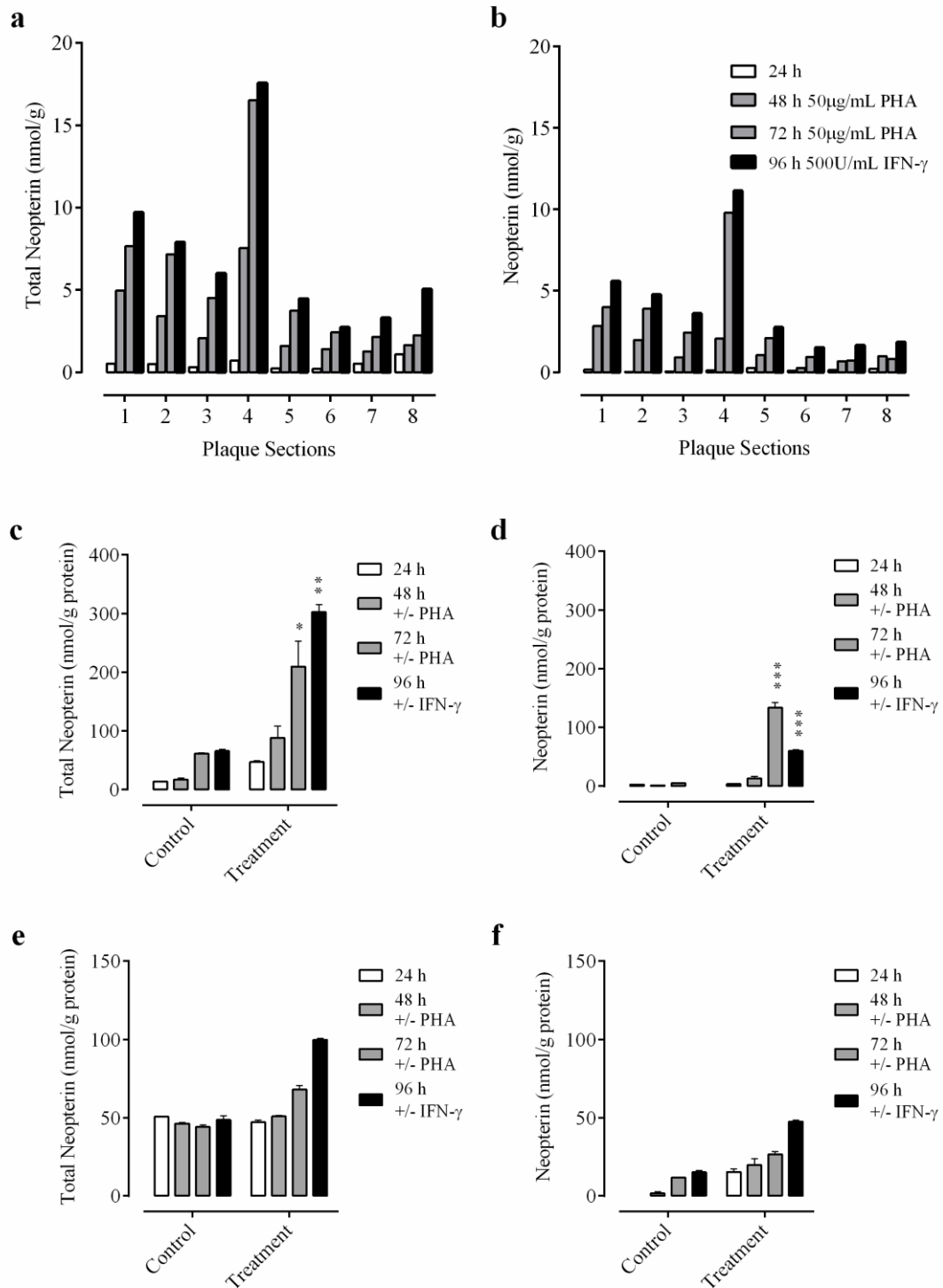


**Figure 3.7 Production of total neopterin and neopterin in media from plaque, macrophages, and PBMC culture stimulated with 50 ng/mL PHA.**

The plaque (a) and (b) was treated with PHA for 2 d following an initial media-only day, 500 U/mL of interferon- $\gamma$  was added on the final day (N=1). The plaque was obtained from a 77-year-old male non-smoker who was suffering from dysarthria and TIAs. Stenosis of the artery was reported as 80–95%. In the HMDM (c) and (d) and PBMC (e) and (f) experiments (N=3), cells were treated with PHA for 2 d following an initial

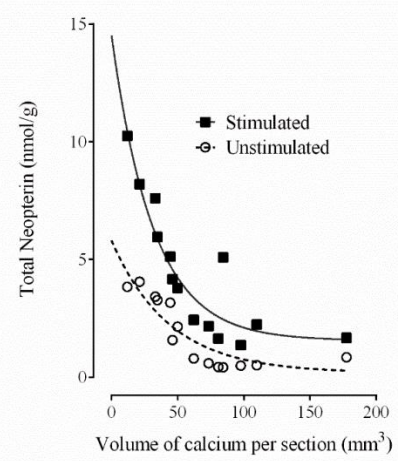
media-only day and 500 U/mL of interferon- $\gamma$  was added on the final day. Error bars represent SEM. Significance is indicated as compared to the previous 24 h period: \* indicates  $p < 0.05$ ; \*\*,  $p < 0.01$ ; \*\*\*,  $p < 0.001$ .

### 3.3.8 Plaque calcium quantification by spectral imaging

Examination of plaque tissue segments shows a variety of structural features (Figure 2.1). It was hypothesised that the measured output of total neopterin may vary from section to section due to the morphology of the tissue and the level of calcification. Because of the nature of the tissue after several days of culture it was not possible to use traditional histology. Instead, to quantify the level of calcification, sections were imaged, and calcium levels quantified by MARS imaging.

Calcium content was inversely related to post-PMA treatment total neopterin values ( $R^2 = 0.91$ ) (a). Plaque sections with vastly differing weights (e.g. 0.166 g vs 0.082 g) but with very similar volumes of calcium (46 mm<sup>3</sup> vs 49 mm<sup>3</sup>) were activated to the same extent (4.2 nmol/g and 3.8 nmol/g total neopterin). Figure 3.8 b to e are material decomposition images of section 5 from the plaque in photographed in Figure 2.1 (and analysed in a). These images taken at different planes through the plaque section, show many spotty calcium deposits and some lipid-rich areas. In comparison, section 7 from the same plaque, which had moderate levels of total neopterin production, is predominantly composed of lipid-rich tissue (f).

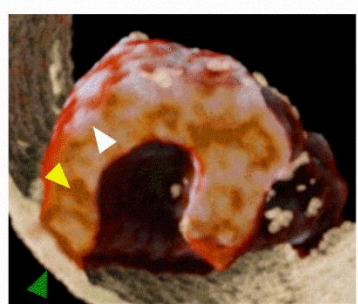
**a**



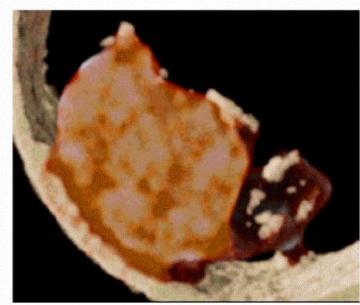
**b**



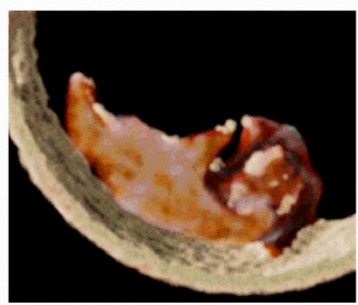
**c**



**d**



**e**



**f**



**g**



**Figure 3.8 MARS imaging of plaque tissue.**

Relationship between total neopterin production in plaque tissue and the volume of calcium present in each section using 14 sections from two PMA-treated plaques, prior to and after stimulation (N=2). R<sup>2</sup> for the non-linear line of best fit was 0.76 for unstimulated plaque and 0.91 for stimulated. (b) – (g) Three-dimensional reconstructions of MARS spectral CT slices using material decomposition for water, lipid, and calcium. Sections 5 (b) – (e) and 7 (f) – (g) of the PMA-treated plaque were selected for examining morphological differences. Tissue samples were retrieved after being cultured and imaged using the MARS spectral scanner. In this slice-through view, (b) – (e) are images from plaque section 5, which are progressing away from the viewer moving along the Z-axis. White arrowheads show examples of calcification; lipid is in yellow. A green arrowhead indicates the polypropylene sample tube, which gives a lipid-like reading. (f) A view of the whole of section 7. (g) A cut-through image midway through section 7.



### 3.4 Discussion

Here it has been shown that macrophages in live plaque tissues can be activated indirectly, possibly via de novo synthesis of interferon- $\gamma$  by Th-1 cells or directly through the addition of exogenous interferon- $\gamma$ . Comparisons to mono-layer tissue culture of either HMDMs or PBMCs demonstrate the effect of the complexity of plaque tissue on its biochemical profile. Live plaque tissue was more likely to respond immediately to stimuli than cells in culture, possibly due to differences in gene expression in the plaque tissue or the milieu of cells available.

Interferon- $\gamma$  stimulation of excised live plaque induced the activation of macrophages confirmed by a rise in total neopterin. This was accompanied by an increase in oxidant generation, which was measured as a rise in neopterin. As in previous work, the response of each section of plaque tissue is highly variable and not related to its location along the length of the plaque (T. Janmale et al., 2015). The macrophage activation was sustained even after the removal of interferon- $\gamma$  from the media. This phenomenon is consistent with other research that indicates interferon- $\gamma$  induces the expression of the enzyme GTPCH-I (Gesierich, Niroomand, & Tiefenbacher, 2003), which controls the rate limiting step in the production of 7,8-dihydroneopterin. The results confirm that atherosclerotic plaque is a source of neopterin, particularly when macrophages are activated. Other studies have previously found that neopterin is increased after events such as stroke (Emsley et al., 2007; Lin et al., 2012) which is associated with macrophage activation (Chiba & Umegaki, 2013). Elevated serum neopterin is also a predictor of major adverse coronary events (Avanzas, Arroyo-Espliguero, Quiles, Roy, & Kaski, 2005). Generation of neopterin from 7,8-dihydroneopterin is evidence of an increase in oxidative stress in the plaque tissue. This is likely due to interferon- $\gamma$  causing an increase the expression of gp91phox and p47phox which form the active NOX complex, generating superoxide (Ellison et al., 2015).

The activation of HMDMs by PMA and PHA was somewhat surprising as the generation of 7,8-dihydroneopterin and neopterin by HMDM cells alone has not been previously reported. PMA is known to activate the NOX complex via protein kinase C activation (Matthews et al., 2016). Total neopterin in plaque tissue treated with PMA rose significantly over 72 h. Initial indications suggest that this is due to de novo synthesis of interferon- $\gamma$  by T cells within the plaque. It was surprising to find that PMA could cause a significant increase in the production of 7,8-dihydroneopterin in a macrophage-only culture in the absence of interferon- $\gamma$ . In vivo

labelling studies have shown that although interferon- $\gamma$  controls the expression of GTPCH-I, the activity of the enzyme is under post-translational control through phosphorylation (Hesslinger, Kremmer, Hultner, Ueffing, & Ziegler, 1998). PMA has been shown to cause hyperphosphorylation of GTPCH-I which induces a substantial rise in enzyme activity (Hesslinger et al., 1998).

These results suggest that both de novo synthesis of interferon- $\gamma$  and phosphorylation of GTPCH-I may be occurring in the PMA treated plaque tissue. Oxidant production as measured by neopterin was much higher in the monolayer cultures (PBMC and HMDM) compared to the PMA-treated plaque tissue. Neopterin generation in the monolayer cultures was expected due to the PMA-induced activation of NOX. In the plaque, most of the 7,8-dihydroneopterin remained unoxidized suggesting that the treatment with PMA had elevated the antioxidant 7,8-dihydroneopterin such that it greatly exceeded any oxidant generation, or that the level of oxidant generation in the plaque was much lower than in tissue culture.

There is an inverse association between the amount of calcification and the macrophage-derived production of 7,8-dihydroneopterin and neopterin in advanced atherosclerotic plaque. This finding suggests that plaque tissue with large volumes of calcium contributes less to the inflammatory burden than tissue with little calcification. From these results it is not possible to distinguish whether the increase in macrophage activation in sections containing smaller volumes of calcium is due to a change in macrophage phenotype related to the presence of microcalcifications or if there is an exclusion of macrophages in highly calcified tissue which lowers the immune activation.

### 3.5 Conclusion

Macrophages present in ex-vivo carotid plaque samples can be stimulated either directly or indirectly via T cells. Macrophage behaviour in live plaque samples varies along the length of the plaque. Cell culture experiments, therefore, have limited use in modelling the inflammatory response within atherosclerotic plaque. In addition, it has been found that the microenvironment of the plaque is associated with differences in macrophage activation, again highlighting the importance of using an ex-vivo system to investigate the role of macrophages in atherosclerosis.

## 4 Relationship between 7,8-dihydroneopterin and neopterin in the presence of superoxide

I was the sole contributor to this chapter.

### 4.1 Introduction

Neopterin is known to be elevated in a wide range of inflammatory conditions including sepsis, cardiovascular disease and HIV. In these diseases, neopterin has been shown to strongly correlate with negative outcomes (Baydar et al., 2009; Pihlstrøm et al., 2014; Wirleitner, Schroecksnadel, Winkler, & Fuchs, 2005). One potential source of neopterin is from HOCl mediated oxidation of 7,8-dihydroneopterin (B. Widner et al., 2000), which is thought to occur through MPO catalyzed conversion of hydrogen peroxide to HOCl in cells (Hampton, Kettle, & Winterbourn, 1998). In reaction mixtures, it has been found that HOCl can oxidize 7,8-dihydroneopterin to neopterin with between 50-80% stoichiometric efficiency (B. Widner et al., 2000), (unpublished data) and this may explain why there is such a dramatic increase in serum neopterin in bacterial inflammatory conditions (140-150 nM cf.  $5 \pm 2$  nM in healthy individuals) (Behnes et al., 2008; Tatzber et al., 1991).

However, in cardiovascular disease, MPO is less likely to be contributing significantly to the generation of neopterin. This is primarily due to the main source of MPO being neutrophils (Shukla & Walsh, 2015), whereas macrophages appear to be the primary inflammatory cell involved in the pathogenesis of cardiovascular disease (see Chapter 1). As identified in the previous chapter, patients with symptomatic cardiovascular disease exhibit a small, compared to bacterial infection, but nevertheless measurable increase in neopterin over healthy patients. With HOCl being an unlikely explanation for the neopterin generated by atherosclerotic plaque, this chapter examines the role of superoxide, one of the main oxidants generated in macrophages (Johnston, Godzik, & Cohn, 1978), as a potential source of neopterin in non-bacterial inflammatory conditions, often referred to as sterile inflammation.

Superoxide is a promising candidate for two reasons. First, several other candidates have been explored previously including hydrogen peroxide and hydroxyl radicals. All oxygen based reactions with 7,8-dihydroneopterin to date have primarily caused a loss of the side chain forming 7,8-dihydroxanthopterin, only HOCl has resulted in oxidation of 7,8-

dihydroneopterin without cleavage of the side chain (Suckling et al., 2008). Secondly, in inflammatory conditions, such as atherosclerosis, there is an increase in NOX activity (Niu et al., 2010) and therefore an increase in superoxide, as well as other related oxidants. There is evidence from earlier research that part of the reason 7,8-dihydroneopterin offers protection against oxLDL mediated cell death is that it reduces the oxidant burden in the cell (S. P. Giese et al., 2010), as 7,8-dihydroneopterin has been shown to reduce DHE fluorescence, a measure of superoxide generation, in cells treated with oxLDL (Katouah, Chen, Othman, & Giese, 2015; Shchepetkina et al., 2017). However, it is unknown if 7,8-dihydroneopterin is acting directly as an antioxidant, or if this reduction in superoxide is through another pathway controlled by 7,8-dihydroneopterin.

The aim of this chapter is to investigate whether superoxide is a potential source of neopterin. Understanding the mechanisms of 7,8-dihydroneopterin oxidation and neopterin formation may improve the utility of neopterin as a biomarker of inflammation and oxidative stress.

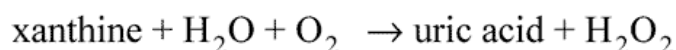
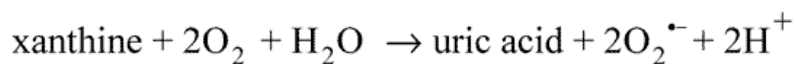
#### 4.1.1 Measuring neopterin formation by superoxide in a xanthine oxidase system

Fridovich (1970) first established the xanthine oxidase reaction system which generates superoxide through the enzymatic hydroxylation of xanthine to uric acid. This system has been chosen for use in this chapter over alternatives, which include superoxide salts and solid state reactions (Hayyan, Hashim, & AlNashef, 2016). These alternatives would require stop flow UV-Vis absorbance measurements and would likely compromise the ability to quantify neopterin via HPLC. The xanthine oxidase enzyme system is well established, and therefore there are known and expected values for how the assay will perform.

Whilst the xanthine oxidase system is the most appropriate for the following experiments, it does have some constraints. One drawback of this system is that neopterin inhibits the enzyme once it reaches above 10  $\mu\text{M}$  (Wede, Altindag, Widner, Wachter, & Fuchs, 1998) and 7,8-dihydroneopterin over 100  $\mu\text{M}$ . High concentrations of neopterin prevent the formation of uric acid so it is thought that neopterin may compete with xanthine for the molybdenum active site. Experiments have been carried out with an excess of xanthine substrate to try to prevent competition occurring in the enzyme active site. In addition, to avoid the inhibitory effects of neopterin most experiments have been carried out at 10  $\mu\text{M}$  of 7,8-dihydroneopterin. This low concentration makes detection slightly more difficult. Fortunately, HPLC is fairly sensitive with 7,8-dihydroneopterin being accurately detected

down to  $\sim 2 \mu\text{M}$  and neopterin down to  $\sim 10 \text{ nM}$ . However, this low concentration of 7,8-dihydroneopterin does prevent the ability to monitor the reaction directly via UV-Vis or fluorescence.

A second consideration is that there is some debate about whether xanthine oxidase is producing purely superoxide, or whether some is hydrogen peroxide (Kelley et al., 2010). In addition, hydrogen peroxide will be produced by the dismutation of superoxide. Superoxide production by xanthine oxidase is typically measured via the cytochrome c assay where  $\text{Fe}^{3+}$  is reduced to  $\text{Fe}^{2+}$ , however, in the presence of hydrogen peroxide there may be a back reaction, where the hydrogen peroxide oxidizes the  $\text{Fe}^{2+}$  (Vandewalle & Petersen, 1987). The reaction of hydrogen peroxide with 7,8-dihydroneopterin is known to be very slow and unlikely to occur in the timeframes of the majority of the experiments detailed here (Maghzal, 1999). Catalase, an enzyme that catalyses the dismutation of hydrogen peroxide to water and oxygen, has been used in specific experiments in this chapter to investigate the role of superoxide alone. Due to the presence of hydrogen peroxide, there is the possibility that the cytochrome c assay is under reading the rate of superoxide production, as the back reaction with hydrogen peroxide masks the superoxide reduction.



#### **Xanthine oxidase catalysed reactions of xanthine with oxygen and the resulting products.**

Finally, one further consideration is that this reaction is generally monitored by cytochrome c reduction as mentioned above. However, 7,8-dihydroneopterin will cause the direct reduction of cytochrome c. To overcome this, an NBT assay is used when 7,8-dihydroneopterin is present in the reaction mixture. This is a colorimetric assay based on two superoxide radicals converting one tetrazolium salt to a formazan dye. This has the advantage that there is no possible back reaction, however NBT has been shown to be slightly less competitive for superoxide than cytochrome c (Auclair, Torres, & Hakim, 1978).

The aim of this chapter is to measure the production of neopterin in the presence of xanthine oxidase generated superoxide using the reactions detailed below. It is already known that superoxide reacts with 7,8-dihydroneopterin at a rate constant of  $10^3 \text{ M}^{-1} \text{ S}^{-1}$ , a second order reaction. This was established using a spin trapping study by K. Oetl et al. (1997). However, measurement of the products of this reaction by HPLC has not previously been attempted.

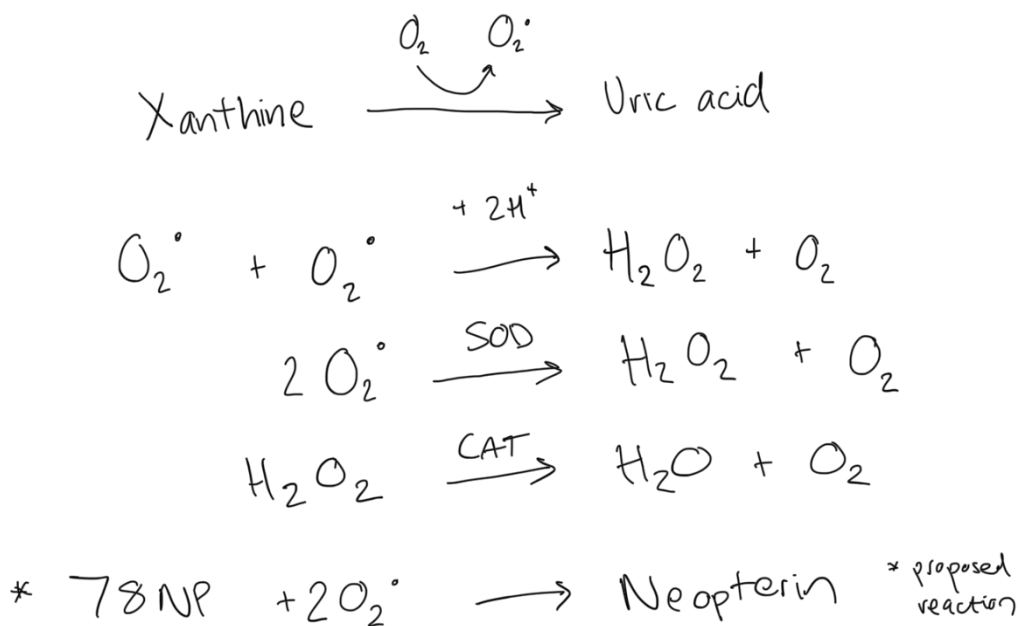
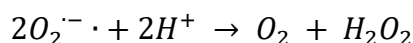


**Diagram of known reactions occurring in the xanthine oxidase system and the proposed oxidation of 7,8-dihydroneopterin.**

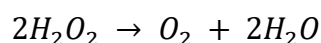
## 4.2 Methods in brief

All xanthine oxidase experiments were carried out in a pH 7.8 potassium phosphate buffer, to limit the production of hydroperoxyl radicals (Halliwell & Gutteridge, 1999), containing 500  $\mu\text{M}$  of xanthine (see Chapter 2) at 25°C shielded from light. All solutions were chelexed prior to use to prevent Fenton reactions occurring. 7,8-dihydroneopterin was diluted from a stock solution directly into the xanthine/potassium phosphate buffer to achieve a final concentration of 10  $\mu\text{M}$  for most experiments, or a suitable dilution achieve the desired final concentration up to a maximum of 130  $\mu\text{M}$ . Concentrations above this could not be achieved due to the need to balance components in the reaction mixture, and the solubility of 7,8-dihydroneopterin.

Enzyme solutions of xanthine oxidase (0.05 U/mL), superoxide dismutase (up to 1000 U/mL) and catalase (up to 1000 U/mL) were prepared fresh in ice cold water. One unit of xanthine oxidase will convert 1  $\mu\text{mole}$  of xanthine to uric acid per minute at pH 7.8 and 25 °C. Superoxide dismutase catalyzes the dismutation of superoxide into molecular oxygen and hydrogen peroxide.



One unit of superoxide dismutase will reduce the rate of cytochrome c reduction by 50% in the presence of 5 mU (or 1.67 mU/mL) xanthine oxidase. Catalase catalyses the decomposition of hydrogen peroxide to molecular oxygen and water at a rate of 1  $\mu\text{mole}$  of hydrogen peroxide per minute pH 7.0 and 25°C.



Enzyme solutions were diluted as necessary, and always added as a 100  $\mu\text{L}$  aliquot (each) as the final addition. Total reaction volume for all experiments was 3 mL.

Reactions were monitored by the cytochrome c assay (see Chapter 2) or NBT assay (see Chapter 2). Measurement of 7,8-dihydroneopterin and neopterin concentrations were carried out via absorbance and fluorescence HPLC using the SCX detection method as described in detail in Chapter 2.

## 4.3 Results

### 4.3.1 Superoxide induced loss of 7,8-dihydroneopterin and generation of neopterin

To test whether 7,8-dihydroneopterin was oxidised by superoxide, increasing initial concentrations of 7,8-dihydroneopterin were incubated with 1.67 mU/mL of xanthine oxidase for 60 minutes. This amount of xanthine oxidase will generate a theoretical 200  $\mu\text{M}$  of superoxide. Figure 4.1 shows neopterin is a product of the reaction between superoxide and 7,8-dihydroneopterin. The amount of 7,8-dihydroneopterin lost or neopterin gained is relatively linear until 50  $\mu\text{M}$  7,8-dihydroneopterin, with approximately 50% of the initial 7,8-dihydroneopterin remaining after 60 minutes. The asymptote for neopterin production is at 25  $\mu\text{M}$  for 200  $\mu\text{M}$  of assumed superoxide generated. However, this asymptote is not reached until an initial concentration of 1200  $\mu\text{M}$  7,8-dihydroneopterin.

The reaction efficiency appears to shift as the concentration of 7,8-dihydroneopterin increases. Figure 4.1a shows that the absolute amount of 7,8-dihydroneopterin lost during the 60 minute incubation with xanthine oxidase continued to increase as the initial concentration of 7,8-dihydroneopterin increased. However, the highest proportion of neopterin gain occurs at the lowest initial concentrations of 7,8-dihydroneopterin. At 10  $\mu\text{M}$  of 7,8-dihydroneopterin starting concentration, 1 neopterin is produced for every 2.2 7,8-dihydroneopterin molecules lost, whereas at 130  $\mu\text{M}$ , 1 neopterin is being produced for every 3.15 7,8-dihydroneopterin molecules lost.



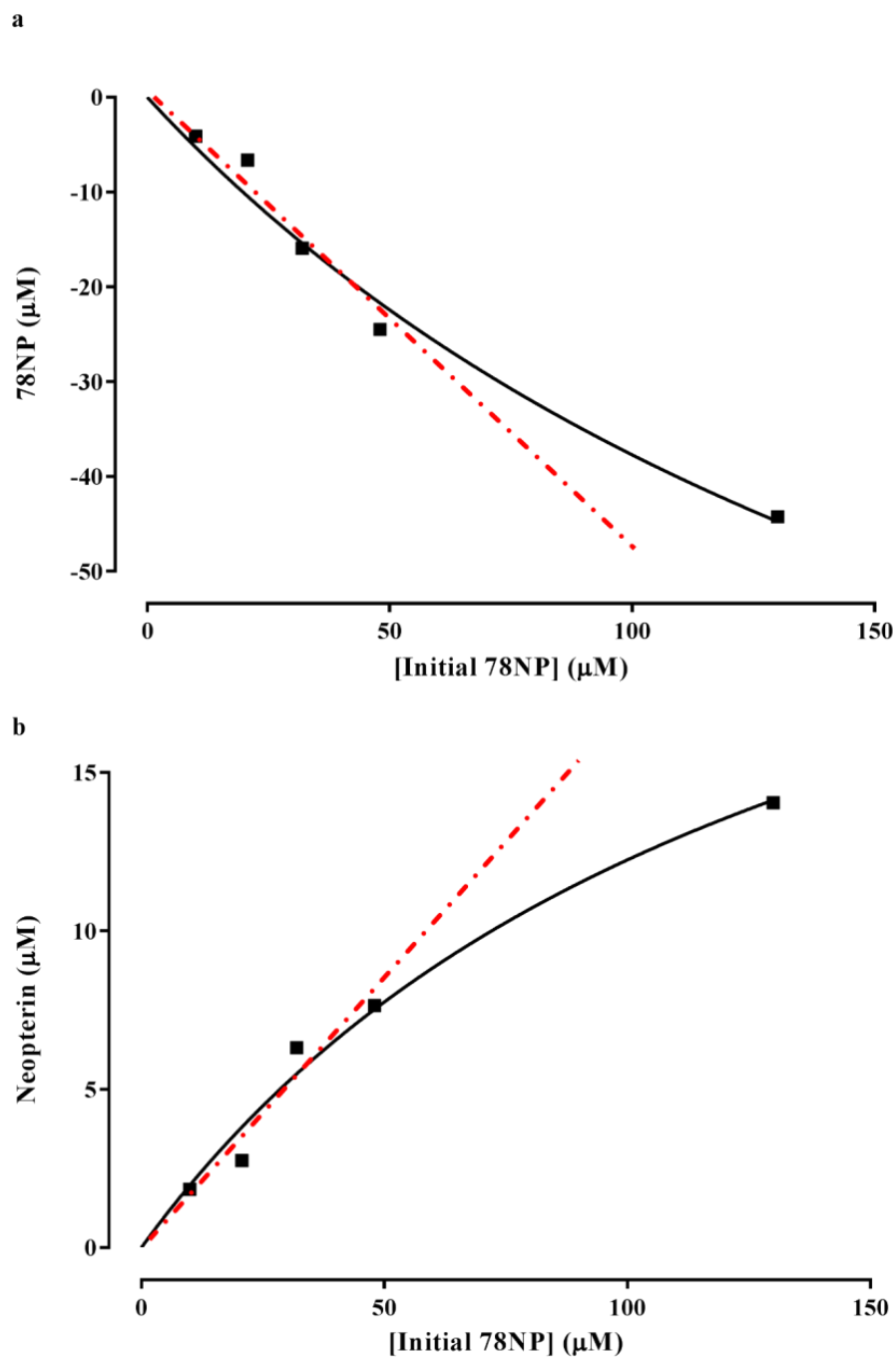


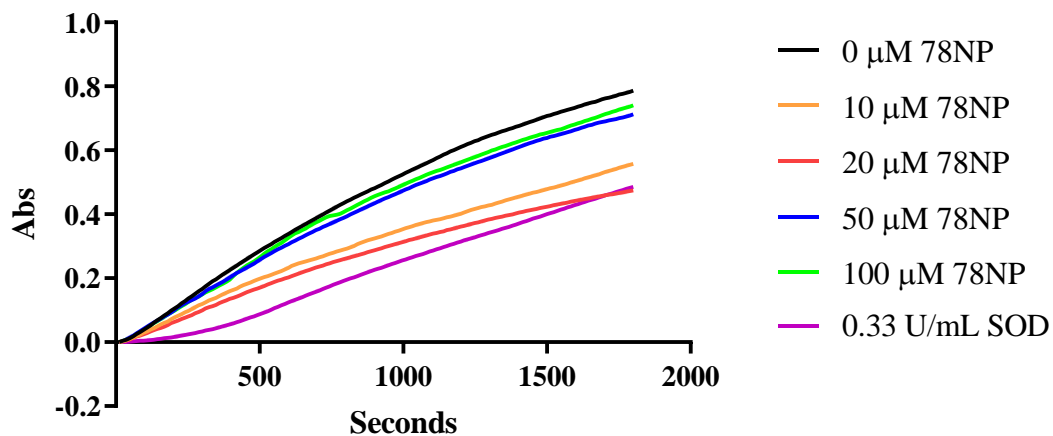
**Figure 4.1 Loss of 7,8-dihydroneopterin and gain of neopterin at different initial concentrations of 7,8-dihydroneopterin after 60 minutes of incubation with 1.67 mU/mL xanthine oxidase.**

The change in 7,8-dihydroneopterin concentration was measured by absorbance at 254nm using the SCX method on HPLC (a). Neopterin was simultaneously measured using fluorescence detection at ex 353 and em 438 (b). The black line is the fitting of a hyperbolic curve to all data points, whereas the red dotted line indicates the initial straight line trend through the first 4 data points. This graph shows results from a single experiment.

#### 4.3.2 Measurement of 7,8-dihydroneopterin superoxide scavenging ability

It is known that neopterin and 7,8-dihydroneopterin have the ability to inhibit the xanthine oxidase enzyme. To test how much inhibition is occurring in this modified xanthine oxidase system where xanthine oxidase is at a concentration of 1.67 mU/mL, an NBT assay was carried out at increasing concentrations of 7,8-dihydroneopterin (Figure 4.2). The measurement of superoxide production by the NBT assay shows that low concentrations of 7,8-dihydroneopterin reduce the amount of superoxide being scavenged by the NBT, however, the higher concentrations of 50  $\mu$ M and 100  $\mu$ M of 7,8-dihydroneopterin have little to no effect on the amount of superoxide being scavenged. One unit of SOD resulted in an approximately 50% reduction in NBT formation as expected, given that definition of a unit of SOD is the amount of enzyme that will reduce xanthine oxidase formation by half. Finally, there is no evidence of inhibition of the enzyme at higher 7,8-dihydroneopterin concentrations which may be due to the increased substrate availability in this modified set up.

a



b

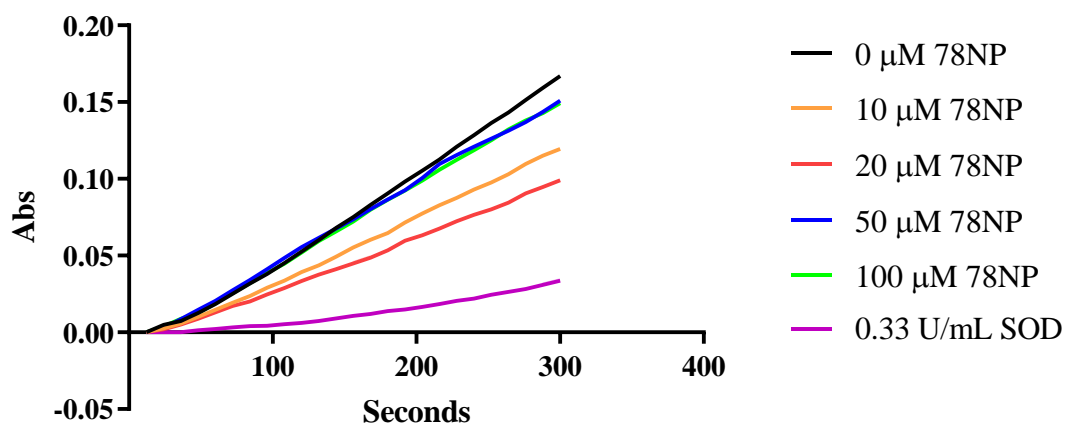


**Figure 4.2 NBT assay of superoxide production with increasing concentrations of 7,8-dihydroneopterin in the presence of 1.67 mU of xanthine oxidase.**

Absorbance of NBT-diformazan product formation with superoxide was measured at 550 nm over a total of 2500 seconds (a) with various concentrations of 7,8-dihydroneopterin. A close up of the first 300 seconds is displayed in (b). This graph shows results from a single experiment.

Measurement of superoxide production by either cytochrome c assay or NBT assay indicated a lower than theoretical rate of superoxide generation (Table 4.1). The cytochrome c assay and NBT assay are generally in agreement with each other; with the cytochrome c assay reading slightly lower than the NBT assay (100.2  $\mu\text{M}$  per hour vs 124.5  $\mu\text{M}$  per hour, respectively).

**Table 4.1 Theoretical and measured values for superoxide production using 1.67 mU/mL of xanthine oxidase**

Units	Theoretical (2 $\mu\text{moles}$ of superoxide from 1 $\mu\text{mole}$ of uric acid per minute)	Measured Cytochrome C reduction	Measured NBT reduction
$\mu\text{moles per minute}$	0.01	0.005	0.006
$\mu\text{M per hour}$	200.0	100.2	124.5

7,8-dihydroneopterin (10  $\mu\text{M}$ ) was incubated with increasing amounts of xanthine oxidase enzyme to measure the effect of variable rates of superoxide generation on the efficiency of the oxidation of 7,8-dihydroneopterin to neopterin. 7,8-dihydroneopterin was incubated with 0.03 mU/mL – 1.67 mU/mL of xanthine oxidase for 60 minutes (Figure 4.3). The amount of superoxide generated during the 60 minutes is  $\sim 112 \mu\text{M}$  (average of the values measured by cytochrome c and NBT assays) at 1.67 mU/mL. For 0.3 mU/mL, 0.17 mU/mL, 0.067 mU/mL and 0.03 mU/mL, the respective superoxide generation is 22.4  $\mu\text{M}$ , 11.2  $\mu\text{M}$ , 4.5  $\mu\text{M}$  and 2.2  $\mu\text{M}$ . The rate of superoxide generation is  $1.87 \mu\text{M min}^{-1}$  at 1.67 mU/mL of xanthine oxidase.

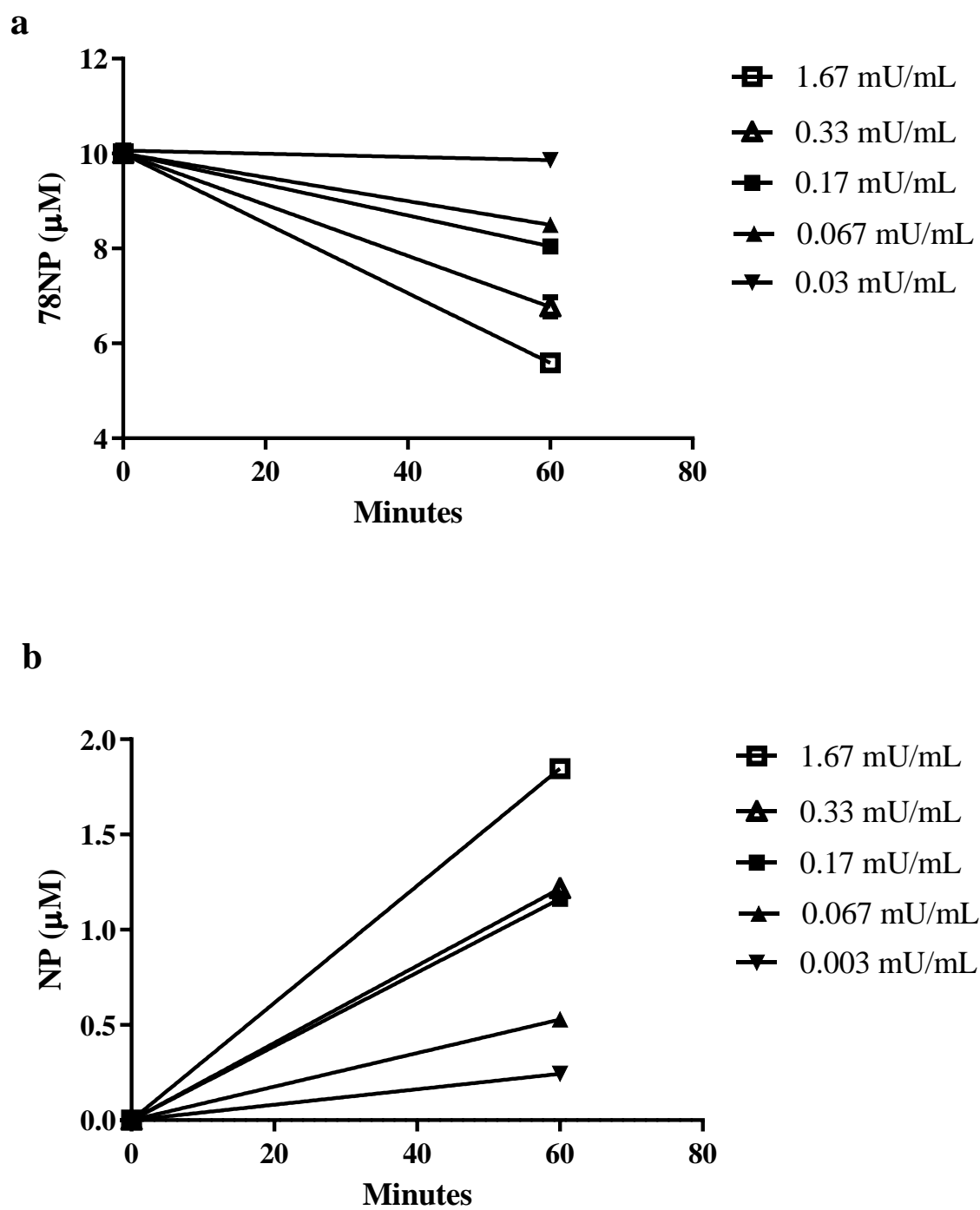
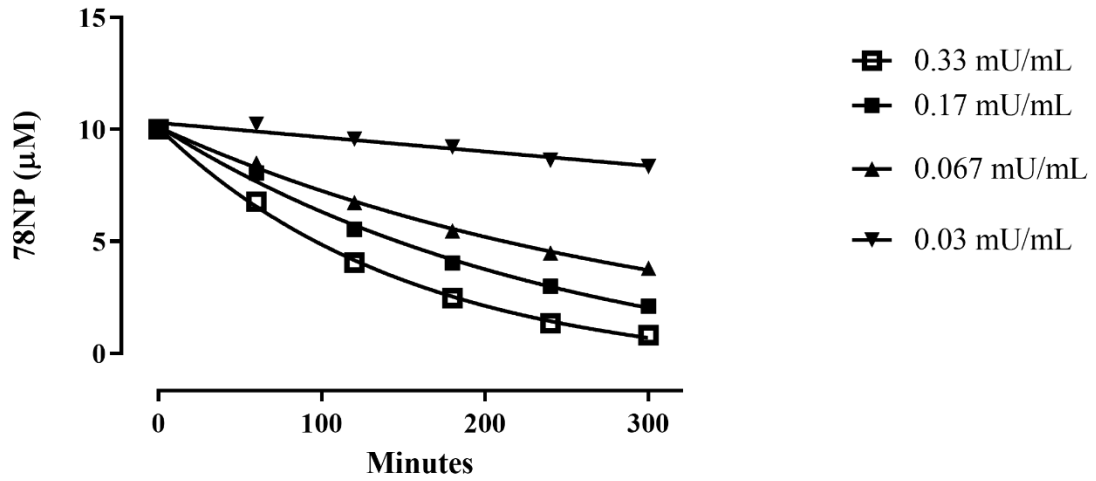


**Figure 4.3 Effect of increasing concentrations of xanthine oxidase enzyme on loss of 7,8-dihydroneopterin and gain of neopterin.** 7,8-dihydroneopterin (10 µM) was incubated with various concentrations of xanthine oxidase enzyme for 60 minutes. The change in 7,8-dihydroneopterin concentration was measured by absorbance at 254nm using the SCX method on HPLC (a). Neopterin was simultaneously measured using fluorescence detection at ex 353 and em 438 (b). Data is mean ± SEM (n=3).

The rate of 7,8-dihydroneopterin loss at 1.67 mU/mL of xanthine oxidase is  $0.074 \mu\text{M min}^{-1}$  and the rate of neopterin gain is  $0.031 \mu\text{M min}^{-1}$ . Clearly the rate of superoxide generation is much higher than the rate of 7,8-dihydroneopterin loss or NP gain, yet in Figure 4.2  $10 \mu\text{M}$  of 7,8-dihydroneopterin results in a 28% reduction of the superoxide output.

A time course of the reaction between superoxide and 7,8-dihydroneopterin at increasing rates of superoxide production shows that 7,8-dihydroneopterin is not completely oxidized by 300 minutes. The remaining 7,8-dihydroneopterin was measured at time 0 and every 30 minutes subsequently for up to 300 minutes (Figure 4.4a). Neopterin gain was assessed at the same intervals (Figure 4.4b). The total superoxide generation over the 300 minute time course was  $112 \mu\text{M}$  at 0.3 mU/mL of xanthine oxidase, and  $56 \mu\text{M}$ ,  $22.4 \mu\text{M}$  and  $11.2 \mu\text{M}$  for 0.17 mU/mL, 0.067 mU/mL and 0.03 mU/mL, respectively. The rate of superoxide generation is  $0.37 \mu\text{M min}^{-1}$  at 0.3 mU/mL of xanthine oxidase. The final concentration of 7,8-dihydroneopterin at the end of the time course in the presence of 0.03 mU/mL of xanthine oxidase was  $8.34 \mu\text{M}$  compared to  $0.81 \mu\text{M}$  with 0.3 mU/mL of xanthine oxidase. At 0.03 mU/mL of xanthine oxidase just  $0.59 \mu\text{M}$  of neopterin was generated over the time course, compared with  $3.7 \mu\text{M}$  of neopterin when 0.3 mU/mL of xanthine oxidase was present. This experiment showed that superoxide is a source of neopterin as increasing the superoxide generation increased the corresponding production of neopterin. As could be expected in a two-electron oxidation, neopterin generation is not a 1:1 ratio to 7,8-dihydroneopterin loss, however, the roughly 1:3 (neopterin gain: 7,8-dihydroneopterin loss) ratio at the highest concentration of enzyme is unusual. Interestingly, the loss of 7,8-dihydroneopterin did not correspond to the theoretical rate of superoxide generation. This will be explored more fully in subsequent experiments. Figure 4.2 and Figure 4.4 confirm that modifying either the concentration of 7,8-dihydroneopterin or the concentration of superoxide will change the rate of reaction, as expected with a second order reaction.

a)



b)

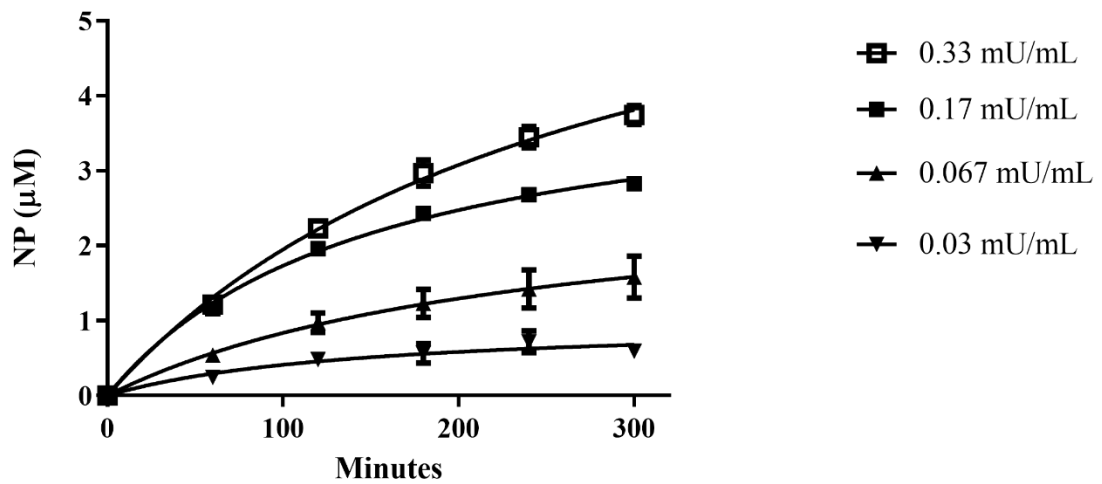


**Figure 4.4 Loss of 7,8-dihydroneopterin and gain of neopterin over time in the presence of increasing concentrations of xanthine oxidase enzyme.**

7,8-dihydroneopterin (10  $\mu\text{M}$ ) was incubated with various concentrations of xanthine oxidase enzyme for 300 minutes. The change in 7,8-dihydroneopterin concentration was measured by absorbance at 254nm using the SCX method on HPLC (a). Neopterin was simultaneously measured using fluorescence detection at ex 353 and em 438 (b). Data is mean  $\pm$  SEM (n=3).

### 4.3.3 Competition between 7,8-dihydroneopterin and superoxide dismutase

Including SOD in the reaction mixture prevented the formation of neopterin and the oxidation of 7,8-dihydroneopterin (

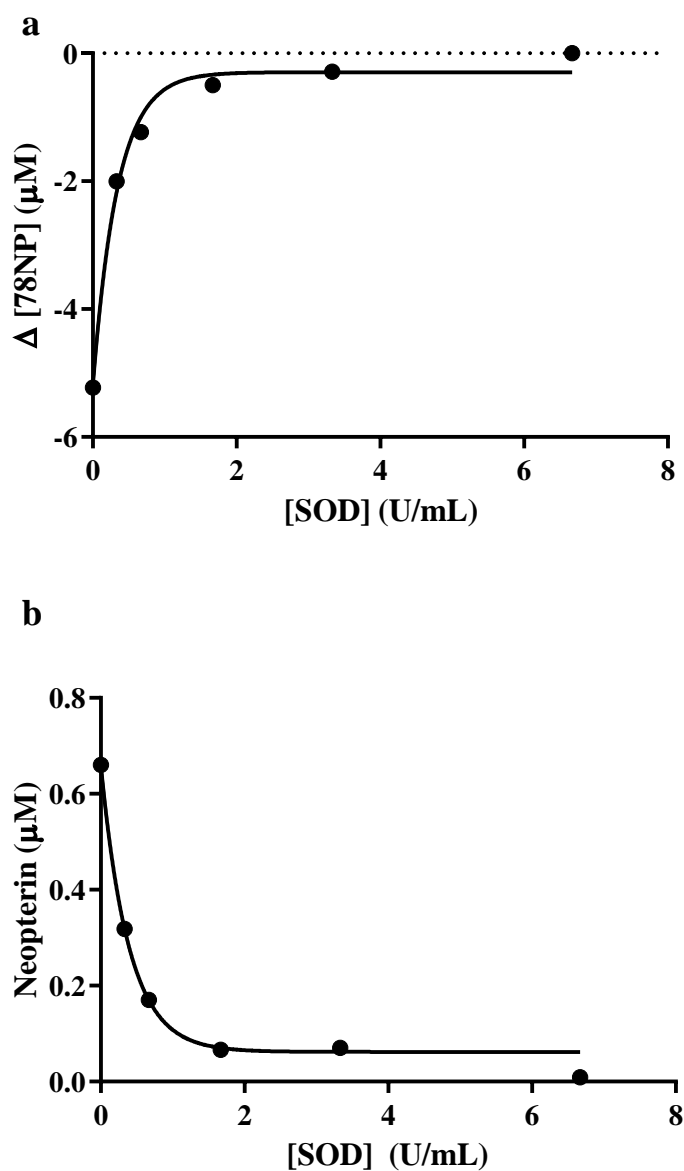
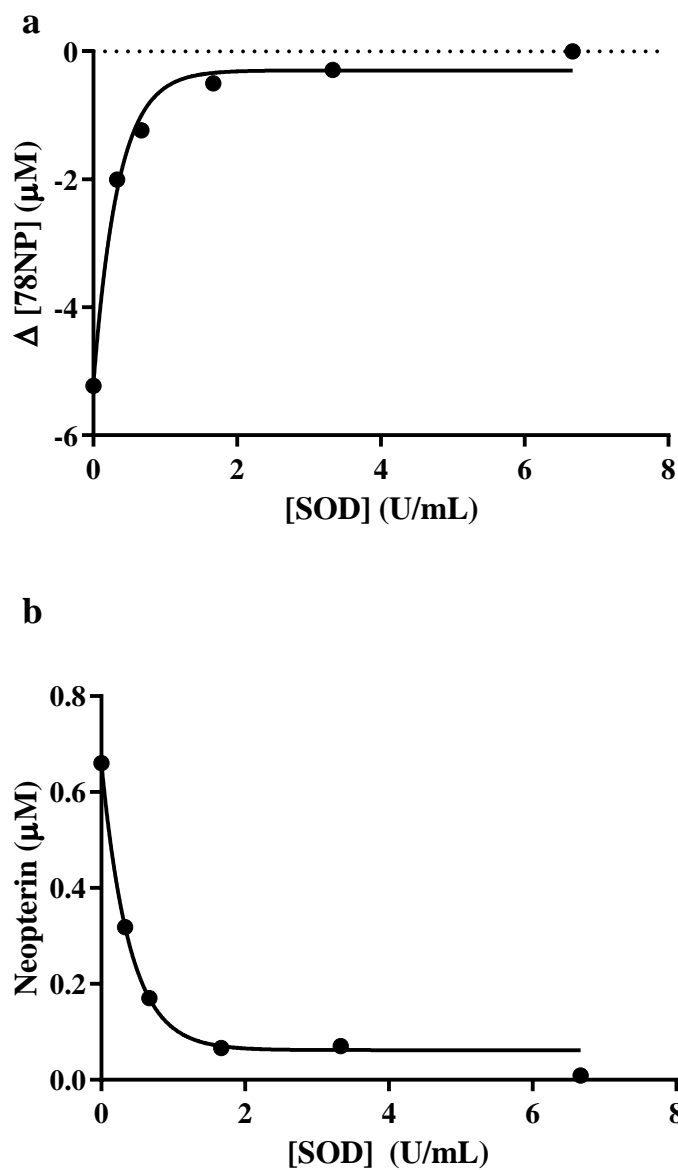


Figure 4.5). By 1.67 U/mL of SOD only a very small amount of neopterin (0.06  $\mu\text{M}$ ) is produced, and by 3.3 U/mL of SOD almost all 7,8-dihydroneopterin loss is abated. This confirms that the production of neopterin is occurring via superoxide, and that hydrogen peroxide generated by xanthine oxidase is not directly contributing to the formation of neopterin.





**Figure 4.5 Effect of increasing concentrations of SOD on loss of 7,8-dihydroneopterin and gain of neopterin in the presence of 1.67 mU/mL of xanthine oxidase for 60 minutes.**

7,8-dihydroneopterin (10  $\mu\text{M}$ ) was incubated with various concentrations of SOD enzyme for 60 minutes. The change in 7,8-dihydroneopterin concentration was measured by absorbance at 254nm using the SCX method on HPLC (a). Neopterin was simultaneously measured using fluorescence detection at ex 353 and em 438 (b). This graph shows results from a single experiment.

To test whether SOD was having any direct effect on 7,8-dihydroneopterin, 10  $\mu\text{M}$  of 7,8-dihydroneopterin was incubated for 30 minutes with 0.3 U/mL of SOD and 1.67 mU/mL of xanthine oxidase in the presence or absence of xanthine (Figure 4.6). As expected, adding SOD in the absence of the enzyme substrate, xanthine, had no effect on the concentration of either 7,8-dihydroneopterin or neopterin. In contrast, adding SOD in the presence of xanthine significantly ( $p = 0.03$ ) decreased the amount of neopterin formed, and prevented the loss of 7,8-dihydroneopterin ( $p = 0.0019$ ). This figure also confirms that there is no direct reaction between xanthine oxidase and 7,8-dihydroneopterin in the absence of the substrate.

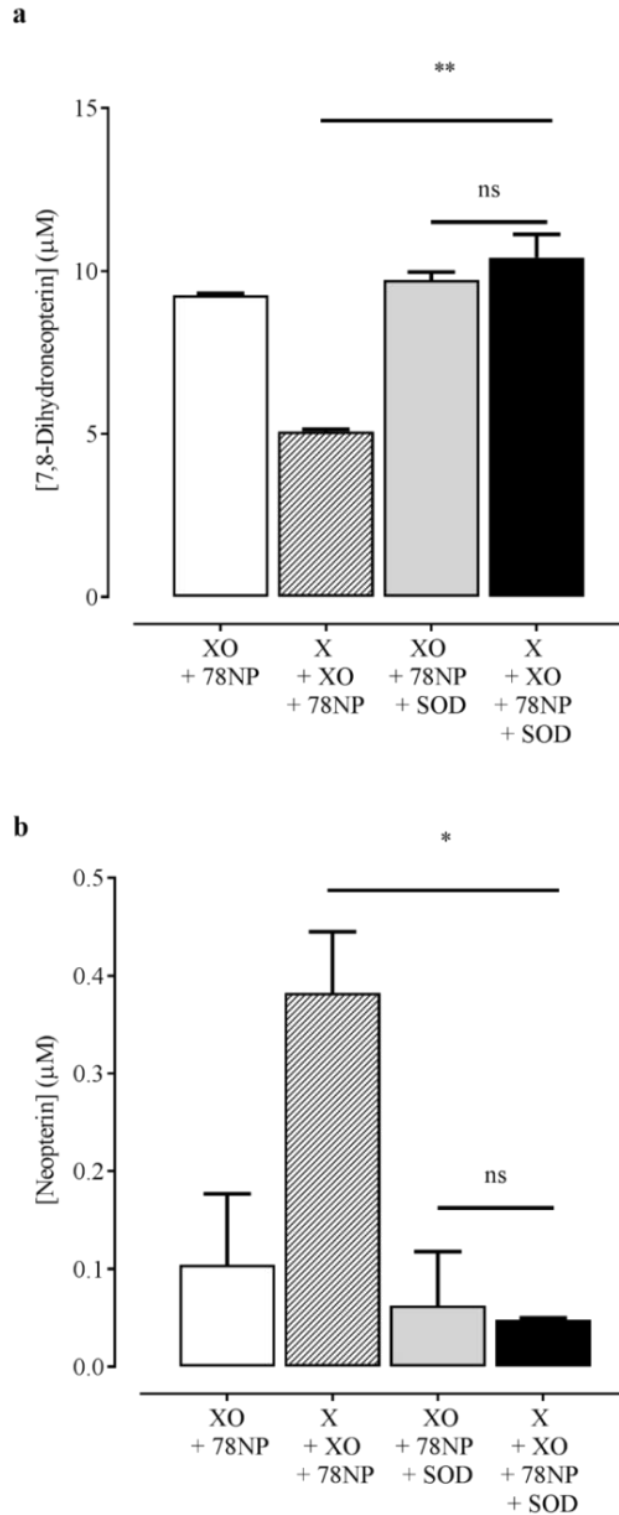


**Figure 4.6 Effect of SOD on loss of 7,8-dihydroneopterin and gain of neopterin in the presence or absence of the enzyme substrate with 1.67 mU/mL of xanthine oxidase for 30 minutes.**

7,8-dihydroneopterin (10 µM) was incubated with 0.3 U/mL of SOD enzyme for 30 minutes in the presence or absence of xanthine. The change in 7,8-dihydroneopterin concentration was measured by absorbance at 254nm using the SCX method on HPLC (a). Neopterin was simultaneously measured using fluorescence detection at ex 353 and em 438 (b).

#### 4.3.4 Initial reactions of 7,8-dihydroneopterin with superoxide

The following two experiments were carried out at 15 minutes to capture the initial reactions to isolate the main mechanism of neopterin formation from 7,8-dihydroneopterin by superoxide. The first experiment uses a low concentration of 7,8-dihydroneopterin (10  $\mu$ M) in the presence of excess of catalase (CAT) and SOD (Figure 4.7). The second experiment was conducted in the same manner but at 100  $\mu$ M of 7,8-dihydroneopterin (Figure 4.8). In Figure 4.7, the addition of SOD completely abolishes any loss of 7,8-dihydroneopterin and results a very small amount of neopterin. Somewhat surprisingly, catalase causes a substantial reduction in 7,8-dihydroneopterin well over and above that caused by the presence of xanthine oxidase alone. The addition of both catalase and SOD together abolishes the protective effect of SOD, but the loss of 7,8-dihydroneopterin is reduced in comparison to catalase alone. The changes in neopterin were small and not statistically significant.

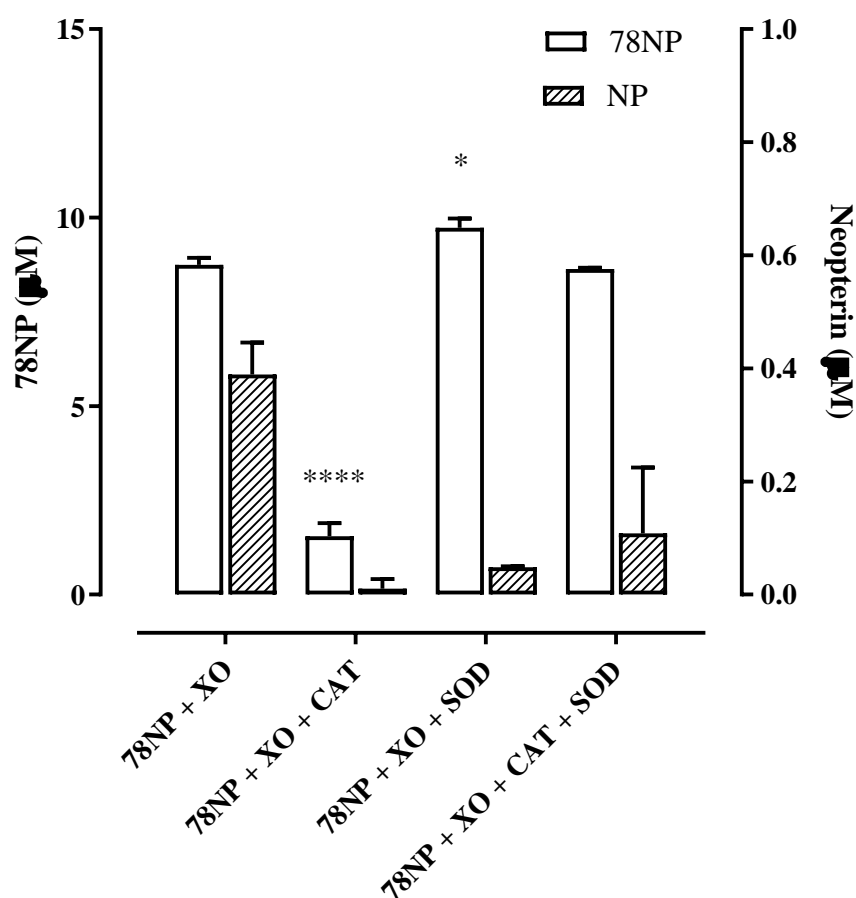


**Figure 4.7 Effect of 33 U/mL of CAT and 100 U of SOD on 10 μM of 7,8-dihydroneopterin in the presence of 1.67 mU/mL of xanthine oxidase for 15 minutes.**

7,8-dihydroneopterin (10 μM) was incubated with 33 U/mL of catalase (CAT) or 33 U/mL of SOD enzyme for 15 minutes in addition to 1.67 mU/mL of xanthine oxidase. The change in 7,8-dihydroneopterin concentration was measured by absorbance at 254nm using the SCX method on HPLC (a). Neopterin was simultaneously measured using fluorescence detection at ex 353 and em 438 (b). Data is mean ± SEM (n=2). A two-way ANOVA was carried out. Significance indicated by \*\*\*\* is  $p < 0.0001$ , \* is  $p < 0.05$ .

In Figure 4.8, 100  $\mu\text{M}$  7,8-dihydroneopterin is outcompeting both catalase and SOD for the xanthine oxidase-generated superoxide. Here in the presence of 7,8-dihydroneopterin alone, generating 28  $\mu\text{M}$  of superoxide results in the loss of 22  $\mu\text{M}$  of 7,8-dihydroneopterin, and an accompanying gain of 11  $\mu\text{M}$  of neopterin (50% of 7,8-dihydroneopterin lost). The loss of 7,8-dihydroneopterin in the presence of catalase that was seen in Figure 4.7 has been abolished at 100  $\mu\text{M}$  7,8-dihydroneopterin. Instead, as in the case of 7,8-dihydroneopterin alone,  $\sim 22 \mu\text{M}$  of 7,8-dihydroneopterin has been oxidized. As also seen in the previous figure, catalase is the most effective at preventing the formation of neopterin, whereas SOD is the most effective at preventing the loss of 7,8-dihydroneopterin. There is a gain of 5.7  $\mu\text{M}$  of neopterin, which is approximately half of the neopterin gain seen in the 7,8-dihydroneopterin alone condition, although this was not found to be a statistically significant difference. The addition of SOD results in a loss of 11  $\mu\text{M}$  of 7,8-dihydroneopterin, half that occurred in the 7,8-dihydroneopterin alone treatment, and a gain of 8.5  $\mu\text{M}$  of neopterin. The neopterin gain is reduced by 23% compared to the 7,8-dihydroneopterin alone treatment but a 1.5-fold increase compared to 7,8-dihydroneopterin with catalase. The presence of both catalase and SOD again lead to the loss of 7,8-dihydroneopterin (11  $\mu\text{M}$ ). The neopterin gain of 6.5  $\mu\text{M}$  is like that produced when incubated with SOD.

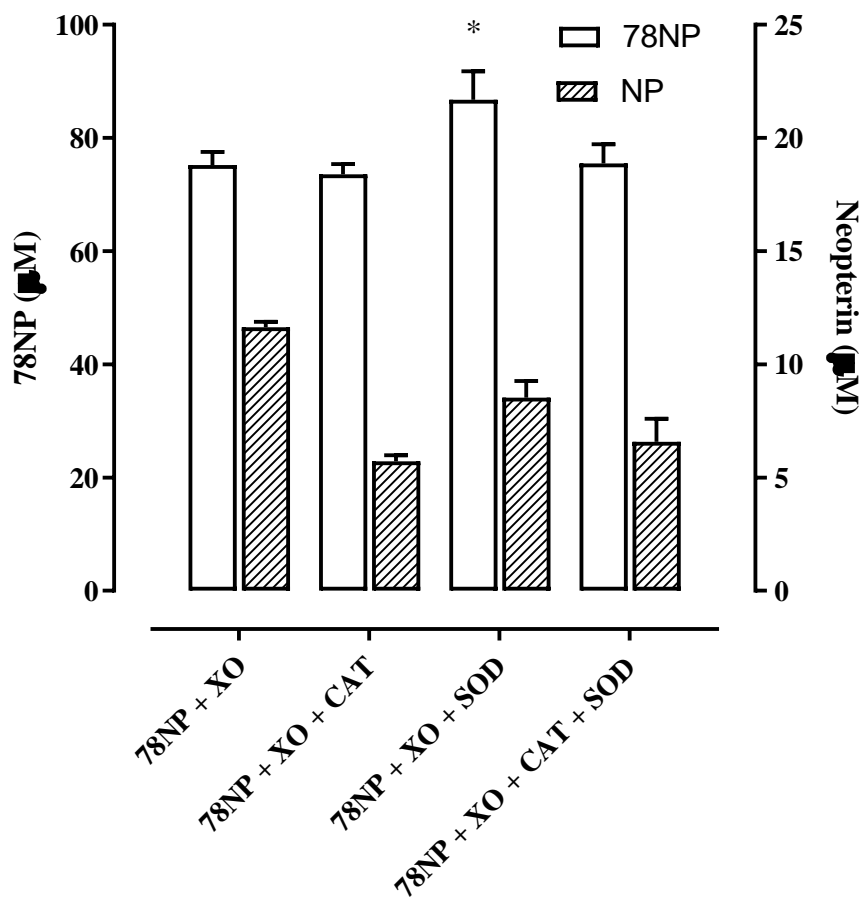


**Figure 4.8 Effect of 33 U/mL of CAT and 33 U/mL of SOD on 100 μM of 7,8-dihydroneopterin in the presence of 1.67 mU/mL of xanthine oxidase for 15 minutes.**

7,8-dihydroneopterin (100 μM) was incubated with 33 U/mL of CAT or 33 U/mL of SOD enzyme in addition to 1.67 mU/mL of xanthine oxidase for 15 minutes. The change in 7,8-dihydroneopterin concentration was measured by absorbance at 254nm using the SCX method on HPLC (a). Neopterin was simultaneously measured using fluorescence detection at ex 353 and em 438 (b). Data is mean ± SEM (n=2). A two-way ANOVA was carried out. Significance indicated as \* is p<0.05.

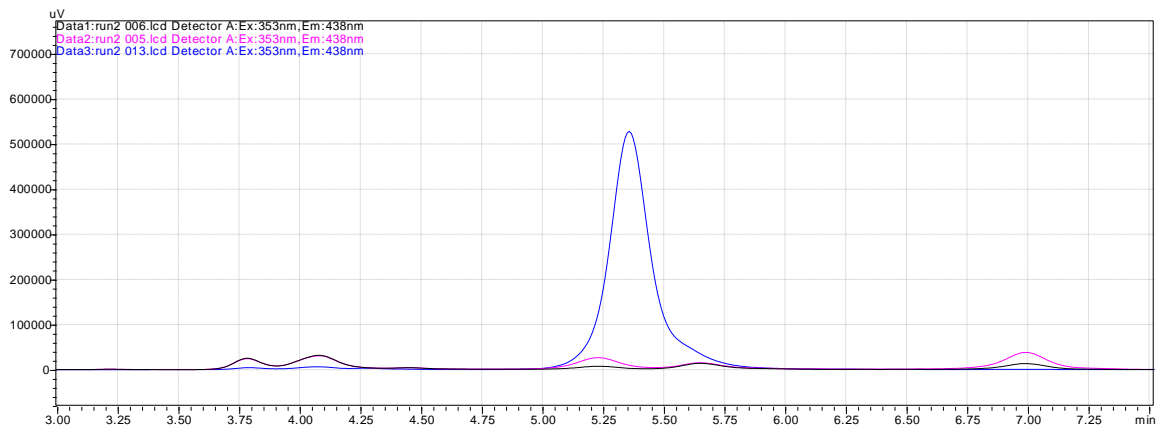
#### 4.3.5 Potential other products of the reaction between superoxide and 7,8-dihydroneopterin

There is a distinct difference between the amount of 7,8-dihydroneopterin consumed by the reaction with superoxide and the amount of neopterin that results. The HPLC chromatograms were examined closely to identify any possible other products. There was no evidence of dihydroxanthopterin or xanthopterin formation, which would be expected to produce distinctive peaks between 4.3 and 5 minutes (Figure 4.9a) in the fluorescence chromatogram (ex. 353nm, em. 438 nm). The peaks visible at 3.8 and 4.1 minutes are likely to be xanthine and uric acid. Neopterin can be seen clearly at 5.4 minutes (blue line = 100 nM neopterin standard). The peak at 7.0 minutes is 7,8-dihydroneopterin. Figure 4.9b is a close up of Figure 4.9a. The black line represents 10  $\mu$ M of 7,8-dihydroneopterin at  $t=0$ , the pink line is 25  $\mu$ M of 7,8-dihydroneopterin at  $t=0$ . Although this is noted as time 0, there was an unavoidable delay of almost two minutes prior to the needle acquiring the sample. At both 10 and 25  $\mu$ M of 7,8-dihydroneopterin, there are distinctive peaks at 5.2 and 5.7 minutes which both sit underneath the 100 nM of neopterin standard (pH 6). After 60 minutes incubation with xanthine oxidase, both peaks have increased in height, but the peak at 5.2 minutes has increased substantially more than the peak at 5.7 minutes (Figure 4.9c). Figure 4.9d is a close up of 10  $\mu$ M of 7,8-dihydroneopterin at  $t=0$  (pink) and  $t=60$  (black) showing the gain in peak height at 5.2 and 5.7 minutes and the corresponding decrease of the peak at 7.0 minutes. Examining the absorbance of the compounds at  $t=0$  (brown, 25  $\mu$ M 7,8-dihydroneopterin; blue 10  $\mu$ M 7,8-dihydroneopterin) and  $t=60$  (pink, 25  $\mu$ M 7,8-dihydroneopterin; black, 10  $\mu$ M 7,8-dihydroneopterin) using the PDA set to 254 nm, identified a distinctive drop in 7,8-dihydroneopterin concentration at 6.8 minutes (Figure 4.9e). There are two non-resolved peaks that form at 5.1 and 5.3 minutes in the  $t=60$  samples that appear to correspond to the 5.2 minute fluorescence peak. There is no absorbance peak that corresponds to the 5.7 minute fluorescence peak.

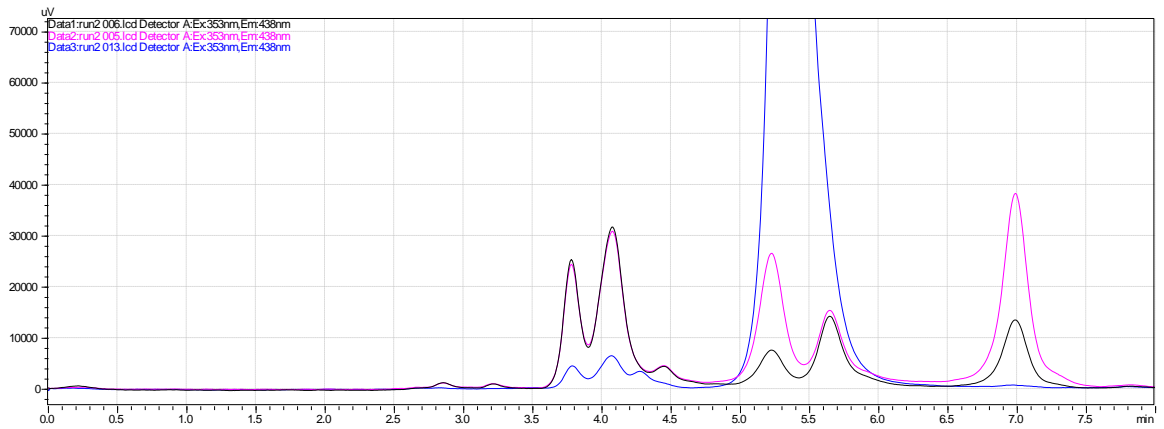
To see if the unidentified peak at 5.7 minutes had any biological relevance, media from a plaque sample was analysed. Figure 4.9f is the fluorescence chromatogram of media from an unstimulated plaque. The black line represents the media injected which has a pH of 7.4, the pink line represents media which has been acidified to pH 6. Interestingly, at pH 6, the neopterin peak at 5.2 minutes is much more distinct, and there is a peak that occurs at 5.7 minutes.



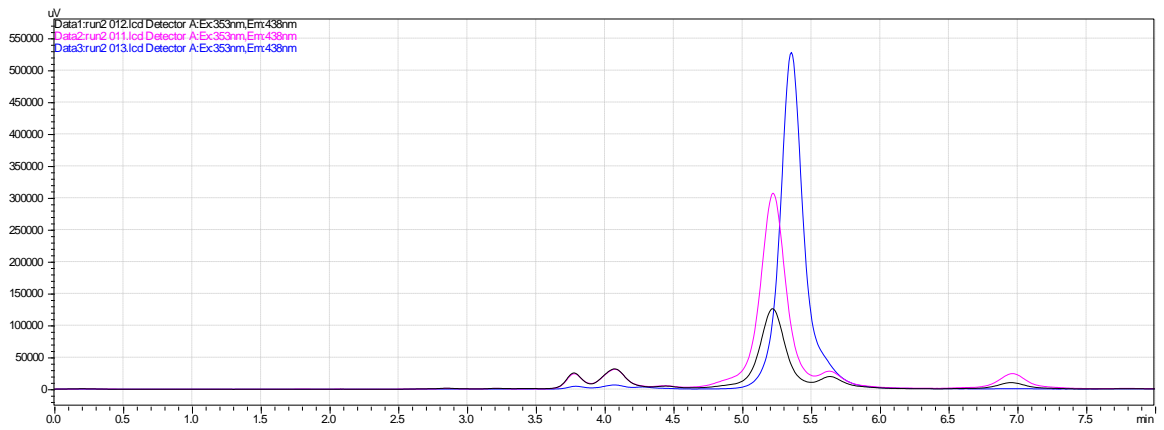
a)



b)



c)



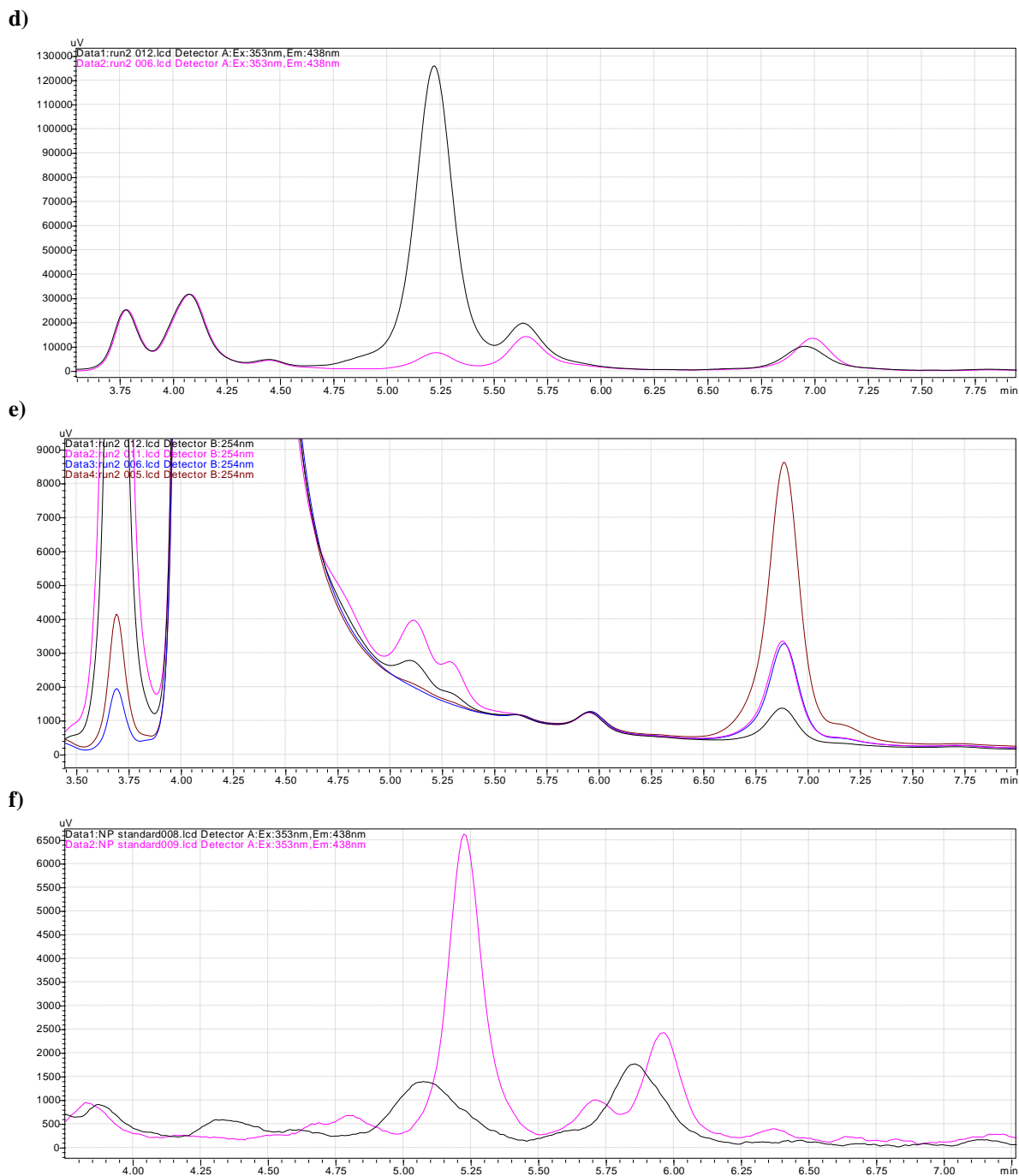


**Figure 4.9 Chromatograms of 7,8-dihydroneopterin and neopterin detection via SCX method.**

(a) Fluorescence chromatogram of injected standard of 100 nM neopterin (blue line), overlaid with the chromatograms from 10  $\mu$ M of 7,8-dihydroneopterin (black) and 25  $\mu$ M of 7,8-dihydroneopterin (pink) at time 0. (b) Close up of the fluorescence chromatogram described in (a). (c) Fluorescence chromatogram of injected standard of 100 nM neopterin (blue line), overlaid with the chromatograms from 10  $\mu$ M of 7,8-dihydroneopterin (black) and 25  $\mu$ M of 7,8-dihydroneopterin (pink) at time 60 minutes. (d) Fluorescence chromatogram of 10  $\mu$ M of 7,8-dihydroneopterin at time 0 (pink) and time 60 minutes (black). (e) Absorbance chromatogram of 10  $\mu$ M of 7,8-dihydroneopterin and 25  $\mu$ M of 7,8-dihydroneopterin at time 0 (blue and brown respectively) and time 60 minutes (black and pink, respectively). (f) Fluorescence chromatogram of plaque media at pH 7.4 (black) and pH 6.0 (pink). The results displayed here are from a single experiment.

#### 4.4 Discussion

The results from this chapter show that the oxidation of 7,8-dihydroneopterin to neopterin is not a straightforward reaction. In Figure 4.10, a potential mechanism is proposed, however, further study is required to confirm this proposed scheme. Using the information that has been gleaned from these experiments, it is possible to begin to form a hypothesis about the reactions occurring. The first piece of information is that superoxide will react with 7,8-dihydroneopterin. Secondly, SOD protects against 7,8-dihydroneopterin loss but at high concentrations 7,8-dihydroneopterin will still scavenge superoxide in the presence of SOD. Thirdly, introducing catalase at high concentrations of 7,8-dihydroneopterin has no effect on superoxide scavenging but lowers the amount of neopterin formed. In reaction 1a, a molecule of superoxide reacts with 7,8-dihydroneopterin to form a deprotonated and charged species and a hydroperoxyl radical (similar to the reactions in Nanni Jr, Stallings, and Sawyer (1980)). The resulting hydroperoxyl radical can participate in several different reactions outlined in 1a, b and c. In reaction 2, the deprotonated and charged species from reaction 1 reacts with a hydroperoxyl radical (generated from reaction 1b), which forms neopterin and hydrogen peroxide. Reaction 2a shows that there are multiple other possible products if the deprotonated and charged species reacts with an alternative oxidant or radical species.

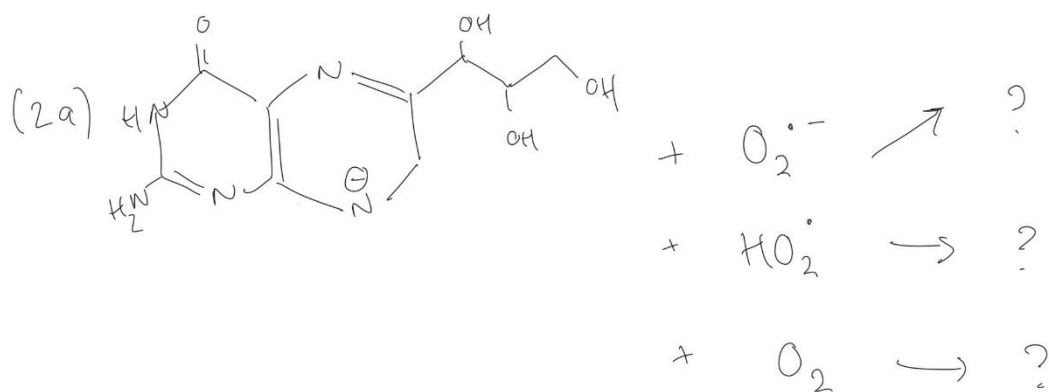
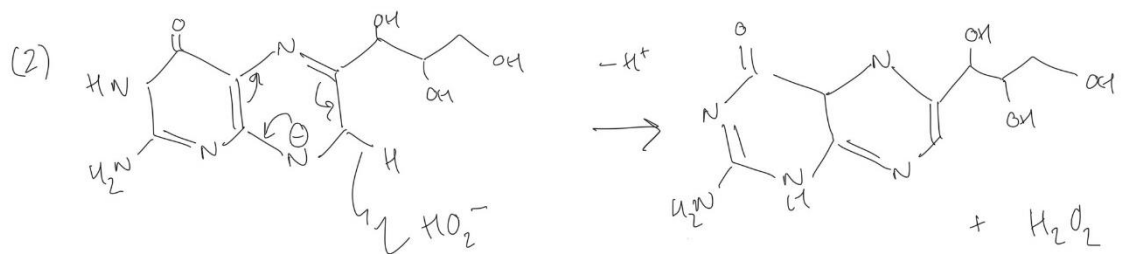
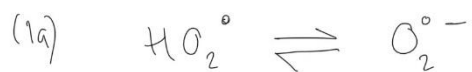
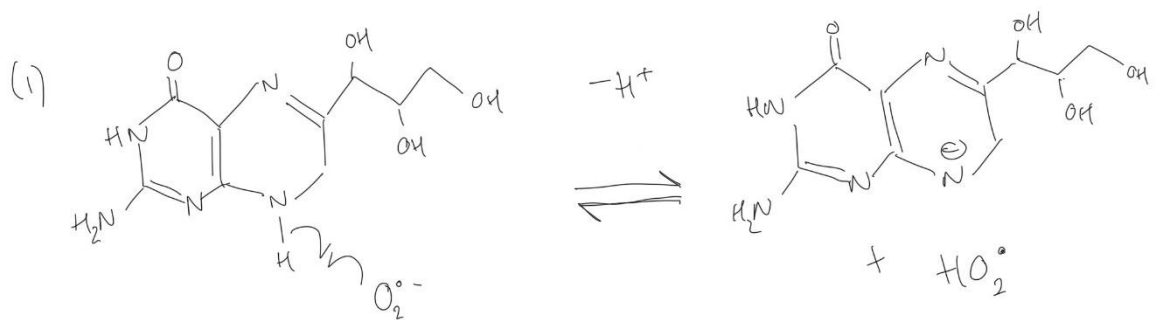


Figure 4.10 Hypothesised reaction mechanisms of 7,8-dihydroneopterin with superoxide.

As 100  $\mu\text{M}$  of 7,8-dihydroneopterin is able to outcompete 33 U/mL of SOD, which is known to react with superoxide at a rate constant of  $2 \times 10^9$ , there is the possibility that the rate of reaction between 7,8-dihydroneopterin and superoxide may actually be faster than the rate constant of  $10^3 \text{ M}^{-1} \text{ S}^{-1}$  that K. Oettl et al. (1997) have established, resulting in a deprotonated-7,8-dihydroneopterin (reaction 1). The additional peak that appears in the HPLC chromatograms adds support to this theory that a relatively stable charged intermediate may be being generated. The rate that K. Oettl et al. (1997) measured may in fact not have been the initial reaction with 7,8-dihydroneopterin which effectively regenerates superoxide (reaction 1a) but a subsequent and slower reaction, for example a reaction of superoxide with the product of reaction 1 (see reaction 2a). This concept is further supported by finding that the presence of catalase in conjunction with SOD removes the protective effect of SOD against 7,8-dihydroneopterin loss. This is likely to occur through the removal of hydroperoxyl radicals from the system caused by a shift in the reactant/product balance in reaction 1c. This in turn could impact the protonated/deprotonated 7,8-dihydroneopterin equilibrium (reaction 1) increasing the favourability of the deprotonated product. Hence, the effect of SOD is likely occurring at a later step in the oxidation process than initially thought, i.e. mitigating the effects of reaction 1b, which may decrease the favourability of reaction 2, the step which forms neopterin. As this mechanism is seeking to establish how neopterin formation occurs, the effects of other oxidants e.g. superoxide, at reaction 2 have not been considered, although these are likely to produce alternative products. This may explain the discrepancy between 7,8-dihydroneopterin loss and neopterin gain.

The NBT experiment provided some surprising results, where low concentrations of 7,8-dihydroneopterin reduced the formation of NBT via superoxide but higher concentrations did not. It is known from Figure 4.1 that 7,8-dihydroneopterin is being oxidized to neopterin in the presence of xanthine oxidase generated superoxide at all concentrations. NBT reacts with superoxide at a rate constant of  $1 \times 10^4 \text{ M/s}$ . If the initial reaction of superoxide with 7,8-dihydroneopterin is faster than this, then it may not be the initial reaction that is being monitored here. Since the reaction is likely to be a two-step mechanism, and superoxide or a superoxide derivative may be involved in both steps of the reaction, it is possible the NBT assay is only capturing the second or rate-limiting step of the reaction. At high concentrations of 7,8-dihydroneopterin, the second step could be less favourable due to the abundance of 7,8-dihydroneopterin, meaning any available superoxide is more likely to react with the NBT. At low concentrations of 7,8-dihydroneopterin, the second step may be more favourable, and this

is likely to be the step that removes superoxide from the system. As the NBT reading for superoxide produced is almost identical in the absence of 7,8-dihydroneopterin and in the presence of 50  $\mu\text{M}$  and 100  $\mu\text{M}$ , this would suggest the initial reaction of 7,8-dihydroneopterin with superoxide is not consuming the superoxide. This would be possible if a proton was abstracted from 7,8-dihydroneopterin in the first reaction forming a hydroperoxyl radical, as the pH of the solution would favour that species reforming superoxide almost instantaneously. Karl Oettl, Greilberger, and Reibnegger (2000) showed that 7,8-dihydroneopterin does not react directly with NBT at concentrations as high as 500  $\mu\text{M}$ . Wede et al. (1998) found that 7,8-dihydroneopterin diminished the production of uric acid up to 40% at 200  $\mu\text{M}$  of 7,8-dihydroneopterin, however, at the same concentration the measured reduction in NBT was only 20%. When they measured the remaining pterins after incubation with NBT, they found no change in the concentration of 7,8-dihydroneopterin. It seems plausible that NBT may be outcompeting the deprotonated-7,8-dihydroneopterin for the hydroperoxyl generated superoxide radicals. In the absence of NBT, 7,8-dihydroneopterin loss does not correlate well to the superoxide production which suggests that 7,8-dihydroneopterin may, cycling between protonated and deprotonated species, with only some 7,8-dihydroneopterin committed to further oxidation reactions.

In the first proposed reaction superoxide is acting as an oxidizing agent, generating a deprotonated form of 7,8-dihydroneopterin and releasing a hydroperoxyl radical. The hydroperoxyl radical is much more reactive than superoxide. The hydroperoxyl radical will react with itself to form hydrogen peroxide (reaction 1c) and oxygen or with superoxide to form oxygen and a hydroperoxyl anion (reaction 1b) (Nanni Jr et al., 1980). The hydroperoxyl radical is in equilibrium with superoxide but at pH 7.8 the equilibrium is heavily in favour of superoxide (reaction 1a) (Augusto & Miyamoto, 2011). It is proposed that neopterin is formed through the reaction of the deprotonated species with a hydroperoxyl anion. In addition to neopterin, this reaction produces hydrogen peroxide. With neopterin formation only occurring in the second step of the reaction, it is no surprise that there is variation in the percentage conversion of 7,8-dihydroneopterin to neopterin. In the case of low superoxide (Figure 4.4, 0.03 mU/mL xanthine oxidase) to 7,8-dihydroneopterin, it appears that reaction 1 predominates. However, as the amount of superoxide increases, the balance shifts further in favour of reaction 2, probably due to an increased likelihood of reaction 1b occurring. Experiments in the presence of catalase showed that removing hydrogen peroxide had a detrimental effect on neopterin generation yet caused a marked decrease in 7,8-

dihydroneopterin concentration. Potentially, removing hydrogen peroxide from the system prevents the deprotonated-7,8-dihydroneopterin from regenerating 7,8-dihydroneopterin, in addition to preventing the forward reaction towards neopterin by increasing hydroperoxyl-hydroperoxyl reactions as discussed earlier.

Finally, whilst following the loss of 7,8-dihydroneopterin and gain of neopterin via HPLC is cost effective and easy, it is worth noting that the SCX method is not particularly sensitive for 7,8-dihydroxanthopterin or xanthopterin, so it is not possible to rule out the potential formation of low (sub 10  $\mu\text{M}$ ) amounts of these products (possibly generated through reaction 2a). Given the identification of an alternative, but unquantified peak at 5.7 minutes, which also appears to have relevance to biological samples, it seems the logical next step would be to monitor this reaction using mass spectrometry. Furthermore, the results with the SCX method, which uses hydrogen-bonding, suggests that the method is much more susceptible to variations in sample pH than initially thought, which strengthens the case for either controlling pH or using a method that is not susceptible.

#### 4.5 Conclusion

From the data presented here, superoxide appears to be necessary for the generation of neopterin in this system but appears to not be the sole oxidant involved. It appears that the balance of neopterin to other products can be modified by the ratio of various oxidants available. It is possible that 7,8-dihydroneopterin may react with multiple molecules of superoxide. The reaction of 7,8-dihydroneopterin with superoxide may generate a deprotonated, charged form, which may be of relevance in biological systems. These reactions may be less favourable in a system that contains other oxidants. Future work is required to confirm the mechanism of oxidation.

## 5 Effect of oxidant modulation on 7,8-dihydroneopterin and neopterin generation in biological systems

### 5.1 Introduction

NOX is a potential source of superoxide in the plaque (Judkins et al., 2009). In this chapter, experiments were conducted with apocynin, a common inhibitor of p47phox containing NOXs (Stolk, Hiltermann, Dijkman, & Verhoeven, 1994). The p47phox subunit is crucial to the activation of NOX through its phosphorylation and subsequent binding to the p22phox domain (Takeya et al., 2003). Interestingly, apocynin is thought to only act as a competitive inhibitor of p47phox binding in NOX when it is in the dimerized form (Ismail, Scapozza, Ruegg, & Dorchies, 2014). The formation of the dimer is via a myeloperoxidase (MPO)-mediated oxidation (Ximenes, Kanegae, Rissato, & Galhiane, 2007). It has also been suggested that the radical form of apocynin generated by MPO may damage thiol groups on the NOX, and prevent NOX activation in that manner (Heumüller et al., 2008). In the absence of MPO, apocynin has been found to act as an antioxidant, although the mechanism of this is not well understood (Kanegae, da Fonseca, Brunetti, de Oliveira Silva, & Ximenes, 2007). There has been some suggestion that the antioxidant activity of apocynin in cells is not direct, but rather is via regulation of Nrf2 which is involved in the synthesis of GSH and peroxiredoxin (Lim et al., 2014).

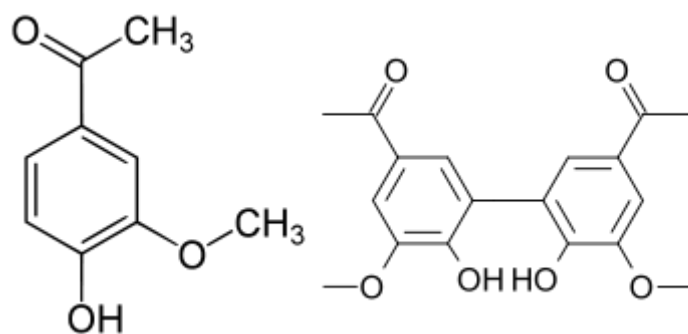


**Figure 5.1 Apocynin and diapocynin molecules**

In order to be confident that any effect seen with apocynin was due to reduction in NOX activity, it was necessary to investigate MPO activity in the plaque tissue. As mentioned earlier, MPO, in addition to oxidizing apocynin, has a role in producing hypochlorite from hydrogen peroxide. If MPO was present in plaque tissue, it would be expected that neopterin could be produced from the reaction between hypochlorite and 7,8-dihydroneopterin. If this is the case, by blocking MPO in plaque tissue, it would be expected that total neopterin would increase



and neopterin would decrease. At the same time, inhibiting MPO could prevent cellular hydrogen peroxide from becoming hypochlorite, increasing the intracellular hydrogen peroxide levels. If the mechanism of 7,8-dihydroneopterin loss and neopterin formation presented in the previous chapter is correct, then it would be expected that an increase in hydrogen peroxide would favour total neopterin regeneration. To test the effect of MPO in the plaque, 4-aminobenzoic acid hydrazide (ABAH) was used as an inhibitor. ABAH irreversibly inactivates MPO (Kettle, Gedye, Hampton, & Winterbourn, 1995; Malle, Furtmüller, Sattler, & Obinger, 2007). This inactivation thought to occur through the oxidation of MPO by ABAH to a radical form. If the radical form interacts with hydrogen peroxide then irreversible inactivation occurs, but in the presence of oxygen, enzyme turnover occurs (Kettle, Gedye, & Winterbourn, 1997).

Finally, to directly confirm the effect of removing superoxide, a plaque was incubated with PEG-SOD, a pegylated form of the enzyme superoxide dismutase, which is membrane-permeable (Pannirselvam, Verma, Anderson, & Triggle, 2002). This was the first experiment to attempt to use intra-plaque controls, which meant the treatment was only added to every second section of plaque. The theory being that the sections either side of the treatment section would help to assess how the tissue may have behaved if the treatment had not been added.

Next, the effect of increasing cellular oxidants on 7,8-dihydroneopterin and neopterin production in plaque was tested using the addition of oxLDL. OxLDL was chosen for use in these experiments for two reasons. One, it is known to increase intracellular oxidant production including superoxide (Stielow et al., 2006), and two, for its biological relevance to the development of atherosclerosis (Pirillo, Norata, & Catapano, 2013). In this series of experiments, several hypotheses were tested. Firstly, was there an effect of oxLDL on 7,8-dihydroneopterin and neopterin in PMA-stimulated cells. Secondly, was this effect specific to the oxidized form, as opposed to native LDL. Finally, was oxLDL toxic to the cells in the plaque? In addition, an experiment with HMDM cells was used to test whether the extracellular response to oxLDL reflects what is occurring intracellularly. Understanding how the balance of oxidants in plaque tissue modulates 7,8-dihydroneopterin and neopterin release is a crucial step in improving the usefulness of 7,8-dihydroneopterin and neopterin as biomarkers of advanced cardiovascular disease.

## 5.2 Methods in brief

Plaques were obtained fresh from Christchurch Hospital and cut into sections and cultured as described in Chapter 2. Total neopterin and neopterin were measured by HPLC as described in Chapter 2. Lactate measurements were conducted by a colorimetric assay as described in Chapter 2.

HMDM cells were cultured in accordance with the method described in Chapter 2. The cells were incubated with oxLDL (2 mg/mL), and/or 50 U/mL of PEG-SOD in the presence or absence of 200  $\mu$ M 7,8-dihydroneopterin for 24 hours. At the end of the 24 hours, the media was removed for analysis. To the remaining cells, 200 $\mu$ L of ice-cold PBS was added and then the cells were scrapped from the plate surface using a pipette tip. The resulting liquid was frozen to ensure cell lysis prior to analysis. Intracellular and extracellular total neopterin and neopterin were measured by HPLC as described in Chapter 2. Protein concentrations were determined using the BCA assay in Chapter 2.

## 5.3 Results

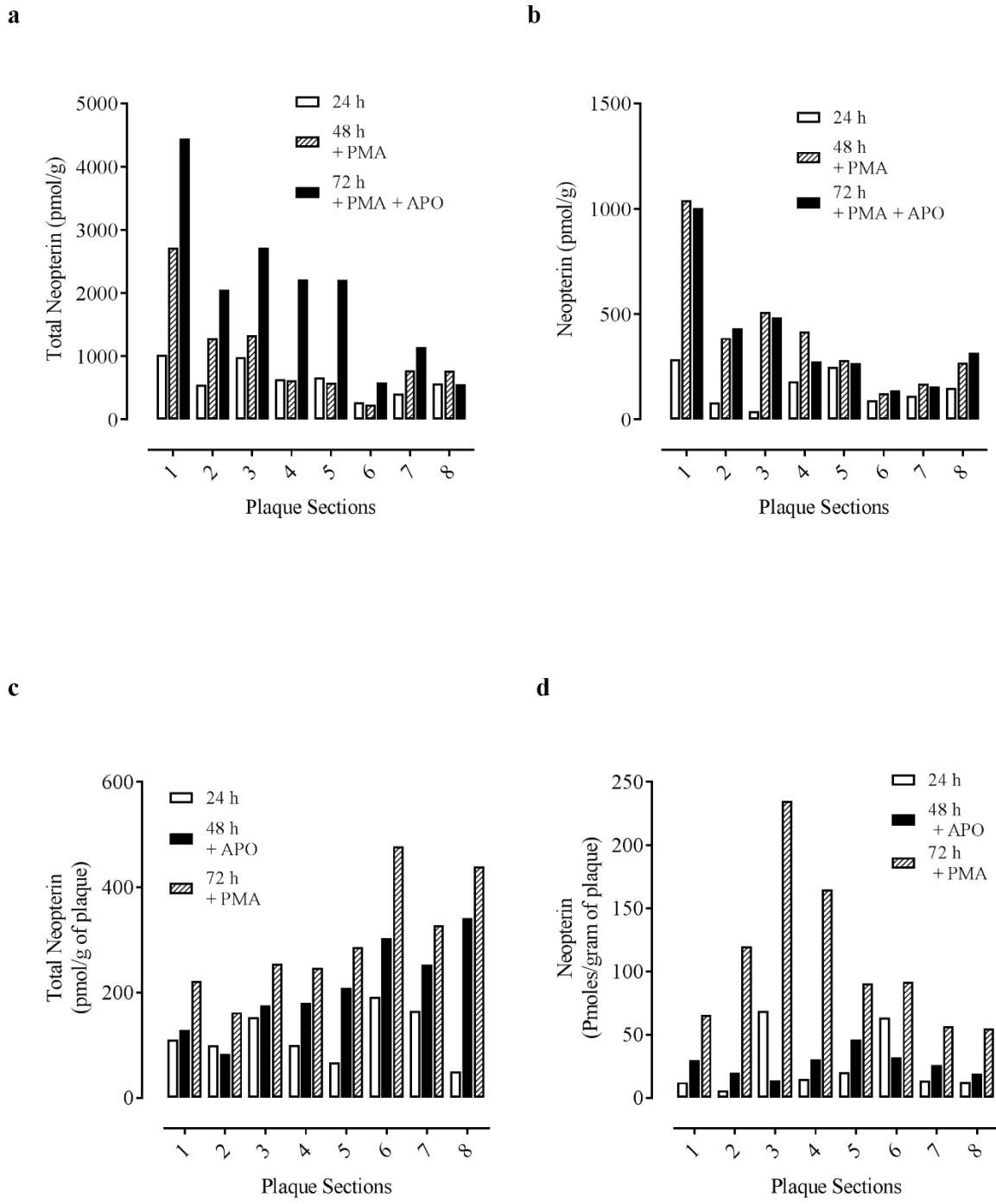
### 5.3.1 Reducing superoxide production by inhibiting NADPH oxidase in plaque

A plaque was collected from the right internal carotid artery of a 73-year-old, non-smoking, diabetic female who had experienced a TIA with leg weakness (Figure 5.2). The patient had a blood pressure of 150/65 and weighed 86.2 kg. Assessment of the carotid artery by ultrasound showed stenosis of 80-85%. Treating PMA stimulated plaque sections with apocynin increased the total neopterin to  $1993 \pm 1277$  pmol/g on average ( $p=0.0079$ , paired t-test) (compared to  $1040 \pm 771$  pmol/g in the PMA only treatment) as shown in a & b, but did not change the neopterin production compared to the previous day ( $385 \pm 277$  pmol/g vs.  $400 \pm 289$  pmol/g; n.s.). Earlier experiments with PMA suggest that typically both total neopterin and neopterin continue to increase with ongoing stimulation of cells; however, plaque tissue is variable in its response to stimuli. It is not possible to know for certain whether the ablation of neopterin generation is directly due to the addition of the apocynin.

In *Figure 5.2c & d*, the plaque from the left internal carotid artery of a 64 year old, recent ex-smoker, non-diabetic male who suffered from a stroke resulting in facial droop and slurred speech was cultured with apocynin prior to the addition of PMA. Blood pressure, weight and stenosis of the artery were not recorded on the patient information form. When apocynin was added before stimulating the plaque, there was an increase in basal total neopterin ( $210 \pm 87$  pmol/g vs  $118 \pm 49$  pmol/g (media only);  $p=0.03$ ), which was unexpected. As the plaque was unstimulated in this case, it is likely that this effect is due to the addition of the apocynin. Interestingly, there was little to no change in neopterin ( $27 \pm 10$  pmol/g vs.  $27 \pm 25$  pmol/g (media only); n.s.). However, upon stimulation with PMA there was a marked increase in neopterin production ( $110 \pm 62$  pmol/g vs  $27 \pm 10$  pmol/g;  $p=0.01$ ). It is not possible to tell from these results whether apocynin is competitively binding to p47phox and therefore preventing NOX activation or acting as an antioxidant.

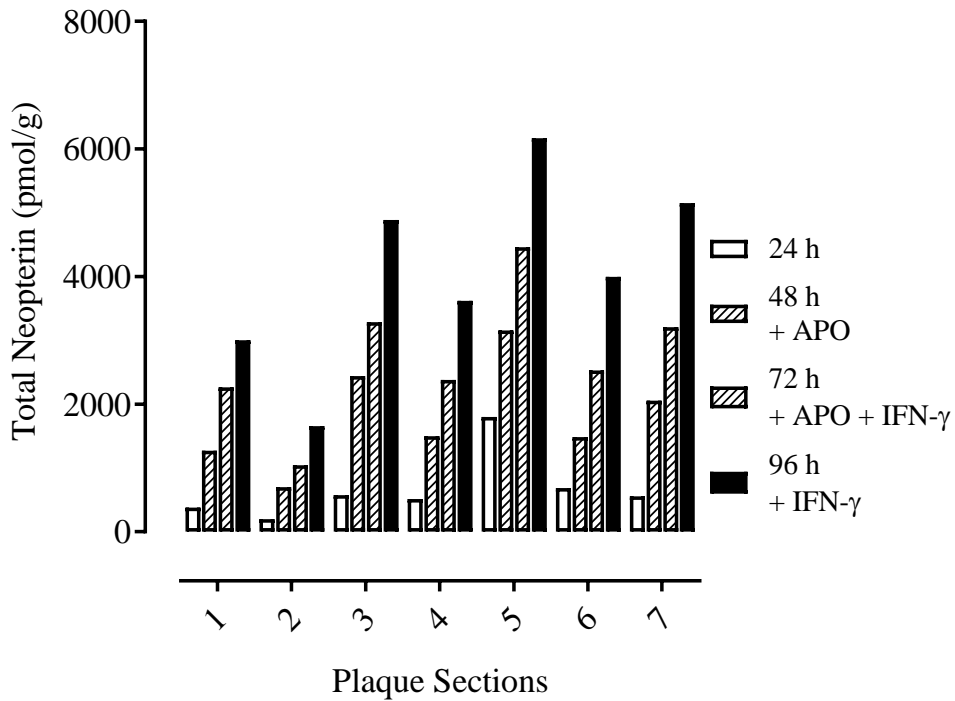
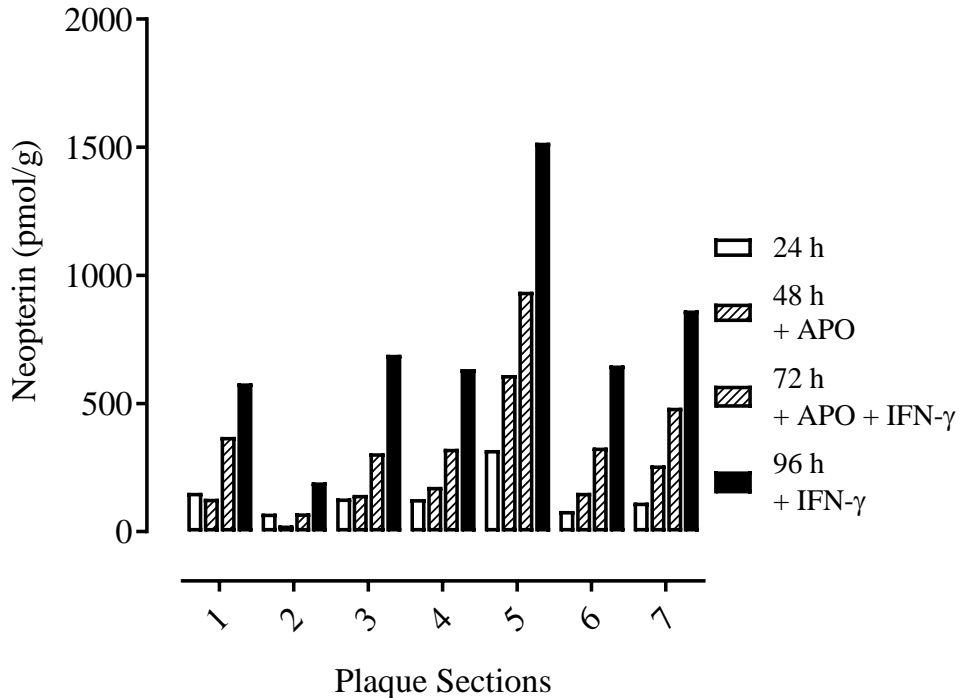
A separate plaque was obtained from the left carotid artery of an 83 year old male who experienced TIAs and weakness in their right hand (Figure 5.3). Stenosis was measured as 50-69%. Figure 5.3a shows that incubation with apocynin alone resulted in the immediate increase in total neopterin ( $1801 \pm 815$  pmol/g vs.  $671 \pm 522$  pmol/g (media only);  $p=0.0007$ ). In most sections, there was only a slight increase in neopterin ( $213 \pm 189$  pmol/g vs.  $142 \pm 83$  pmol/g

(media only); n.s.) accompanying the rise in total neopterin (Figure 5.3b). Incubation of apocynin in conjunction with interferon-gamma continued the increase in total neopterin (average increase  $936 \pm 306$  pmol/g;  $p=0.0002$ ), however, this time there was an accompanying increase in neopterin ( $190 \pm 87$  pmol/g;  $p=0.0012$ ). Finally, incubation with interferon-gamma alone caused a further increase in both total neopterin ( $1332 \pm 498$  pmol/g;  $p=0.0004$ ) and neopterin ( $330 \pm 146$  pmol/g;  $p=0.001$ ). Apocynin is unable to abolish the interferon-gamma induced production of neopterin, however, the ratio of total neopterin to neopterin appears unexpectedly high.



**Figure 5.2 Effect of 100  $\mu$ M of apocynin before or after stimulation using 5 $\mu$ M of PMA on total neopterin and neopterin production in plaque.**

(a) and (b) show the total neopterin and neopterin measured in a plaque from a 73-year-old, non-smoking, diabetic female. The plaque was cultured with PMA after the initial media only day and then with PMA and apocynin. This work was carried out by Sean Cross. (c) and (d) show the total neopterin and neopterin measured in a plaque from a 64-year-old, non-diabetic, recent ex-smoker male. The plaque was cultured with apocynin after the initial media only day and then with PMA.

**a****b**

**Figure 5.3 Effect of 100  $\mu$ M of apocynin (a and b) before IFN- $\gamma$  (500 U/mL) stimulation on total neopterin and neopterin production in plaque.**

(a) and (b) show the total neopterin and neopterin measured in a plaque from a 64-year-old, non-diabetic, recent ex-smoking male. The plaque was cultured with apocynin after the initial media only day and then with apocynin and IFN- $\gamma$ . On the final day, the plaque was cultured with IFN- $\gamma$  alone.

### 5.3.2 Experiments with interferon-gamma and ABAH

An experiment with interferon-gamma alone found that after two days of interferon-gamma stimulation, there were between 2-3 pmol/g of total neopterin per 1 pmol/g of neopterin (Figure 5.4). This plaque from the bifurcation of the right common and internal carotid artery had been obtained from a 56 year old diabetic, non smoking male who weighed 107 kg. The patient had experienced amaurosis fugax (blindness) in both eyes. Stenosis of the artery was reported as 80-90%.

A plaque from the left internal carotid artery was obtained from a 64 year old, non-smoking, non-diabetic male (Figure 5.5). The patient experienced TIAs and sensory loss in their right arm. Stenosis of the artery was recorded as 50-69%. Attempting to inhibit myeloperoxidase activity using ABAH had no effect on total neopterin ( $96 \pm 61$  pmol/g vs.  $118 \pm 48$  pmol/g (media only); n.s.) or neopterin ( $59 \pm 22$  pmol/g vs.  $83 \pm 51$  pmol/g (media only); n.s.) in the absence of stimulants ( a & b). Co-incubation of ABAH and interferon-gamma resulted in an increase in both total neopterin ( $319 \pm 109$  pmol/g vs.  $96 \pm 61$  pmol/g (ABAH only);  $p=0.0007$ ) and neopterin ( $184 \pm 91$  pmol/g vs.  $59 \pm 22$  pmol/g (ABAH only);  $p=0.01$ ). Further stimulation with interferon-gamma alone caused an increase in total neopterin in all sections (average increase  $139 \pm 69$  pmol/g;  $p=0.0018$ ), and neopterin in sections 3, 5, 6, and 7 (average increase for all sections  $87 \pm 82$  pmol/g;  $p=0.0312$ ). ABAH does not appear to have an effect on plaque with neither a gain of total neopterin or the ability to prevent the formation of neopterin.

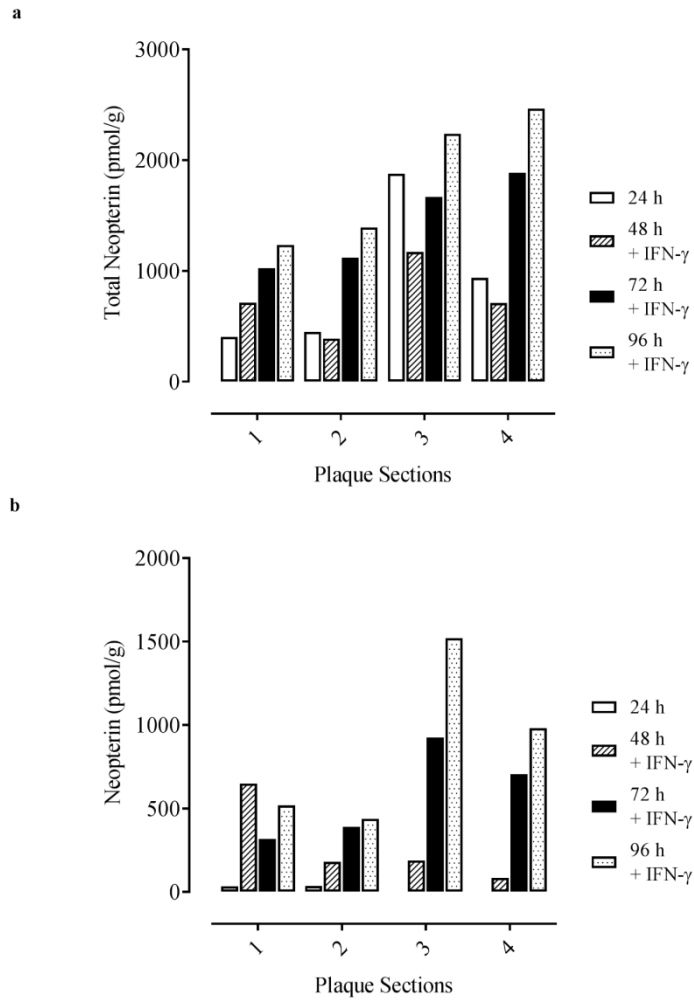


**Figure 5.4 Effect of IFN- $\gamma$  (500 U/mL) stimulation on total neopterin and neopterin production in plaque.** (a) and (b) show the total neopterin and neopterin measured in the media from a plaque obtained from a 56-year-old, non-smoking, diabetic male. The plaque was cultured for 3 days with IFN- $\gamma$  after the initial media only day.



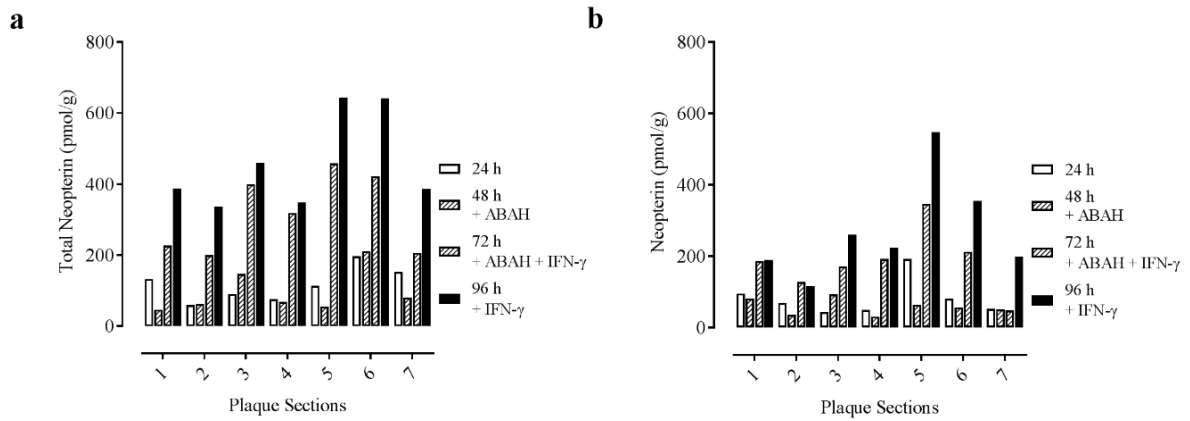


**Figure 5.5 Effect of 1 mM of ABAH (a and b) before IFN- $\gamma$  (500 U/mL) stimulation on total neopterin and neopterin production in plaque.**

(a) and (b) show the total neopterin and neopterin measured in the media of a plaque obtained from a 73-year-old, non-smoking, diabetic female. The plaque was cultured with ABAH after the initial media only day and then with ABAH and IFN- $\gamma$ . On the final day, the plaque was cultured with IFN- $\gamma$  alone.

### 5.3.3 Removing superoxide in plaque culture directly using PEG-SOD

The previous experiments with ABAH and apocynin do not conclusively implicate superoxide in the formation of neopterin. Therefore, it was thought to test removing the superoxide directly using PEG-SOD (Figure 5.6). The plaque from the right internal carotid artery of a 69-year-old female, both a smoker and diabetic, was obtained. The patient had had a stroke in their right frontal lobe. Stenosis of the artery was described as 50-69%. PMA was added to the plaque tissue for two days to reach the maximal level of macrophage stimulation, and then on the final day, either PMA was added (in sections 1, 3, 5, and 7) as a control or PMA and PEG-SOD (sections 2, 4, 6, 8) to test the effect of removing superoxide. PMA stimulation increased total neopterin in all sections at 48 hours ( $1368 \pm 1054$  pmol/g) and in 7 out of 8 sections at 72 hours ( $3562 \pm 2328$  pmol/g). Interestingly, from the lactate data it can be seen that peak glycolysis occurs at 72 hours coinciding with peak total neopterin production (Figure 5.6 e & f). At 96 hours, PEG-SOD treated section 2 showed a sustained increase in total neopterin, whereas sections 4, 6, and 8 showed a slight decrease (mean increase  $225 \pm 2277$  pmol/g; n.s. c.f. PMA only). Sections 1 and 3 experienced a dramatic decrease in total neopterin, whereas 5 and 7 had a slight increase (mean decrease  $79 \pm 138$  pmol/g; n.s. c.f. PEG-SOD). From b it can be observed that pattern of total neopterin across the sections of the plaque does not appear to change with the addition of PEG-SOD. Neopterin increased in 7 sections at 48 hours, and in 5 sections at 72 hours. At 96 hours there was a decrease in neopterin across all sections, regardless of whether PEG-SOD was added or not.

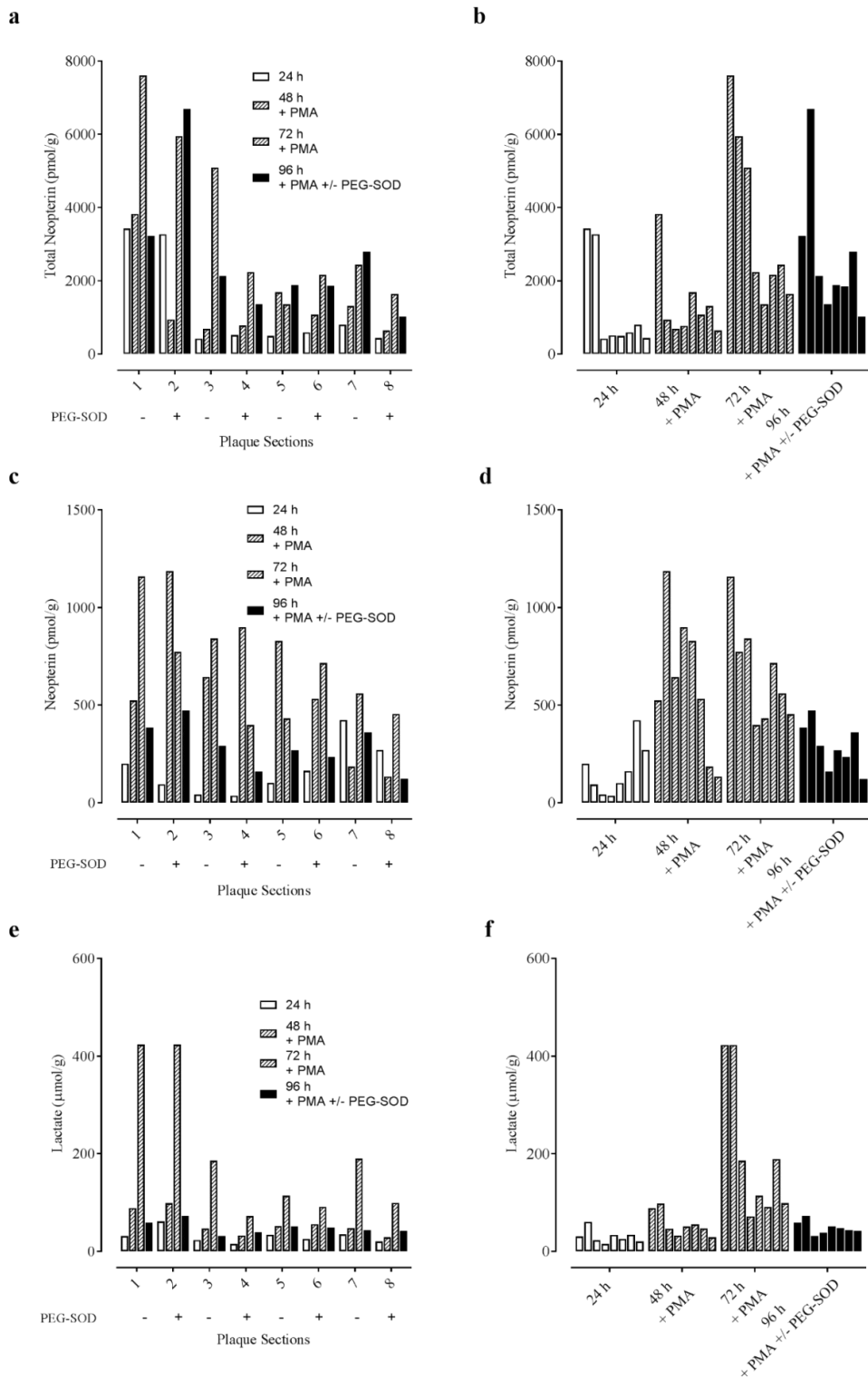


**Figure 5.6 Effect of  $5\mu\text{M}$  of PMA and PEG-SOD ( $50\text{ U/mL}$ ) on total neopterin (a and b), neopterin (c and d) and lactate (e and f) production in plaque.**

(a) shows the total neopterin measured in the media from a plaque obtained from a 69-year-old, smoking, diabetic female graphed according to each section, whereas (b) displays the same data per day. The plaque was cultured with PMA for two days after the initial media only day and then with PMA and PEG-SOD. (c) and (d) show the neopterin measured from the same plaque. (e) and (f) show the measured lactate levels.

#### 5.3.4 Increasing the oxidant production in plaque by adding oxidized LDL

Adding oxLDL to plaque culture after stimulating with PMA caused an increase in neopterin output (Figure 5.7). The plaque from the right internal carotid artery was obtained from an 81-year-old non-smoking, non-diabetic male. The patient had experienced a stroke and had previously had a plaque from their left internal carotid artery removed in 2005. Stenosis of the artery was reported as 50-69%. In the absence of oxLDL, sections 1, 3, 7 experienced an increase in total neopterin compared to the previous day. In section 5, however, total neopterin decreased substantially from the previous day. The overall effect was no statistically significant change in total neopterin. In sections treated with oxLDL the results were also mixed, 2 of the sections (2, 8) had an increase in total neopterin, whereas sections 4 and 6 had a decrease. In the case of neopterin, all sections treated with oxLDL showed an increase, and d shows that these sections are clearly producing more neopterin than the neighbouring sections, however, on the average difference in neopterin of 149 pmol/g between sections with oxLDL and without oxLDL is not significant. Combining sections showed there was no significant difference between those treated with and without oxLDL (Figure 5.8). OxLDL had no obvious effect on lactate production.

A second experiment was conducted using native LDL (n-LDL) as the control instead of PBS. Sections were incubated with either nLDL (sections 1, 3, 5, 7) or oxLDL (2, 4, 6, 8) for two days (Figure 5.9). This plaque from the left carotid artery of an 85-year-old, non-diabetic male had been obtained. The patient had experienced a TIA and the stenosis of the artery was reported as 70-80%. Lactate was assessed to see if oxLDL influenced plaque metabolism. In sections incubated with nLDL, total neopterin increased at 48 hours ( $307 \pm 92$  pmol/g vs.  $156 \pm 81$  pmol/g (media only);  $p=0.017$ ). At 72 hours, total neopterin decreased in section 1, remained relatively constant in section 7, and increased in sections 3 and 5. OxLDL treatment resulted in an increase in total neopterin in all sections at 48 hours (mean =  $423 \pm 187$  pmol/g) and in section 2 at 72 hours. Sections 4 and 6 experienced a slight decrease in total neopterin at 72 hours. Treatment with oxLDL caused a continual increase in neopterin in all plaque sections (mean values:  $35 \pm 19$  pmol/g, 24 h.;  $203 \pm 99$  pmol/g, 48 h;  $233 \pm 131$  pmol/g, 72 h). Sections 4 and 6 both seem to produce much more neopterin than the surrounding sections. OxLDL treatment appeared to have no effect on lactate levels (figure 5.7). In contrast, nLDL treatment increased neopterin at 48 hours ( $96 \pm 31$  pmol/g vs.  $31 \pm 8$  pmol/g; n.s.), although this was not statistically significant, but the effect at 72 hours was more variable (mean  $103 \pm$

84 pmol/g). Intriguingly, sections treated with nLDL experienced a large decrease in lactate production at 72 hours, which did not occur in the oxLDL treatment.

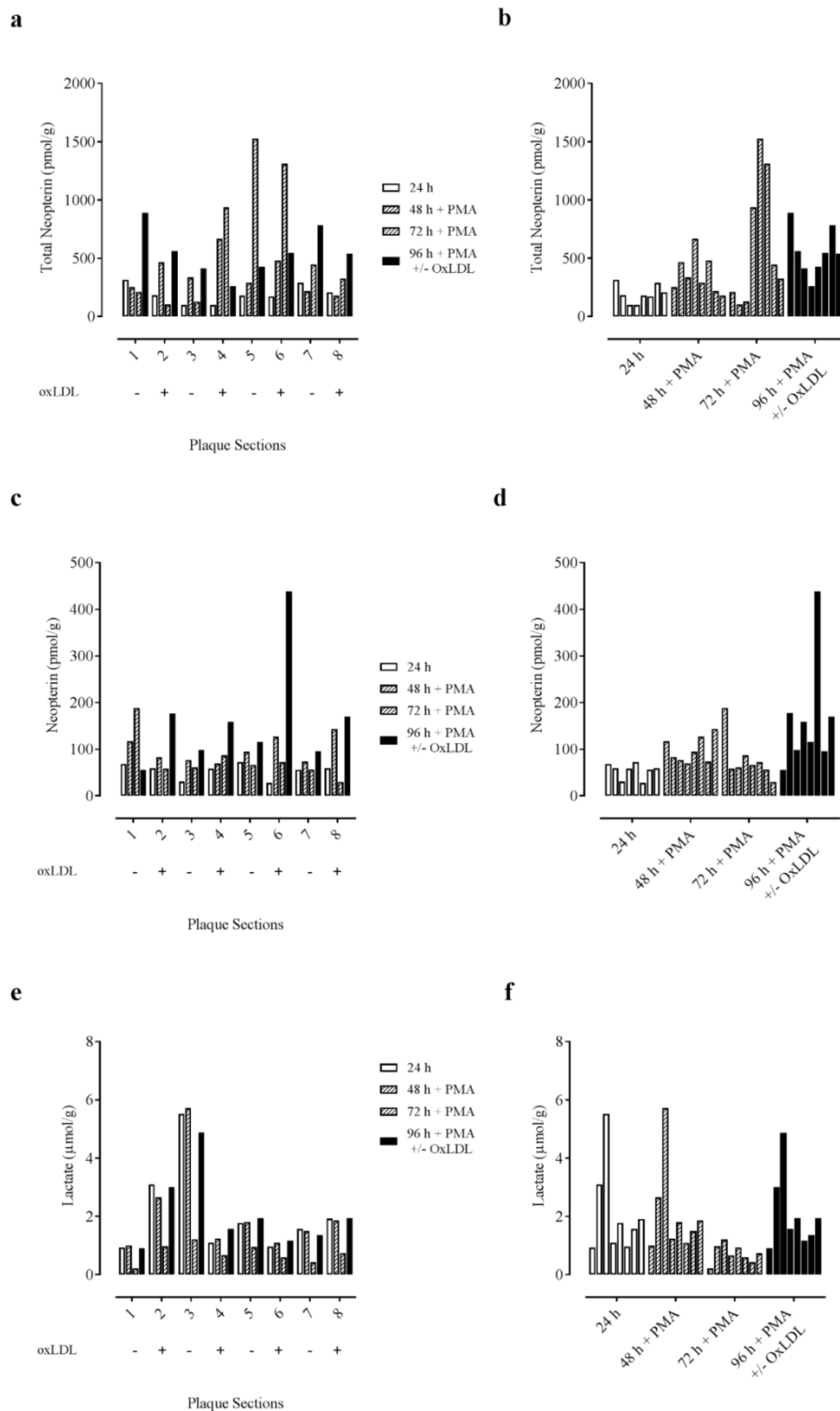


**Figure 5.7 Effect of 5µM of PMA and OxLDL (2 mg/mL) on total neopterin (a and b), neopterin (c and d) and lactate (e and f) production in plaque.**

(a) shows the total neopterin measured in the media from a plaque obtained from an 81-year-old, non-smoking, non-diabetic male graphed according to each section, whereas (b) displays the same data per day. The plaque was cultured with PMA for two days after the initial media only day and then with either PMA alone or PMA and oxLDL. (c) and (d) show the neopterin measured from the same plaque. (e) and (f) show the measured lactate levels.

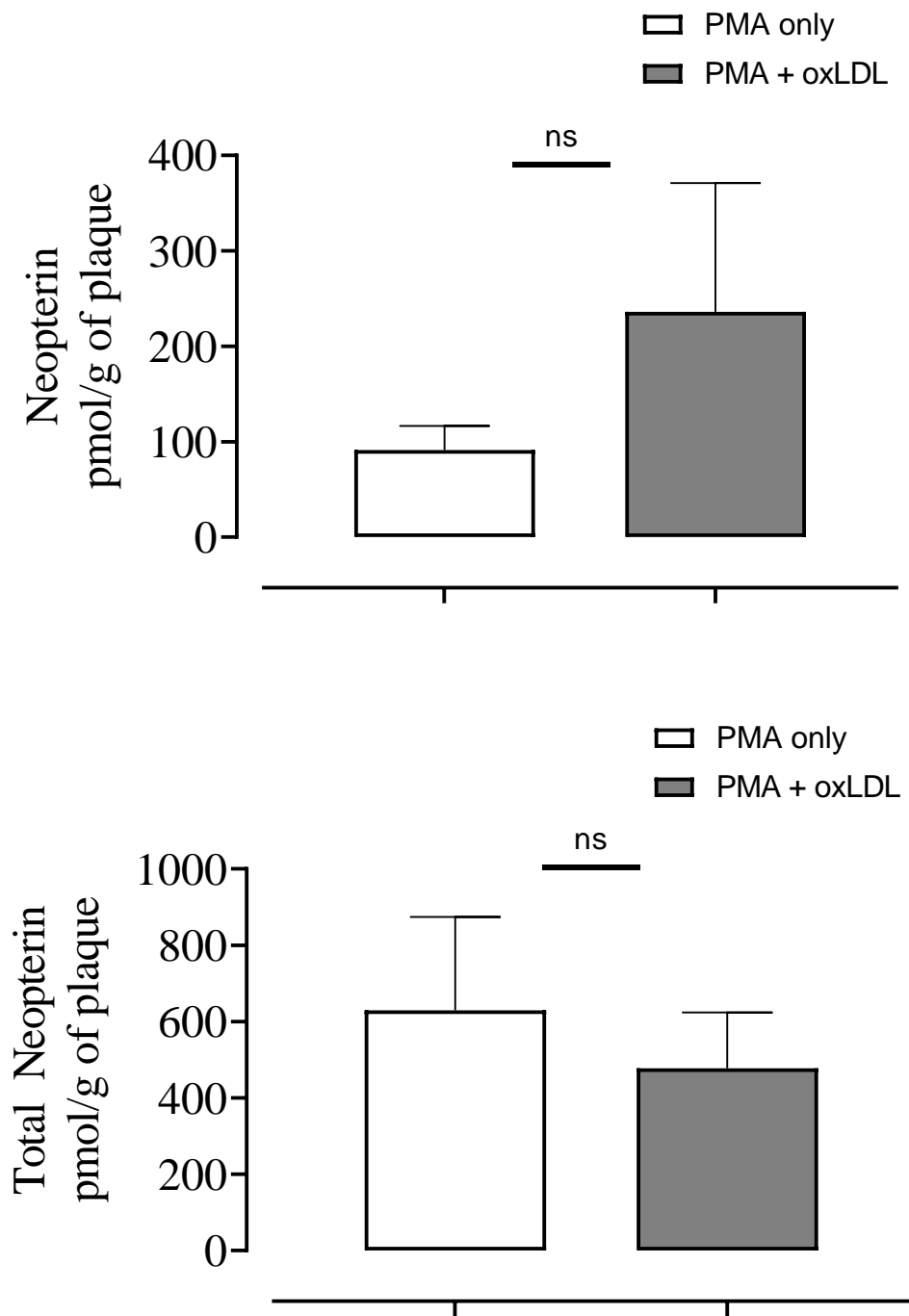
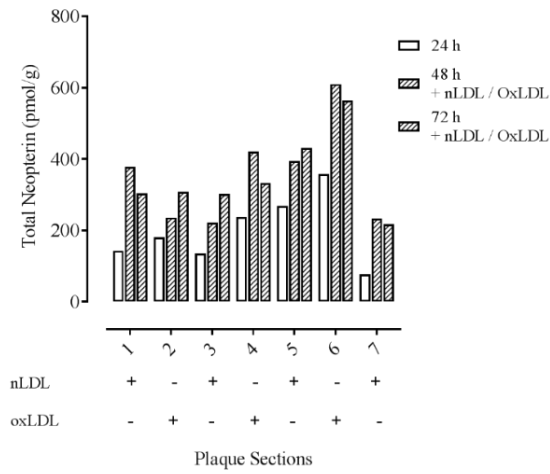


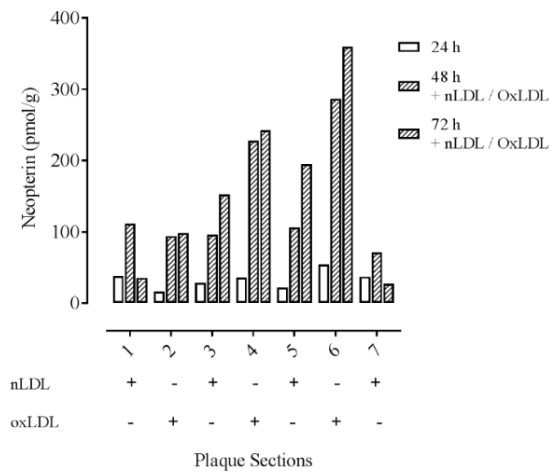
**Figure 5.8 Combined plaque sections after incubation with 5 $\mu$ M of PMA with or without OxLDL (2 mg/mL) on neopterin (a) and total neopterin (b)**

shows the total neopterin measured in the media from a plaque obtained from an 81-year-old, non-smoking, non-diabetic male. Data is mean with SD. An unpaired t-test was carried out on each dataset (n=4). There was no statistical difference between the presence or absence of oxLDL for either neopterin (p=0.0795) or total neopterin (p=0.3296).

**a**



**b**



**c**

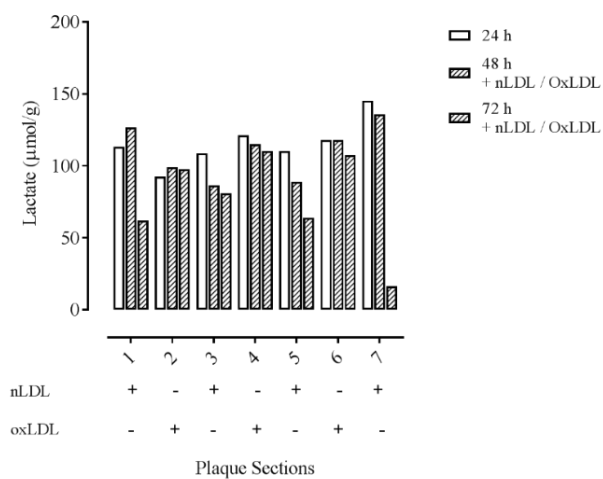


**Figure 5.9 Effect of OxLDL (2 mg/mL) and nLDL (2 mg/mL) on total neopterin (a), neopterin (b) and lactate (c) production in plaque.**

(a) shows the total neopterin measured in the media from a plaque obtained from an 81-year-old, non-smoking, non-diabetic male. The plaque was cultured with either nLDL or oxLDL for two days after the initial media only day (b) shows the neopterin measured from the same plaque. (c) shows the measured lactate levels.



### 5.3.5 Increasing and inhibiting oxidants in macrophages

In HMDM cells with no exogenous 7,8-dihydroneopterin, the experiment took place over 12 hours, to prevent major cell loss because of oxLDL toxicity. Treatment with oxLDL caused a small but non-significant rise in intracellular total neopterin (Figure 5.10). Co-incubation of oxLDL with PEG-SOD resulted in 91.5 pmol/mg protein of total neopterin. OxLDL and PEG-SOD with oxLDL both resulted in a decrease in intracellular neopterin compared to a cell only control (10 pmol/mg and 8.8 pmol/mg respectively, c.f. 14.8 pmol/g for the control). However, the extracellular results were the opposite. OxLDL alone and oxLDL with PEG-SOD decreased total neopterin compared to the control (84 pmol/g and 53 pmol/g respectively, c.f. 150 pmol/g for the control) and increased neopterin (11 pmol/g and 16 pmol/g respectively, c.f. 8.9 pmol/g for the control). When the intra- and extracellular results are combined, in the absence of exogenous 7,8-dihydroneopterin, oxLDL decreased total neopterin, whether PEG-SOD is present or not, but there is little to no effect on neopterin. PEG-SOD appears to influence the location of the total neopterin and neopterin, increasing intracellular total neopterin and extracellular neopterin.

In HMDM cells with exogenous 7,8-dihydroneopterin, the experiment was carried out at 24 hours to better match the plaque experiments. OxLDL toxicity is unlikely to be an issue in the presence of exogenous 7,8-dihydroneopterin which is known to protect against cell death. Photographs of the cells show no evidence of cell death (Figure 5.12). The addition of PEG-SOD without oxLDL significantly ( $p=0.01$ ) increased intracellular total neopterin by 3090 pmol/g (Figure 5.11). PEG-SOD in the presence of oxLDL ablated the decrease in total neopterin that occurred in the oxLDL only treatment. OxLDL caused a small decrease (70 pmol/g) in neopterin, however, this was not statistically significant. HMDMs treated with oxLDL had significantly less extracellular total neopterin compared to the control ( $p<0.0001$ ), whereas the introduction of PEG-SOD in the absence of oxLDL cause a significant rise in total neopterin (35.70 nmol/g) compared to the control. As occurred in the intracellular results, PEG-SOD in conjunction with oxLDL ablated the decrease in total neopterin that occurred within the oxLDL only treatment. Finally, treatment with oxLDL in the presence or absence of PEG-SOD had no effect on neopterin, however, treatment with PEG-SOD alone significantly decreased extracellular neopterin. PEG-SOD appears to be better at protecting cells from extracellular 7,8-dihydroneopterin loss in the presence of exogenous 7,8-dihydroneopterin.

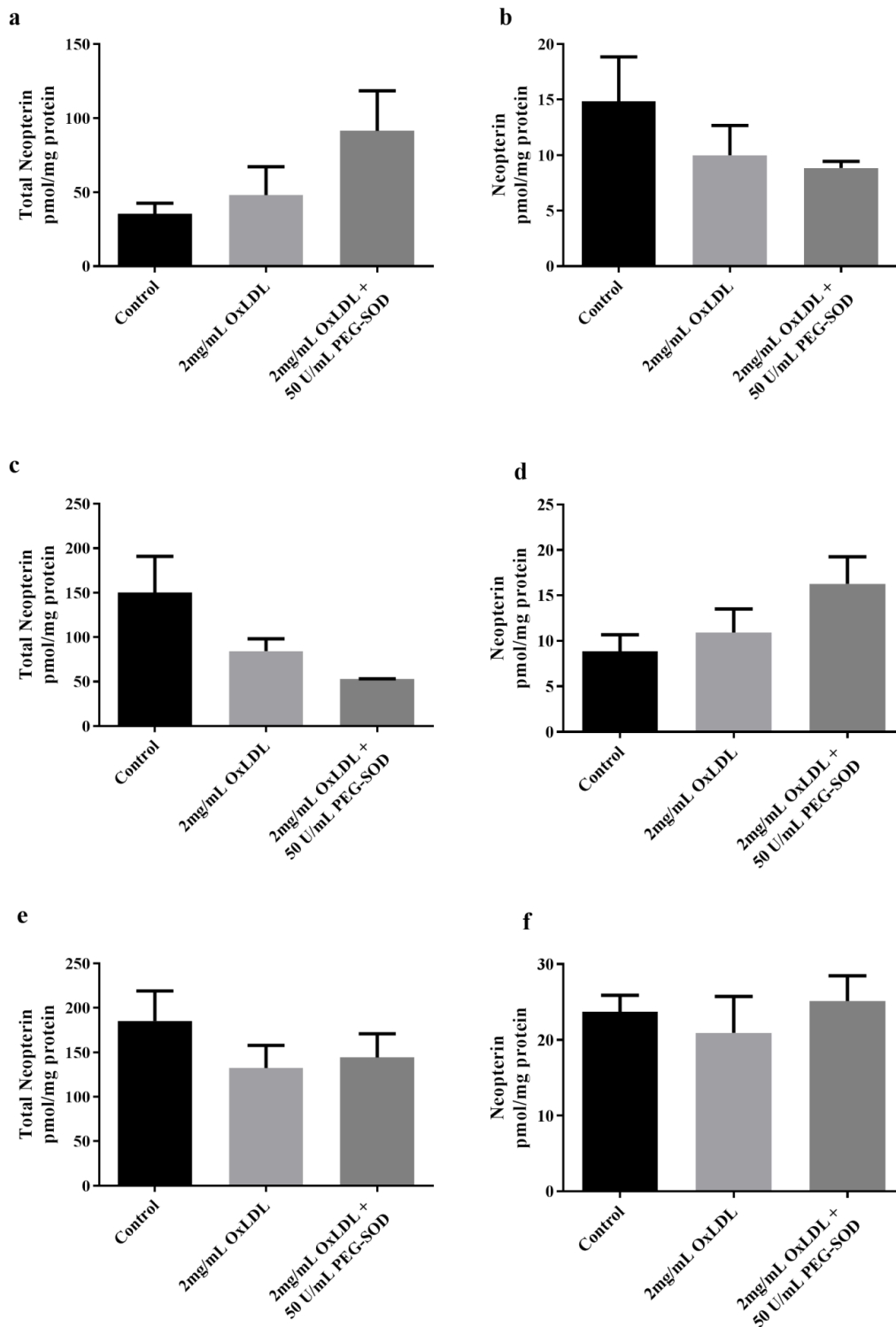


**Figure 5.10 Effect of 2mg/mL of oxLDL and 50 U/mL of PEG-SOD on intracellular and extracellular total neopterin and neopterin on HMDM cells in the absence of exogenous 7,8-dihydroneopterin.**

HMDM cells with either PBS, 2 mg/mL of oxLDL, 2 mg/mL of oxLDL with 50 U/mL of PEG-SOD or 50 U/mL of PEG-SOD alone for 12 hours (n=3). Intracellular total neopterin and neopterin were measured in a HMDM culture (a) and (b), and extracellular total neopterin and neopterin (c) and (d). (e) and (f) represent the combined intracellular and extracellular values. Error bars represent SEM. A one-way ANOVA was performed, and there was no statistically significant difference between any of the data.

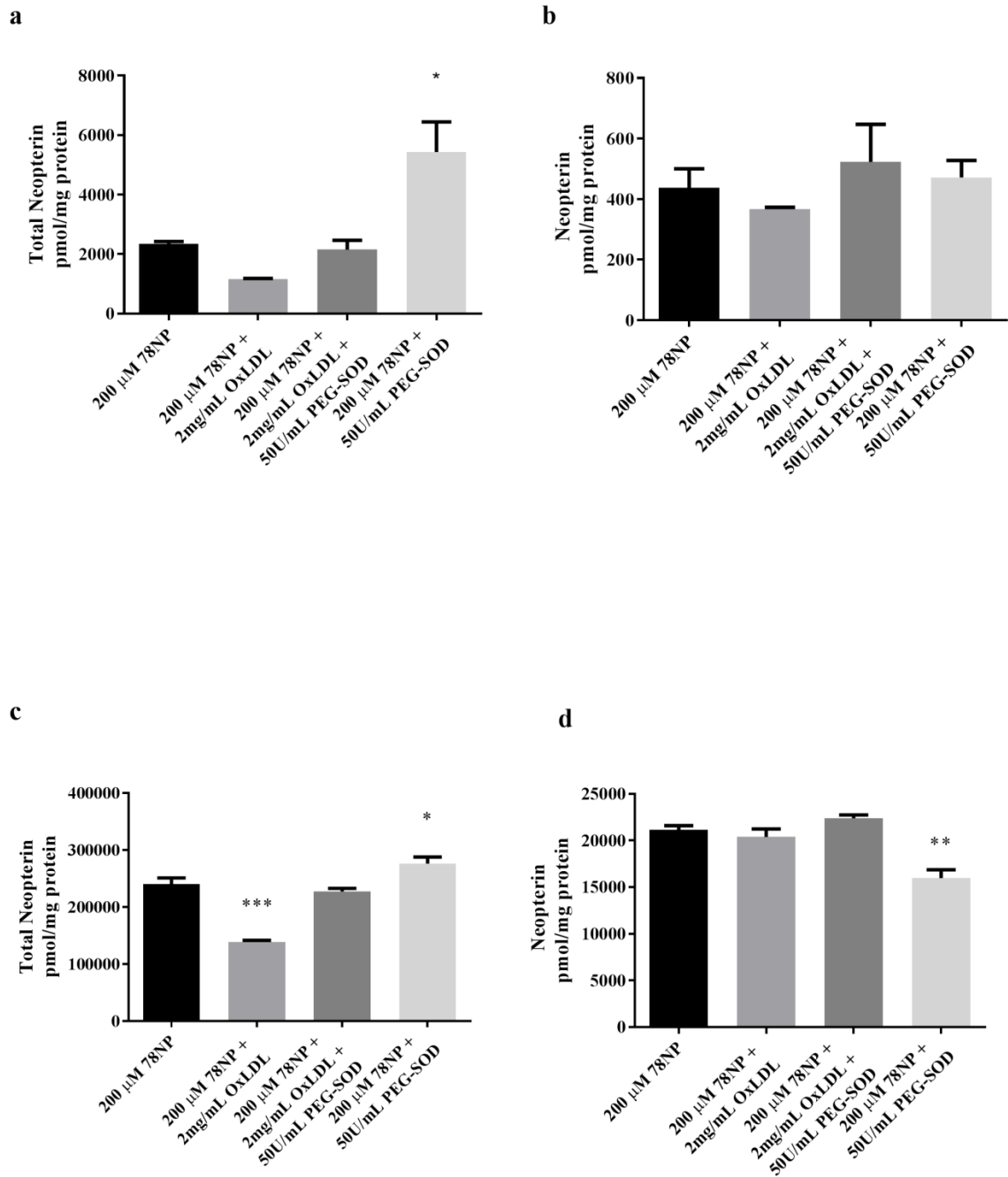


**Figure 5.11** Effect of 2 mg/mL of oxLDL and 50 U/mL of PEG-SOD on intracellular and extracellular total neopterin and neopterin on HMDM cells in the presence of exogenous 7,8-dihydroneopterin (200  $\mu$ M).

HMDM cells were incubated in 200  $\mu$ M of 7,8-dihydroneopterin for two hours prior to the addition of either PBS, 2 mg/mL of oxLDL, 2 mg/mL of oxLDL with 50 U/mL of PEG-SOD or 50 U/mL of PEG-SOD alone for 24 hours (n=3). Intracellular total neopterin and neopterin were measured in a HMDM culture (a) and (b), and extracellular total neopterin and neopterin (c) and (d). Error bars represent SEM. Significance is indicated as compared to the 7,8-dihydroneopterin only control: \* indicates  $p < 0.05$ ; \*\*,  $p < 0.01$ ; \*\*\*,  $p < 0.001$ .

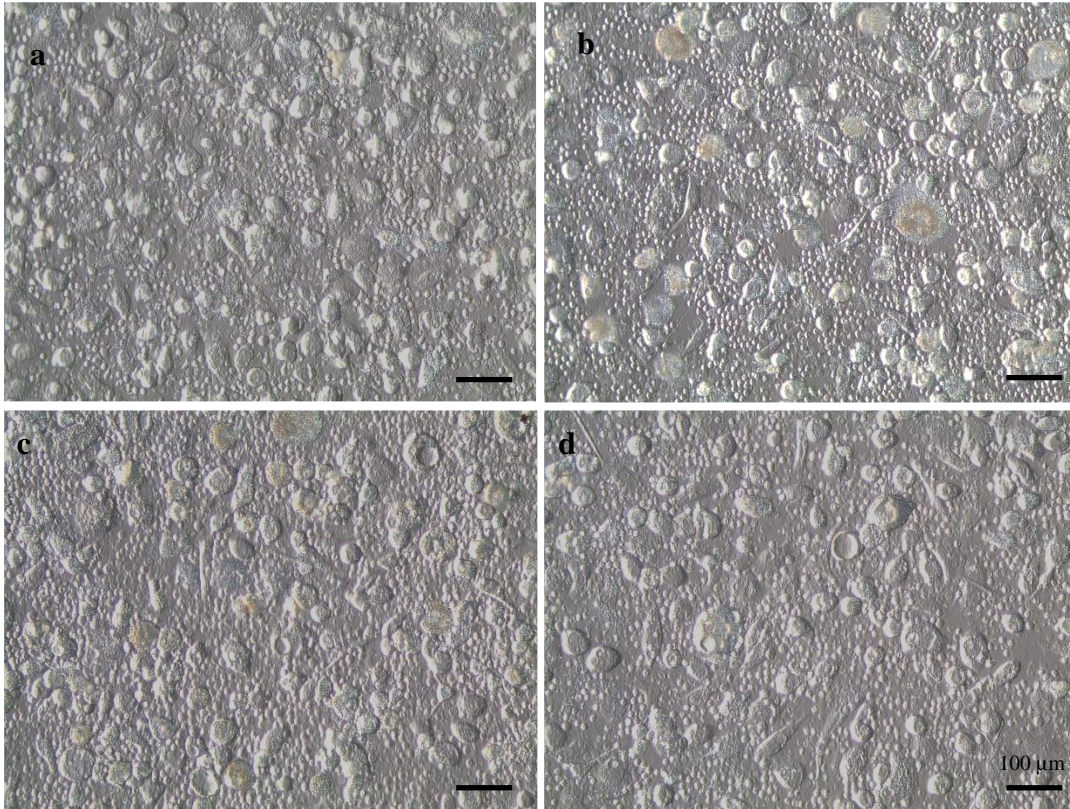
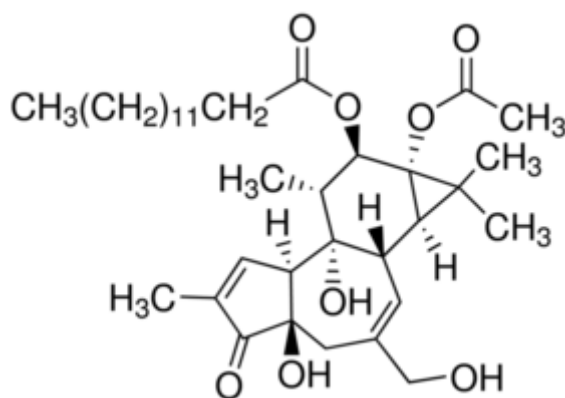


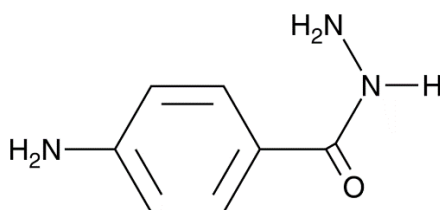
**Figure 5.12 Light microscopy of HMDM cells after 24 hours culture.** a) represents HMDMs that were treated with 78NP only, b) had both 78NP and oxLDL, c) had 78NP, oxLDL, and PEG-SOD, and d) had 78NP and PEG-SOD.

## 5.4 Discussion

The effect of ABAH on plaque appears to be muted. One might suggest that it is not possible to know whether the ABAH molecule inhibited MPO, as there was no change in measured total neopterin or neopterin. Comparing the ABAH molecule to apocynin (Figure 5.13) or PMA, which have both been found to act upon plaque, there is no immediate reason to believe that this molecule would not be taken up by the plaque. This plaque responded to the introduction of IFN- $\gamma$ , so it is unlikely there is anything relating specifically to this plaque that would prevent uptake from occurring, although it is recommended that for future experiments as secondary marker is used to confirm uptake of the target molecule. Furthermore, the use of ABAH to inhibit MPO is well characterized in cell culture experiments (Kettle et al., 1995). A possible reason for the limited effect is significant amounts of MPO are not present in plaque at this advanced stage. Sugiyama et al. (2001) identified some MPO-positive macrophages in ruptured plaque (~118 per 100x field of view). However, it was clear not all macrophages in the plaque were producing MPO. In addition, they found little evidence of MPO-positive neutrophils. This suggests that the processes occurring in plaque are likely quite separate to the rapid neopterin generation seen in bacterial conditions like sepsis.



PMA



ABAH

Figure 5.13 Chemical structures of PMA and ABAH

As the results indicate that MPO may not be particularly active in the plaque, then it is possible that apocynin may be having an antioxidant effect in the plaque culture experiments rather than directly inhibiting NOX. This hypothesis could be confirmed through direct measurement of MPO in the plaque. This may explain why the effect on total neopterin is much larger than the effect on neopterin. It may also explain why removing apocynin from the media produced an immediate increase neopterin. A comparison to other known antioxidant in plaque culture would be useful to further understand this effect. Whilst the experiments with apocynin do not give a clear answer on the involvement of NOX in the generation of superoxide in plaque, they do show that adding 100  $\mu$ M apocynin is not enough to prevent neopterin formation.

The effect of PEG-SOD and oxLDL in HMDMs seems to be at complete odds with the plaque data. Excess 7,8-dihydroneopterin in plaque culture was generated using PMA but was likely to be lower than the 200  $\mu$ M 7,8-dihydroneopterin added to HMDM culture. PMA also has the effect of generating superoxide, but PEG-SOD in plaque did not seem to have any major effect on total neopterin or neopterin, so potentially PMA is not generating a large number of oxidants. This is backed up by the evidence that generally in plaque tissue treated with PMA the amount of total neopterin being generated is 5-7x higher than the amount of neopterin being produced. The PEG-SOD was carried out in a high responder plaque, whereas the oxLDL experiment was carried out in a low-responder plaque.

It seems from this work that is very easy to increase 7,8-dihydroneopterin or neopterin production in plaque tissue but shutting down this process is a much more difficult task. If anything, these results appear to suggest that the cells in plaque tissue are responding correctly. The cells identify a threat or increase in oxidants, there is a burst of antioxidant activity, and then there is a slow down once the threat has been dealt with. Perhaps, but incubating the plaque tissue with such high levels of stimulants to ensure a response, it is mimicking a situation of bacterial threat. It would be interesting to experiment with constant low doses of oxidants to measure the response in a situation that is likely to be more similar to the slower progression of atherosclerosis. Particularly of note from these experiments and those in Chapter 4, is that the plaque clearly has the capability to produce significant quantities of both 7,8-dihydroneopterin and neopterin, however, it is very rare that they do on the media only day. This seems to suggest that the plaques, although they are vulnerable, and have often recently ruptured, are not in an activated state.

### 5.4.1 Plaque Culture

Plaque culture provides an effective system to test how the plaque tissue truly behaves but this has several aspects that are not possible to control. These begin at the patient level, with a wide age range, patients on a mixture of different drug treatments, and different patient histories (smoker, diabetic). It is not possible to know how these variables impact the result that is seen in the tissue. If enough plaques could be collected it may be possible to do a multi-factorial statistical assessment to find which changes at the patient level have a significant impact on biomarkers. At present, with just receiving plaques from a single hospital that services a population of less than 500,000 it is too difficult to obtain enough numbers to conduct this kind of study. However, the ability to do large scale testing is further limited by time constraints. Each plaque culture and analysis takes a minimum of a week. For the meantime that limits the research to studies where relative changes in biomarkers are assessed as opposed to absolute biomarker levels. Despite these limitations, these experiments are beneficial in the context that many of these questions have never been explored in plaque tissue previously.

At the experimental level there are also several factors at play. It is not possible to cut the sections to be the same size, as even if the sections are sliced at the same width, they vary in diameter and thickness. This will always result in variations in surface to volume ratio. Again, it is unknown whether this difference in tissue size has implications for the results. Typically, treatments are added at a standard dose without considering the size or weight of the tissue. It is possible some of the differences in the response of the tissue may be due to some pieces receiving a dose of 20  $\mu\text{M}$  per gram and others receiving 8  $\mu\text{M}$  per gram. This issue becomes fraught when considering that the weight of the piece of tissue may be greatly affected by the volume of calcium present. Ideally, one would know the cellular (or non-calcified) composition of the tissue before beginning the experiment, however, with the time required to process the material decomposition of the MARS image, this is not currently feasible. However, it is likely with improvements to the system, this should be feasible soon. Fortunately, this is not such an issue for considering how typical drug treatments impact plaque inflammation status, which would normally be delivered as a bolus *in vivo*, for example, understanding the effects of statins. For this reason, this is probably the best avenue to exploit with the plaque culture system going forward.

The method employed here has been to carry out a single experiment per donated plaque. This limits the ability to carry out statistical analysis as even though the plaque is cut into 7 or 8

sections, the n value per experiment is 1. But with the very limited supply of plaques available, carrying out the same experiment across multiple plaques would greatly limit the number of questions that could be investigated. Proposed here is a new method, which would overcome some of these issues. This new method has been developed based on the results from the plaque experiments in this thesis. This would involve using two sections from each plaque to conduct an experiment, one from the outer edge, and one from the inner part, as the experiments in this thesis have shown that these two areas behave differently. In an 8 section plaque experiment 1 would be conducted on sections 1 and 5, experiment 2 on sections 2 and 6 and so on. This would allow four experiments per plaque. These same experiments would then be repeated across five separate plaques. That would provide four experiments with n=5 and a total of 10 data points each, which should be enough to carry out statistical analyses. This should reduce variation, as showed that plaque segments from similar parts of the plaque behave more similarly to each other than those from different regions within a single plaque.

There is difficulty in modifying just a single variable at a time due to temporal effects. The experiment with a single dose of interferon gamma showed the prolonged effect the stimulation had even the interferon gamma was removed from the media. This continued effect is most likely due to modifications at the DNA and RNA level, which from time of stimulation can take 24-48 hours to reach their peak. This becomes difficult if you are adding a different treatment each day and trying to isolate the effect of that treatment. The experiment with PMA + PEG-SOD showed this. If all segments had had PEG-SOD added on the final day, the decrease in neopterin and total neopterin would have been thought to be due to the addition of the PEG-SOD, but the control cells which only had PMA showed a decrease was also naturally occurring. The reason for stimulating the plaques was two –fold: one, to produce a signal that is high enough to be easily assayed by HPLC and two, to mimic an active plaque amid inflammation. However, the amount of stimulus added is probably excessive compared to what would be normally found, and it may be better to investigate plaque behaviour without artificial stimulation. This would make the HPLC assay more difficult as the changes in neopterin would be much subtler, but this could be overcome by spiking the samples with a known concentration of neopterin to give greater clarity to the peaks. If the plaque has not been pre-stimulated, then it is possible to be confident that the effect measured is due to the stimulus added. To assess, combinations of effects, its best to carry these out in separate experiments. For example, a single experiment with oxLDL, and then a second experiment testing the effect of oxLDL with 7,8-dihydroneopterin. These two experiments would be carried out as described earlier so the



only difference would be that they were using different sections from plaques, but the data points would be made up by the same patients, which should eliminate plaque to plaque variation.

## 5.5 Conclusion

Oxidant production in excised plaque tissue can be modulated through the addition of exogenous stimulants. This provides a system to test the response of plaques to other compounds such as statins or other medications patients may be receiving to learn how this affects the oxidative biomarkers that are measured in clinical settings.

## 6 Plaque baseline production of 7,8-dihydroneopterin and neopterin: correlation to plasma markers

In this chapter, I collected, cultured and carried out the analysis for 11 of the plaques. 5 plaques were prepared by Sean Cross. All data interpretation in the chapter is my own.

### 6.1 Introduction

Neopterin has shown promise as an inflammatory biomarker for cardiovascular disease. However, the relationship of neopterin and 7,8-dihydroneopterin as measured in the plasma compared to its production in excised plaque tissue has not previously been explored. In fact, there is no evidence from the literature of a plasma biomarker being compared to its production in a live tissue counterpart. It is hypothesized that plaque tissue is a major source of plasma neopterin and 7,8-dihydroneopterin *in vivo* (Adachi et al., 2007; S. P. Giese et al., 2008). As mentioned previously, due to its small size, neopterin diffuses out of tissue into the plasma. Neopterin is cleared fairly rapidly from the plasma into the urine via glomerular filtration (Werner et al., 1987), but it is less clear whether 7,8-dihydroneopterin is cleared as effectively as neopterin. At present, there is a lack of studies investigating plasma 7,8-dihydroneopterin levels. The aim of this chapter is to investigate whether there is a relationship between plasma total neopterin, 7,8-dihydroneopterin or neopterin and their plaque counterparts. This likely depends on whether the excised piece of tissue is representative of the level of inflammation occurring in the patient's cardiovascular system as a whole. Due to the small nature of this study, correlations have been carried out on an unadjusted dataset. It is recognized that factors such as age and sex are known to affect patient neopterin levels (M. E. Spencer et al., 2010), but given that this work is exploring the relationship between matched plasma and tissue samples, these factors are unlikely to have a major effect. In addition, the correlation of blood lactate with the inflammatory markers is also considered. Lactate was already being monitored in the plaque media as a method for obtaining glycolytic activity, plasma (or blood) lactate has previously been identified as being increased during carotid atherosclerosis (Shantha et al., 2013). Blood lactate has also been hypothesized as a marker of oxidative capacity (Mongraw-Chaffin et al., 2012).

## 6.2 Methods in brief

This chapter examines the baseline plaque production of neopterin and total neopterin (and by subtraction, 7,8-dihydroneopterin). All readings were taken from the supernatant from the second day of culture, after an initial wash out day. The plaques at this stage were only incubated with human serum containing media. No stimulants were added. The plasma samples that were analysed were obtained just prior to surgery. Neopterin and total neopterin levels in the media and plasma were determined HPLC as previously described.

In this chapter, total neopterin and neopterin values are standardized by the plaque section weight. Correlations are carried out using the average value i.e. total neopterin or neopterin output per plaque (standardized per gram) divided by the number of sections. This analysis was limited to plaques that were suitable for tissue culture (n = 16). Plaques examined were 112, 113, 114, 116, 119, 120, 122, 123, 126, 127, 129, 131, 134, 135, 137, 138 – refer to Appendix B. Not all plaques had a blood sample supplied by the surgeon. Four plaques without plasma samples have been excluded from the correlation (n=12). One plaque was not correctly assessed for lactate and has been excluded (n=11).

Media lactate concentrations were determined using a lactate assay as described in Chapter 2.

## 6.3 Results

### 6.3.1 Variation in whole plaque and plaque section weight

The number of sections produced by each plaque is limited by the length of the excised specimen. Only one plaque produced less than five sections (**Table 6.1**). Five plaques produced seven sections and ten plaques that produced eight sections. The average section weights are similar but there is a wide standard deviation, particularly for sections 2 and 3. Although the procedure aimed to produce sections of a consistent width, this was not always possible due to areas of dense calcification that caused the scalpel blade to deflect. Even if the width was consistent, it was not possible to control the tissue diameter or volume (level of stenosis) within or between plaques. Plaque total weight ranged between 0.4 g and 1.4 g with most plaques weighing between 0.7 and 0.9 g (**Figure 6.1**). Tissue thickness and the amount of calcification present likely contributed to this variation.

**Table 6.1 Average weight per plaque section from all cultured plaques.**

Each plaque was sectioned into pieces of approximately 2mm width. This resulted in between 4 and 8 plaque sections depending on the length of the piece of tissue. Individual tissue culture plates were weighed. The plaque section was then placed into the plate and reweighed. The plate weight was then subtracted to find the section weight.

Section	Average Weight (g)	SD	N
1	0.085	0.055	16
2	0.089	0.095	16
3	0.090	0.087	16
4	0.092	0.045	16
5	0.093	0.056	15
6	0.095	0.045	15
7	0.101	0.038	15
8	0.103	0.044	10

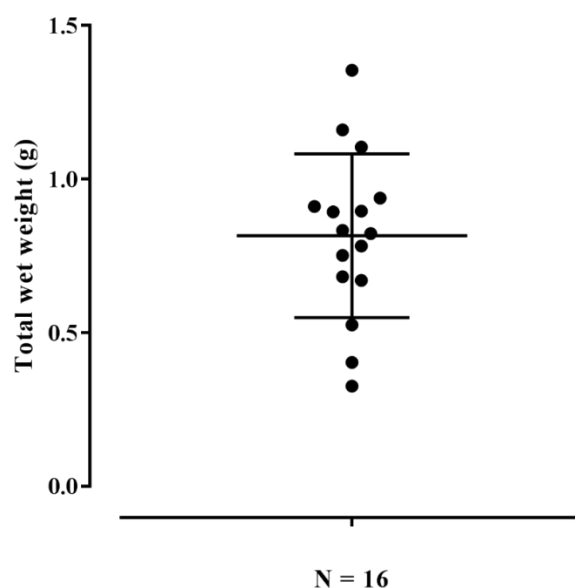


**Figure 6.1 Mean and Standard Deviation of Total Plaque Weight from Cultured Plaques.**  
Plaques were weighed whole prior to sectioning, immediately after arrival in the laboratory.

### 6.3.2 Variation in total neopterin and neopterin in media and plasma between individuals

The average total neopterin output in plaque was most variable in sections 1, 2, 3, 8 (**Figure 6.2**). Total neopterin values had a much wider range than neopterin (0 – 7800 pmol/g vs 0 – 1100 pmol/g respectively). Neopterin showed a relatively similar amount of variation across all sections, with mean neopterin values close to 250 pmol/g for all sections. A comparison of the total plaque output of total neopterin compared to neopterin clearly demonstrates this difference in variation between the two (**Figure 6.3**). The graph of total plaque output suggests that some patients have a much higher antioxidant capacity being generated by their plaques than others, as evidenced by the difference between the total neopterin and neopterin values. Interestingly, by comparison plasma does not show such a clear difference with neopterin and total neopterin values varying by roughly similar ranges (15- 45 nM for total neopterin and 8 – 30 nM for neopterin) (**Figure 6.4**). The next section examines the relationship between plaque antioxidant capacity and plasma antioxidant capacity.

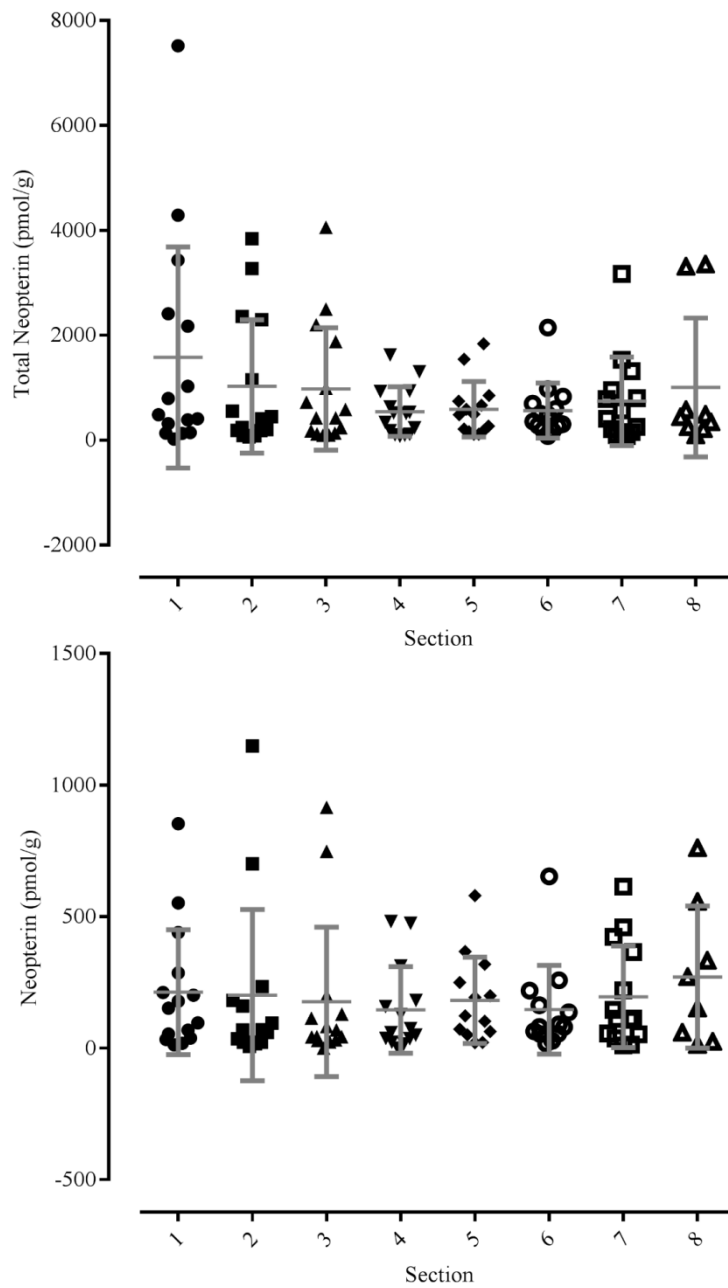


**Figure 6.2 Mean and Standard Deviation of Baseline Total Neopterin and Neopterin produced in all cultured plaque sections.**

The plaques were incubated in RPMI-1640, supplemented with 10% human serum for 24 h. The media from the cultured plaque sections were assayed for neopterin and total neopterin using the SCX HPLC method. A one-way ANOVA was performed. There was no statistical difference in total neopterin or neopterin production between sections.

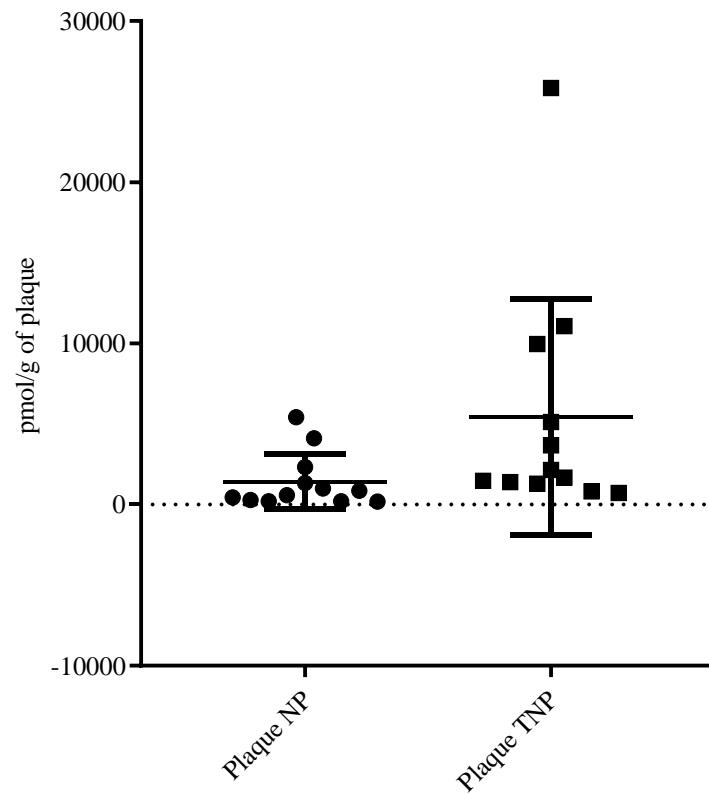


**Figure 6.3 Mean and Standard Deviation of Baseline Neopterin and Total Neopterin produced in all cultured plaques.**

The plaques were incubated in RPMI-1640, supplemented with 10% human serum for 24 h. The media from the cultured plaque sections were assayed for neopterin and total neopterin using the SCX HPLC method. Neopterin and total neopterin values from the sections of each plaque were summed together. A paired t-test was performed (n=12). There was no statistical difference between total neopterin and neopterin production (p=0.068).

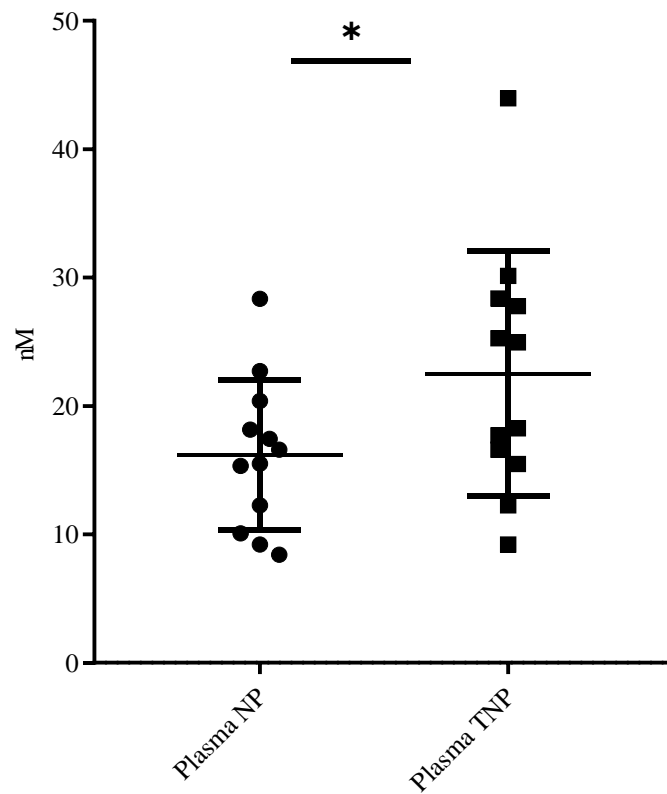


**Figure 6.4 Mean and Standard Deviation of Neopterin and Total Neopterin in patient plasma samples.**

Patient plasma samples were obtained immediately prior to surgery. The plasma was separated from the red blood cells by centrifugation. The plasma samples were assayed for neopterin and total neopterin using the SCX HPLC method. A paired t-test was performed (n=12). There was a statistical between neopterin and total neopterin in the plasma samples (p=0.0157).



### 6.3.3 Relationship between neopterin, 7,8-dihydroneopterin and total neopterin

The table below (Table 6.2) shows the relationship between total neopterin, neopterin and 7,8-dihydroneopterin values in the plasma of carotid endarterectomy patients. The table has been arranged according to their 7,8-dihydroneopterin concentration. Quartiles were determined from the patient data. The 1st quartile is labelled low; however, this term low means relative to the other patients as opposed to healthy controls. The lowest neopterin value measured in this cohort was 8.42 nM (maximum; 28.3 nM) whereas the reported healthy range for neopterin is 5-7 nM (Tatzber et al., 1991). Patients with low 7,8-dihydroneopterin (less than 2.3 nM) exhibited high or very high neopterin levels, with only one patient with low levels of total neopterin. This suggests this group is experiencing increased oxidative stress. Patients with high or very high 7,8-dihydroneopterin levels had variable neopterin and total neopterin levels. This suggests that high 7,8-dihydroneopterin levels are not purely due to high inflammation or low oxidation but rather a complex interplay between the two. As this study was open to all patients undergoing endarterectomy surgery at Christchurch Hospital, this is a cross-sectional group. The information about the patient's co-morbidities and percent stenosis have been recorded in the table below but there are not enough data points in each category to assess any relationship between % stenosis, disease severity or co-morbidities and 7,8-dihydroneopterin values.

Not all patients with plasma samples had their plaques cultured, and conversely, not all patients with cultured plaques had plasma samples available. contains the values from all the plaques that were cultured. Patients without values in this table either did not have blood samples supplied or the sample was stored in a way that prevented accurate neopterin/total neopterin analysis. Of note is that the group that had the highest levels of plasma 7,8-dihydroneopterin are the same group that show the lowest plaque levels of 7,8-dihydroneopterin. This is a relationship that is worth investigating further. Here we have only examined the plaque output. The relationship between total neopterin and 7,8-dihydroneopterin appears to be much more straightforward in plaque culture, for example, low total neopterin typically results in low 7,8-dihydroneopterin. Patients with very high total neopterin typically also had very high levels of 7,8-dihydroneopterin and neopterin. It is not yet understood how total neopterin and neopterin levels in the plaque tissue impact the patients' health outcomes.

**Table 6.2 Patient data arranged by plasma 7,8-dihydroneopterin level**

1<sup>st</sup> quartile = low; 2<sup>nd</sup> and 3<sup>rd</sup> quartiles = high, 4<sup>th</sup> quartile = v.high

#	Age	Event	Smoker	Diabetic	Weight	% Stenosis	Sex	Total Neopterin	Neopterin	78NP
1	81	stroke			82	50-69	M	High	V.High	Low
2	70	TIA	no	yes		50-69	M	High	High	Low
3	83	TIA				50-69	M	High	V.High	Low
4	89	weakness		no		60-70	M	Low	High	Low
5	83	TIA	no	no		50-69	M	Low	High	High
6	75	TIA	no	yes		<50	M	High	V.High	High
7	79	TIA				50-69	M	V.High	High	High
8	65	dysphasia	ex	no	70	80-99	M	High	High	High
9	64	stroke	recent ex				M	Low	Low	High
10	64	TIA	no	no	65	50-69	M	Low	Low	High
11	68	TIA	no	no	93		M	High	High	V.High
12	75	Stroke	no	no	60	60	F	V.High	High	V.High
13	81	stroke	no	no		50-69	M	V.High	Low	V.High
14	56	Amaurosis	no	yes	107	80-90	M	V.High	Low	V.High

**Table 6.3 Patient data arranged by plaque 7,8-dihydroneopterin level**

#	Age	Event	Smoker	Diabetic	Weight	% Stenosis	Sex	Total Neopterin	Neopterin	78NP
11	68	TIA	no	no	93		M	Low	Low	Low
10	64	TIA	no	no	65	50-69	M	Low	High	Low
13	81	stroke	no	no		50-69	M	Low	Low	Low
12	75	Stroke	no	no	60	60	F	Low	High	Low
6	75	TIA	no	yes		<50	M	High	High	High
	73	TIA		yes	86	80-85	F	High	High	High
3	83	TIA				50-69	M	High	High	High
14	56	Amaurosis	no	yes	107	80-90	M	High	Low	High
5	83	TIA	no	no		50-69	M	V.High	V.High	High
9	64	stroke	recent ex				M	Low	Low	High
	85	TIA		yes		70-80	M	Low	Low	High
	69	Stroke	yes	yes		50-69	F	High	High	V.High
	82	TIA	no			80-95	M	V.High	V.High	V.High
2	70	TIA	no	yes		50-69	M	V.High	V.High	V.High
8	65	dysphasia	ex	no	70	80-99	M	V.High	V.High	V.High

#### 6.3.4 Correlation between plasma and plaque values of neopterin, total neopterin, and 7,8-dihydroneopterin

Where both plasma and plaque data were available, the relationship between the plasma biomarkers and those released into the tissue culture media were assessed. There were no significant correlations between average plaque neopterin and plasma neopterin, plaque total neopterin and plasma total neopterin, and plaque 7,8-dihydroneopterin and plasma 7,8-dihydroneopterin. The relationship of plaque total neopterin to plasma total neopterin was completely random ( $r=-0.09$ ). Plasma neopterin to plaque neopterin had the strongest correlation of  $r=-0.40$ , but the residuals (the distance between the line of best fit and the data points) are large. The data suggests that there is no relationship between total neopterin in plaque and plasma, but it may be worth exploring the relationship between plaque and plasma neopterin with a larger dataset where adjustments for age, sex and co-morbidities are possible.

The correlation between plasma total neopterin and plaque neopterin is very close to 0 ( $r=-0.08$ , n.s.), but this is somewhat expected, as it would have been unlikely for plasma total neopterin to have a bearing on plaque neopterin that is being measured *ex vivo*. It is not possible to rule out that there would be a relationship between these two values *in vivo*, where there is more chance of an interplay between plasma and plaque. There was a very slight correlation ( $r=-0.22$ ) between plasma neopterin and plaque total neopterin but again the small sample size makes generating meaningful statistics difficult.

Intracellular plaque values have not been assessed as these plaques were used for further experimentation in the subsequent days after the baseline assessment was carried out.

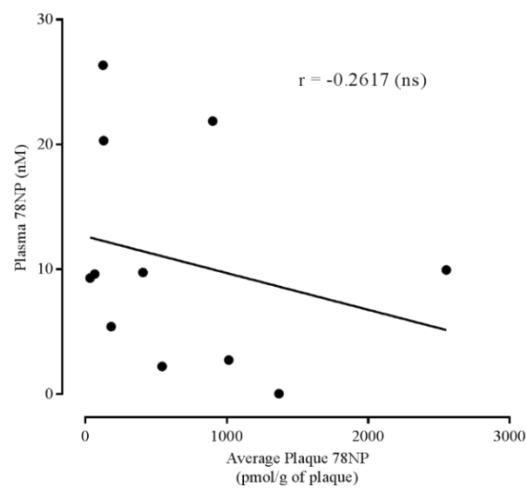
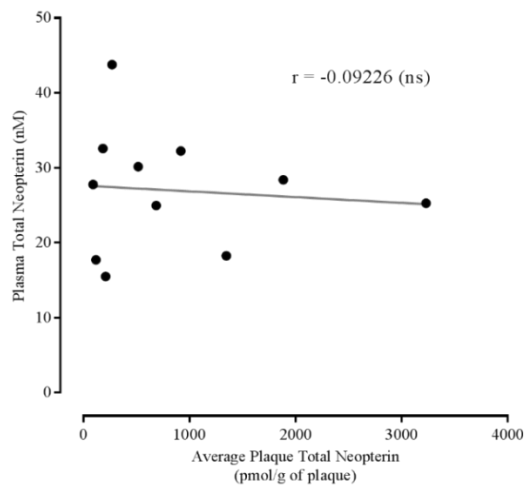
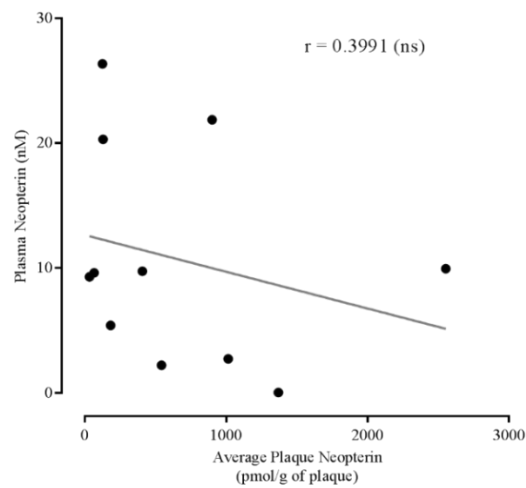


**Figure 6.5 Correlation of (a) plaque neopterin to plasma neopterin, (b) plaque total neopterin to plasma total neopterin, and (c) plaque 7,8-dihydroneopterin to plasma 7,8-dihydroneopterin.**

The plaques were incubated in RPMI-1640, supplemented with 10% human serum for 24 h. Patient plasma samples were obtained immediately prior to surgery. The plasma was separated from the red blood cells by centrifugation. The plasma samples and cultured media were assayed for neopterin and total neopterin using the SCX HPLC method. A Pearson correlation was performed, and a regression line applied to the dataset.

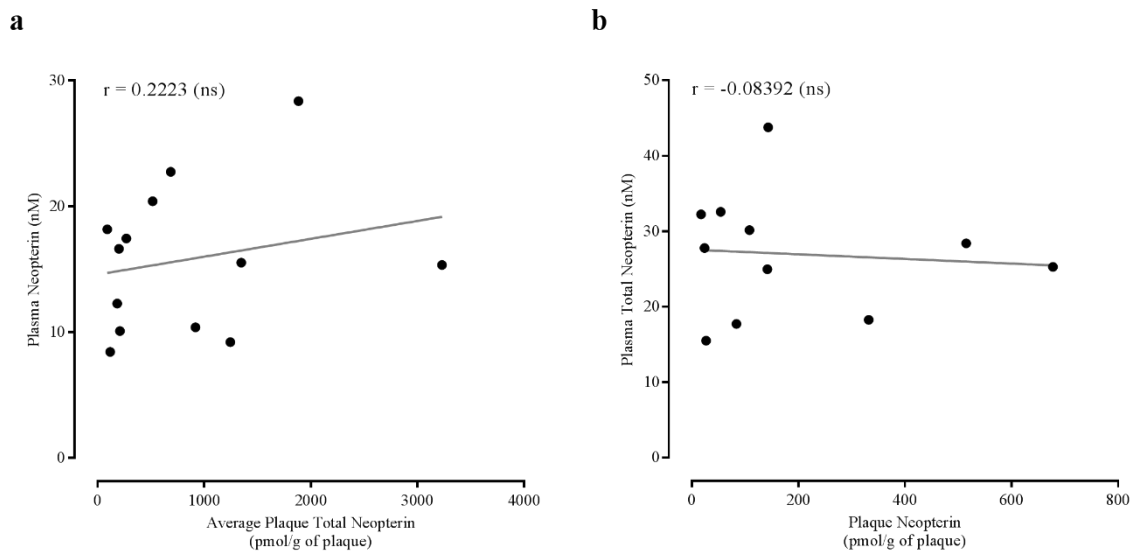


**Figure 6.6 Correlation of (a) plaque total neopterin to plasma neopterin and (b) plaque neopterin to plasma total neopterin.**

The plaques were incubated in RPMI-1640, supplemented with 10% human serum for 24 h. Patient plasma samples were obtained immediately prior to surgery. The plasma was separated from the red blood cells by centrifugation. The plasma samples and cultured media were assayed for neopterin and total neopterin using the SCX HPLC method. A Pearson correlation was performed, and a regression line applied to the dataset.

### 6.3.5 Correlation of blood and plaque lactate values to plaque total neopterin and neopterin values

Blood lactate has previously been identified as being positively correlated with carotid atherosclerosis (Shantha et al., 2013). A normal blood lactate value is between 0.5 and 1.0 mM (Mongraw-Chaffin et al., 2012). Blood lactate, measured in the plasma, increased with plaque total neopterin (Figure 6.7). The Pearson correlation coefficient for this was 0.62, which was significant. Neither the relationship of blood lactate to neopterin nor 7,8-dihydroneopterin were significant, although both had a positive association. There was no correlation between plaque lactate and blood lactate (Figure 6.8). There was also no relationship between the amount of neopterin or total neopterin generated by a plaque and the amount of lactate generated by the plaque (Figure 6.9).

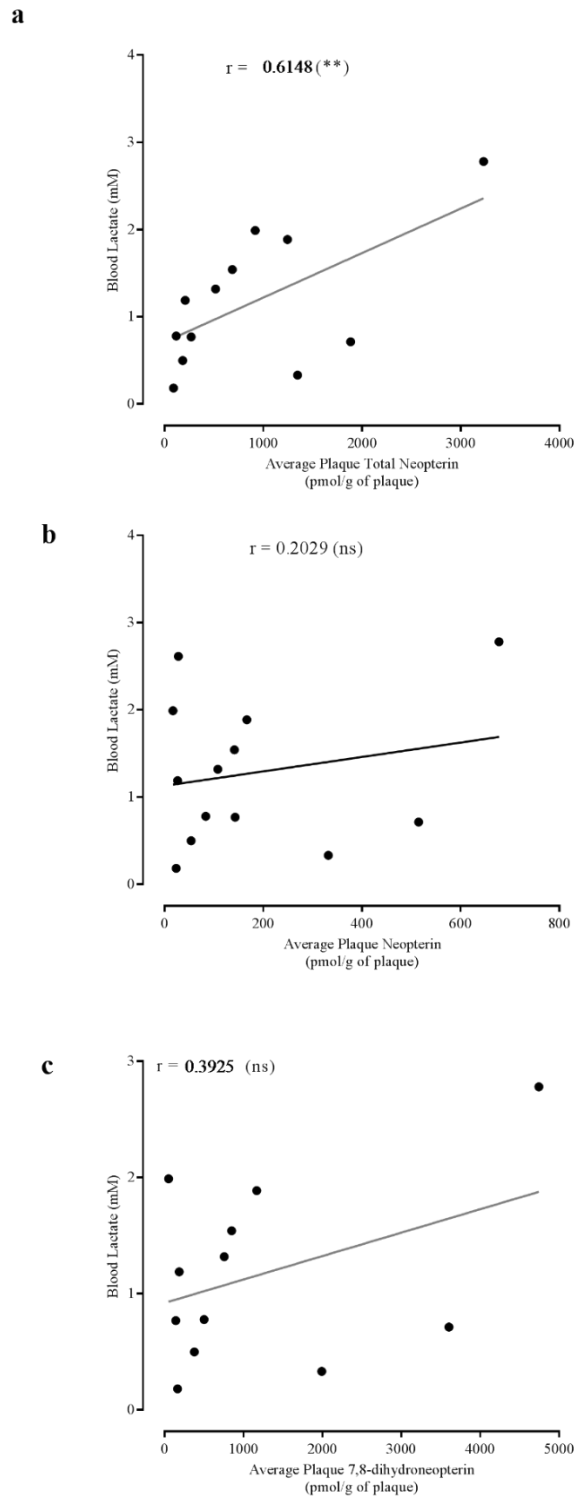


**Figure 6.7 Correlation of blood lactate to plaque total neopterin (a), neopterin (b) and 7,8-dihydroneopterin (c).**

The plaques were incubated in RPMI-1640, supplemented with 10% human serum for 24 h. Patient plasma samples were obtained immediately prior to surgery. The plasma was separated from the red blood cells by centrifugation. Lactate was measured in the plasma samples using a colorimetric lactate assay kit and cultured media were assayed for neopterin and total neopterin using the SCX HPLC method. A Pearson correlation was performed and a regression line applied to the dataset.

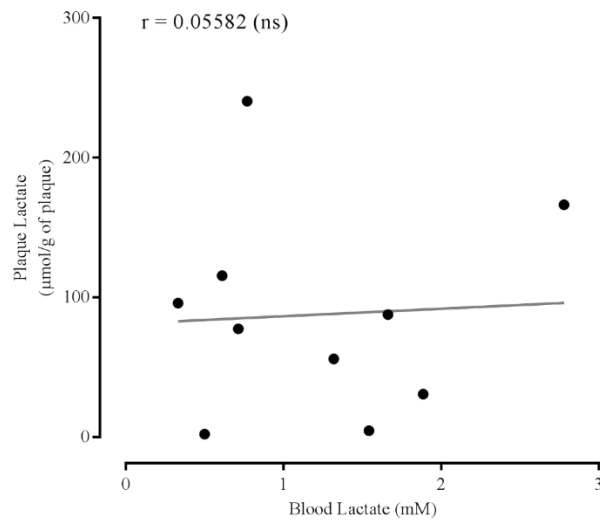


**Figure 6.8 Correlation of Blood Lactate to Plaque Lactate.**

The plaques were incubated in RPMI-1640, supplemented with 10% human serum for 24 h. Patient plasma samples were obtained immediately prior to surgery. The plasma was separated from the red blood cells by centrifugation. Lactate was measured in the plasma and plaque media samples using a colorimetric lactate assay kit. A Pearson correlation was performed and a regression line applied to the dataset.

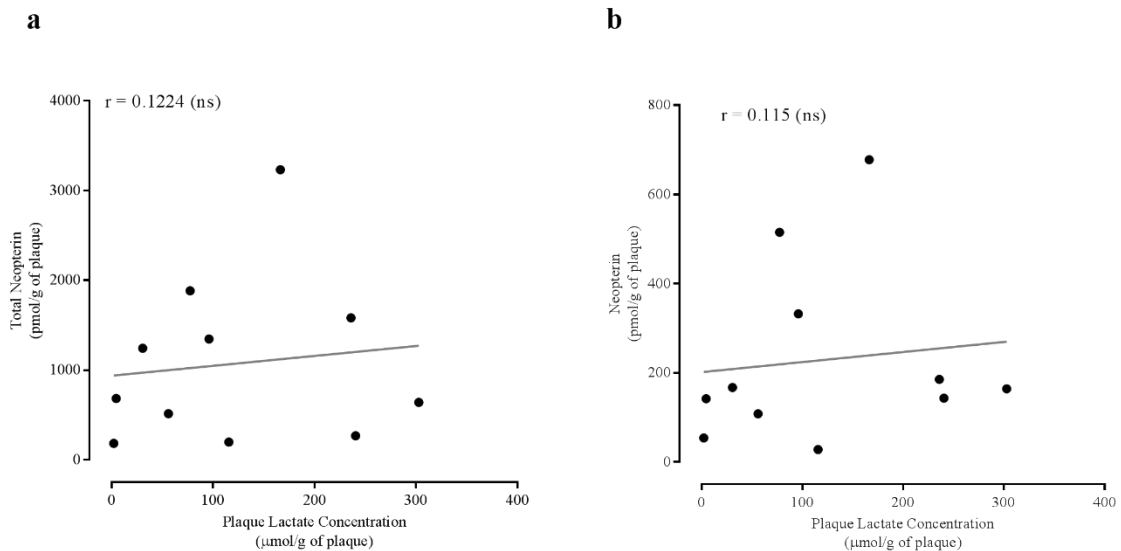


**Figure 6.9 Correlation of plaque lactate to plaque (a) total neopterin and (b) neopterin.**

The plaques were incubated in RPMI-1640, supplemented with 10% human serum for 24 h. Patient plasma samples were obtained immediately prior to surgery. The plasma was separated from the red blood cells by centrifugation. Lactate was measured in the plaque media samples using a colorimetric lactate assay kit and the plasma samples were assayed for neopterin and total neopterin using the SCX HPLC method. A Pearson correlation was performed and a regression line applied to the dataset.

## 6.4 Discussion

Total neopterin, neopterin and 7,8-dihydroneopterin values obtained from plaque culture do not appear to be correlated with their plasma counterparts from the results presented here. The initial study here comparing the levels of plaque neopterin and total neopterin to the plasma biomarkers shows some promising trends, however, the study is impeded by the small sample size. It was difficult to determine if there are any outliers in the dataset, so all points available are contributing to the dataset.

It was interesting to find that high 7,8-dihydroneopterin levels in plasma were often not reflected in the plaque tissue. This raises some questions about whether 7,8-dihydroneopterin is intended to act as an antioxidant at source or whether it is generated elsewhere and enters the plasma to be transported to appropriate locations around the body. The literature is surprisingly silent on the *in vivo* role of 7,8-dihydroneopterin (S. P. Giese et al., 2008; S. P. Giese et al., 1995). Entering the plasma would allow 7,8-dihydroneopterin to counter sudden oxidative bursts which individual cells may be too slow to react to. It is known that upregulating 7,8-dihydroneopterin from the gene level takes 24-48 hours to reach a maximum level of output (Burrowes, 2012). Previous work carried out in this laboratory has shown that 7,8-dihydroneopterin is taken up into the cell via ENT/CNT transport (Tejraj Janmale, 2013), yet cells making 7,8-dihydroneopterin seem to leak significant amounts to the extracellular space, an interesting and largely unexplored dynamic, which may have physiological relevance.

Total neopterin in plaque was found to be correlated with blood lactate levels. Blood lactate is associated with mitochondrial dysfunction (Yeo et al., 2008), and in particular endothelial cell dysfunction and has previously been found to be associated with carotid atherosclerosis (Mongraw-Chaffin et al., 2012; Shantha et al., 2013). It is unknown whether there is any link between blood lactate and total neopterin, or whether they are separately upregulated in carotid atherosclerosis. It may be worth exploring whether there is any association between macrophage activation and endothelial dysfunction.

This work confirms previous results found in this laboratory that the levels of neopterin and total neopterin vary through the different regions of the plaque (Tejraj Janmale, 2013; T. Janmale et al., 2015) and that there is a large amount of variation amongst individuals. Obtaining healthy controls for live plaque tissue for comparison is largely not possible due to the fact healthy tissue is generally not removed from patients. However, the ends of the plaque



tissue tend to appear less diseased than the central regions, which may explain why the ends tends to show higher levels of cellular activation. Interestingly, histological studies have found that cellular density increases in the shoulder and cap regions of the plaque, but where macrophages make up 46% of the shoulder region, they only contribute 1.6% to the cap (Docherty, Carswell, Friel, & Mercer, 2018).

## 6.5 Conclusion

Whilst the results here do not show a correlation between plaque and plasma values except in the case of total neopterin and blood lactate, there may be a relationship between some of these values. Obtaining further data points would allow a multivariate analysis to look at the impact of sources of variation, e.g. co morbidities, on this relationship. There is significant value to being able to draw conclusions about a patient's plaque or their cardiovascular system from their plasma levels of biomarkers, so it is certainly worth continuing to explore this further as samples become available.

## 7 Developing imaging procedures for assessing plaque vulnerability

The research was carried out in collaboration with Harshil Gulati (summer student), and Emily Searle (MSc candidate), as part of a summer studentship funded by Callaghan Innovation. For this body of work, I contributed to the design of the experiments and carried out all manual preparation of the plaque samples including the photography. I conducted the scanning and material decomposition of the plaques in Fig 7.3 and assisted Harshil with the plaque in 7.14, Emily conducted the scanning and material decomposition of the remain plaques. I prepared the chemical and blood phantoms. The scanning and material decomposition was carried out by Emily. Raj Panta provided technical assistance for modifying the scanner calibration. All interpretation of the results here is my own.

The work in this chapter relating to section 7.8.3 is being published as a conference proceeding in the *Journal of Instrumentation*.

### 7.1 Introduction

Plaque vulnerability, the breakdown of structural integrity in the plaque resulting in thrombus formation (Hansson, Libby, & Tabas, 2015), is the key to whether a patient is at risk of an adverse event. Yet, these small changes in the structure of the plaque are incredibly difficult to study or assess in humans due to the quality of information achieved using current imaging techniques. As early as 2012, the MARS scanner has been shown to be able to non-invasively identify components that are thought to contribute to the destabilization of plaque (Zainon et al., 2012). The research conducted here investigates optimizing MARS scanning to identify components of the plaque that have been identified in the literature as being related to plaque vulnerability, including calcium and lipid. It continues to build on the previous work using the improved hardware, detection and material decomposition algorithms and by investigating the identification of intraplaque haemorrhage using ferric nitrate. The MARS project brings together a range of disciplines, ranging from medical physics to software development, and is constantly evolving. Many of the research projects currently being conducted to are contributed to by numerous people in the team. These ongoing developments include a concerted effort to improve the quality and performance of the system. In the time since the initial research was conducted and even over the course of this thesis, the system was upgraded from single chip to a 3-chip camera. This dramatically reduced the time need to scan a sample, from around an

hour per sample, to now around 10 minutes. Other improvements to the scanner have reduced the time required for reconstruction and analysis. The small animal scanner is now at a level of development where relatively high throughput can be achieved. One of the aims of this work is to demonstrate that MARS spectral scanning has reached a level of quality and stability where it is now possible to design larger sample size studies to investigate plaque morphology.

#### 7.1.1 Principles of spectral CT for quantitative material assessment

Traditional CT uses energy integrating detectors to measure the intensity of photons passing through an object. The denser the material, the fewer the photons that reach the detector. This ignores the fact that each incoming photon has its own energy. The energy of the photon gives information about the material in the object. Photon counting detectors such as Medipix3, used by the MARS scanner, measure the energy of each arriving photon, and then allocate that photon to an energy bin. These energy bins or thresholds are flexible and user-defined. By measuring reference materials, characteristic curves for known materials can be generated. These are used to quantitatively assess materials in an unknown sample using a process called material decomposition. It is only possible to separate materials if there is a substantial enough difference between the characteristic curves of the materials. For example, separating glucose from fructose would be impossible, but separating gold from iodine is quite feasible.

#### 7.1.2 Separating iron from calcium in spectral CT

Traditional CT is not typically used to discriminate iron as its attenuation profile too like other materials (**Figure 7.1**). Separating the iron and calcium signal with spectral CT is challenging, as whilst spectral CT is capable of distinguishing and quantifying multiple materials at once, this becomes problematic if the spectral signals are not distinct. As can be seen from **Figure 7.2** below, the k-edges, which give high-z materials their distinctive spectral signal, in iron and calcium are relatively close to one another, and sit outside of the diagnostic energy range. Whilst this is challenging, parameters on the scanner such as the energy bins and the choice of material concentrations in the calibration phantom can be modified. This work builds on previous calibration and protocol testing looking at improving the separation of the two materials. The aim here is to show that iron and calcium separation can be achieved in a biological sample containing haemorrhage.

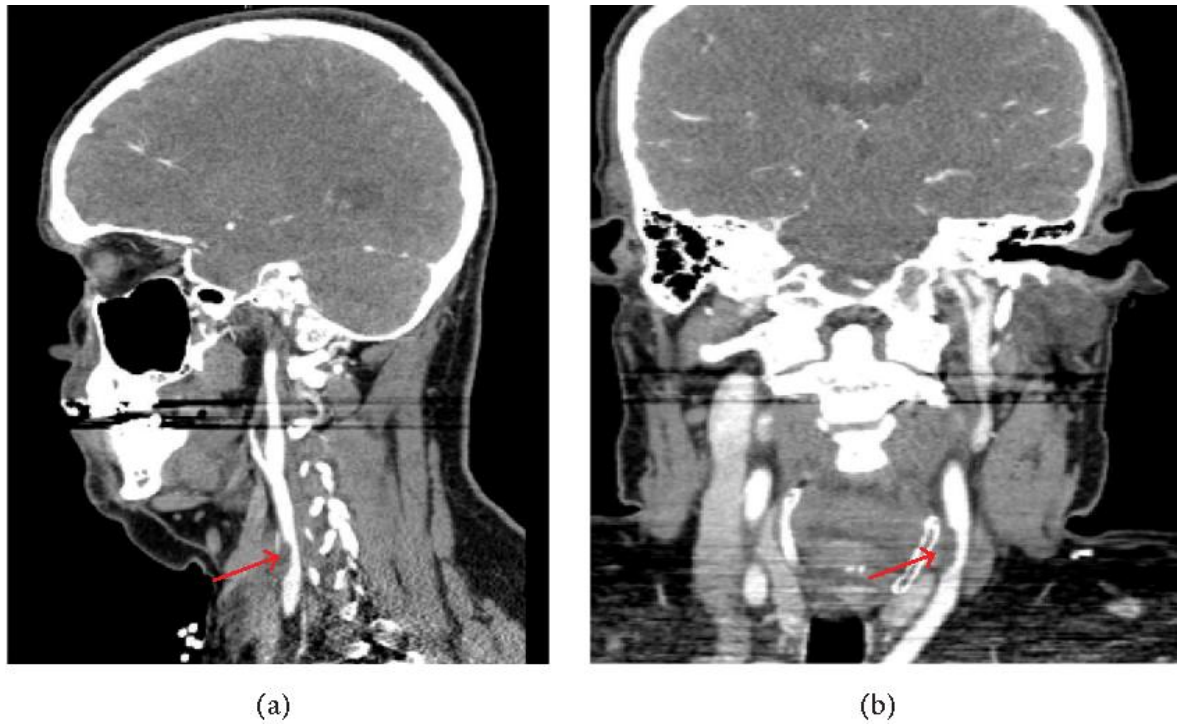


**Figure 7.1** Image of a thrombus taken by traditional CT. Image reproduced from Roshal (2016). Permission has been sought from the publisher.

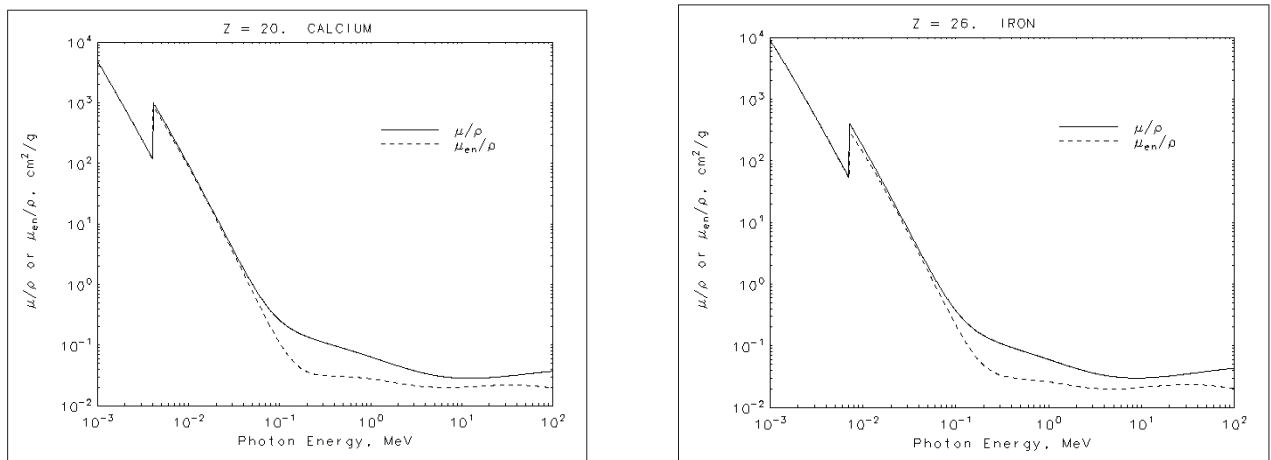


**Figure 7.2** Spectral signal and k-edge of calcium and iron. Images reproduced from Hubbell and Seltzer (1995). Permission has been sought from the publisher.

## 7.2 Methods in brief

### 7.2.1 MARS spectral scanning protocols

Phantoms were designed as described in Chapter 2. Plaque imaging for lipid, water and calcium was conducted using 2mm Aluminium filtration with energy bands beginning at 18, 30, 40, 50 and 60 keV, tube voltage 118 kVp, tube current 13  $\mu$ A and exposure time of 200ms. When

assessing iron content as well, thresholds were set at 20, 28, 36 and 44 keV, with a tube voltage of 80 kVp, a tube current of 55  $\mu$ A and 100ms exposure time. For the plaque with haemorrhage, 2mm Al filtration was used with a tube voltage of 120 kVp, tube current of 36  $\mu$ A. Energy thresholds were set at 18, 29, 45, and 75 keV. Exposure time was 100 ms with 720 projections captured.

### 7.2.2 Method developed for calculating plaque volume by using ImageJ

Total plaque volume provides interesting insight into the size of the plaque sample relative to its weight. This provides information about the density of the tissue, and a tool by which to compare between plaque samples. For example, to investigate whether plaque volume increases with age or percent stenosis. To obtain total plaque volume the area containing all materials excluding the sample tube were measured. This was carried out by cropping out the sample tube and using the image thresholding technique in ImageJ as follows:

Reconstructed energy images were opened in ImageJ. The cropping tool was used to select the area inside the tube, and then selecting to delete everything outside of the highlighted area. The stack was converted to a hyperstack and the dimensionality reduced to ensure only one energy image from each slice was used. The threshold was then adjusted to make sure the highlighted area included all regions of the plaque. The analyse particles tool was then used to measure the resulting thresholded areas. The area of each slice was multiplied by the slice thickness to achieve a volume. The volumes from each slice were added together to get the total plaque volume.

### 7.2.3 Calculating plaque calcium volume by using ImageJ

The calcium volume was calculated in much the same way but instead of using the energy reconstruction, the material decomposition files were used. The material decomposition images from the hydroxyapatite channel were loaded into image J. As these were material decomposition there was no need to reduce dimensionality as there was only one image per slice. The thresholding tool was used making sure that all the calcium, no matter what density, was selected to ensure microcalcifications were captured. The analyse particles tool was then used as described above and the volume calculation was performed.

## 7.3 Results and Discussion

### 7.3.1 Identification of calcium as a marker of plaque vulnerability

In Chapter 3, it was found that volume of calcium was inversely related to the amount of plaque activation. MARS spectral CT is able to identify both dense calcification (**Figure 7.3**, top) and microcalcification (**Figure 7.3**, bottom). Section 5 has calcification evenly dispersed throughout the section, whereas section 4 has one area of dense calcification on the surface of the tissue, and then very fine microcalcification throughout the rest of the tissue. Interestingly these two sections were immediately adjacent to one another in a single plaque specimen. It is possible that the calcification in section 5 was so dense that scalpel blade essentially skimmed the outside of it, resulting in these two very different sections.

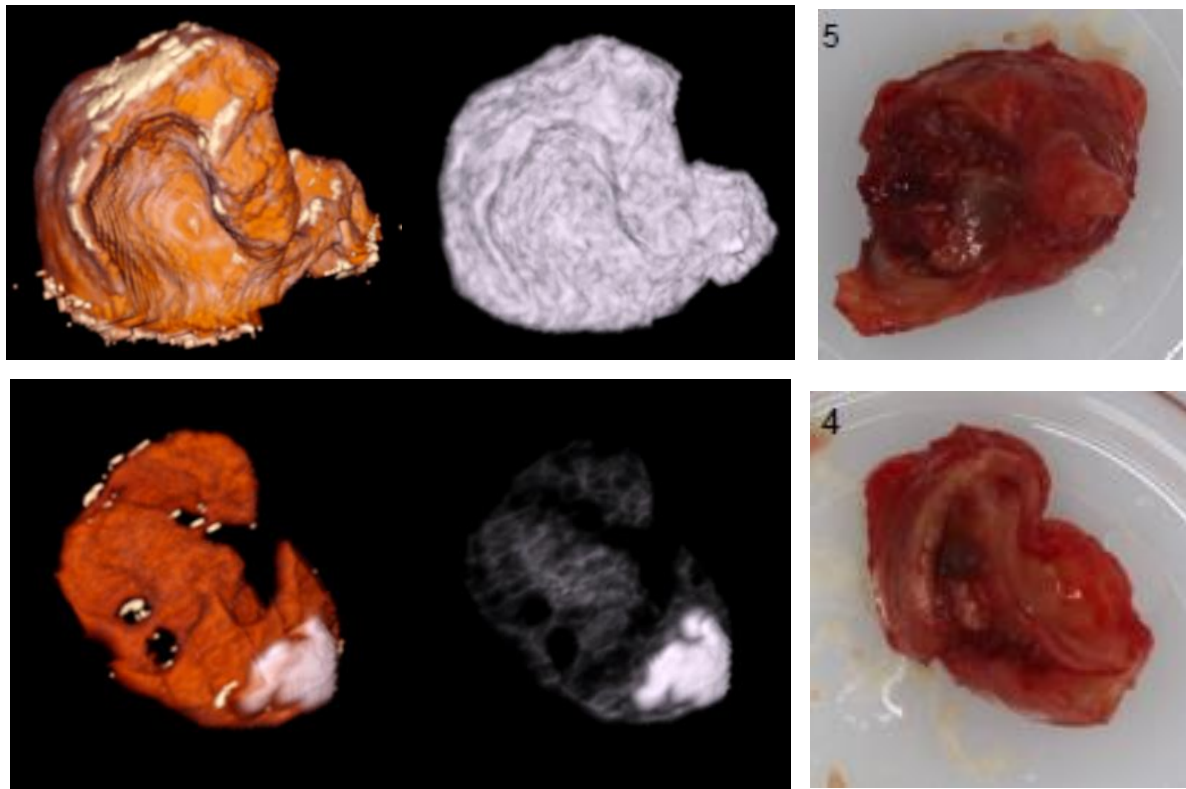


**Figure 7.3 MARS images of plaque sections 5 (top) and 4 (bottom) of plaque 120 displaying two different types of calcification from within a single plaque.**

Red represents soft tissue (water), calcium is in white, and lipid is in beige. Images on the left include all material channels. Images on the right highlight just the calcium channel. The colour scheme is the same for the top and bottom images. The plaque section in the top image contains more lipid than the section in the bottom which is predominately soft tissue and calcium.

Examining a small number of plaque specimens showed wide variation (2.8% - 29%) in the percentage of the plaque made up of calcium deposition (**Table 7.1** ). Calcium score is not traditionally measured in carotid arteries, but this information may be of relevance for clinicians.

**Table 7.1 Plaque volume and total volume of calcification in a selection of plaques**

Plaque Number	82	115	118	136
Ages (yrs.)	75	81	73	82
% stenosis	60-69	50-69	severe critical narrowing	75
Plaque volume (mm <sup>3</sup> )	1379.36	987.52	762.76	1223.51
Total Assigned Calcium Volume(mm <sup>3</sup> )	38.07	63.14	219.61	147.15
Calcium as % of total volume	2.8%	6.4%	29%	12%

### 7.3.2 Investigation of inconsistent plaque lipid values in material decomposition

Each MARS scanner comes with factory designed protocols in which the parameters have been set to provide the best results for an experimental sample. The plaque protocol was designed with the goal of accurately separating lipid, calcium and soft tissue. This protocol had been used successfully for over a year to generate material decomposition of plaque tissue. **Figure 7.4** to **Figure 7.7** were the first examples of receiving an unexpected result using this well-established scanning protocol. Plaques previously scanned using the protocol produced a distribution of lipid, soft tissue and calcium consistent with literature descriptions of plaque morphology and composition (as demonstrated in **Figure 7.3**). The plaques in **Figure 7.4** to **Figure 7.7** are notable in the lack of lipid signal present. In addition to the lack of lipid signal, the images appear to lack the complexity that previous images contained. For example, whilst calcium has been identified, there seems to be no evidence of microcalcification. In all the images, soft tissue seems to be the dominant material, but even within this, the density appears to be too consistent.

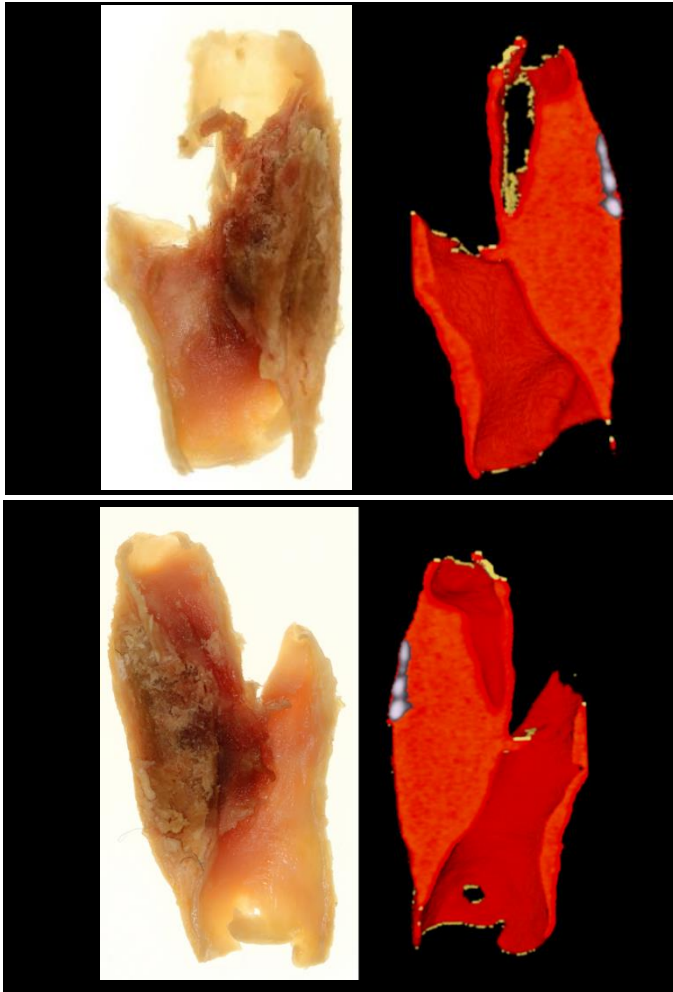


**Figure 7.4 Photograph (left) and MARS image (right) of Plaque 82.**  
This plaque was obtained from an 80-year-old male. No other clinical information was supplied.

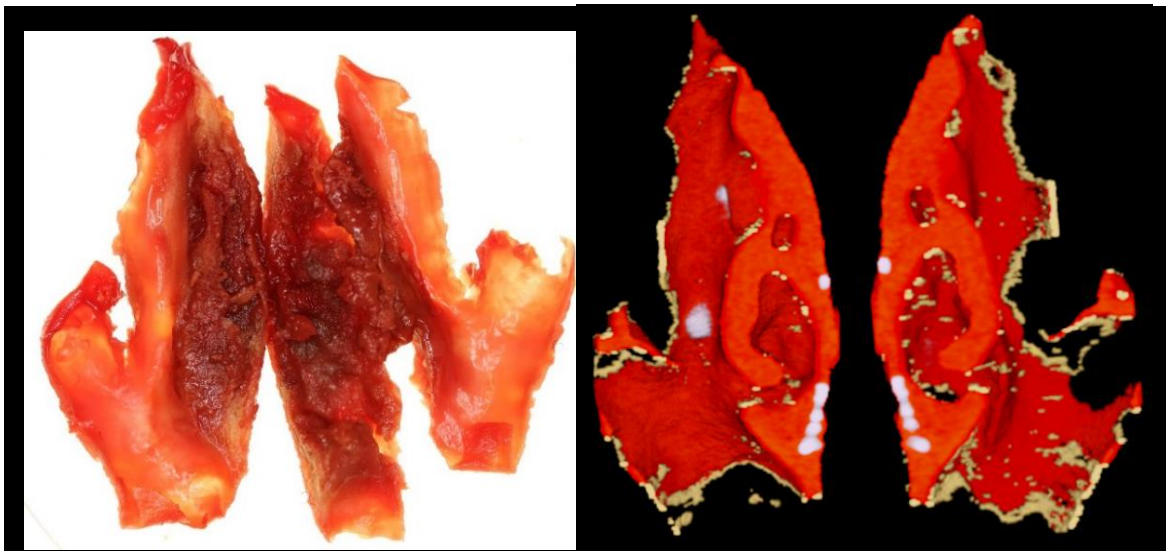


**Figure 7.5 Photograph (left) and MARS image (right) of Plaque 115**  
This plaque was obtained left internal carotid artery of an 81-year-old male who had suffered from a stroke and hypertension. Stenosis was recorded as 50-69%.



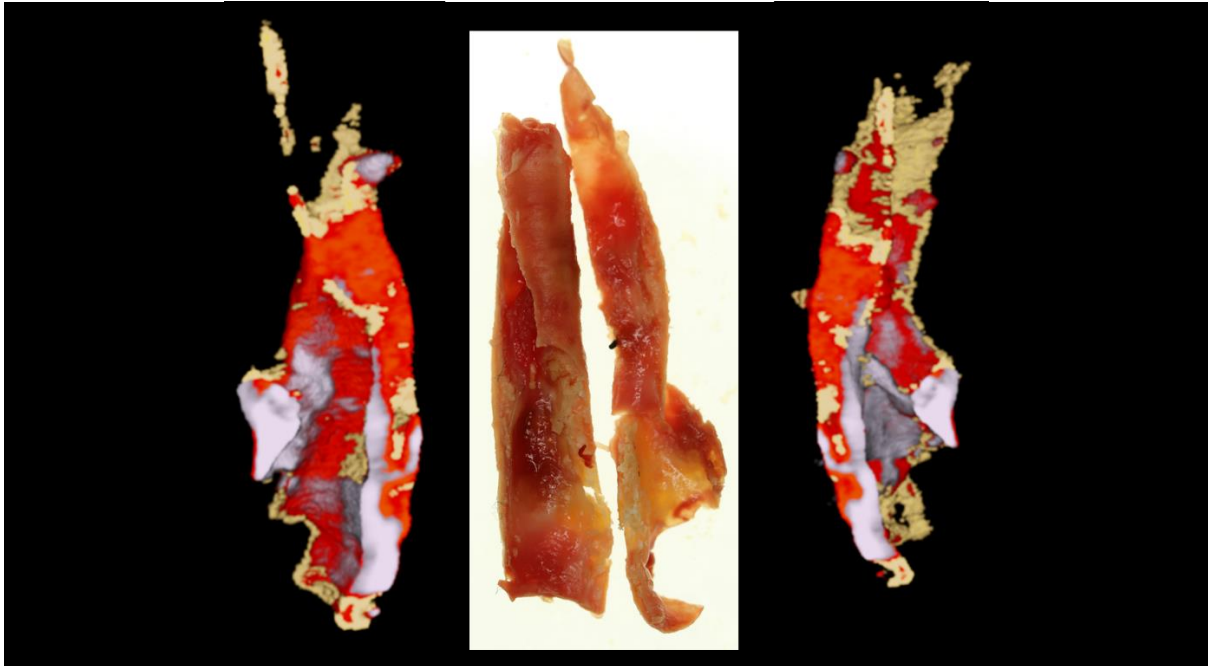


**Figure 7.6 Photograph (centre) and MARS image (left and right) of Plaque 118.**

The plaque was obtained from the right internal carotid artery of a 73-year-old diabetic male who had a TIA and expressive dysphasia. The stenosis was described as severe critical narrowing.

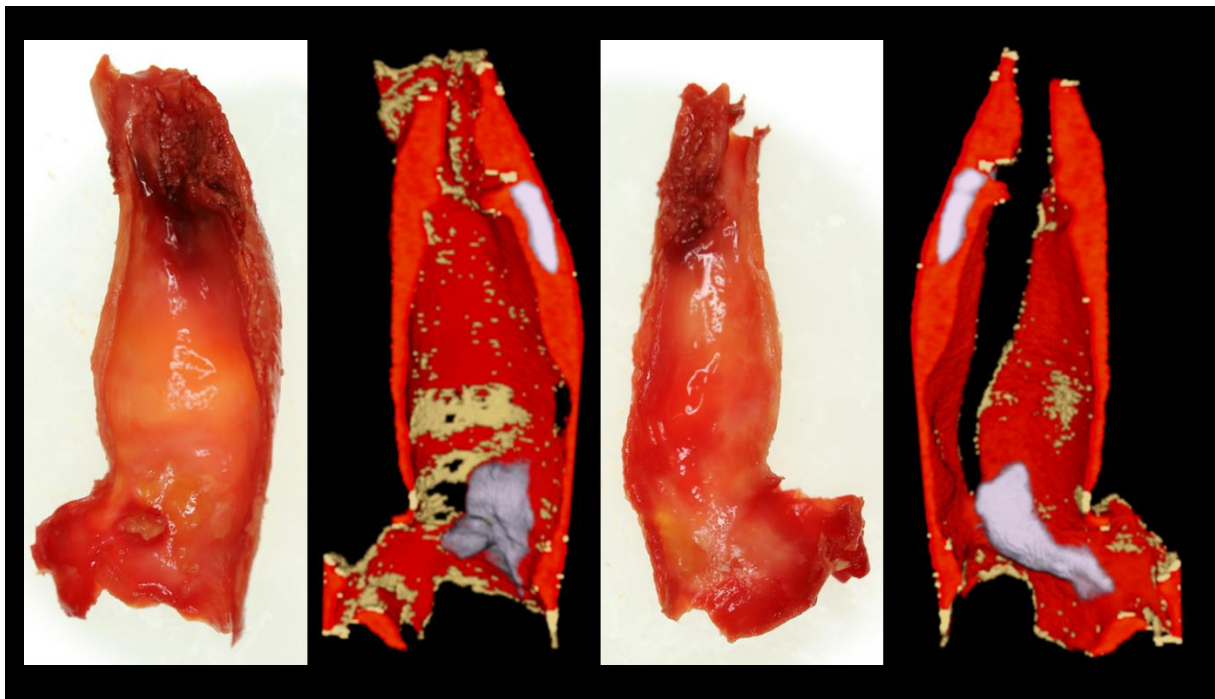


**Figure 7.7 Photograph (first and third image) and MARS image (second and fourth image) of Plaque 136.**

The plaque was obtained the left internal carotid artery of an 82-year-old male who had suffered a stroke. Stenosis was recorded as 75%.

The first assessment of the situation was that the MARS images appeared to lack definition compared to previous plaque scans. It was also noted that the datasets appeared to contain almost no lipid. After establishing that this was not due to the colour scheme selected but due

to an inherent issue in the data set several hypotheses for what could have caused the problem were formulated. Firstly, it was thought that perhaps the plaques chosen may have been of a more fibrous phenotype. It seemed relatively unlikely that five separate plaques selected at random would all display this phenotype. To assess this, plaques were stained with oil red O to rule out the issue being a lack of lipid in the plaque material itself (**Figure 7.8** and **Figure 7.9**). This seemed unlikely to be the case but was relatively easy to test. The areas of gruel in two separate plaques both stained with the oil red O as well as areas around the edge of the tissue showing that lipid is present in the plaque samples. This suggests that there was a problem with the material decomposition computation or the scanner itself.

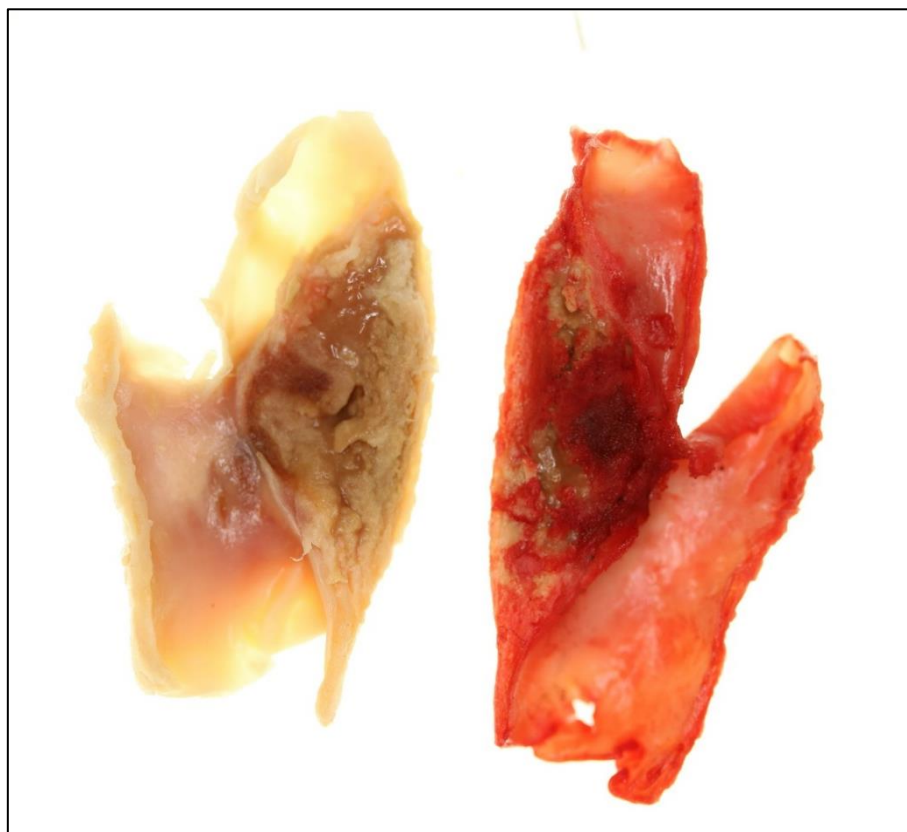


**Figure 7.8** Photograph of Plaque 82 unstained (left) or stained with oil red o (right)

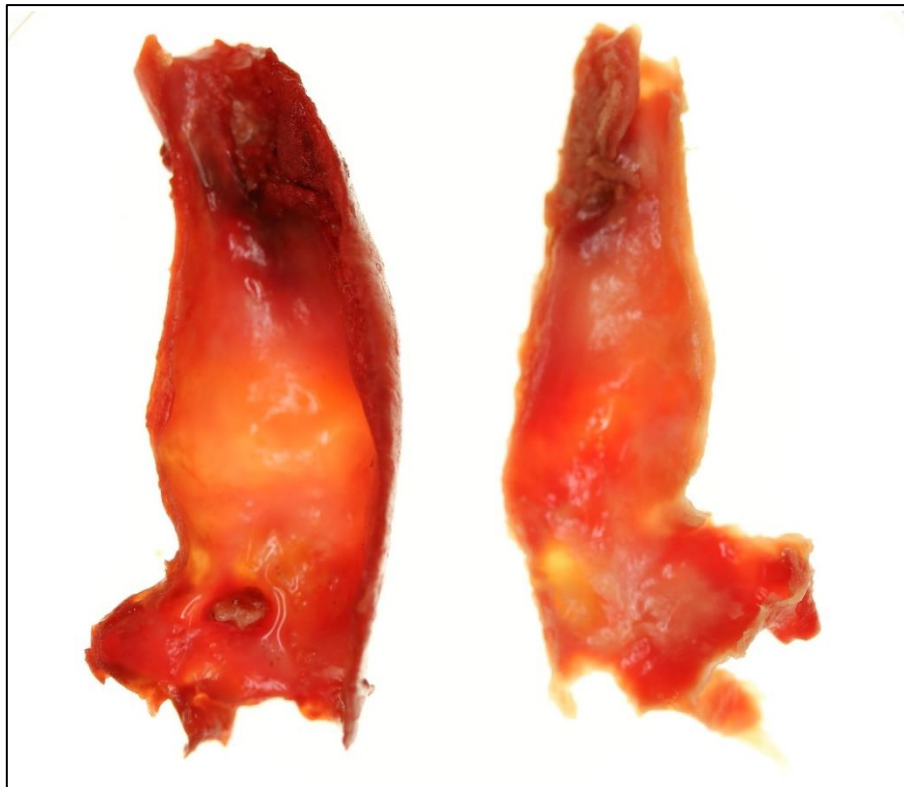


**Figure 7.9 Photograph of Plaque 136 stained with oil red o (left) or unstained (right)**

Secondly, it was noted that these scans were carried out after the installation of a new 3 sensor camera on the scanner. It was thought that a material decomposition calibration of the scanner was not performed at the time the camera was changed over (1 chip upgraded to 3 chips). A recalibration of the scanner was performed, which improved the automatic reconstruction of scans to some extent, but is unlikely to explain the lack of lipid in the material decomposition images above as the MARS images shown in **Figure 7.4** to **Figure 7.7** were produced using a manual calibration using values that were obtained from a phantom performed at the same time as the scan. It was noted that linear attenuation values between scans can be variable, which is why it is recommend that a phantom be scanned along with the samples of interest.

Thirdly, it was noted that extremely low levels of calcium had been identified in nearly all voxels. It was thought that perhaps microcalcification was preventing the lipid signal from being seen due to the partitioning in the material decomposition algorithm. A plan was made to test this by swapping the values for lipid and water, so that voxels made up of lipid and calcium could possibly be identified. However, before this could be implemented it was noted that there were inconsistencies in the phantom used to produce the plaque images. Given that

micro calcification had never had such a dramatic impact on lipid values previously, it was decided that examining the phantom MD in more detail would be a better direction to pursue.

A closer examination of the phantom used for the material decomposition for these plaques found that the material decomposition was not correctly identifying the materials (Table 7.2). Lipid is identifying as 60% water, and only 34% lipid, a large misclassification. Water was identifying correctly with no misclassification of lipid or hydroxyapatite (calcium) present. However, hydroxyapatite was not classifying correctly. The measured concentration was at most half the expected value (200 mg/ml in the 400 mg/mL sample). The 400 mg/ml hydroxyapatite sample recorded 3.37 g/mL of water, which is not physically possible. In examining the phantom, it was noted that the lipid vial was placed in the centre which is not recommended due to the possibility of increased beam hardening in the middle of the phantom. This may have contributed to the poor resolution of water from lipid. In addition, the water vial was next to the highest concentration of hydroxyapatite, which is also likely to cause beam hardening. It is recommended that for each protocol a range of normal linear attenuation and material decomposition values are established, so that errors can quickly be identified, and the source of the error can be tracked down. It would be worthwhile to quantify the effect of phantom layout on linear attenuation values to establish whether the placement of vials is having a detrimental impact on the material decomposition.

**Table 7.2 Measurements from the phantom used to calibrate the MD for the previous images.**

Water Content (g/mL)		Lipid Content (g/mL)		Hydroxyapatite Content (g/mL)	
Water	1.03	Water	0.01	Water	0.00
Lipid	0.61	Lipid	0.34	Lipid	0.00
Ha00	1.10	Ha00	0.00	Ha00	0.00
Ha50	1.21	Ha50	0.00	Ha50	0.03
Ha100	1.31	Ha100	0.00	Ha100	0.06
Ha200	1.51	Ha200	0.00	Ha200	0.11
Ha400	3.37	Ha400	0.00	Ha400	0.21

### 7.3.3 Imaging intraplaque haemorrhage

Intraplaque haemorrhage is associated with plaque vulnerability (Michel, Virmani, Arbustini, & Pasterkamp, 2011). Whilst conducting the plaque culture experiments described in chapter 4 it was noted that neovascularization and haemorrhage were relatively common features (Figure 7.10). However, these plaques did not always survive the four days in culture intact (Figure 7.10) which meant they could not be scanned later. From experience, it was known that plaques that had a darker discolouration on the exterior tended to contain areas of intraplaque haemorrhage. Whilst it would also be interesting to investigate neovascularization, plaque haemorrhage was selected as the first target due to the higher likelihood of being able to identify it using spectral imaging. At present, neovascularization sits just below the resolution the MARS spectral scanner. It was unknown whether it would be possible to separate calcium from iron, as they are relatively close to each other on the periodic table (Fe 26, Ca 20), and it was uncertain if the k-edge of iron and calcium would sit in different energy bins. Ferric nitrate was chosen to represent iron due to its similarity to the form of iron likely to be found *in vivo*. An initial test carried out by Ms Searle showed that using ferric nitrate phantoms, iron should be identified within blood clots.

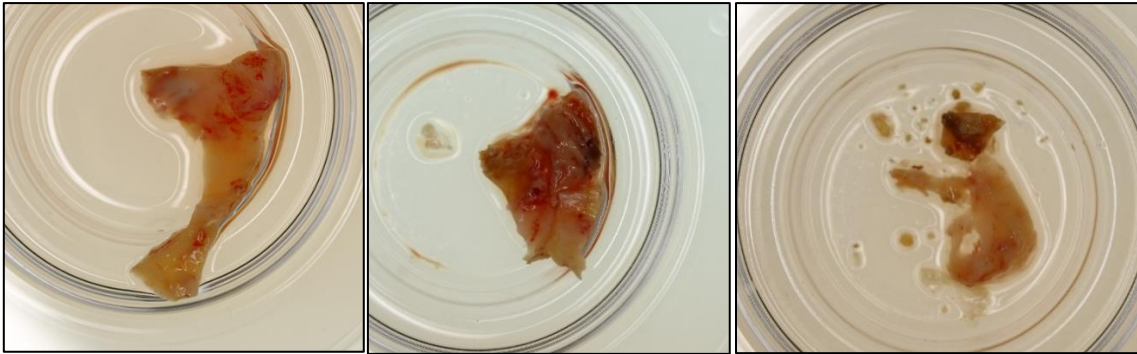


**Figure 7.10 Evidence of neovascularization and intraplaque haemorrhage in plaque sections**



**Figure 7.11 Plaque 158 with suspected intraplaque haemorrhage**

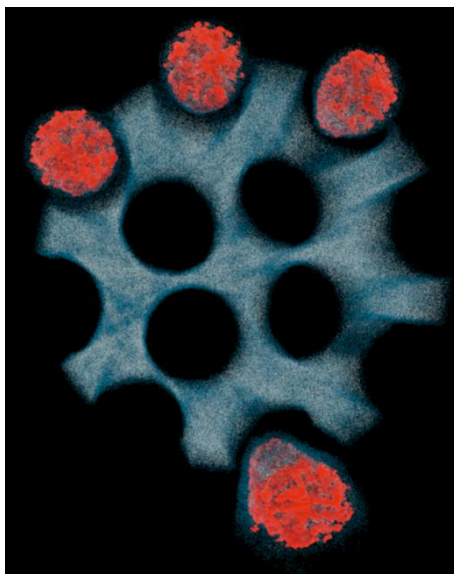


**Figure 7.12 Ferric Nitrate signal in blood clots**

Given the issues that had occurred previously with quantification of materials in the phantom, the misidentification and quantification of the calibration phantom for this scan was carefully assessed. Figure 7.13 shows the measured concentration of ferric nitrate against the given concentration. At all concentrations ferric nitrate is measured as less than the actual concentration. This is mainly due to the overlap between calcium and ferric nitrate which is not unexpected. Interestingly, the values for ferric nitrate are much higher in the plaque (in the order of g/mL rather than mg) than we are using for the phantom. It may be possible to increase the concentrations of ferric nitrate to improve the separation between ferric nitrate and calcium. It is much easier to modify the ferric nitrate values as these are solutions are prepared in the laboratory whereas the hydroxyapatite calibration standards are purchased in predetermined concentrations.

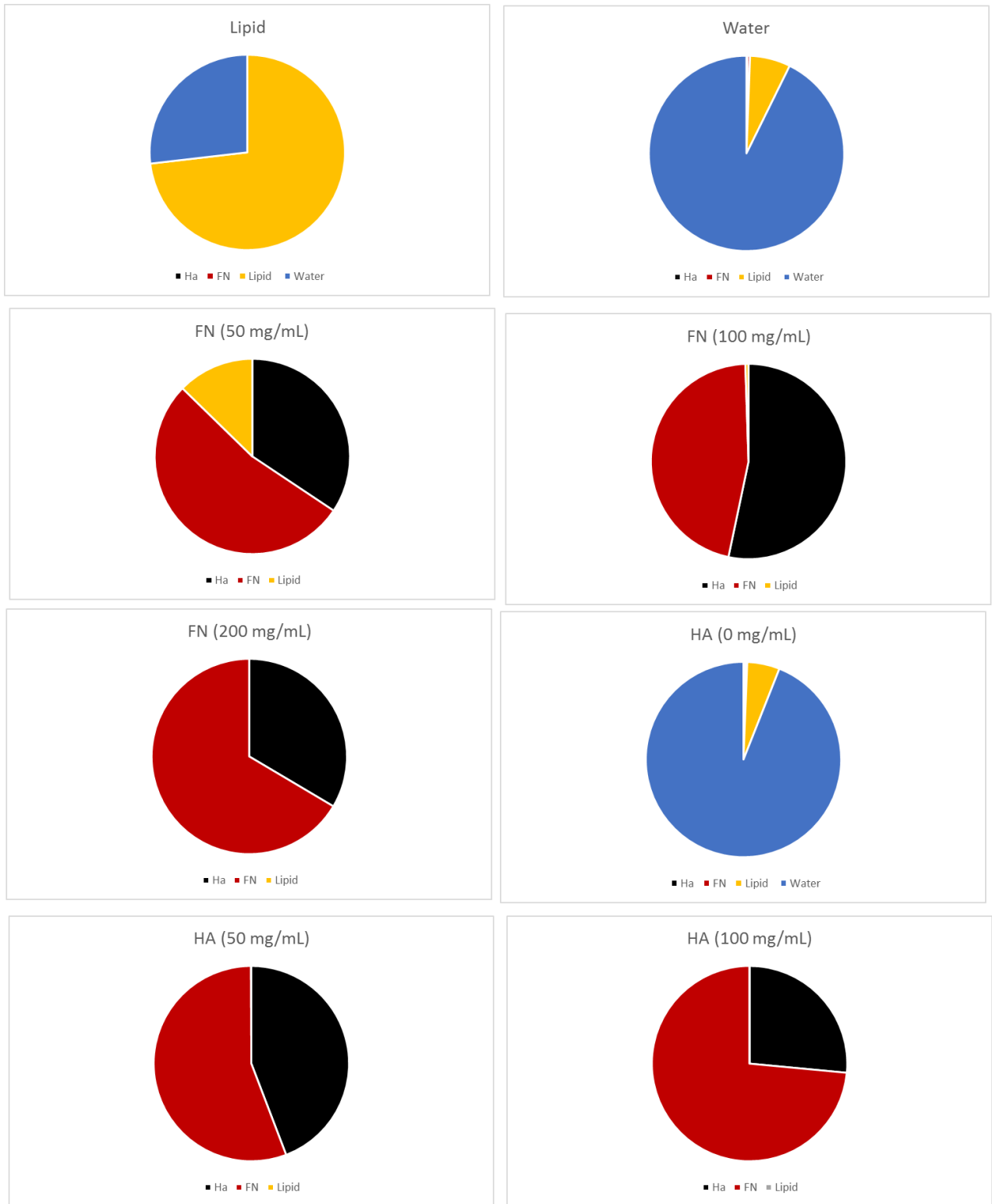


**Figure 7.13 Misidentification of materials**



The plaque selected for this experiment was obtained from the right internal carotid artery of a 74-year-old male smoker who weighed 62 kg (Figure 7.14). The patient had suffered a stroke in his retina. The patient had a blood pressure of 154/70. An ultrasound had identified the stenosis to be 70%. The cut that can be seen in the photo of the plaque is caused by the procedure used to remove it. The plaque measures 32 mm in length and 14 mm in width. A bifurcation is clearly identifiable. In the cut images, the bifurcation sits at the rear the right-hand segment. There is a distinctive discoloration under the tissue in the central region of the plaque. Tissue at the extremities of the plaque seems relatively smooth and healthy. This plaque contains a typical necrotic core. Areas of dark brown discolouration within the necrotic core can be seen, as well as voids and areas of yellow deposits, most likely lipid. The fibrous cap containing the necrotic core can be seen at the outer edges. This layer has eroded in the centre of the necrotic region. On the right hand cut section, there is an area of what appears to be ulceration in centre of the necrotic core.

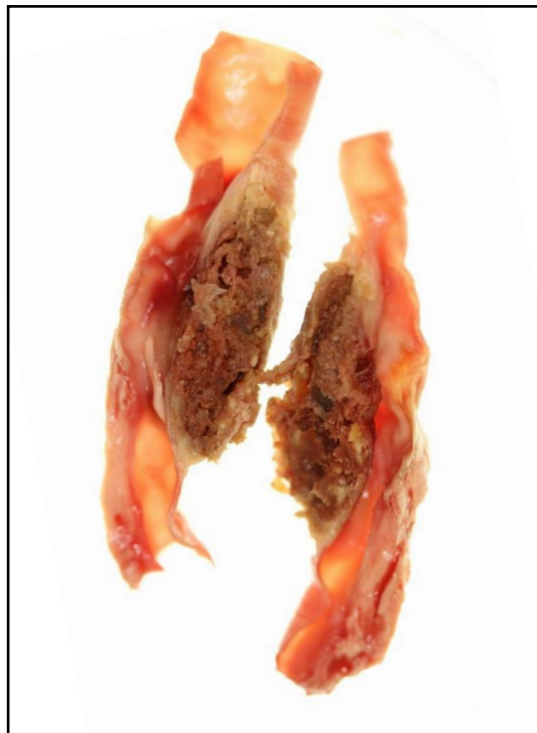


**Figure 7.14 Photographs of Plaque 158, back view, front view, sagittal slice view.**

The plaque was obtained from the right internal carotid artery of a 74-year-old male smoker weighing 62 kg. The patient had suffered a retinal stroke. Ultrasound identified the stenosis at 70%. The top image shows the front and back of the specimen prior to it being cut open. The bottom image is after a single cut was performed through the length of the plaque. The open plaque reveals a gruelly mass consistent with an advanced plaque.

Analysis of the plaque using MARS spectral scanning found the discoloration to be caused by deposits of a material that identified as ferric nitrate like, which is most likely to be intraplaque haemorrhage (**Figure 7.15**). Further analysis of the plaque shows regions of dense calcification as well as distinct microcalcification. A closer examination of the bifurcation shows an area of fibrous cap erosion.

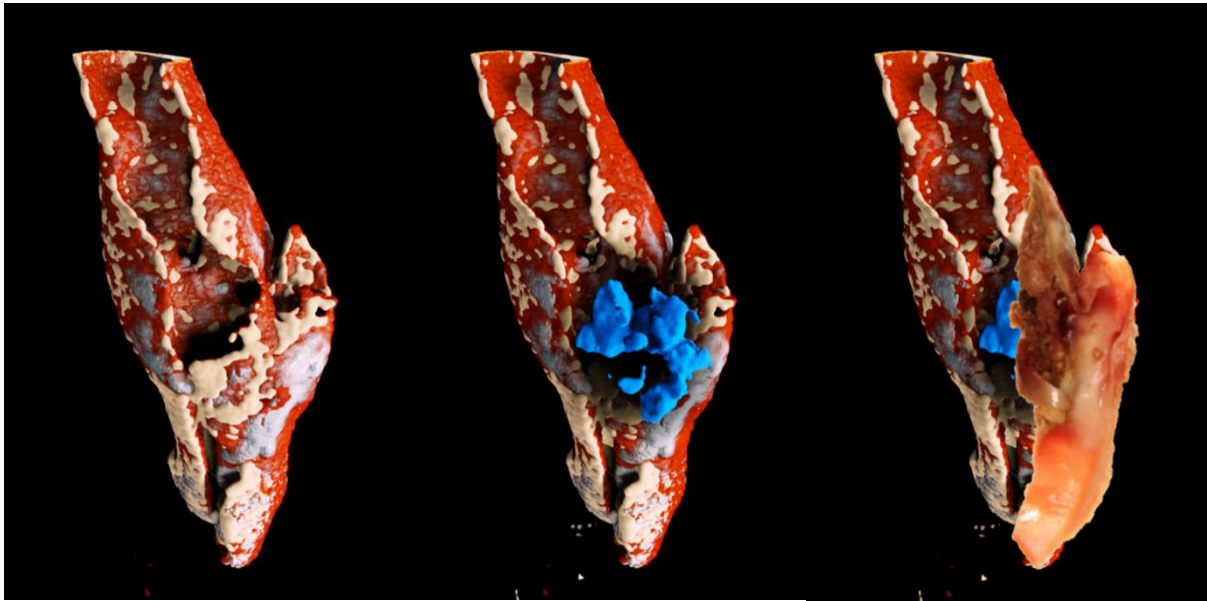


**Figure 7.15** 3D visualisation of plaque 158 from MARS Vision of the whole plaque (left), magic lens to show intraplaque haemorrhage (centre, blue), and with photo of the interior of the bifurcation overlain (right).

Red represents the soft tissue, beige represents lipid, white represents calcium and blue represents iron. The image on the left is a 3D mesh, showing just the materials present on the surface of the tissue. The image in the centre has a circular magic lens applied which will reveal only iron, all other materials are stripped away.

A close up of the area associated with the intraplaque haemorrhage within the bifurcation reveals an area where the fibrous cap appears to have failed and a portion of the necrotic core appears to have eroded (Figure 7.16). Given that this patient suffered a stroke in their retina, it is likely that this is the source of the stroke. Interestingly, the area where the fibrous cap appears to have eroded is mostly identifying as calcification, while the area where there is ulceration is coated in lipid. The areas closest to the eroded cap appear to contain lipid deposits as well as several distinct areas of intraplaque haemorrhage. Further examination using the magic lens tool which strips away all layers except the one that has been selected shows that there are spotty iron deposits throughout the region potentially associated with the rupture. This may explain the distinctive red coloration in the tissue. Sequential axial slices show remnants of the lipid rich area that has most likely ruptured.

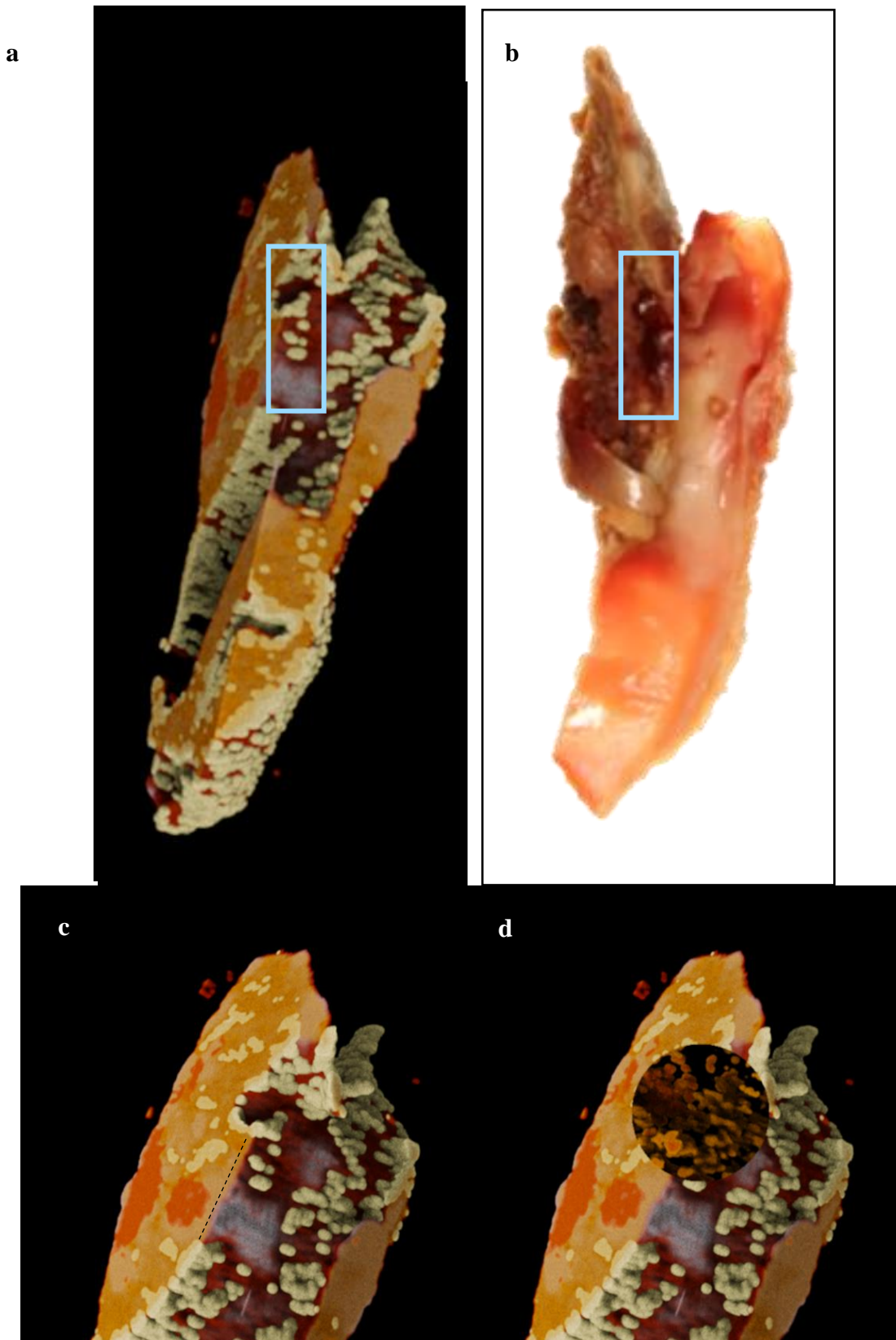


**Figure 7.16** MARS image of plaque bifurcation (a), photograph of plaque bifurcation (b), close up of MARS image of plaque bifurcation (c) and with magic lens for iron (d). Orange-red represents soft tissue, beige is lipid, white is calcium, and iron is in dark red-maroon. The blue box in (a) and (b) highlights the area of ulceration. Black dashed line in (c) indicates area of thin fibrous cap erosion. The area of normal fibrous cap below it can be seen as containing lipid.

Examining just prior to the ulceration, it can be seen that some of the lipid core remains (Figure 7.17a, yellow arrow). There is evidence of surface disruption surrounding the ulceration. An area directly to the left of the lipid core contains iron deposits as indicated by the red arrow. To the right is an area where calcification (white arrow) has reached the surface of the tissue. There is lipid coating the bottom of the ulceration. The ulceration is roughly 2mm in diameter. 95% of ruptured fibrous caps are less than 65  $\mu\text{M}$  thick possibly composed of foam cells (Burke et al., 1997). Figure 7.17 b and c appear to be consistent with this measurement as the remaining cap is close to a single voxel (90  $\mu\text{M}$ ) in thickness. These images show a high degree of complexity in the distribution of lipid, soft tissue, calcium and iron. This shows that the issues of material identification in section 7.3.2 associated with the scans in Figure 7.4 - Figure 7.7 have been resolved by using better constructed phantoms for calibration.

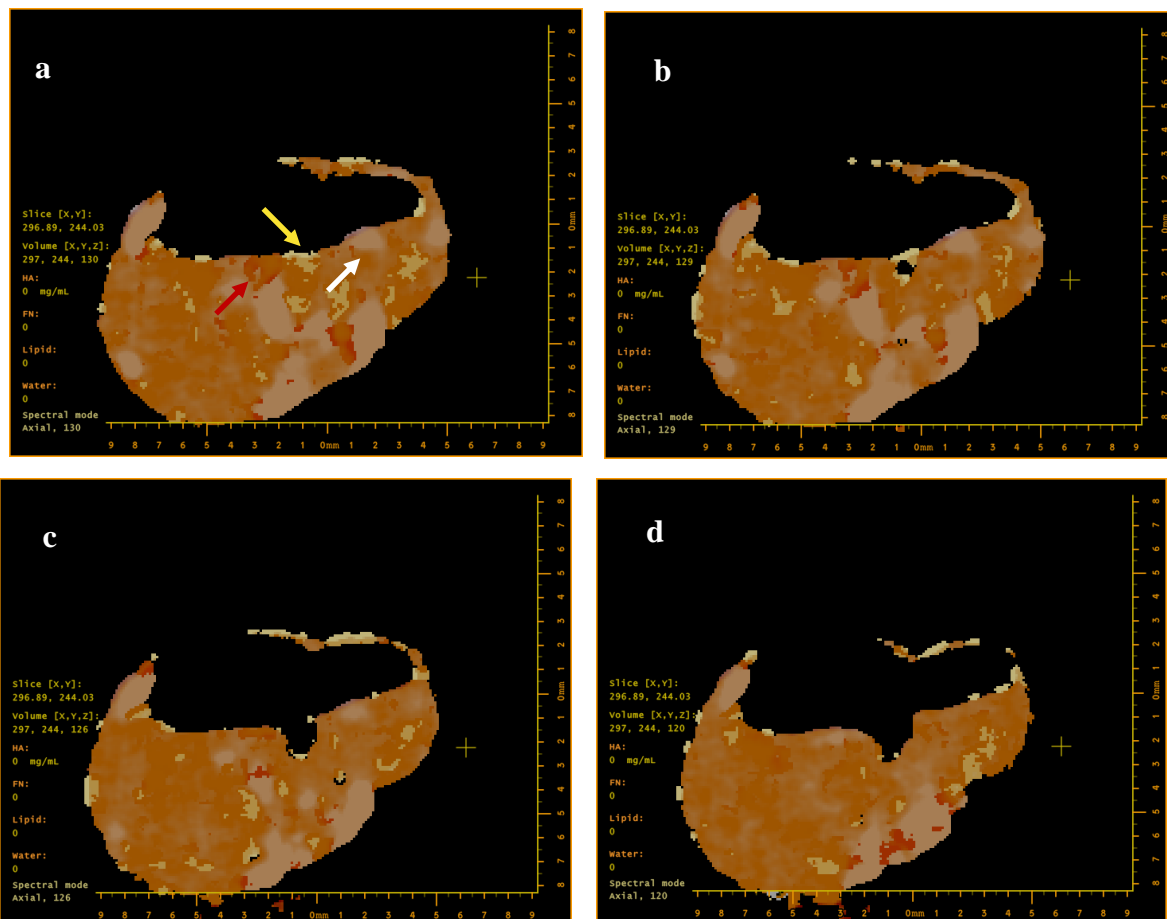


**Figure 7.17** Axial slices (a-d) showing the progression of an ulceration in plaque 158 in four separate slices. Orange-red represents soft tissue, beige is lipid (yellow arrow), white is calcium (white arrow), and iron is in dark red-maroon (red arrow).

Figure 7.18 shows the benefit of being able to examine the entire plaque tissue. Current histology techniques would have meant that areas of interest need to be preselected through the choice of where to slice the plaque with the potential to miss crucial or interesting results. The number of histological slices that can be produced per sample is generally limited due to practicality reasons. Here it is easy to identify the distribution of the materials of interest, e.g. iron, across the entire sample. In this sample, the intraplaque haemorrhage is co-localized with areas of denser calcification. While there is a small possibility this is due to misidentification of materials, this finding is consistent with histological studies on excised carotid plaque specimens (Bini et al., 1999).

Figure 7.18a also contains multiple air pockets in the tissue, which possibly indicate areas of previous ulceration and remodelling. Again, these air pockets would be very difficult to visualise using histology due to the methods used to prepare samples. Many methods end up washing away some of the principal components such as microcalcifications or cholesterol crystals, which means it would be difficult to identify whether a void had truly been a void in the tissue or was just an artefact from the histology procedure. Figure 7.18 b (black arrow) indicates another ulceration, which can be identified in the photographs (again indicated by a black arrow in Figure 7.19) as well as in the 3D model. As this ulceration is on the part of the plaque that leads to the brain, it is possible that this patient may have had a silent infarction, which is known to occur in up to 15% of patients with high grade stenosis (Brott et al., 1994).

In Figure 7.18 b and c, tissue with a healthy appearance gives a strong lipid signal on both the interior and exterior walls but as the tissue becomes more diseased the lipid signal on the tissue surface disappears. This suggests that with further analysis of the distribution and thickness of lipid on the plaque surface, it should be possible to create a tool to analyse the surface for areas of disruption and weakness which contribute to plaque vulnerability.

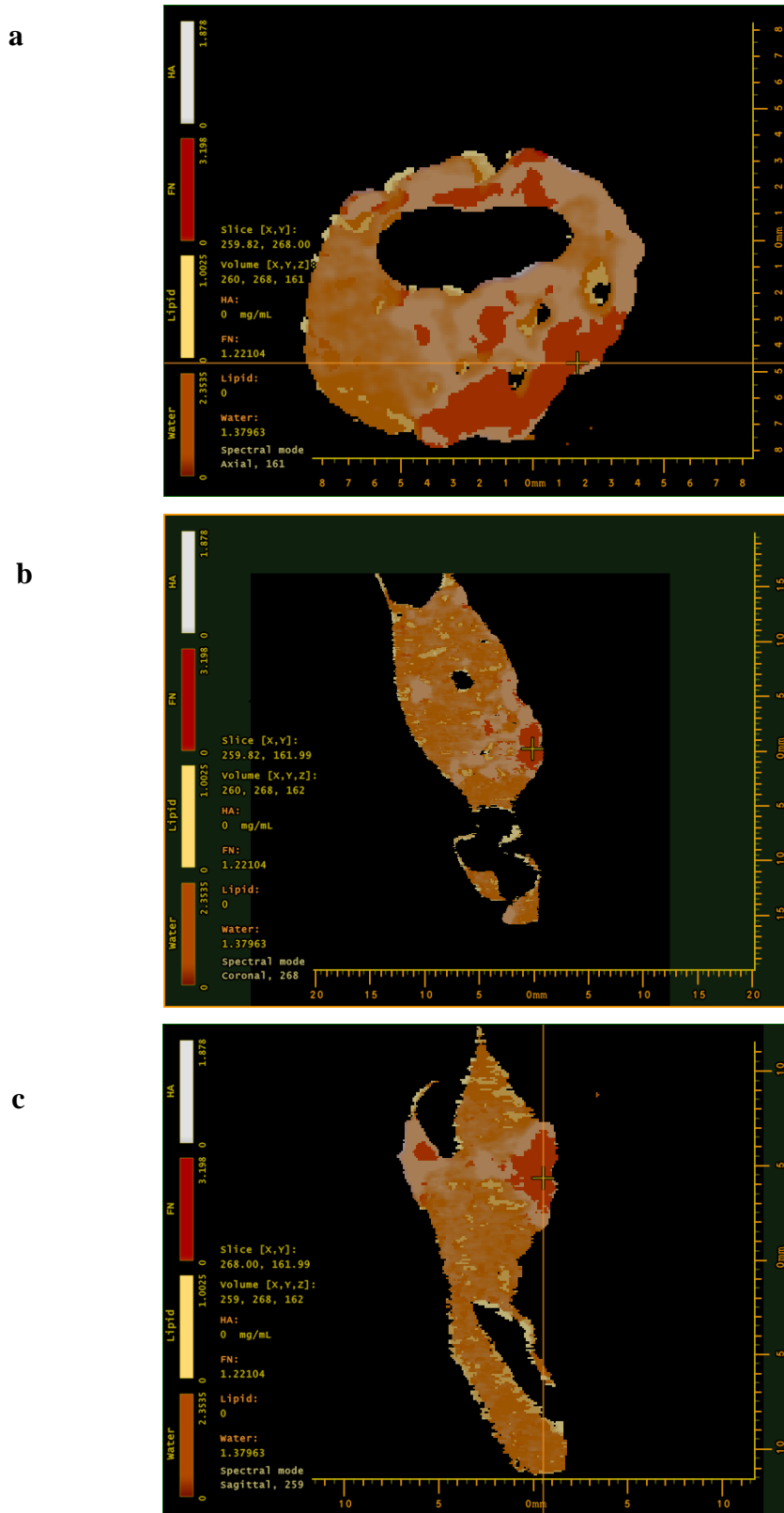


**Figure 7.18 Axial, coronal and sagittal slices from plaque 158.**

Orange-red represents soft tissue, beige is lipid, white is calcium, and iron is in dark red-maroon as identified in the colour scale bar on the left of each image.

To further characterize this plaque, it was sliced open horizontally. Figure 7.19 and Figure 7.20 compare photographic images of the plaque to an example from an axial slice of the 3D rendered MARS image. The dashed arrows on Figure 7.19 indicates where the axial slice was taken from. The red circles identify areas of increased iron deposits, and the yellow circle, lipid. The solid black line identifies an area of ulceration which was discussed previously. In figure 7.20, calcium is in white, lipid in yellow, iron is dark red and soft tissue is in orange.



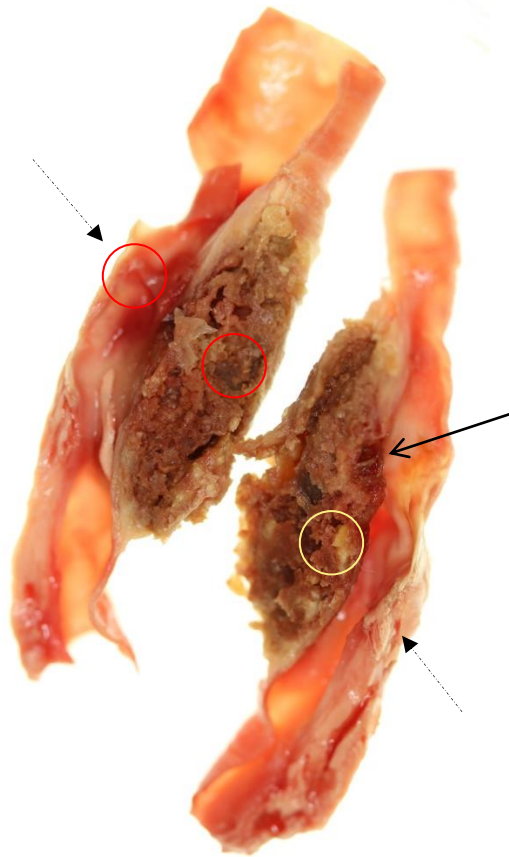


**Figure 7.19 Photograph of Plaque 158 cut in half.**

Red circles indicate areas of potential iron deposits and yellow for lipid. The solid arrow indicates an area of ulceration. The dashed arrows indicate approximately where the axial slice was selected from.



**Figure 7.20 Axial 3D MARS image of plaque 158.**

Orange-red represents soft tissue, beige is lipid, white is calcium, and iron is in dark red-maroon. Red circles indicate areas of potential iron deposits and yellow for lipid. The dashed white line represents the horizontal cut in the plaque

#### 7.4 Conclusion

Overall, there is excellent alignment between the photographic evidence and the MARS material image. This shows that MARS imaging is now at a stage where it can produce high quality, material decomposition images with good alignment to expected results. With high level images such as these it is now possible to start exploring ways to quantify plaque vulnerability across a range of subjects, using some of the methods suggested here such as plaque surface disruption, quantification of the amount of haemorrhage or microcalcification. It may be possible to move from the current cross-sectional approach to a more targeted approach analysing, for example, the differences in plaques based on the age of the patient. This could initially be conducted from the catalogue of frozen plaques that are currently stored. In addition, it may be worth also obtaining frozen plaque samples from other hospitals to increase the sample size for each grouping.

By resolving the issue around lipid detection and introducing detection of intraplaque haemorrhage, MARS imaging of vulnerable plaque is now sufficiently advanced to begin use as a quantitative tool. It is now possible to successfully obtain the distribution and concentration of microcalcification across the plaque, and there is initial evidence supporting the ability to detect ulceration and disturbances in the fibrous cap. Furthermore, a technique for identifying intraplaque haemorrhage has been successfully tested in blood clots and plaque tissue.

## 8 Imaging of nanoparticle probes targeting macrophages

The research was carried out in collaboration with Emily Searle (MSc candidate) and Dr Aamir Raja (Research Fellow, University of Otago), as part of a short project funded by a Grant-In-Aid from the Heart Foundation of New Zealand. For this body of work, I contributed to the design of the experiments and prepared the labelled LDL. I conducted all aspects relating to cell culture. Emily conducted the scanning and material decomposition of the samples. All interpretation of the results here is my own.

The work in this chapter was presented as a poster at the Society for Biomaterials meeting, Atlanta, GA, USA, 2018.

### 8.1 Introduction

For the last 30 years, iodine has been the primary contrast agent for imaging with CT (Riederer & Mistretta, 1977). Recently, it has been shown that two contrast agents (iodine and gadolinium) can be detected simultaneously using dual energy CT (Badea, Holbrook, Clark, & Ghaghada, 2018). However, spectral CT introduces the ability to capture the k-edge of multiple materials simultaneously (Moghiseh et al., 2016). This has opened the development of new contrast agents for CT. One of the most utilized of these new contrast agents has been gold nanoparticles due to their flexibility for attachment of antibodies, sensitivity of detection, and ease of use (Cormode et al., 2010; Hainfeld, Slatkin, Focella, & Smilowitz, 2006; Haller et al., 2015; Park, Pramanick, Kim, Lee, & Kim, 2017).

Here, the uptake of non-functionalized gold nanoparticles in HMDM cells has been explored in the presence and absence of human serum. In addition, functionalized nanoparticles were produced by using contrast agent, either iodine or gold nanoparticles, attached to a natural nanoparticle, LDL. Using LDL would be significantly more cost effective than antibody targeting. The advantage to using gold in the nanoparticle form is the ability to attach many more atoms of gold than if it were in an ionic form (Liu, Atwater, Wang, & Huo, 2007).

To test the *in vitro* uptake of labelled LDL a monocyte-like cell culture line, U937, which can be differentiated into macrophage-like cells has been used. Monocytes and macrophages have been identified as a key target, as these cells are involved in the very first stages of the development of the atherosclerotic lesion (Biessen & Wouters, 2017). Monocytes and macrophages take up LDL, which has become oxidised in the intima, via the scavenger receptor CD36 (Ceolotto et al., 2017; Chistiakov, Bobryshev, & Orekhov, 2016; Shchepetkina et al.,

2017). This process is uncontrolled and eventually the cells become full of toxic oxLDL and become necrotic, causing the formation of the necrotic core (Bekkering et al., 2014; Boshuizen et al., 2016).

The work in this chapter was focused on the methodology around producing contrast-enhanced LDL and is the first step towards a wider aim of developing spectral imaging techniques in conjunction with nanoparticle contrast agents that may allow atherosclerosis to be diagnosed at an early stage, where intervention will be much more effective.

## 8.2 Methods in brief

Plasma was obtained from healthy donors under ethics approval CTY/98/07/069 granted by the Upper South (B) Regional Ethics Committee. LDL was isolated from donor plasma using a centrifugation gradient separation method as described by Giese and Esterbauer (1994) as described in detail in Chapter 2. Isolated LDL was washed with phosphate buffered saline (PBS) using an Amicon Ultra-15 membrane filter centrifugation tubes (Millipore, USA) at 3000 g, 4°C for 30 minutes, and repeated twice. LDL concentration was adjusted to 10 mg (LDL total mass) per mL, which was determined using a total cholesterol assay kit (Roche Diagnostics, Germany), assuming the total cholesterol accounts for 31.69% of the LDL particle (MW 2500kDa).

Iodinated LDL (I-LDL) was prepared by gently mixing 500  $\mu$ L of 20 mM ICl in 2M NaCl with 1 mL of 10 mg/mL LDL. This solution was washed using the ultra-membrane filter tubes as described above. Native LDL (n-LDL) was prepared in the same manner except with the addition of 500  $\mu$ L of PBS rather than ICl. Gold nanoparticle labelled LDL (Au-LDL) was prepared by mixing 500  $\mu$ L of 0.5 mg/mL AuNPs with 1 mL of 10 mg/mL LDL (method modified from Handley, Arbeeny, and Chien (1981)). All solutions were filter sterilized through a 0.22  $\mu$ m filter prior to use in cell culture. Precipitation of LDL was initially carried out using 50% Trichloroacetic acid (TCA)/50% H<sub>2</sub>O. Upon scanning the pellets, the native LDL pellet registered as containing as much iodine as the I-LDL

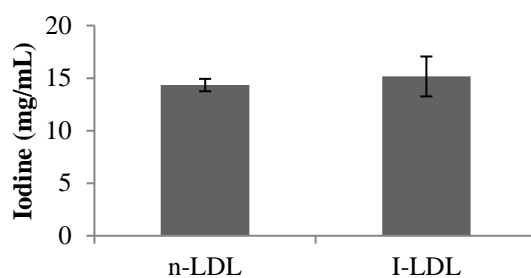


**Figure 8.1 Iodine measurement by spectral CT of pellets of n-LDL and I-LDL.** The iodine concentration was measured by selecting five regions of interest each of the same size within the pellet. Error bars are SD.

As the signal was consistent in both the pellet and the liquid region above the pellet which contained TCA, it was suspected that the misidentification was being caused by the TCA, possibly due to the high chlorine content. For subsequent experiments precipitated LDL was obtained by adding 500  $\mu$ L of acetonitrile (ACN) to 500  $\mu$ L of LDL (native, iodinated or Au-labelled) in 1.7 mL Eppendorf tubes and vortexing for 30 seconds. Precipitates were then centrifuged at 15,000 RPM for 10 minutes at 4°C to form pellets. The ACN supernatant was then removed and the pellets were carefully removed from the Eppendorf tubes and placed into PCR tubes for MARS spectral scanning. ACN precipitated pellets did not result in the misidentification of iodine.

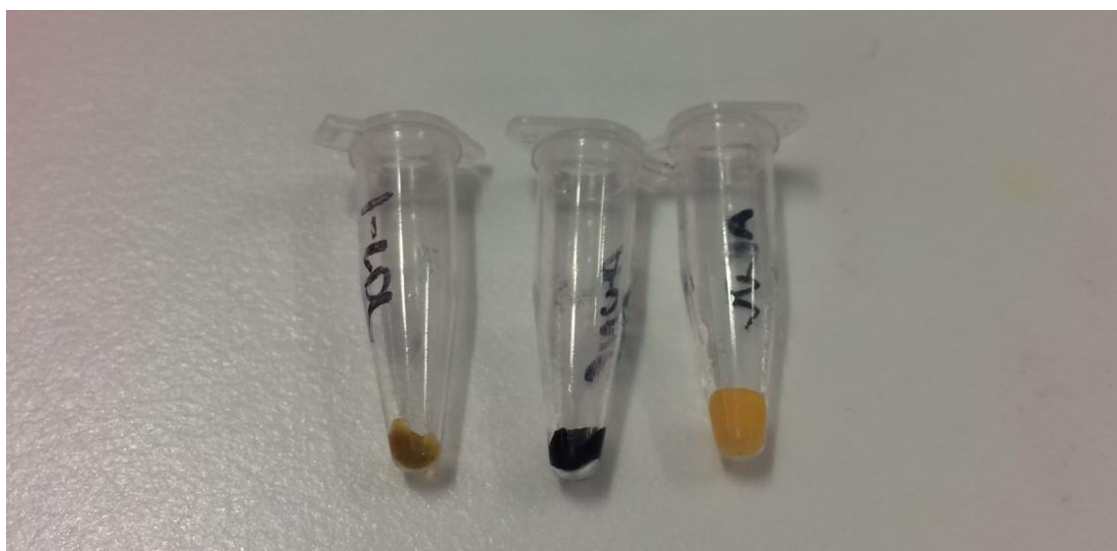


**Figure 8.2 ACN precipitated pellets of I-LDL, Au-LDL and n-LDL (left to right)**

For cell experiments, U937 cells were cultured in RPMI-1640 media containing 5% FBS. U937s were plated into 12 well plates (Nunc, Thermo Fisher Scientific, NZ Ltd) and differentiated for 24 hours with the addition of 100 ng/mL of phorbol-12-meristate-13-acetate

(PMA). Cells were then treated with n-LDL, Au-LDL and I-LDL at a final concentration of 2 mg/mL for 24 hours. The supernatant was then removed and the U937 cells were lifted from the plate using 200uL of Accutase which was incubated at room temperature for 15 minutes. The resulting liquid was transferred to PCR tubes and the cells were pelleted by centrifugation (1500 RPM, 5 minutes 20°C).

The MARS Spectral scanner (V 6.0) was used to image the tubes containing the samples of LDL (native, iodinated, and Au-labelled). For the initial analysis, the sample holder contained the liquid and precipitated LDL samples, in both their native form (control) and iodinated (I-LDL). In addition, samples of water, lipid, 9 mg/mL iodine and 18 mg/ml iodine were present, which are necessary for the calibration of the scan and analysis of results. In the same manner for the subsequent scan, the sample holder included the Eppendorf tubes of precipitated LDL (native, iodinated, and Au-labelled), accompanied by water, lipid, 9 mg/ml iodine, 18 mg/mL iodine, 4 mg/mL gold chloride ( $\text{AuCl}_3$ ) and 8 mg/mL  $\text{AuCl}_3$ . For the final scan, the sample holder contained the PCR tubes of cells treated with n-LDL, I-LDL and Au-LDL, along with samples of water, lipid, 9 mg/ml iodine, 18 mg/mL iodine, 4 mg/mL  $\text{AuCl}_3$  and 8 mg/mL  $\text{AuCl}_3$ .

The above experiments were imaged using a Factory AI Protocol with a filtration of 2mm of aluminium, which blocks low energy photons which would typically not penetrate the skin in a human scan. Using this filtration helps improve the ability to translate this research directly to human scale imaging. The samples were scanned using a tube voltage of 118 kVp, a tube current of 13 $\mu$ A, and an exposure time of 300ms per projection. There were 720 projections representing one full rotation of the camera gantry. Four energy bins were used, these in the range 18 – 29.9 keV, 29.9 – 44.9 keV, 44.9-77.9 keV, and 77.9 keV- 120 keV. This energy range expresses the k-edge of iodine at approximately 33.2 keV and captures the increase in attenuation of gold in the higher energy band, representing the k-edge of gold at approximately 80.7 keV.

## 8.3 Results

### 8.3.1 Non-functionalized gold nanoparticle uptake in macrophages

In previous experiments conducted in this laboratory, it was noticed that non-functionalized gold nanoparticles tended to clump in the cell culture media. Although it was still possible to get enough nanoparticle uptake, this took up to 72 hours. This experiment compared the uptake of non-functionalized gold nanoparticles after 24 hours of incubation with HMDM cells in the presence or absence of human serum (Figure 8.3). After 24 hours in the presence of serum, the media no longer contains the pink hue that is typical of gold nanoparticles in solution, however, there is no visual evidence of gold nanoparticle uptake in the HMDM cells. In HMDM cells incubated with gold nanoparticles in the absence of serum, the cells contain dark deposits of gold nanoparticles after 24 hours. This suggests that a component of the human serum is preventing uptake of non-functionalized gold nanoparticles.

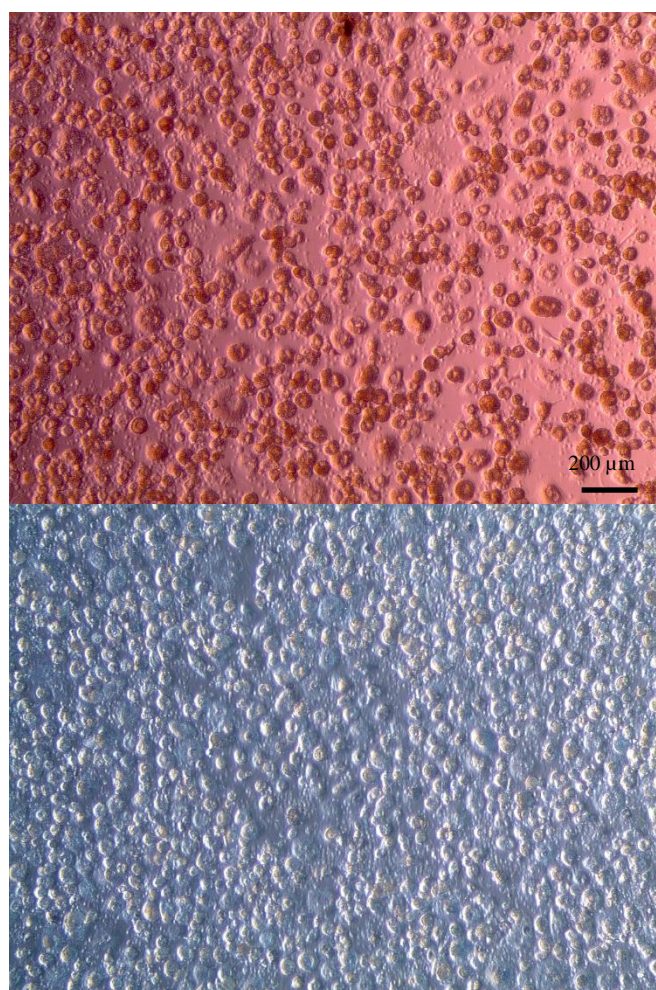


**Figure 8.3 Macrophages with 10 % Human Serum and Gold Nanoparticles prior to (top) and after (bottom) 24 hour incubation.**

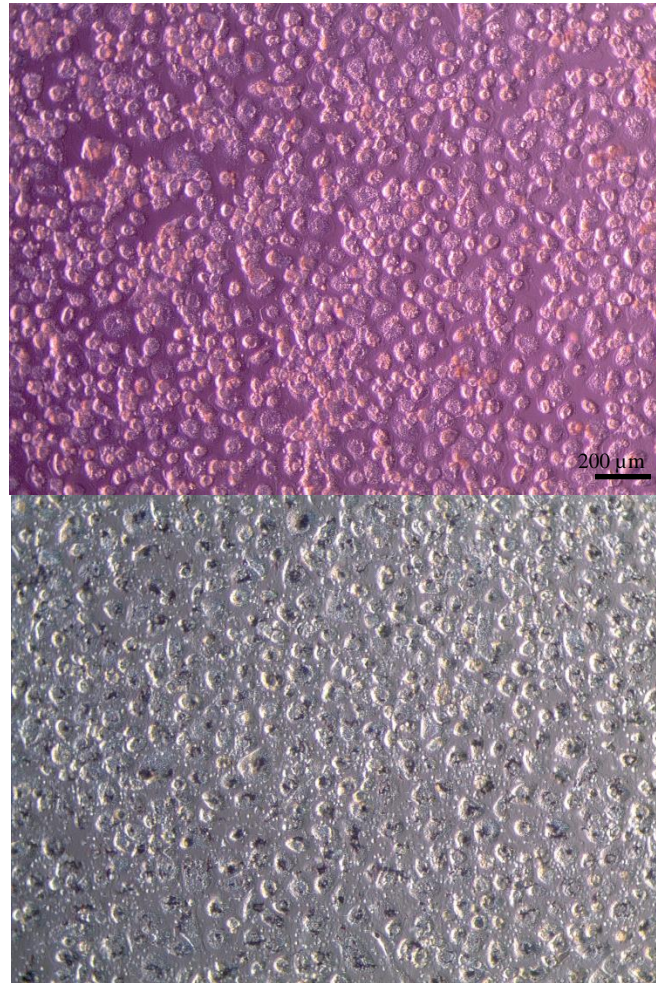


**Figure 8.4 Macrophages without Human Serum and Gold Nanoparticles prior to (top) and after (bottom) 24 hour incubation.**

The cells were then lifted from the plate using 200  $\mu$ L Accutase (as described in the Methods in brief) and pelleted so that they could be examined by spectral CT. The cells that had been incubated with gold nanoparticles in the presence of human serum showed no signal for gold, the same as the controls which did not contain nanoparticles. The HMDMs that had been incubated with gold nanoparticles in the absence of serum did identify positively as containing gold. This suggests that there may be difficulty in using non-functionalized gold nanoparticle to identify macrophages *in vivo*. To combat this issue, the next section of this thesis investigates using LDL particles as a way of functionalizing the contrast agent to target macrophage cells.





**Figure 8.5** Photo of layout of vials (left) and MARS image (right) of macrophages with non-functionalized gold nanoparticles.

### 8.3.2 Modified LDL as a probe for macrophage like cells

Liquid and precipitated LDL was prepared in either its native form (control) or I-LDL. At 10 mg/mL LDL, there was no measurable iodine in the liquid sample as measured by MARS scanning and subsequent material decomposition. In the precipitate, both the control (n-LDL) and the I-LDL gave a significant iodine signal in the material decomposition of the spectral images. All further precipitations were carried out using ACN. Precipitates containing 10 mg of Au-LDL or I-LDL produced a significant signal. To investigate whether the uptake of I-LDL or Au-LDL could be measured in monocyte-like and macrophage-like cells, we incubated un-differentiated and PMA-treated Au-LDL and I-LDL at 2 mg/mL. There was little colour change seen in pelleted U937 cells (2 million per pellet), whether the cells were differentiated to be macrophage-like using PMA or not. The colour of the cell media had not changed as it typically would if labelled-LDL was being taken up. This suggests there was poor uptake of the I-LDL and Au-LDL in U937 cells. Examination of the U937 cells by microscopy shows that cells have changed morphology due to the addition of PMA to increase LDL uptake (Figure 8.6). There is no evidence of gold clustering inside the cells (Figure 8.7) as was seen with the non-functionalized gold nanoparticles in HMDMs. Cells incubated with I-LDL appear to have undergone significant lysis, suggesting there may be a toxicity issue (Figure 8.8). Therefore, it

is not surprising that the MARS image of the pelleted cells did not indicate the presence of gold or iodine in the pelleted cells (Figure 8.9).

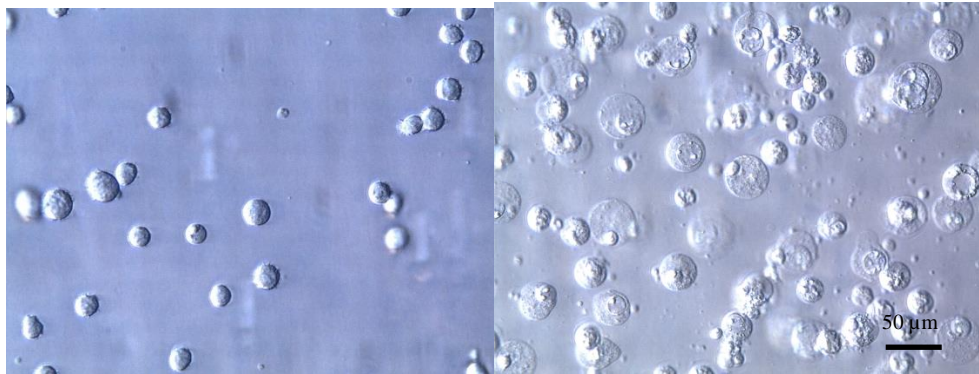


**Figure 8.6** PMA-treated U937 cells before (left) and after (right) 24 hours incubation with n-LDL

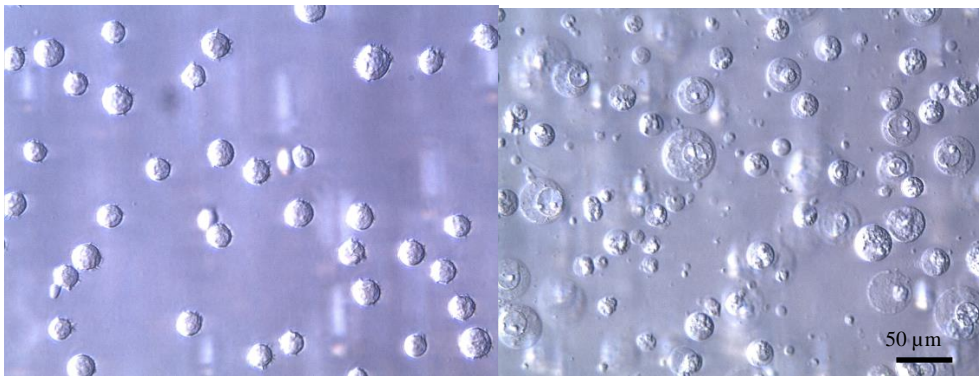


**Figure 8.7** PMA- treated U937 cells before (left) and after (right) 24 hours incubation with Au-LDL

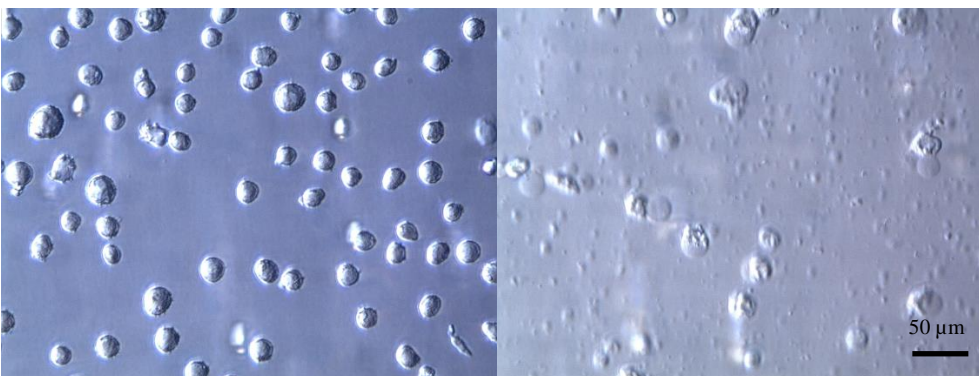


**Figure 8.8** PMA-treated U937 cells before (left) and after (right) 24 hours incubation with I-LDL

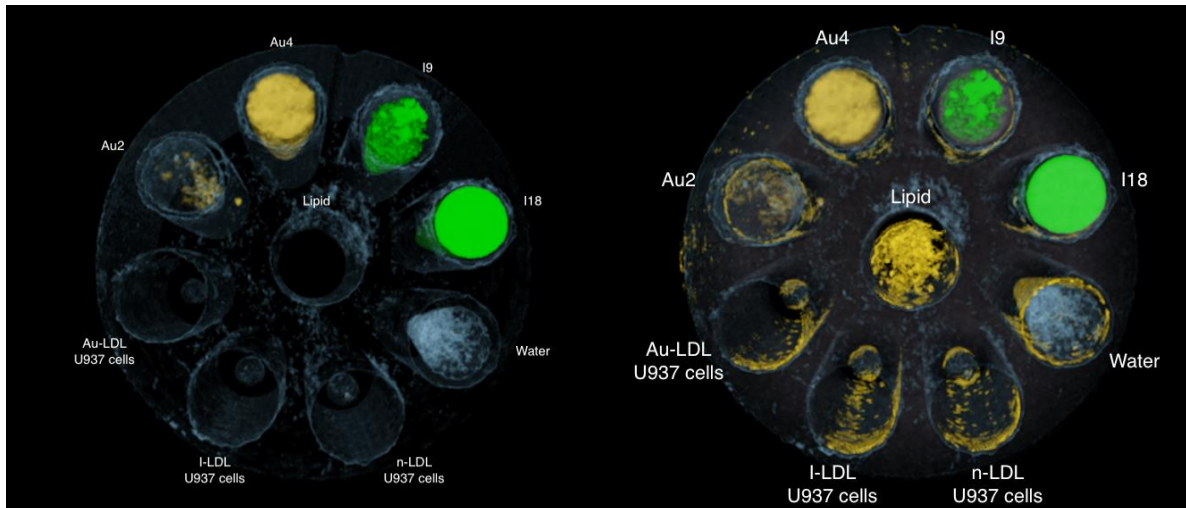


**Figure 8.9** MARS images of U937 cells incubated with modified LDL without (left) and with (right) lipid channel

#### 8.4 Discussion

Non-functionalized gold nanoparticles can be measured in macrophages in the absence of serum with a shorter incubation of 24 hours, but the presence of serum slows the uptake of the nanoparticles. Non-functionalized gold nanoparticles have been used successfully to investigate tumour neovascularization in a mouse model with spectral CT (unpublished). There was no evidence of the non-functionalised gold lodging in macrophages during the experiments conducted in this thesis however there were some key differences in that a much smaller nanoparticle was used for the tumour experiment, and the incubation time was longer. The tumour experiment also had the advantage that the leaky vessels enhanced the retention of gold nanoparticles. It is most likely that for gold-nanoparticles to be useful for *in vivo* experiments investigating macrophages they will need a form of targeting, such as to a cell surface receptor like CD68 or CD36.

LDL showed some promise as a low-cost way to target macrophages, however, getting the contrast enhanced LDL to be taken up in U937 cells proved difficult. The reason for using LDL was that it is already an approved therapy. Whilst oxLDL would be more effectively taken up by the cell due to unregulated uptake via CD36, oxLDL is toxic to cells, limiting its value for use in humans. There was an expectation that LDL may be sufficient to introduce the nanoparticle into the cell, and then for the LDL to be recycled via ABCAI. It is worth noting the maximum concentration of LDL that could be added to the cells was 2 mg/mL which is much lower than the 10mg/mL used for the precipitates. It was thought that if the cells had taken up the labelled LDL, there may have been a concentrating effect. It is possible that the

modification of LDL means that it is no longer recognized by the LDL receptor on U937 cells or that LDL uptake is severely limited by the number of receptors available (Tontonoz, Nagy, Alvarez, Thomazy, & Evans, 1998). An alternative possibility is that normal cell feedback mechanisms that are part of the regulation of cholesterol metabolism prevented significant uptake (Brown & Goldstein, 1983). Cormode et al. (2010) have used an alternative method that involves dissolving the lipid membrane of the LDL particle to insert the gold nanoparticles inside the LDL, and could see the uptake of these nanoparticles into the cell using TEM. This may be worth trialling with the MARS system. Otherwise, it may be possible to use modified LDL, such as acetylated-LDL or oxLDL which would avoid the normal regulation of cholesterol metabolism, and increase the amount accumulated in the cell (Jerome, Cox, Griffin, & Ullery, 2008).

## 8.5 Conclusion

Gold nanoparticles show promise as a contrast agent due to their ability to collect within macrophages which makes detection easier using tools such as MARS spectral CT. Developing viable methods for delivering gold nanoparticles targeted to macrophages or areas of increased inflammation is an ongoing research area.

## 9 General Discussion and Future Directions

Assessing how this work sits alongside the current literature is a difficult task. For many of these experiments, for example, the plaque culture, there are no directly comparable results to draw upon. Spectral CT is such a new technology that whilst groups in the US are also experimenting with using it to investigate plaque specimens, no results are currently available. For neopterin, despite the fact it is routinely used to assess inflammation there are no studies investigating the mechanism of its formation.

### 9.1 Biomarkers of inflammation

One of the specific aims of this thesis was to investigate the inflammatory response of macrophages within excised atherosclerotic plaque and the relation of the clinical biomarker neopterin, and its parent compound, 7,8-dihydroneopterin, to the morphology of the plaque. In addition, to explore the role of superoxide, a reactive oxygen species produced by NADPH oxidase in macrophages, in the oxidation of 7,8-dihydroneopterin to neopterin.

Neopterin is generated from superoxide induced oxidation of 7,8-dihydroneopterin, possibly via a stable charged intermediate. It is worth exploring the possibility of this intermediate further using techniques such as mass spectrometry, as this may be crucial to elucidating a mechanism for neopterin production in vivo that does not involve hypochlorite. One aspect that was not tested here was the effect of pH on the efficiency of neopterin generation. It is known that in the plaque environment there is a wide range of pH, anywhere from pH 6 - 8 (Naghavi et al., 2002), and this may help to explain why some sections of the plaque produce more neopterin than others.

A further goal of this thesis was to investigate the relationship between plaque morphology and its biochemical response, particularly release of neopterin and 7,8-dihydroneopterin, to stimuli. Plaque total neopterin output (macrophage activation) is correlated to plasma lactate values, which are known to be associated with the degree of carotid atherosclerosis present, and inversely correlated to calcium volume. The results here indicate that there is new information to be obtained by measuring total neopterin in a clinical setting. This has recently been demonstrated in the case of patients with muscular dystrophy (Angus Lindsay, Schmiechen, Chamberlain, Ervasti, & Lowe, 2018). Further research is needed to understand how high levels of total neopterin in patient plasma contribute to positive or negative clinical outcomes.

## 9.2 Future of MARS imaging

Another goal of this project was to develop techniques in conjunction with others that will identify macrophages and regions of interest within the plaque. In this thesis it has now been shown that key hallmarks of vulnerable plaque can be identified using MARS imaging. Much of this work has been focused on the identification of the markers as opposed to quantification. This project is now at a stage where it can move into characterizing and cataloguing plaques based on their morphology and composition. The next steps for this work are to assess how plaque vulnerability markers change across the population based on the vulnerable plaques that have already been collected. This work can move beyond the intrinsic markers discussed here to investigating macrophage density or phenotype using suitable nanoparticle-based contrast agents with specific antibodies bound. It is worth noting that some of this work has already been attempted by others using methods such as histology. The distinct value to repeating this work using MARS imaging is the ability to capture all the information from each plaque. However, a common criticism of this type of work is that by their nature all these plaques are vulnerable. Accessing plaques from autopsy is a possibility but as the patient is no longer alive, there is no way to know whether the plaque would have been vulnerable or not. These are two of the main reasons why establishing the triggers of plaque vulnerability has been so difficult in the past. MARS imaging is likely to solve this issue in the future, as the results obtained using excised specimens in the small animal scanner are directly translatable to human scale imaging. Within the next 5 to 10 years it should be possible to conduct a long-term study to follow plaque development and vulnerability in a clinical setting within minimal harm to those involved. In the meantime, cataloguing of existing plaques will help to identify which features should be explored first when the human scale technology is available.

## 9.3 Conclusion

This thesis investigated the relationship between plaque morphology and the biochemical markers of inflammation, 7,8-dihydroneopterin and neopterin. It was found that plaque total neopterin is inversely related to calcium deposition. This finding is significant as this is the first evidence that plaque morphology may influence inflammatory biomarkers. The biochemical response of plaque tissue is likely to be varied due to differences in morphology, which has implications for treatment of plaques *in vivo*. In addition, this thesis explored the role of superoxide in the oxidation of 7,8-dihydroneopterin to neopterin. It was found that oxidation to neopterin did occur, but this could be modulated using SOD and catalase. A possible mechanism for the oxidation to neopterin was hypothesized based on the evidence

presented here. This new evidence that superoxide has a role in neopterin formation is significant, as it adds to the evidence that both total neopterin and neopterin should be considered as clinical biomarkers for atherosclerosis. Finally, it has been shown here that using MARS spectral CT, images of plaque with regions of interest such as necrotic core, intraplaque haemorrhage and microcalcification can be obtained. This demonstrates this work is now ready for translation to human scale imaging where non-invasive images of the key hallmarks of vulnerable plaque will have an impact on how atherosclerosis is diagnosed and treated in the future.

#### 9.4 Summary

Understanding the complex reactions that form neopterin from 7,8-dihydroneopterin are important for the utility of both neopterin and 7,8-dihydroneopterin as biomarkers of inflammation. Plaque culture experiments showed that modulation of oxidants influenced the balance of both neopterin and 7,8-dihydroneopterin, and that there is a differential response across the plaque tissue, dependent on the level of calcification. This is significant as this is a first step towards being able to relate macrophage activity in vulnerable tissue to plasma markers which would help to improve clinical assessment of atherosclerosis.

MARS imaging of plaque tissue produces high quality images with excellent differentiation of key hallmarks of plaque vulnerability, including lipid pools within the necrotic core and microcalcification, which are highly consistent with visual inspection of the tissue. Intraplaque haemorrhage can be identified and differentiated from calcification in ex-vivo plaque tissue. This is significant as iron and calcium cannot be distinguished using traditional CT methods, and it provides a further tool to assess plaque vulnerability.

## References

- Abo, A., Pick, E., Hall, A., Totty, N., Teahan, C. G., & Segal, A. W. J. N. (1991). Activation of the NADPH oxidase involves the small GTP-binding protein p21rac1. *353*(6345), 668.
- Adachi, T., Naruko, T., Itoh, A., Komatsu, R., Abe, Y., Shirai, N., . . . Ueda, M. (2007). Neopterin is associated with plaque inflammation and destabilisation in human coronary atherosclerotic lesions. *Heart*, *93*(12), 1537-1541.  
doi:10.1136/hrt.2006.109736
- Adamik, B., Kübler-Kielb, J., Golebiowska, B., Gamian, A., & Kübler, A. J. I. c. m. (2000). Effect of sepsis and cardiac surgery with cardiopulmonary bypass on plasma level of nitric oxide metabolites, neopterin, and procalcitonin: correlation with mortality and postoperative complications. *26*(9), 1259-1267.
- Agarwal, A., Aponte-Mellado, A., Premkumar, B. J., Shaman, A., Gupta, S. J. R. b., & endocrinology. (2012). The effects of oxidative stress on female reproduction: a review. *10*(1), 49.
- Agil, A., Fuller, C. J., & Jialal, I. (1995). SUSCEPTIBILITY OF PLASMA TO FERROUS IRON HYDROGEN PEROXIDE-MEDIATED OXIDATION - DEMONSTRATION OF A POSSIBLE FENTON REACTION. *Clinical Chemistry*, *41*(2), 220-225.
- Alberti, K. G. M. M., Eckel, R. H., Grundy, S. M., Zimmet, P. Z., Cleeman, J. I., Donato, K. A., . . . Smith, S. C., Jr. (2009). Harmonizing the Metabolic Syndrome A Joint Interim Statement of the International Diabetes Federation Task Force on Epidemiology and Prevention; National Heart, Lung, and Blood Institute; American Heart Association; World Heart Federation; International Atherosclerosis Society; and International Association for the Study of Obesity. *Circulation*, *120*(16), 1640-1645.  
doi:10.1161/circulationaha.109.192644
- Alexander, M. R., Moehle, C. W., Johnson, J. L., Yang, Z., Lee, J. K., Jackson, C. L., & Owens, G. K. (2012). Genetic inactivation of IL-1 signaling enhances atherosclerotic plaque instability and reduces outward vessel remodeling in advanced atherosclerosis in mice. *The Journal of clinical investigation*, *122*(1), 70-79.
- Altenhöfer, S., Radermacher, K. A., Kleikers, P. W., Winkler, K., Schmidt, H. H. J. A., & signaling, r. (2015). Evolution of NADPH oxidase inhibitors: selectivity and mechanisms for target engagement. *23*(5), 406-427.
- Anderson, N. G., & Butler, A. P. (2014). Clinical applications of spectral molecular imaging: potential and challenges. *Contrast media & molecular imaging*, *9*(1), 3-12.
- Aroney, C. N. (2012). A Suggested Paradigm for Coronary Risk Screening in Asymptomatic Persons-Assessment of Total Coronary Atheromatous Burden. *Heart Lung and Circulation*, *21*(8), 449-454. doi:10.1016/j.hlc.2012.02.008
- Auclair, C., Torres, M., & Hakim, J. (1978). Superoxide anion involvement in NBT reduction catalyzed by nadph-cytochrome P-450 reductase: A pitfall. *Febs Letters*, *89*(1), 26-28.
- Augusto, O., & Miyamoto, S. (2011). Oxygen radicals and related species. *Principles of free radical biomedicine*, *1*, 19-42.
- Avanzas, P., Arroyo-Espliguero, R., Quiles, J., Roy, D., & Kaski, J. C. (2005). Elevated serum neopterin predicts future adverse cardiac events in patients with chronic stable angina pectoris. *European Heart Journal*, *26*(5), 457-463.  
doi:10.1093/eurheartj/ehi111



- Badea, C., Holbrook, M., Clark, D., & Ghaghada, K. (2018). *Spectral imaging of iodine and gadolinium nanoparticles using dual-energy CT*. Paper presented at the Medical Imaging 2018: Physics of Medical Imaging.
- Bánfi, B., Tirone, F., Durussel, I., Knisz, J., Moskwa, P., Molnár, G. Z., . . . Cox, J. A. J. J. o. B. C. (2004). Mechanism of Ca<sup>2+</sup> activation of the NADPH oxidase NOX5.
- Barnett, H. J. M., & Collaborators, N. (1998). Final results of the North American Symptomatic Carotid Endarterectomy Trial (NASCET). *Stroke*, 29(1), 286-286.
- Baydar, T., Yuksel, O., Sahin, T. T., Dikmen, K., Girgin, G., Sipahi, H., . . . Sare, M. (2009). Neopterin as a prognostic biomarker in intensive care unit patients. *Journal of critical care*, 24(3), 318-321.
- Beauchamp, C., & Fridovich, I. (1971). Superoxide dismutase: improved assays and an assay applicable to acrylamide gels. *Analytical Biochemistry*, 44(1), 276-287.
- Bedard, K., & Krause, K.-H. J. P. r. (2007). The NOX family of ROS-generating NADPH oxidases: physiology and pathophysiology. 87(1), 245-313.
- Behnes, M., Brueckmann, M., Wiessner, M., Kettenmann, E., Liebetrau, C., Lang, S., . . . Hoffmann, U. (2008). Time-course of neopterin levels in patients suffering from severe sepsis treated with and without Drotrecogin-alpha (activated). *Scandinavian journal of infectious diseases*, 40(6-7), 503-508.
- Bekkering, S., Quintin, J., Joosten, L. A. B., van der Meer, J. W. M., Netea, M. G., & Riksen, N. P. (2014). OXLDL INDUCES LONG-TERM PRO-INFLAMMATORY CYTOKINE PRODUCTION AND FOAM CELL FORMATION VIA EPIGENETIC REPROGRAMMING OF MONOCYTES. *Atherosclerosis*, 235(2), E40-E40.
- Ben-Sasson, S. Z., Hu-Li, J., Quiel, J., Cauchetaux, S., Ratner, M., Shapira, I., . . . Paul, W. E. (2009). IL-1 acts directly on CD4 T cells to enhance their antigen-driven expansion and differentiation. *Proceedings of the National Academy of Sciences*, 106(17), 7119-7124.
- Biessen, E. A. L., & Wouters, K. (2017). Macrophage complexity in human atherosclerosis: opportunities for treatment? *Current Opinion in Lipidology*, 28(5), 419-426. doi:10.1097/mol.0000000000000447
- Boshuizen, M. C. S., Hoeksema, M. A., Neele, A. E., van der Velden, S., Hamers, A. A. J., Van den Bossche, J., . . . de Winther, M. P. J. (2016). Interferon-beta promotes macrophage foam cell formation by altering both cholesterol influx and efflux mechanisms. *Cytokine*, 77, 220-226. doi:10.1016/j.cyto.2015.09.016
- Bots, M. L., Hofman, A., & Grobbee, D. E. (1997). Increased common carotid intima-media thickness - Adaptive response or a reflection of atherosclerosis? Findings from the Rotterdam study. *Stroke*, 28(12), 2442-2447. doi:10.1161/01.str.28.12.2442
- Bove, A. A., Santamore, W. P., Homko, C., Kashem, A., Cross, R., McConnell, T. R., . . . Menapace, F. (2011). Treatment of patients with intermediate cardiovascular risk: Are clinical measures enough? *Journal of Nuclear Cardiology*, 18(6), 1021-1025. doi:10.1007/s12350-011-9415-7
- Boyaud, F., & Inguibert, N. (2011). Soluble fms-like tyrosine kinase-1 antibody for diagnosis purposes (WO2010075475). *Expert Opinion on Therapeutic Patents*, 21(6), 971-975. doi:10.1517/13543776.2011.577071
- Brott, T., Tomsick, T., Feinberg, W., Johnson, C., Biller, J., Broderick, J., . . . Locklear, J. (1994). BASE-LINE SILENT CEREBRAL INFARCTION IN THE ASYMPTOMATIC CAROTID ATHEROSCLEROSIS STUDY. *Stroke*, 25(6), 1122-1129.
- Brown, M. S., & Goldstein, J. L. (1983). Lipoprotein metabolism in the macrophage: implications for cholesterol deposition in atherosclerosis. *Annual review of biochemistry*, 52(1), 223-261.

- Budoff, M. J., Achenbach, S., Blumenthal, R. S., Carr, J. J., Goldin, J. G., Greenland, P., . . . Wieggers, S. E. (2006). Assessment of coronary artery disease by cardiac computed tomography - A scientific statement from the American Heart Association committee on cardiovascular imaging and intervention, council on cardiovascular radiology and intervention, and Committee on Cardiac Imaging, Council on Clinical Cardiology. *Circulation*, *114*(16), 1761-1791. doi:10.1161/circulationaha.106.178458
- Burrowes, H. M. (2012). Macrophage Activation and Differentiation with Cholesterol Crystals.
- Butler, A. P. H., Anderson, N. G., Tipples, R., Cook, N., Watts, R., Meyer, J., . . . Butler, P. H. (2008). Bio-medical X-ray imaging with spectroscopic pixel detectors. *Nuclear Instruments & Methods in Physics Research Section a-Accelerators Spectrometers Detectors and Associated Equipment*, *591*(1), 141-146. doi:10.1016/j.nima.2008.03.039
- Byrne, Jonathan A, Grieve, D. J., Bendall, J. K., Li, J.-M., Gove, C., Lambeth, J. D., . . . Shah, A. M. J. C. r. (2003). Contrasting roles of NADPH oxidase isoforms in pressure-overload versus angiotensin II-induced cardiac hypertrophy. *93*(9), 802-805.
- Ceolotto, G., Giannella, A., Albiero, M., Kuppusamy, M., Radu, C., Simioni, P., . . . de Kreutzenberg, S. V. (2017). miR-30c-5p regulates macrophage-mediated inflammation and pro-atherosclerosis pathways. *Cardiovascular Research*, *113*(13), 1627-1638. doi:10.1093/cvr/cvx157
- CF, N. (1986). Peroxide and pteridine: a hypothesis on the regulation of macrophage antimicrobial activity by interferon gamma. *Interferon*, *7*, 125-143.
- Chen, Y. H., Shi, W., Liang, X. L., Liang, Y. Z., & Fu, X. (2011). Effect of blood sample type on the measurement of advanced oxidation protein products as a biomarker of inflammation and oxidative stress in hemodialysis patients. *Biomarkers*, *16*(2), 129-135. doi:10.3109/1354750x.2010.535172
- Chiba, T., & Umegaki, K. (2013). Pivotal Roles of Monocytes/Macrophages in Stroke. *Mediators of Inflammation*, *10*. doi:10.1155/2013/759103
- Chinetti-Gbaguidi, G., Baron, M., Bouhrel, M. A., Vanhoutte, J., Copin, C., Sebti, Y., . . . Tailleux, A. (2011). Human atherosclerotic plaque alternative macrophages display low cholesterol handling but high phagocytosis because of distinct activities of the PPAR $\gamma$  and LXR $\alpha$  pathways. *Circulation Research*, CIRCRESAHA. 110.233775.
- Chinetti-Gbaguidi, G., Colin, S., & Staels, B. (2015). Macrophage subsets in atherosclerosis. *Nature Reviews Cardiology*, *12*(1), 10.
- Chistiakov, D. A., Bobryshev, Y. V., & Orekhov, A. N. (2016). Macrophage-mediated cholesterol handling in atherosclerosis. *Journal of Cellular and Molecular Medicine*, *20*(1), 17-28. doi:10.1111/jcmm.12689
- Chung, T. (2002). Current imaging status - Cardiac MRI. *Pediatric Chest Imaging*, 285-296.
- Cormode, D. P., Roessl, E., Thran, A., Skajaa, T., Gordon, R. E., Schlomka, J. P., . . . Fayad, Z. A. (2010). Atherosclerotic Plaque Composition: Analysis with Multicolor CT and Targeted Gold Nanoparticles. *Radiology*, *256*(3), 774-782. doi:10.1148/radiol.10092473
- Criqui, M. H., Denenberg, J. O., Ix, J. H., McClelland, R. L., Wassel, C. L., Rifkin, D. E., . . . Allison, M. A. (2014). Calcium Density of Coronary Artery Plaque and Risk of Incident Cardiovascular Events. *JAMA : the journal of the American Medical Association*, *311*(3), 271-278. doi:10.1001/jama.2013.282535
- Crossman, D. C., Morton, A. C., Gunn, J. P., Greenwood, J. P., Hall, A. S., Fox, K. A., . . . Foley, C. E. (2008). Investigation of the effect of Interleukin-1 receptor antagonist (IL-1ra) on markers of inflammation in non-ST elevation acute coronary syndromes (The MRC-ILA-HEART Study). *Trials*, *9*(1), 8.

- Culling, C. F. A., Allison, R., & Barr, W. (2014). *Cellular pathology technique*: Elsevier.
- Dantola, M. L., Thomas, A. H., Braun, A. M., Oliveros, E., & Lorente, C. (2007). Singlet oxygen (O-2((1)Delta(g))) quenching by dihydropterins. *Journal of Physical Chemistry A*, *111*(20), 4280-4288. doi:10.1021/jp071278h
- Davies, S. P. M. (2015). *7, 8-Dihydroneopterin and Its Effect on the Formation of Foam Cells: A Thesis Submitted in Partial Fulfilment of the Requirements for the Degree of Master of Science in Biochemistry at the University of Canterbury, New Zealand, School of Biological Sciences, University of Canterbury*. University of Canterbury,
- De Rosa, S., Cirillo, P., Pacileo, M., Petrillo, G., D'Ascoli, G. L., Maresca, F., . . . Chiariello, M. (2011). Neopterin: From Forgotten Biomarker to Leading Actor in Cardiovascular Pathophysiology. *Current Vascular Pharmacology*, *9*(2), 188-199. doi:10.2174/157016111794519372
- Detrano, R. C., Wong, N. D., Doherty, T. M., Shavelle, R. M., Tang, W. Y., Ginzton, L. E., . . . Narahara, K. A. (1999). Coronary calcium does not accurately predict near-term future coronary events in high-risk adults. *Circulation*, *99*(20), 2633-2638.
- Dhamoon, M. S., Sciacca, R. R., Rundek, T., Sacco, R. L., & Elkind, M. S. V. (2006). Recurrent stroke and cardiac risks after first ischemic stroke - The Northern Manhattan Study. *Neurology*, *66*(5), 641-646. doi:10.1212/01.wnl.0000201253.93811.f6
- Di Marco, E., Gray, S., Chew, P., Koulis, C., Ziegler, A., Szyndralewicz, C., . . . Slattery, R. (2014). Pharmacological inhibition of NOX reduces atherosclerotic lesions, vascular ROS and immune-inflammatory responses in diabetic Apoe<sup>-/-</sup> mice. *Diabetologia*, *57*(3), 633-642.
- Docherty, C. K., Carswell, A., Friel, E., & Mercer, J. R. (2018). Impaired mitochondrial respiration in human carotid plaque atherosclerosis: A potential role for Pink1 in vascular smooth muscle cell energetics. *Atherosclerosis*, *268*, 1-11.
- Duewell, P., Kono, H., Rayner, K. J., Sirois, C. M., Vladimer, G., Bauernfeind, F. G., . . . Schnurr, M. (2010). NLRP3 inflammasomes are required for atherogenesis and activated by cholesterol crystals. *Nature*, *464*(7293), 1357.
- Elliott, M. R., Koster, K. M., & Murphy, P. S. (2017). Efferocytosis signaling in the regulation of macrophage inflammatory responses. *The Journal of Immunology*, *198*(4), 1387-1394.
- Ellison, M. A., Thurman, G., Gearheart, C. M., Seewald, R. H., Porter, C. C., & Ambruso, D. R. (2015). INF-gamma Enhances Nox2 Activity by Upregulating phox Proteins When Applied to Differentiating PLB-985 Cells but Does Not Induce Nox2 Activity by Itself. *PLoS One*, *10*(8), 19. doi:10.1371/journal.pone.0136766
- Emsley, H. C. A., Smith, C. J., Gavin, C. M., Georgiou, R. F., Vail, A., Barberan, E. M., . . . Hopkins, S. J. (2007). Clinical outcome following acute ischaemic stroke relates to both activation and autoregulatory inhibition of cytokine production. *Bmc Neurology*, *7*, 12. doi:10.1186/1471-2377-7-5
- Endo, A. (2017). Discovery and Development of Statins. *Natural Product Communications*, *12*(8), 1153-1156.
- Erbel, C., Wolf, A., Lasitschka, F., Linden, F., Domschke, G., Akhavanpoor, M., . . . Gleissner, C. A. (2015). Prevalence of M4 macrophages within human coronary atherosclerotic plaques is associated with features of plaque instability. *International Journal of Cardiology*, *186*, 219-225.
- Favalli, V., Serio, A., Giuliani, L. P., & Arbustini, E. (2017). 'Precision and personalized medicine,' a dream that comes true? *Journal of Cardiovascular Medicine*, *18*, e1-e6. doi:10.2459/jcm.0000000000000423

- Feasby, T. E., & Barnett, H. J. M. (2007). Improving the appropriateness of carotid endarterectomy. *Neurology*, *68*(3), 172-173. doi:10.1212/01.wnl.0000254507.52005.7d
- Feigin, V., Carter, K., Hackett, M., Barber, P. A., McNaughton, H., Dyal, L., . . . Auckland Regional Community, S. (2006). Ethnic disparities in incidence of stroke subtypes: Auckland Regional Community Stroke Study, 2002-2003. *Lancet Neurology*, *5*(2), 130-139. doi:10.1016/s1474-4422(05)70325-2
- Firoz, C. K., Jabir, N. R., Kamal, M. A., Alama, M. N., Damanhour, G. A., Khan, W., . . . Tabrez, S. (2015). Neopterin: An immune biomarker of coronary artery disease and its association with other CAD markers. *Iubmb Life*, *67*(6), 453-459. doi:10.1002/iub.1390
- Fisher, M. R., Steinberg, F. L., & Rogers, L. F. (1987). FUNCTIONAL CARDIAC MRI. *Investigative radiology*, *22*(9), S29-S29. doi:10.1097/00004424-198709000-00132
- Flavall, E. A., Crone, E. M., Moore, G. A., & Gieseg, S. P. (2008). Dissociation of neopterin and 7,8-dihydroneopterin from plasma components before HPLC analysis. *Journal of Chromatography B-Analytical Technologies in the Biomedical and Life Sciences*, *863*(1), 167-171. doi:10.1016/j.jchromb.2007.12.019
- Formanowicz, D., Radom, M., Rybarczyk, A., & Formanowicz, P. (2018). The role of Fenton reaction in ROS-induced toxicity underlying atherosclerosis - modeled and analyzed using a Petri net-based approach. *Biosystems*, *165*, 71-87. doi:10.1016/j.biosystems.2018.01.002
- Fornai, F., Carrizzo, A., Forte, M., Ambrosio, M., Damato, A., Ferrucci, M., . . . Vecchione, C. (2016). The inflammatory protein Pentraxin 3 in cardiovascular disease. *Immunity & Ageing*, *13*. doi:10.1186/s12979-016-0080-1
- Fridovich, I. (1970). Quantitative aspects of the production of superoxide anion radical by milk xanthine oxidase. *Journal of Biological Chemistry*, *245*(16), 4053-4057.
- Galaska, R., Kulawiak-Galaska, D., Wegrzyn, A., Wasag, B., Chmara, M., Borowiec, J., . . . Gruchala, M. (2016). Assessment of Subclinical Atherosclerosis Using Computed Tomography Calcium Scores in Patients with Familial and Nonfamilial Hypercholesterolemia. *Journal of Atherosclerosis and Thrombosis*, *23*(5), 588-595.
- Galkina, E., & Ley, K. (2009). Immune and inflammatory mechanisms of atherosclerosis. *Annual review of immunology*, *27*, 165-197.
- Gao, H., & Long, Q. (2008). Effects of varied lipid core volume and fibrous cap thickness on stress distribution in carotid arterial plaques. *Journal of Biomechanics*, *41*(14), 3053-3059. doi:10.1016/j.jbiomech.2008.07.011
- Geng, S., Chen, K., Yuan, R., Peng, L., Maitra, U., Diao, N., . . . Qi, C.-F. (2016). The persistence of low-grade inflammatory monocytes contributes to aggravated atherosclerosis. *Nature communications*, *7*, 13436.
- Gerry, A. B., Satchell, L., & Leake, D. S. (2008). A novel method for production of lipid hydroperoxide-or oxysterol-rich low-density lipoprotein. *Atherosclerosis*, *197*(2), 579-587.
- Gesierich, A., Niroomand, F., & Tiefenbacher, C. P. (2003). Role of human GTP cyclohydrolase I and its regulatory protein in tetrahydrobiopterin metabolism. *Basic Research in Cardiology*, *98*(2), 69-75. doi:10.1007/s00395-003-0394-y
- Gieseg, S., Duggan, S., & Gebicki, J. M. (2000). Peroxidation of proteins before lipids in U937 cells exposed to peroxy radicals. *Biochemical Journal*, *350*, 215-218. doi:10.1042/0264-6021:3500215
- Gieseg, S. P., Amit, Z., Yang, Y. T., Shchepetkina, A., & Katouah, H. (2010). Oxidant Production, oxLDL Uptake, and CD36 Levels in Human Monocyte-Derived Macrophages Are Downregulated by the Macrophage-Generated Antioxidant 7,8-

- Dihydroneopterin. *Antioxidants & Redox Signaling*, 13(10), 1525-1534.  
doi:10.1089/ars.2009.3065
- Giese, S. P., Crone, E. M., Flavall, E. A., & Amit, Z. (2008). Potential to inhibit growth of atherosclerotic plaque development through modulation of macrophage neopterin/7,8-dihydroneopterin synthesis. *British Journal of Pharmacology*, 153(4), 627-635.  
doi:10.1038/sj.bjp.0707408
- Giese, S. P., & Esterbauer, H. (1994). LOW-DENSITY-LIPOPROTEIN IS SATURABLE BY PROOXIDANT COPPER. *Febs Letters*, 343(3), 188-194. doi:10.1016/0014-5793(94)80553-9
- Giese, S. P., Leake, D. S., Flavall, E. M., Amit, Z., Reid, L., & Yang, Y.-T. J. F. b. (2009). Macrophage antioxidant protection within atherosclerotic plaques. *14*(1), 230-246.
- Giese, S. P., Reibnegger, G., Wachter, H., & Esterbauer, H. (1995). 7,8-DIHYDRONEOPTERIN INHIBITS LOW-DENSITY-LIPOPROTEIN OXIDATION IN-VITRO - EVIDENCE THAT THIS MACROPHAGE SECRETED PTERIDINE IS AN ANTIOXIDANT. *Free Radical Research*, 23(2), 123-136.  
doi:10.3109/10715769509064027
- Gostner, J. M., & Fuchs, D. (2016). Biomarkers for the role of macrophages in the development and progression of atherosclerosis. *Atherosclerosis*, 255, 117-118.  
doi:10.1016/j.atherosclerosis.2016.10.046
- Gostner, J. M., Raggl, E., Becker, K., Uberall, F., Schennach, H., Pease, J. E., & Fuchs, D. (2015). Bisphenol A suppresses Th1-type immune response in human peripheral blood mononuclear cells in vitro. *Immunology Letters*, 168(2), 285-292.  
doi:10.1016/j.imlet.2015.10.006
- Gruson, D., Hermans, M. P., Ferracin, B., Ahn, S. A., & Rousseau, M. F. (2016). Sflt-1 in heart failure: relation with disease severity and biomarkers. *Scandinavian Journal of Clinical & Laboratory Investigation*, 76(5), 411-416.  
doi:10.1080/00365513.2016.1190863
- Gu, H. M., & Zhang, D. W. (2015). Hypercholesterolemia, low density lipoprotein receptor and proprotein convertase subtilisin/kexin-type 9. *Journal of Biomedical Research*, 29(5), 356-361. doi:10.7555/jbr.29.20150067
- Gupta, A., Baradaran, H., Schweitzer, A. D., Kamel, H., Pandya, A., Delgado, D., . . . Sanelli, P. C. (2013). Carotid Plaque MRI and Stroke Risk A Systematic Review and Meta-analysis. *Stroke*, 44(11), 3071-3077. doi:10.1161/strokeaha.113.002551
- Hainfeld, J., Slatkin, D., Focella, T., & Smilowitz, H. (2006). Gold nanoparticles: a new X-ray contrast agent. *The British journal of radiology*, 79(939), 248-253.
- Halade, G. V., Jin, Y. F., & Lindsey, M. L. (2013). Matrix metalloproteinase (MMP)-9: A proximal biomarker for cardiac remodeling and a distal biomarker for inflammation. *Pharmacology & Therapeutics*, 139(1), 32-40. doi:10.1016/j.pharmthera.2013.03.009
- Haller, E., Lindner, W., & Lammerhofer, M. (2015). Gold nanoparticle-antibody conjugates for specific extraction and subsequent analysis by liquid chromatography-tandem mass spectrometry of malondialdehyde-modified low density lipoprotein as biomarker for cardiovascular risk. *Analytica Chimica Acta*, 857, 53-63.  
doi:10.1016/j.aca.2014.12.024
- Halliday, A., Mansfield, A., Marro, J., Peto, C., Peto, R., Potter, J., . . . Grp, A. C. (2004). Prevention of disabling and fatal strokes by successful carotid endarterectomy in patients without recent neurological symptoms: randomised controlled trial. *Lancet*, 363(9420), 1491-1502.
- Halliwell, B., & Gutteridge, J. M. (1999). Free radicals in biology and medicine. In: Oxford university press, Oxford.

- Hampton, M. B., Kettle, A. J., & Winterbourn, C. C. (1998). Inside the neutrophil phagosome: oxidants, myeloperoxidase, and bacterial killing. *Blood*, *92*(9), 3007-3017.
- Handley, D. A., Arbeeny, C. M., & Chien, S. (1981). COLLOIDAL GOLD LOW-DENSITY LIPOPROTEIN CONJUGATES AS MEMBRANE-RECEPTOR PROBES. *Arteriosclerosis*, *1*(1), 67-67.
- Hansson, G. K., Libby, P., & Tabas, I. (2015). Inflammation and plaque vulnerability. *Journal of Internal Medicine*, *278*(5), 483-493.
- Hashimoto, D., Chow, A., Noizat, C., Teo, P., Beasley, M. B., Leboeuf, M., . . . Lucas, D. (2013). Tissue-resident macrophages self-maintain locally throughout adult life with minimal contribution from circulating monocytes. *Immunity*, *38*(4), 792-804.
- Hayyan, M., Hashim, M. A., & AlNashef, I. M. (2016). Superoxide ion: generation and chemical implications. *Chemical reviews*, *116*(5), 3029-3085.
- He, W., Zhang, H. Q., Shi, C. Y., Chen, J., & Gao, J. (2013). Fly through ultrasound imaging in assessment of carotid atherosclerosis: a pictorial essay. *Clinical Imaging*, *37*(5), 811-820. doi:10.1016/j.clinimag.2013.03.002
- Herbin, O., Regelman, A. G., Ramkhalawon, B., Weinstein, E. G., Moore, K. J., & Alexandropoulos, K. (2016). Monocyte Adhesion and Plaque Recruitment During Atherosclerosis Development Is Regulated by the Adapter Protein Chat-H/SHEP1. *Arteriosclerosis Thrombosis and Vascular Biology*, *36*(9), 1791-1801. doi:10.1161/atvbaha.116.308014
- Hesslinger, C., Kremmer, E., Hultner, L., Ueffing, M., & Ziegler, I. (1998). Phosphorylation of GTP cyclohydrolase I and modulation of its activity in rodent mast cells - GTP cyclohydrolase I hyperphosphorylation is coupled to high affinity IgE receptor signaling and involves protein kinase C. *Journal of Biological Chemistry*, *273*(34), 21616-21622. doi:10.1074/jbc.273.34.21616
- Heumüller, S., Wind, S., Barbosa-Sicard, E., Schmidt, H. H., Busse, R., Schröder, K., & Brandes, R. P. (2008). Apocynin is not an inhibitor of vascular NADPH oxidases but an antioxidant. *Hypertension*, *51*(2), 211-217.
- Hollan, I., Nebuloni, M., Bottazzi, B., Mikkelsen, K., Forre, O., Meroni, P. L., & Feiring Heart Biopsy Study, G. (2010). PENTRAXIN 3 (PTX3), A NOVEL CARDIOVASCULAR BIOMARKER, IS EXPRESSED IN VASCULAR SPECIMENS OF PATIENTS WITH CORONARY ARTERY DISEASE (CAD). *Atherosclerosis Supplements*, *11*(2), 97-97. doi:10.1016/s1567-5688(10)70447-5
- Howell, K. W., Meng, X. Z., Fullerton, D. A., Jin, C. H., Reece, T. B., & Cleveland, J. C. (2011). Toll-like Receptor 4 Mediates Oxidized LDL-Induced Macrophage Differentiation to Foam Cells. *Journal of Surgical Research*, *171*(1), E27-E31. doi:10.1016/j.jss.2011.06.033
- Hsu, J. J., Lim, J., Tintut, Y., & Demer, L. L. (2016). Cell-matrix mechanics and pattern formation in inflammatory cardiovascular calcification. *Heart*, *102*(21), 1710-1715. doi:10.1136/heartjnl-2016-309667
- Hubbell, J. H., & Seltzer, S. M. (1995). *Tables of X-ray mass attenuation coefficients and mass energy-absorption coefficients 1 keV to 20 MeV for elements Z= 1 to 92 and 48 additional substances of dosimetric interest*. Retrieved from
- Huber, C., Batchelor, J. R., Fuchs, D., Hausen, A., Lang, A., Niederwieser, D., . . . Wachter, H. (1984). Immune-response associated production of neopterin - release from macrophages primarily under control of interferon-gamma. *Journal of Experimental Medicine*, *160*(1), 310-316. doi:10.1084/jem.160.1.310

- Huber, C., Batchelor, J. R., Fuchs, D., Hausen, A., Lang, A., Niederwieser, D., . . . Wachter, H. J. J. o. E. M. (1984). Immune response-associated production of neopterin. Release from macrophages primarily under control of interferon-gamma. *160*(1), 310-316.
- Imanishi, T., Ikejima, H., Tsujioka, H., Kuroi, A., Ishibashi, K., Komukai, K., . . . Akasaka, T. (2010). Association of monocyte subset counts with coronary fibrous cap thickness in patients with unstable angina pectoris. *Atherosclerosis*, *212*(2), 628-635.
- Ismail, H. M., Scapozza, L., Ruegg, U. T., & Dorchies, O. M. (2014). Diapocynin, a dimer of the NADPH oxidase inhibitor apocynin, reduces ROS production and prevents force loss in eccentrically contracting dystrophic muscle. *PLoS One*, *9*(10), e110708.
- Janmale, T. (2013). *Formation, Transport and Detection of 7, 8-dihydroneopterin: A Thesis Submitted in Partial Fulfilment of the Requirements for the Degree of Doctor of Philosophy in Biochemistry, School of Biological Sciences, University of Canterbury, New Zealand*. University of Canterbury,
- Janmale, T., Genet, R., Crone, E., Flavall, E., Firth, C., Pirker, J., . . . Gieseg, S. P. (2015). Neopterin and 7,8-dihydroneopterin are generated within atherosclerotic plaques. *Pteridines*, *26*(3), 93-103. doi:10.1515/pterid-2015-0004
- Jenkins, S. J., Ruckerl, D., Cook, P. C., Jones, L. H., Finkelman, F. D., van Rooijen, N., . . . Allen, J. E. (2011). Local macrophage proliferation, rather than recruitment from the blood, is a signature of TH2 inflammation. *Science*, *332*(6035), 1284-1288.
- Jerome, W. G., Cox, B. E., Griffin, E. E., & Ullery, J. C. (2008). Lysosomal cholesterol accumulation inhibits subsequent hydrolysis of lipoprotein cholesteryl ester. *Microscopy and Microanalysis*, *14*(2), 138-149.
- Johnson, J. L., & Newby, A. C. (2009). Macrophage heterogeneity in atherosclerotic plaques. *Current Opinion in Lipidology*, *20*(5), 370.
- Johnston, J. R., Godzik, C. A., & Cohn, Z. A. (1978). Increased superoxide anion production by immunologically activated and chemically elicited macrophages. *Journal of Experimental Medicine*, *148*(1), 115-129.
- Judkins, C. P., Diep, H., Broughton, B. R., Mast, A. E., Hooker, E. U., Miller, A. A., . . . Drummond, G. R. (2009). Direct evidence of a role for Nox2 in superoxide production, reduced nitric oxide bioavailability, and early atherosclerotic plaque formation in ApoE<sup>-/-</sup> mice. *American Journal of Physiology-Heart and Circulatory Physiology*, *298*(1), H24-H32.
- Kadl, A., Meher, A. K., Sharma, P. R., Lee, M. Y., Doran, A. C., Johnstone, S. R., . . . Chen, W. (2010). Identification of a Novel Macrophage Phenotype That Develops in Response to Atherogenic Phospholipids via Nrf2 Novelty and Significance. *Circulation Research*, *107*(6), 737-746.
- Kanegae, M. P., da Fonseca, L. M., Brunetti, I. L., de Oliveira Silva, S., & Ximenes, V. F. (2007). The reactivity of ortho-methoxy-substituted catechol radicals with sulfhydryl groups: contribution for the comprehension of the mechanism of inhibition of NADPH oxidase by apocynin. *Biochemical pharmacology*, *74*(3), 457-464.
- Kaski, J. C., Consuegra-Sanchez, L., Fernandez-Berges, D. J., Cruz-Fernandez, J. M., Garcia-Moll, X., Marrugat, J., . . . Investigators, S. (2008). Elevated serum neopterin levels and adverse cardiac events at 6 months follow-up in Mediterranean patients with non-ST-segment elevation acute coronary syndrome. *Atherosclerosis*, *201*(1), 176-183. doi:10.1016/j.atherosclerosis.2008.01.009
- Katouah, H., Chen, A., Othman, I., & Gieseg, S. P. (2015). Oxidised low density lipoprotein causes human macrophage cell death through oxidant generation and inhibition of key catabolic enzymes. *International Journal of Biochemistry & Cell Biology*, *67*, 34-42. doi:10.1016/j.biocel.2015.08.001

- Kavurma, M. M., Rayner, K. J., & Karunakaran, D. (2017). The walking dead: macrophage inflammation and death in atherosclerosis. *Current Opinion in Lipidology*, 28(2), 91-98. doi:10.1097/mol.0000000000000394
- Kelley, E. E., Khoo, N. K. H., Hundley, N. J., Malik, U. Z., Freeman, B. A., & Tarpey, M. M. (2010). Hydrogen peroxide is the major oxidant product of xanthine oxidase. *Free Radical Biology and Medicine*, 48(4), 493-498. doi:10.1016/j.freeradbiomed.2009.11.012
- Kettle, A. J., Gedye, C. A., Hampton, M. B., & Winterbourn, C. C. (1995). Inhibition of myeloperoxidase by benzoic acid hydrazides. *Biochemical Journal*, 308(Pt 2), 559.
- Kettle, A. J., Gedye, C. A., & Winterbourn, C. C. (1997). Mechanism of inactivation of myeloperoxidase by 4-aminobenzoic acid hydrazide. *Biochemical Journal*, 321(Pt 2), 503.
- Kojima, Y., Downing, K., Kundu, R., Miller, C., Dewey, F., Lancero, H., . . . Schadt, E. (2014). Cyclin-dependent kinase inhibitor 2B regulates efferocytosis and atherosclerosis. *The Journal of clinical investigation*, 124(3), 1083-1097.
- Konety, S. H., Koene, R. J., Norby, F. L., Wilsdon, T., Alonso, A., Siscovick, D., . . . Folsom, A. R. (2016). Echocardiographic Predictors of Sudden Cardiac Death The Atherosclerosis Risk in Communities Study and Cardiovascular Health Study. *Circulation-Cardiovascular Imaging*, 9(8). doi:10.1161/circimaging.115.004431
- Kong, Y. Z., Yu, X. Y., Tang, J. J., Ouyang, X. S., Huang, X. R., Fingerle-Rowson, G., . . . Lan, H. Y. (2005). Macrophage migration inhibitory factor induces MMP-9 expression: implications for destabilization of human atherosclerotic plaques. *Atherosclerosis*, 178(1), 207-215. doi:10.1016/j.atherosclerosis.2004.08.030
- Konstantino, Y., Nguyen, T. T., Wolk, R., Aiello, R. J., Terra, S. G., & Fryburg, D. A. (2009). Potential implications of matrix metalloproteinase-9 in assessment and treatment of coronary artery disease. *Biomarkers*, 14(2), 118-129. doi:10.1080/13547500902765140
- Lambeth, J. D., Kawahara, T., Diebold, B. J. F. R. B., & Medicine. (2007). Regulation of Nox and Duox enzymatic activity and expression. 43(3), 319-331.
- Li, H., Gu, B., Zhang, Y., Lewis, D. F., & Wang, Y. (2005). Hypoxia-induced increase in soluble Flt-1 production correlates with enhanced oxidative stress in trophoblast cells from the human placenta. *Placenta*, 26(2-3), 210-217. doi:10.1016/j.placenta.2004.05.004
- Li, N., McLaren, J. E., Michael, D. R., Clement, M., Fielding, C. A., & Ramji, D. P. (2010). ERK is integral to the IFN- $\gamma$ -mediated activation of STAT1, the expression of key genes implicated in atherosclerosis, and the uptake of modified lipoproteins by human macrophages. *The Journal of Immunology*, 185(5), 3041-3048.
- Lim, J. L., Wilhelmus, M. M., de Vries, H. E., Drukarch, B., Hoozemans, J. J., & van Horssen, J. J. A. o. t. (2014). Antioxidative defense mechanisms controlled by Nrf2: state-of-the-art and clinical perspectives in neurodegenerative diseases. 88(10), 1773-1786.
- Lin, H. S., Tsai, T. H., Liu, C. F., Lu, C. H., Chang, W. N., Chen, S. F., . . . Yip, H. K. (2012). Serum level and prognostic value of neopterin in patients after ischemic stroke. *Clinical Biochemistry*, 45(18), 1596-1601. doi:10.1016/j.clinbiochem.2012.07.113
- Lindsay, A., Carr, S., Othman, M. I., Marks, E., Davies, S., Petersen, C., . . . Giese, S. P. (2015). The physiological and mononuclear cell activation response to cryotherapy following a mixed martial arts contest: a pilot study. *Pteridines*, 26(4), 143-151. doi:10.1515/pterid-2015-0010



- Lindsay, A., Janmale, T., Draper, N., & Gieseg, S. P. (2014). Measurement of changes in urinary neopterin and total neopterin in body builders using SCX HPLC. *Pteridines*, 25(2), 53-62. doi:10.1515/pteridines-2014-0003
- Lindsay, A., Othman, M. I., Prebble, H., Davies, S., & Gieseg, S. P. (2016). Repetitive cryotherapy attenuates the in vitro and in vivo mononuclear cell activation response. *Experimental Physiology*, 101(7), 851-865. doi:10.1113/ep085795
- Lindsay, A., Schmiechen, A., Chamberlain, C. M., Ervasti, J. M., & Lowe, D. A. (2018). Neopterin/7, 8-dihydroneopterin is elevated in Duchenne muscular dystrophy patients and protects mdx skeletal muscle function. *Experimental Physiology*.
- Liu, X., Atwater, M., Wang, J., & Huo, Q. (2007). Extinction coefficient of gold nanoparticles with different sizes and different capping ligands. *Colloids and Surfaces B: Biointerfaces*, 58(1), 3-7.
- Lloyd-Jones, D. M., Larson, M. G., Beiser, A., Leip, E., D'Agostino, R. B., Wilson, P. W., & Levy, D. (2000). Framingham risk score and lifetime risk of coronary heart disease. *Circulation*, 102(18), 842-842.
- Loscalzo, J. (2012). Personalized Cardiovascular Medicine and Drug Development Time for a New Paradigm. *Circulation*, 125(4), 638-645. doi:10.1161/circulationaha.111.089243
- Macmahon, S., Norton, R., Jackson, R., Mackie, M. J., Cheng, A., Vanderhoorn, S., . . . McCulloch, A. (1995). FLETCHER CHALLENGE-UNIVERSITY OF AUCKLAND HEART-AND-HEALTH STUDY - DESIGN AND BASE-LINE FINDINGS. *New Zealand Medical Journal*, 108(1013), 499-502.
- Maghzal, G. J. (1999). *Red Blood Cell Membrane Protection from Oxidative Damage by 7, 8-dihydroneopterin: A Thesis Submitted in Partial Fulfilment of the Requirements for the Degree of Master of Science in Cellular and Molecular Biology at the University of Canterbury, New Zealand*. University of Canterbury,
- Malle, E., Furtmüller, P., Sattler, W., & Obinger, C. (2007). Myeloperoxidase: a target for new drug development? *British Journal of Pharmacology*, 152(6), 838-854.
- Mantovani, A., Sica, A., & Locati, M. (2005). Macrophage polarization comes of age. *Immunity*, 23(4), 344-346.
- Marques, L., Negre-Salvayre, A., Costa, L., & Canonne-Hergaux, F. (2016). Iron gene expression profile in atherogenic Mox macrophages. *Biochimica et Biophysica Acta (BBA)-Molecular Basis of Disease*, 1862(6), 1137-1146.
- Martinon, F. (2010). Signaling by ROS drives inflammasome activation. *European journal of immunology*, 40(3), 616-619.
- Matthews, A. T., Lee, J. H., Borazjani, A., Mangum, L. C., Hou, X., & Ross, M. K. (2016). Oxyradical stress increases the biosynthesis of 2-arachidonoylglycerol: involvement of NADPH oxidase. *American Journal of Physiology-Cell Physiology*, 311(6), C960-C974. doi:10.1152/ajpcell.00251.2015
- McCord, J. M., & Fridovich, I. (1968). The reduction of cytochrome c by milk xanthine oxidase. *Journal of Biological Chemistry*, 243(21), 5753-5760.
- Michel, J.-B., Virmani, R., Arbustini, E., & Pasterkamp, G. (2011). Intraplaque haemorrhages as the trigger of plaque vulnerability. *European Heart Journal*, 32(16), 1977-1985.
- Moghiseh, M., Aamir, R., Panta, R. K., de Ruyter, N., Chernoglazov, A., Healy, J., . . . Anderson, N. (2016). Discrimination of multiple high-Z materials by multi-energy spectral CT—A phantom study. *JSM Biomed. Imaging Data Pap*.
- Mohamed, H. A. (2007). Negative exercise stress test Does it mean anything? *The Libyan journal of medicine*, 2(2), 103-105. doi:10.4176/070103
- Mongraw-Chaffin, M. L., Matsushita, K., Brancati, F. L., Astor, B. C., Coresh, J., Crawford, S. O., . . . Young, J. H. (2012). Diabetes medication use and blood lactate level among

- participants with type 2 diabetes: the atherosclerosis risk in communities carotid MRI study. *PLoS One*, 7(12), e51237.
- Moran, A. E., Forouzanfar, M. H., Roth, G. A., Mensah, G. A., Ezzati, M., Murray, C. J. L., & Naghavi, M. (2014). Temporal Trends in Ischemic Heart Disease Mortality in 21 World Regions, 1980 to 2010 The Global Burden of Disease 2010 Study. *Circulation*, 129(14), 1483-1492. doi:10.1161/circulationaha.113.004042
- Moss, A. J., Williams, M. C., Newby, D. E., & Nicol, E. D. (2017). The Updated NICE Guidelines: Cardiac CT as the First-Line Test for Coronary Artery Disease. *Current Cardiovascular Imaging Reports*, 10(5). doi:10.1007/s12410-017-9412-6
- Mozaffarian, D., Benjamin, E. J., Go, A. S., Arnett, D. K., Blaha, M. J., Cushman, M., . . . Stroke Stat, S. (2016). Heart Disease and Stroke Statistics-2016 Update A Report From the American Heart Association. *Circulation*, 133(4), E38-E360. doi:10.1161/cir.0000000000000350
- Naghavi, M., John, R., Naguib, S., Siadaty, M. S., Grasu, R., Kurian, K., . . . Madjid, M. (2002). pH Heterogeneity of human and rabbit atherosclerotic plaques; a new insight into detection of vulnerable plaque. *Atherosclerosis*, 164(1), 27-35.
- Nakanishi, K., & Homma, S. (2016). Role of echocardiography in patients with stroke. *Journal of Cardiology*, 68(1-2), 91-99. doi:10.1016/j.jjcc.2016.05.001
- Nanni Jr, E. J., Stallings, M. D., & Sawyer, D. T. (1980). Does superoxide ion oxidize catechol, alpha-tocopherol, and ascorbic acid by direct electron transfer? *Journal of the American Chemical Society*, 102(13), 4481-4485.
- Narasimhulu, C. A., Fernandez-Ruiz, I., Selvarajan, K., Jiang, X. T., Sengupta, B., Riad, A., & Parthasarathy, S. (2016). Atherosclerosis - do we know enough already to prevent it? *Current Opinion in Pharmacology*, 27, 92-102. doi:10.1016/j.coph.2016.02.006
- Natarajan, S., Glick, H., Criqui, M., Horowitz, D., Lipsitz, S. R., & Kinoshian, B. (2003). Cholesterol measures to identify and treat individuals at risk for coronary heart disease. *American Journal of Preventive Medicine*, 25(1), 50-57. doi:10.1016/s0749-3797(03)00092-8
- Niederwieser, A., Blau, N., Wang, M., Joller, P., Amares, M., & Cardesa-Garcia, J. (1984). GTP cyclohydrolase I deficiency, a new enzyme defect causing hyperphenylalaninemia with neopterin, biopterin, dopamine, and serotonin deficiencies and muscular hypotonia. *European journal of pediatrics*, 141(4), 208-214.
- Niu, X.-L., Madamanchi, N. R., Vendrov, A. E., Tchivilev, I., Rojas, M., Madamanchi, C., . . . Smith, A. (2010). Nox activator 1: a potential target for modulation of vascular reactive oxygen species in atherosclerotic arteries. *Circulation*, 121(4), 549-559.
- Noelia, A., Bensinger, S. J., Hong, C., Beceiro, S., Bradley, M. N., Zelcer, N., . . . Gallardo, G. (2009). Apoptotic cells promote their own clearance and immune tolerance through activation of the nuclear receptor LXR. *Immunity*, 31(2), 245-258.
- Oettl, K., Dikalov, S., Freisleben, H. J., Mlekusch, W., & Reibnegger, G. (1997). Spin trapping study of antioxidant properties of neopterin and 7,8-dihydroneopterin. *Biochemical and Biophysical Research Communications*, 234(3), 774-778. doi:10.1006/bbrc.1997.6712
- Oettl, K., Greilberger, J., & Reibnegger, G. (2000). Dihydroneopterin and the generation of superoxide from iron ions. *Pteridines*, 11(2), 60-63.
- Olson, F. J., Schmidt, C., Gummesson, A., Sigurdardottir, V., Hulthe, J., Wiklund, O., & Fagerberg, B. (2008). Circulating matrix metalloproteinase 9 levels in relation to sampling methods, femoral and carotid atherosclerosis. *Journal of Internal Medicine*, 263(6), 626-635. doi:10.1111/j.1365-2796.2008.01927.x

- Otsuka, F., Kramer, M. C. A., Woudstra, P., Yahagi, K., Ladich, E., Finn, A. V., . . . Virmani, R. (2015). Natural progression of atherosclerosis from pathologic intimal thickening to late fibroatheroma in human coronary arteries: A pathology study. *Atherosclerosis*, *241*(2), 772-782. doi:10.1016/j.atherosclerosis.2015.05.011
- Owens, A. P., & Mackman, N. (2012). Sources of tissue factor that contribute to thrombosis after rupture of an atherosclerotic plaque. *Thrombosis Research*, *129*, S30-S33. doi:10.1016/j.thromres.2012.02.026
- Pannirselvam, M., Verma, S., Anderson, T. J., & Triggle, C. R. (2002). Cellular basis of endothelial dysfunction in small mesenteric arteries from spontaneously diabetic (db/db<sup>-/-</sup>) mice: role of decreased tetrahydrobiopterin bioavailability. *British Journal of Pharmacology*, *136*(2), 255-263.
- Park, J., Pramanick, S., Kim, J., Lee, J., & Kim, W. J. (2017). Nitric oxide-activatable gold nanoparticles for specific targeting and photo-thermal ablation of macrophages. *Chemical Communications*, *53*(81), 11229-11232. doi:10.1039/c7cc06420a
- Pencina, M. J., D'Agostino, R. B., Larson, M. G., Massaro, J. M., & Vasan, R. S. (2009). Predicting the 30-Year Risk of Cardiovascular Disease The Framingham Heart Study. *Circulation*, *119*(24), 3078-U3061. doi:10.1161/circulationaha.108.816694
- Pihlstrøm, H., Mjøen, G., März, W., Olav Dahle, D., Abedini, S., Holme, I., . . . Holdaas, H. (2014). Neopterin is associated with cardiovascular events and all-cause mortality in renal transplant patients. *Clinical Transplantation*, *28*(1), 111-119.
- Pirillo, A., Norata, G. D., & Catapano, A. L. (2013). LOX-1, OxLDL, and atherosclerosis. *Mediators of Inflammation*, *2013*.
- Psychogios, K., Stathopoulos, P., Takis, K., Vemmou, A., Manios, E., Spegos, K., & Vemmos, K. (2015). The Pathophysiological Mechanism Is an Independent Predictor of Long-Term Outcome in Stroke Patients with Large Vessel Atherosclerosis. *Journal of Stroke & Cerebrovascular Diseases*, *24*(11), 2580-2587. doi:10.1016/j.jstrokecerebrovasdis.2015.07.011
- Rajendran, K., Walsh, M., De Ruitter, N., Chernoglazov, A., Panta, R., Butler, A., . . . Woodfield, T. J. J. o. I. (2014). Reducing beam hardening effects and metal artefacts in spectral CT using Medipix3RX. *9*(03), P03015.
- Ridker, P. M., & Antman, E. M. (1999). Pathogenesis and pathology of coronary heart disease syndromes. *Journal of Thrombosis and Thrombolysis*, *8*(3), 167-189. doi:10.1023/a:1008997801820
- Ridker, P. M., Everett, B. M., Thuren, T., MacFadyen, J. G., Chang, W. H., Ballantyne, C., . . . Anker, S. D. (2017). Antiinflammatory therapy with canakinumab for atherosclerotic disease. *New England Journal of Medicine*, *377*(12), 1119-1131.
- Riederer, S. J., & Mistretta, C. (1977). Selective iodine imaging using K-edge energies in computerized x-ray tomography. *Medical Physics*, *4*(6), 474-481.
- Rifai, N., & Ridker, P. M. (2001). High-sensitivity C-reactive protein: A novel and promising marker of coronary heart disease. *Clinical Chemistry*, *47*(3), 403-411.
- Robbins, C. S., Hilgendorf, I., Weber, G. F., Theurl, I., Iwamoto, Y., Figueiredo, J.-L., . . . Smyth, D. (2013). Local proliferation dominates lesional macrophage accumulation in atherosclerosis. *Nature medicine*, *19*(9), 1166.
- Rodriguez-Palomares, J. F., & Masip, A. E. (2016). Aortic Calcium Score and Vascular Atherosclerosis in Asymptomatic Individuals: Beyond the Coronary Arteries. *Revista Espanola De Cardiologia*, *69*(9), 813-816. doi:10.1016/j.rec.2016.05.006
- Roeder, R. K., Curtis, T. E., Nallathamby, P. D., Irimata, L. E., McGinnity, T. L., Cole, L. E., . . . Dahl, K. D. C. (2017). *Nanoparticle imaging probes for molecular imaging with computed tomography and application to cancer imaging*. Paper presented at the Medical Imaging 2017: Physics of Medical Imaging.

- Roshal, D. (2016). Embolic stroke due to a common carotid artery thrombus in a young patient with severe iron-deficiency anemia without thrombocytosis. *Case reports in neurological medicine*, 2016.
- S Antonopoulos, A., Margaritis, M., Lee, R., Channon, K., & Antoniades, C. (2012). Statins as anti-inflammatory agents in atherogenesis: molecular mechanisms and lessons from the recent clinical trials. *Current pharmaceutical design*, 18(11), 1519-1530.
- Scharnagl, H., Kleber, M. E., Genser, B., Kickmaier, S., Renner, W., Weihrauch, G., . . . Malle, E. (2014). Association of myeloperoxidase with total and cardiovascular mortality in individuals undergoing coronary angiography-The LURIC study. *International Journal of Cardiology*, 174(1), 96-105. doi:10.1016/j.ijcard.2014.03.168
- Schnabel, R. B., Schulz, A., Messow, C. M., Lubos, E., Wild, P. S., Zeller, T., . . . Blankenberg, S. (2010). Multiple marker approach to risk stratification in patients with stable coronary artery disease. *European Heart Journal*, 31(24), 3024-3031. doi:10.1093/eurheartj/ehq322
- Shantha, G. P. S., Wasserman, B., Astor, B. C., Coresh, J., Brancati, F., Sharrett, A. R., & Young, J. H. (2013). Association of blood lactate with carotid atherosclerosis: The Atherosclerosis Risk in Communities (ARIC) Carotid MRI Study. *Atherosclerosis*, 228(1), 249-255.
- Shaw, L. J., Raggi, P., Schisterman, E., Berman, D. S., & Callister, T. Q. (2003). Prognostic value of cardiac risk factors and coronary artery calcium screening for all-cause mortality. *Radiology*, 228(3), 826-833. doi:10.1148/radiol.2283021006
- Shchepetkina, A. A., Hock, B. D., Miller, A., Kennedy, M. A., & Giese, S. P. (2017). Effect of 7,8-dihydroneopterin mediated CD36 down regulation and oxidant scavenging on oxidised low-density lipoprotein induced cell death in human macrophages. *International Journal of Biochemistry & Cell Biology*, 87, 27-33. doi:10.1016/j.biocel.2017.03.017
- Sheedy, F. J., Grebe, A., Rayner, K. J., Kalantari, P., Ramkhalawon, B., Carpenter, S. B., . . . Golenbock, D. T. (2013). CD36 coordinates NLRP3 inflammasome activation by facilitating intracellular nucleation of soluble ligands into particulate ligands in sterile inflammation. *Nature immunology*, 14(8), 812.
- Shukla, J., & Walsh, S. W. (2015). Neutrophil release of myeloperoxidase in systemic vasculature of obese women may put them at risk for preeclampsia. *Reproductive Sciences*, 22(3), 300-307.
- Signorelli, S. S., Anzaldi, M., Libra, M., Navolanic, P. M., Malaponte, G., Mangano, K., . . . Neri, S. (2016). Plasma Levels of Inflammatory Biomarkers in Peripheral Arterial Disease: Results of a Cohort Study. *Angiology*, 67(9), 870-874. doi:10.1177/0003319716633339
- Silvestre-Roig, C., de Winther, M. P., Weber, C., Daemen, M. J., Lutgens, E., & Soehnlein, O. (2014). Atherosclerotic Plaque Destabilization Mechanisms, Models, and Therapeutic Strategies. *Circulation Research*, 114(1), 214-226. doi:10.1161/circresaha.114.302355
- Skopec, I. S., Vezikova, N. N., Marusenko, I. M., Barysheva, O. Y., Malafeev, A. V., & Malygin, A. N. (2016). Correlation of inflammation biomarkers with the traditional risk factors in patients with acute coronary syndrome. *Rational Pharmacotherapy in Cardiology*, 12(2), 166-170. doi:10.20996/1819-6446-2016-12-2-166-170
- Smith, P. K., Krohn, R. I., Hermanson, G., Mallia, A., Gartner, F., Provenzano, M., . . . Klenk, D. (1985). Measurement of protein using bicinchoninic acid. *Analytical Biochemistry*, 150(1), 76-85.

- Spencer, M. E., Jain, A., Matteini, A., Beamer, B. A., Wang, N.-Y., Leng, S. X., . . . Fedarko, N. S. (2010). Serum levels of the immune activation marker neopterin change with age and gender and are modified by race, BMI, and percentage of body fat. *Journals of Gerontology Series A: Biomedical Sciences and Medical Sciences*, 65(8), 858-865.
- Spencer, M. P., & Reid, J. M. (1979). QUANTITATION OF CAROTID STENOSIS WITH CONTINUOUS-WAVE (C-W) DOPPLER ULTRASOUND. *Stroke*, 10(3), 326-330. doi:10.1161/01.str.10.3.326
- Stein, J. H., Korcarz, C. E., Hurst, R. T., Lonn, E., Kendall, C. B., Mohler, E. R., . . . Post, W. S. (2008). Use of carotid ultrasound to identify subclinical vascular disease and evaluate cardiovascular disease risk: A consensus statement from the American society of echocardiography carotid intima-media thickness task force endorsed by the society for vascular medicine. *Journal of the American Society of Echocardiography*, 21(2), 93-111. doi:10.1016/j.echo.2007.11.011
- Stielow, C., Catar, R. A., Muller, G., Wingler, K., Scheurer, P., Schmidt, H. H., & Morawietz, H. (2006). Novel Nox inhibitor of oxLDL-induced reactive oxygen species formation in human endothelial cells. *Biochemical and Biophysical Research Communications*, 344(1), 200-205.
- Stocker, R., & Keaney Jr, J. F. (2004). Role of oxidative modifications in atherosclerosis. *Physiological reviews*, 84(4), 1381-1478.
- Stöger, J. L., Gijbels, M. J., van der Velden, S., Manca, M., van der Loos, C. M., Biessen, E. A., . . . de Winther, M. P. (2012). Distribution of macrophage polarization markers in human atherosclerosis. *Atherosclerosis*, 225(2), 461-468.
- Stolk, J., Hiltermann, T., Dijkman, J., & Verhoeven, A. (1994). Characteristics of the inhibition of NADPH oxidase activation in neutrophils by apocynin, a methoxy-substituted catechol. *American journal of respiratory cell and molecular biology*, 11(1), 95-102.
- Suckling, C. J., Gibson, C. L., Huggan, J. K., Morthala, R. R., Clarke, B., Kununthur, S., . . . Papale, D. (2008). 6-Acetyl-7, 7-dimethyl-5, 6, 7, 8-tetrahydropterin is an activator of nitric oxide synthases. *Bioorganic & medicinal chemistry letters*, 18(5), 1563-1566.
- Symons, R., Reich, D. S., Bagheri, M., Cork, T. E., Krauss, B., Ulzheimer, S., . . . Pourmorteza, A. (2017). Photon-Counting Computed Tomography for Vascular Imaging of the Head and Neck: First In Vivo Human Results. *Investigative radiology*. doi:10.1097/rli.0000000000000418
- Tabas, I. (2009). Macrophage Apoptosis in Atherosclerosis: Consequences on Plaque Progression and the Role of Endoplasmic Reticulum Stress. *Antioxidants & Redox Signaling*, 11(9), 2333-2339. doi:10.1089/ars.2009.2469
- Tabas, I. (2010). Macrophage death and defective inflammation resolution in atherosclerosis. *Nature Reviews Immunology*, 10(1), 36.
- Tabas, I., & Bornfeldt, K. E. (2016). Macrophage phenotype and function in different stages of atherosclerosis. *Circulation Research*, 118(4), 653-667.
- Takeya, R., Ueno, N., Kami, K., Taura, M., Kohjima, M., Izaki, T., . . . Sumimoto, H. (2003). Novel human homologues of p47phox and p67phox participate in activation of superoxide-producing NADPH oxidases. *Journal of Biological Chemistry*, 278(27), 25234-25246.
- Tang, J., Lobatto, M. E., Hassing, L., van der Staay, S., van Rijs, S. M., Calcagno, C., . . . Sanchez-Gaytan, B. L. (2015). Inhibiting macrophage proliferation suppresses atherosclerotic plaque inflammation. *Science advances*, 1(3), e1400223.
- Tatzber, F., Rabl, H., Koriska, K., Erhart, U., Puhl, H., Waeg, G., . . . Esterbauer, H. (1991). Elevated serum neopterin levels in atherosclerosis. *Atherosclerosis*, 89(2-3), 203-208.

- Thorp, E. B. (2010). Mechanisms of failed apoptotic cell clearance by phagocyte subsets in cardiovascular disease. *Apoptosis*, *15*(9), 1124-1136.
- Tontonoz, P., Nagy, L., Alvarez, J. G., Thomazy, V. A., & Evans, R. M. (1998). PPAR $\gamma$  promotes monocyte/macrophage differentiation and uptake of oxidized LDL. *Cell*, *93*(2), 241-252.
- Ueno, N., Takeya, R., Miyano, K., Kikuchi, H., & Sumimoto, H. J. J. o. B. C. (2005). The NADPH Oxidase Nox3 Constitutively Produces Superoxide in a p22phox-dependent Manner ITS REGULATION BY OXIDASE ORGANIZERS AND ACTIVATORS. *280*(24), 23328-23339.
- Ulrich, C., Heine, G. H., Gerhart, M. K., Kohler, H., & Girndt, M. (2008). Proinflammatory CD14+CD16+ monocytes are associated with subclinical atherosclerosis in renal transplant patients. *American Journal of Transplantation*, *8*(1), 103-110. doi:10.1111/j.1600-6143.2007.02035.x
- Ulzheimer, S., & Kalender, W. A. (2003). Assessment of calcium scoring performance in cardiac computed tomography. *European Radiology*, *13*(3), 484-497. doi:10.1007/s00330-002-1746-y
- Van Tits, L., Stienstra, R., Van Lent, P., Netea, M., & Stalenhoef, A. (2011). Oxidized LDL enhances pro-inflammatory responses of alternatively activated M2 macrophages: a crucial role for Krüppel-like factor 2. *Atherosclerosis*, *214*(2), 345-349.
- Vandewalle, P., & Petersen, N. (1987). Oxidation of reduced cytochrome c by hydrogen peroxide. *Febs Letters*, *210*(2), 195-198.
- Videm, V., Wiseth, R., Gunnes, S., Madsen, H. O., & Garred, P. (2007). Multiple inflammatory markers in patients with significant coronary artery disease. *International Journal of Cardiology*, *118*(1), 81-87. doi:10.1016/j.ijcard.2006.07.005
- Wang, J., Tan, G. J., Han, L. N., Bai, Y. Y., He, M., & Liu, H. B. (2017). Novel biomarkers for cardiovascular risk prediction. *Journal of Geriatric Cardiology*, *14*(2), 135-150. doi:10.11909/j.issn.1671-5411.2017.02.008
- Wede, I., Altindag, Z. Z., Widner, B., Wachter, H., & Fuchs, D. (1998). Inhibition of xanthine oxidase by pterins. *Free Radical Research*, *29*(4), 331-338. doi:10.1080/10715769800300371
- Werner, E., Bichler, A., Daxenbichler, G., Fuchs, D., Fuiith, L., Hausen, A., . . . Wachter, H. (1987). Determination of neopterin in serum and urine. *Clinical Chemistry*, *33*(1), 62-66.
- Widner, B., Enzinger, C., Laich, A., Wirleitner, B., & Fuchs, D. (2002). Hyperhomocysteinemia, pteridines and oxidative stress. *Current drug metabolism*, *3*(2), 225-232.
- Widner, B., Mayr, C., Wirleitner, B., & Fuchs, D. (2000). Oxidation of 7,8-dihydroneopterin by hypochlorous acid yields neopterin. *Biochemical and Biophysical Research Communications*, *275*(2), 307-311. doi:10.1006/bbrc.2000.3323
- Wilson, P. W. F., D'Agostino, R. B., Levy, D., Belanger, A. M., Silbershatz, H., & Kannel, W. B. (1998). Prediction of coronary heart disease using risk factor categories. *Circulation*, *97*(18), 1837-1847.
- Wirleitner, B., Schroecksnadel, K., Winkler, C., & Fuchs, D. (2005). Neopterin in HIV-1 infection. *Molecular immunology*, *42*(2), 183-194.
- Wolf, D., Zirlik, A., & Ley, K. (2015). Beyond vascular inflammation-recent advances in understanding atherosclerosis. *Cellular and Molecular Life Sciences*, *72*(20), 3853-3869. doi:10.1007/s00018-015-1971-6
- Ximenes, V. F., Kanegae, M. P., Rissato, S. R., & Galhiane, M. S. (2007). The oxidation of apocynin catalyzed by myeloperoxidase: proposal for NADPH oxidase inhibition. *Archives of Biochemistry and Biophysics*, *457*(2), 134-141.

- Xu, L., Perrard, X. D., Perrard, J. L., Yang, D. L., Xiao, X. H., Teng, B. B., . . . Wu, H. Z. (2015). Foamy Monocytes Form Early and Contribute to Nascent Atherosclerosis in Mice With Hypercholesterolemia. *Arteriosclerosis Thrombosis and Vascular Biology*, 35(8), 1787-1797. doi:10.1161/atvbaha.115.305609
- Yamashita, T., Kawashima, S., Ozaki, M., Takeuchi, S., Inoue, N., & Hirata, K. I. (2000). Inhibition of monocyte/macrophage infiltration by propagermanium reduces atherosclerosis in apolipoprotein E knockout mice. *Circulation*, 102(18), 308-308.
- Yeandle, A. (2017). Regulation of the CD36 scavenger receptor by the antioxidant 7, 8-dihydroneopterin.
- Yeo, T. W., Lampah, D. A., Gitawati, R., Tjitra, E., Kenangalem, E., McNeil, Y. R., . . . Lopansri, B. K. (2008). Recovery of endothelial function in severe falciparum malaria: relationship with improvement in plasma L-arginine and blood lactate concentrations. *The Journal of infectious diseases*, 198(4), 602-608.
- Zainon, R., Butler, P. H., Gieseg, S. P., Janmale, T., Ronaldson, J. P., Anderson, N. G., . . . Ieee. (2014). *High Resolution Spectral Micro-CT Imaging of Atherosclerotic Plaque*.
- Zainon, R., Ronaldson, J. P., Janmale, T., Scott, N. J., Buckenham, T. M., Butler, A. P. H., . . . Anderson, N. G. (2012). Spectral CT of carotid atherosclerotic plaque: comparison with histology. *European Radiology*, 22(12), 2581-2588. doi:10.1007/s00330-012-2538-7
- Zhang, Y. Y., Tong, X. Z., Xia, W. H., Xie, W. L., Yu, B. B., Zhang, B., . . . Tao, J. (2016). Increased plasma neopterin levels are associated with reduced endothelial function and arterial elasticity in hypertension. *Journal of Human Hypertension*, 30(7), 436-441. doi:10.1038/jhh.2015.72
- Zuo, H., Ueland, P. M., Ulvik, A., Eussen, S., Vollset, S. E., Nygard, O., . . . Tell, G. S. (2016). 9 Plasma Biomarkers of Inflammation, the Kynurenine Pathway, and Risks of All-Cause, Cancer, and Cardiovascular Disease Mortality. *American Journal of Epidemiology*, 183(4), 249-258. doi:10.1093/aje/kwv242



Contents lists available at ScienceDirect

Immunobiology

journal homepage: [www.elsevier.com/locate/imbio](http://www.elsevier.com/locate/imbio)

## Induced macrophage activation in live excised atherosclerotic plaque

Hannah Prebble<sup>a</sup>, Sean Cross<sup>a</sup>, Edward Marks<sup>a</sup>, Joe Healy<sup>a</sup>, Emily Searle<sup>b</sup>, Raja Aamir<sup>c</sup>, Anthony Butler<sup>b,c</sup>, Justin Roake<sup>d</sup>, Barry Hock<sup>c</sup>, Nigel Anderson<sup>c</sup>, Steven P. Gieseg<sup>a,c,\*</sup>

<sup>a</sup> Free Radical Biochemistry Laboratory, School of Biological Sciences, University of Canterbury, Private Bag 4800, Christchurch, New Zealand

<sup>b</sup> School of Physics and Astronomy, University of Canterbury, Private Bag 4800, Christchurch, New Zealand

<sup>c</sup> Department of Radiology, University of Otago Christchurch, PO Box 4345, Christchurch, New Zealand

<sup>d</sup> Department of Vascular Surgery, Christchurch Hospital, Private Bag 4710, Christchurch, New Zealand

\* Hematology Research Group, Department of Pathology, Christchurch Hospital, Private Bag 4710, Christchurch, New Zealand

### ARTICLE INFO

#### Keywords:

Carotid plaque  
Macrophage  
Neopterin  
Inflammation  
Spectral X-ray-imaging

### ABSTRACT

Atherosclerotic plaques are complex tissues containing many different cell types. Macrophages contribute to inflammation, formation of the necrotic core, and plaque rupture. We examined whether macrophages in plaque can be activated and compared this to monolayer cells. The volume of calcium in the plaque was compared to the level of macrophage activation measured by total neopterin output. Carotid plaque samples were cut into 3 mm sections and cultured for up to 96 h. Live sections were stimulated with interferon- $\gamma$ , phytohaemagglutinin or phorbol 12-myristate 13-acetate. Macrophage activation and oxidative stress were monitored by total neopterin (oxidized and non-oxidized 7,8-dihydroneopterin) and neopterin levels every 24 h for up to 4 d. The calcium content of two plaques was investigated by spectral imaging. Direct stimulation of macrophages in plaque sections with interferon- $\gamma$  caused a sustained increase in neopterin ( $p = .037$ ) and total neopterin ( $p = .003$ ). The addition of phorbol 12-myristate 13-acetate to plaque had no significant effect on total neopterin production ( $p = .073$ ) but increased neopterin ( $p = .037$ ) whereas phytohaemagglutinin caused a significant increase in both neopterin and total neopterin ( $p = .0279$  and  $.0168$ ). There was an inverse association ( $R^2 = 0.91$ ) between the volume of calcium and macrophage activation as measured by total neopterin production in stimulated plaque tissue. Resident macrophages within excised carotid plaque activated either directly or indirectly generate the biomarkers 7,8-dihydroneopterin and neopterin. Macrophage activation rather than the oxidative environment is associated with plaque calcification.

### 1. Introduction

Atherosclerotic plaques are complex tissues made up of a number of different cell types and cellular subsets which form in the arterial wall (Stary et al., 1995). Monocytes, a macrophage precursor cell, infiltrate the arterial wall in early atherosclerosis. Once resident, macrophages promote inflammation through the generation of oxidants and the release of inflammatory cytokines (Biessen and Wouters, 2017). Macrophages continue the progression of an atherosclerotic lesion by taking up toxic oxidized low-density lipoprotein (oxLDL) in an uncontrolled manner, causing foam cell formation and eventual cell necrosis (Kavurma et al., 2017; Howell et al., 2011). The subsequent release of lipids from dying macrophages promotes the formation of a lipid or necrotic core in the arterial wall (Silvestre-Roig et al., 2014; Tabas, 2009; Otsuka et al., 2015). This necrotic core is separated from the

blood by a thin fibrous cap. Over time, resident macrophages may release matrix metalloproteinases degrading the fibrous cap (Kong et al., 2005), making the plaque prone to rupture (Gao and Long, 2008). Plaque rupture opens the contents of the necrotic core to the blood clotting factors triggering thrombosis (Owens and Mackman, 2012). The thrombus can then break away from the site of plaque rupture and obstruct small vessels. These infarcts typically occur in the brain or heart and often result in death (Psychogios et al., 2015).

Given the high rate of mortality associated with atherosclerosis, there is a strong emphasis on improving detection and diagnosis of the disease. In recent years, there have been significant improvements in various imaging modalities to detect atherosclerosis (Tarkin et al., 2016), and there has been a shift towards identifying biomarkers of the disease, which would provide a non-invasive means of diagnosing and monitoring atherosclerosis (De Rosa et al., 2011; Soeki and Sata, 2016).

\* Corresponding author at: School of Biological Sciences, University of Canterbury, Private Bag 4800, Christchurch, New Zealand.

E-mail addresses: [hannah.prebble@pg.canterbury.ac.nz](mailto:hannah.prebble@pg.canterbury.ac.nz) (H. Prebble), [sean.cross@canterbury.ac.nz](mailto:sean.cross@canterbury.ac.nz) (S. Cross), [joe.healy@pg.canterbury.ac.nz](mailto:joe.healy@pg.canterbury.ac.nz) (J. Healy), [emily.searle@pg.canterbury.ac.nz](mailto:emily.searle@pg.canterbury.ac.nz) (E. Searle), [Raja.Aamir@otago.ac.nz](mailto:Raja.Aamir@otago.ac.nz) (R. Aamir), [Anthony.Butler@otago.ac.nz](mailto:Anthony.Butler@otago.ac.nz) (A. Butler), [justin.roake@cdhb.health.nz](mailto:justin.roake@cdhb.health.nz) (J. Roake), [barry.hock@otago.ac.nz](mailto:barry.hock@otago.ac.nz) (B. Hock), [Nigel.Anderson@otago.ac.nz](mailto:Nigel.Anderson@otago.ac.nz) (N. Anderson), [steven.gieseg@canterbury.ac.nz](mailto:steven.gieseg@canterbury.ac.nz) (S.P. Gieseg).

<https://doi.org/10.1016/j.imbio.2018.03.002>

Received 20 December 2017; Received in revised form 29 January 2018; Accepted 22 March 2018  
0171-2985/ © 2018 Elsevier GmbH. All rights reserved.



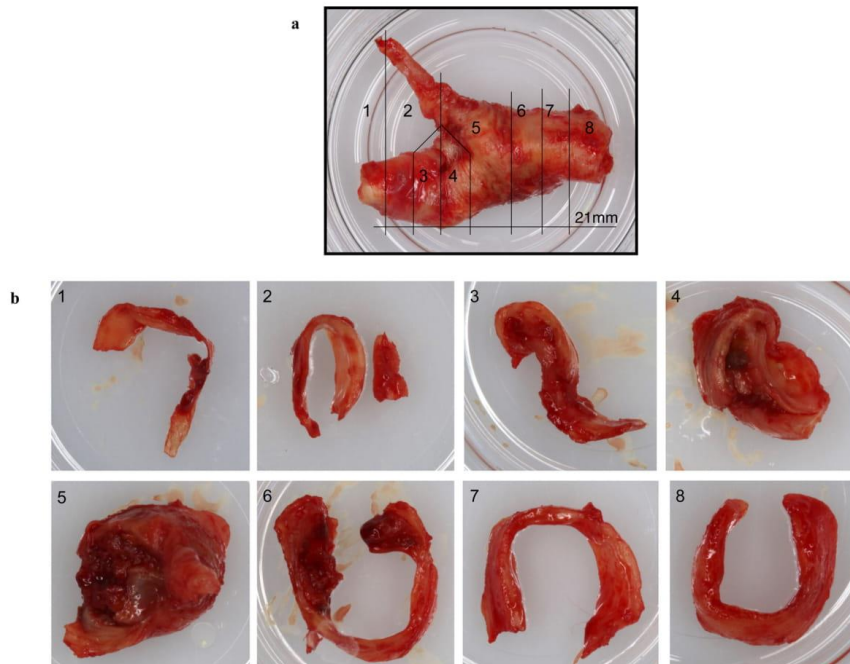


**Fig. 1.** Example of an Internal Carotid Artery plaque prior to (a) and post sectioning procedure (b). Each section was then placed into an individual organ culture dish for the length of the experiment. The plaque was obtained from a 65-year-old male non-smoker who was suffering from dysphasia and amaurosis fugax. Stenosis of the artery was reported as 80–99%. This plaque was used in the experiments conducted in Fig. 5. All plaque culture experiments were carried out on plaques sectioned in this manner.

Given the key role macrophages play in the development of vulnerable plaque, we have examined the macrophage specific compounds 7,8-dihydroneopterin and its oxidation product neopterin as potential as biomarkers of plaque growth and inflammation. Activated macrophages, those which are displaying an M1 phenotype, produce significant quantities of a guanosine triphosphate (GTP)-derived antioxidant, 7,8-dihydroneopterin, which is oxidized *in vivo* to a highly fluorescent compound, neopterin (Wachter et al., 1989; Giesege et al., 2001; Giesege et al., 2008). 7,8-Dihydroneopterin can block cell mediated low density lipoprotein (LDL) oxidation, oxidized LDL induced macrophage death, and down regulate CD36 a key scavenger receptor for oxidized LDL involved in the formation of foam cells (Shchepetkina et al., 2017), a key constituent of plaques. Neopterin has been used clinically to measure immune cell activation in several pathologies including cardiovascular disease (Tang et al., 2016; Ray et al., 2007).

Clinical studies have found that neopterin is elevated in serum of patients with acute ischaemic stroke and myocardial infarction (Elayalwar et al., 2016; Srivastava et al., 2014), and there is prognostic value for patients at risk of ischaemic heart disease or acute coronary syndrome (Vengen et al., 2009; Zeng et al., 2016). To date, there has been little research into the *in vivo* generation of neopterin and most research into the role of neopterin has made use of isolated cultures of macrophages or peripheral blood mononuclear cells (PBMC), however, this approach does not allow for the investigation of the more complex interactions between array of cell types (smooth muscle cells, macrophages, monocytes, T cells) and cytokines within the plaque tissue (Wolf et al., 2015; Hsu et al., 2016). In this study, we overcome this disadvantage of mono layer cultures by activating resident macrophages in live carotid plaque tissue samples from carotid

endarterectomy patients. We used three different known macrophage stimulants, interferon- $\gamma$ , PMA and PHA and compared activation within the plaque tissue with traditional monolayer cultures in the presence and absence of T cells. Interferon- $\gamma$  directly induces the production of 7,8-dihydroneopterin in macrophages via the enzyme GTP cyclohydrolase I (GTPCH-I), while PMA and PHA are known to activate T cells, which produce interferon- $\gamma$  in response (Schroeksnadel et al., 2011; Jenny et al., 2011; Gostner et al., 2015). Thus, PMA and PHA are capable of indirectly increasing 7,8-dihydroneopterin. As 7,8-dihydroneopterin and its oxidation product neopterin are of low molecular weight, they easily diffuse out of the plaque into the blood stream or tissue culture media and can be measured as serum markers of macrophage activity and oxidation (Giesege et al., 2008).

Typically, in clinical settings only serum neopterin levels are analysed. In this study, we take this system further by measuring both neopterin and 7,8-dihydroneopterin. Neopterin can be measured directly and 7,8-dihydroneopterin indirectly by artificial oxidation to neopterin. In a sample that has undergone this artificial oxidation, we refer to the measured value as ‘total neopterin’ as the value given contains both the artificially oxidized 7,8-dihydroneopterin and any biologically produced neopterin (Lindsay et al., 2014; Lindsay et al., 2016). The concentration of 7,8-dihydroneopterin alone can be inferred by subtracting the known neopterin value which was measured in the non-oxidized sample. The advantage to measuring both is that we can measure both the amount of oxidation (as neopterin) and the level of macrophage activation (as total neopterin) occurring in the tissue. In doing this, we found that macrophage activation but not the level of oxidation appears to be associated with the amount of calcification in the plaque tissue.

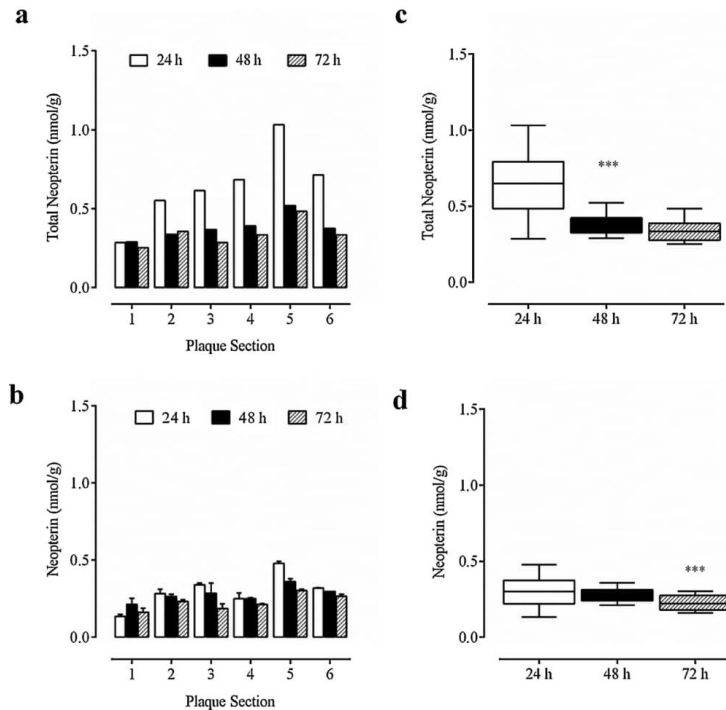


**Fig. 2.** Production of total neopterin and neopterin in media from an unstimulated plaque (N = 1). The plaque was retrieved from a 49-year-old male ex-smoker who presented with a stroke, retinal ischaemia, and familial hypercholesterolaemia. Ultrasound of the artery determined 60–69% stenosis. The plaque was incubated in RPMI-1640, supplemented with 10% human serum for a total of 72 h. (a) shows the total neopterin produced, as measured by HPLC at each media change. (b) shows the neopterin for the same time periods. Plaque total neopterin and neopterin concentrations for each section are given in nmol/g of plaque. (c) and (d) compare the mean and range of plaque total neopterin and neopterin at each time point (N = 6). Significance is indicated as compared to the previous 24 h period: \*\*\* indicates  $p < 0.001$ .

## 2. Materials and methods

All solutions were prepared using nanopure water purified using a Millipore Q system. All chemicals and reagents were of analytical reagent grade and supplied by Sigma-Aldrich (St Louis, MO, USA) or BDH Chemicals New Zealand Limited (Auckland, NZ) unless otherwise stated. Neopterin and 7,8-dihydroneopterin were obtained from Schirck's Laboratories (Bauma, Switzerland).

Freshly excised carotid plaque tissue was obtained from consenting patients undergoing endarterectomy (ethics approval CTY/01/04/036 granted by the New Zealand Upper South B Ethics Committee). Plaques were placed on ice and transported to the laboratory. Plaque tissue was cut into sections approximately 3 mm thick (Fig. 1), weighed (average plaque section weight was  $0.14 \text{ g} \pm 0.02 \text{ g}$ ). Plaque sections were cultured in individual centre-well organ culture dishes (BD Falcon, NJ, USA) in 2 mL of RPMI-1640 containing penicillin (100 U/mL) and streptomycin (100 g/mL), supplemented with 10% human serum. Human serum was prepared from whole blood and stored at  $-80^\circ\text{C}$  until required. Sectioned plaques were incubated for 24 h prior to any experimental treatment. The media were changed every 24 h and the media were collected for lactate measurement and HPLC analysis of neopterin and total neopterin. Neopterin levels in the media were determined by isocratic HPLC using Phenomenex™ SCX column on a Shimadzu 20A HPLC with fluorescence detection of the eluting neopterin as previous described (Lindsay et al., 2014; Janmale et al., 2015). Media proteins were removed by acetonitrile precipitation (Flavall et al., 2008). Due to the non-fluorescent nature of 7,8-dihydroneopterin, this was first oxidized to neopterin using acidic iodide, and then measured as total neopterin (Flavall et al., 2008). Media lactate concentration were determined using the Lactate Assay Kit from Roche Diagnostics NZ LTD (Auckland, NZ) which is an enzymatic based

absorbance assay.

Primary cultures of human PBMC (a mixture of lymphocytes and monocytes) were isolated from fresh whole blood donated under ethics approval CTY/98/07/069. The mononuclear cells were prepared by density gradient centrifugation over Lymphoprep™ (Axis-Shield PoC AS, Oslo, Norway), as described by the manufacturer, and washed in sterile phosphate-buffered saline (PBS) containing 150 mM sodium chloride and 10 mM sodium dihydrogen orthophosphate pH 7.4. The cells were plated in 12-well tissue culture plates (Nunc, ThermoFisher Scientific, Auckland, NZ) at  $5 \times 10^6$  cells per mL in Roswell Park Memorial Institute (RPMI)-1640 containing penicillin (100 U/mL) and streptomycin (100 g/mL), supplemented with 10% human serum. Human monocyte-derived macrophages (HMDM) were prepared from the PBMC preparation by incubating for 40 h in serum-free RPMI before plating at  $5 \times 10^6$  cells/well in RPMI-1640, as described for the PBMC, except  $3 \mu\text{g/mL}$  of granulocyte-macrophage colony-stimulating factor (GM-CSF) was added to the media on the first day after plating but not added during subsequent media changes, which occurred every 3 d. The monocytes differentiated into adherent macrophages over 7–14 d. Fourteen plaque sections from two plaques were scanned using a MARS spectral scanner (MARS Bioimaging Ltd, New Zealand) using a 2 mm Aluminium filter at 30, 40, 50 and 60 keV and material decomposition carried out using MARSvision software (Butler et al., 2008; Zainon et al., 2012). Image J was used for additional image analysis.

All statistical analysis was carried out using Prism software (GraphPad Software Inc, USA). One-way analysis of variance (ANOVA) was performed on all plaque data, using each section as a replicate. One-way ANOVA was performed on cell culture data. Plaque results are from individual plaques unless stated otherwise and each plaque is from a separate patient. Cell culture results are mean  $\pm$  SEM of three independent experiments. Significance is indicated as \*,  $p < 0.05$ ; \*\*,  $p < 0.01$ ; \*\*\*,  $p < 0.001$ .

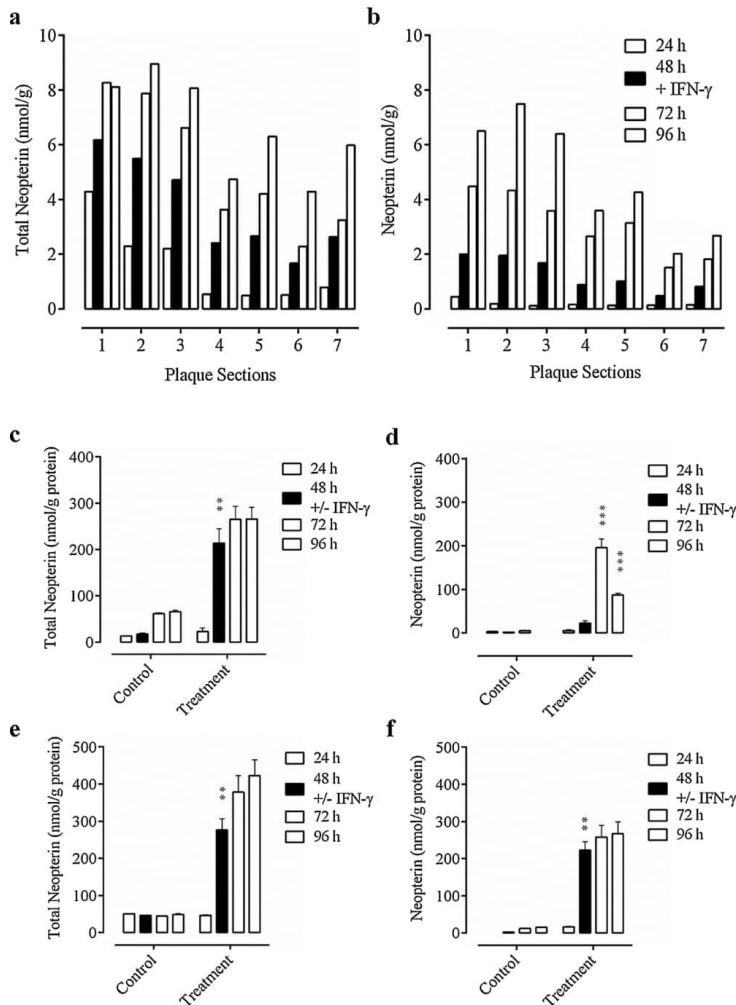


**Fig. 3.** Production of total neopterin and neopterin in media from plaque, macrophages, and PBMC culture stimulated with 500 U/mL of interferon- $\gamma$ . Interferon- $\gamma$  stimulation of the plaque or cells occurred in a single dose after 48 h. Subsequent media changes contained RPMI-1640 with 10% human serum only. (a) and (b) show the total neopterin and neopterin measured in the interferon- $\gamma$  treated plaque (N = 1) obtained from an 82-year-old male non-smoker who presented with a transient ischaemic attack and right upper limb weakness; 80–95% stenosis of the artery was determined by ultrasound. The plaque tissue exhibited moderate levels of calcification. Unrelated human HMDM and PBMCs were analysed. Total neopterin and neopterin were also measured in a HMDM culture (c) and (d), and in a PBMC culture (e) and (f) (N = 3). Error bars represent SEM. Significance is indicated as compared to the previous 24 h period: \*\* indicates  $p < 0.01$ ; \*\*\*,  $p < 0.001$ .

$p < 0.01$ ; \*\*\*,  $p < 0.001$ .

### 3. Results

#### 3.1. 7,8-Dihydroneopterin and neopterin formation in unstimulated plaque

Unstimulated plaque in tissue culture produces both 7,8-dihydroneopterin (measured as total neopterin) and neopterin. The plaque was retrieved from a 49-year-old male ex-smoker who presented with a stroke, retinal ischaemia, and familial hypercholesterolaemia and cut into sections before being cultured. The mean total neopterin produced by the plaque at 72 h was  $0.34 \pm 0.08$  nmol/g and the mean neopterin was  $0.23 \pm 0.05$  nmol/g. The incubation of unstimulated plaque for 72 h resulted in a significant decrease ( $-0.27$  nmol/g,  $p < 0.0001$ ) in total neopterin at 48 h, but then no further change (Fig. 2a). Mean neopterin did not significantly decrease ( $-0.05$  nmol/g,  $p = 0.0005$ )

until 72 h (Fig. 2b). Neither mean neopterin nor total neopterin increased at any point, which is consistent with the plaque being unstimulated.

#### 3.2. Direct activation of plaque macrophages by interferon- $\gamma$ in cultured plaque

Interferon- $\gamma$ , generated *in vitro* by T helper-1-type (Th-1) cells, is a key stimulator of the macrophage inflammatory response (Huber et al., 1984). A single addition of interferon- $\gamma$  (500 U/mL) to a plaque obtained from an 82-year-old male non-smoker who presented with a transient ischaemic attack and right upper limb weakness caused a sustained rise in total neopterin and neopterin (Fig. 3a and b). The initial levels of total neopterin before the addition of the interferon- $\gamma$  ranged from 0.48 nmol/g to 4.28 nmol/g, suggesting this patient had higher, but also more variable, levels of baseline inflammation in their

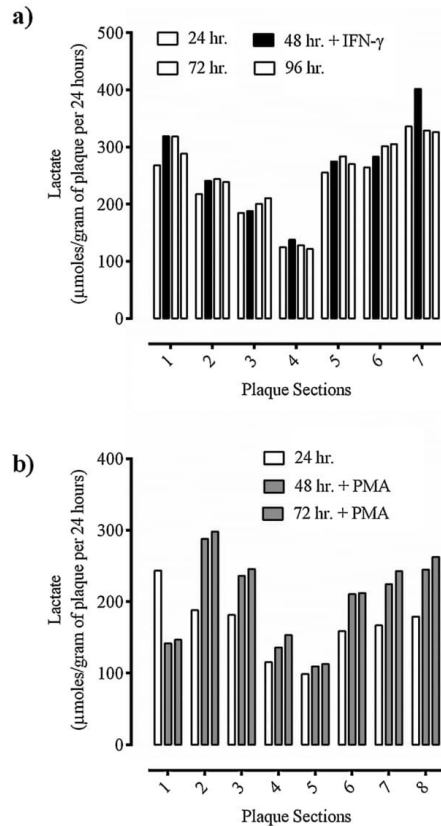


Fig. 4. Analysis of plaque lactate release into the media where a) corresponds to the plaque in Fig. 3 and b) with Fig. 5.

plaque tissue, compared to the plaque analysed in Fig. 2, which ranged from 0.28 nmol/g to 1.03 nmol/g. Neopterin was < 0.44 nmol/g for 8 sections prior to interferon- $\gamma$  addition. For all sections, there was a significant rise in both the mean total neopterin which increased by 4.89 nmol/g ( $p = 0.003$ ) and neopterin (2.82 nmol/g  $p = 0.037$ ) over the 72 h. The magnitude of rise was different for each section, with some sections responding slowly to the interferon- $\gamma$  stimulation (Fig. 3, sections 5–7). This demonstrates that along the length of the plaque there are marked differences in inflammatory activity as well as differing levels of oxidative stress. The high levels of lactate released from the plaques confirmed that the plaques remained metabolically active during the entire incubation. The lactate levels ranged from 121.7  $\mu$ mol/g/24 h to 318.4  $\mu$ mol/g/24 h (Fig. 4).

### 3.3. Direct activation of plaque macrophages by interferon- $\gamma$ in cell culture

To better understand the dynamic behaviour of neopterin-releasing cells within the plaque, we examined unrelated cultured HMDM and PBMC. The interferon- $\gamma$  activation of the HMDM cells produced a significant 29-fold increase in total neopterin ( $p = 0.004$ ) after 24 h (Fig. 3c). The level remained around 200 nmol/g cell protein for the whole 72 h period. However, there was no significant neopterin formation until 48 h after adding interferon- $\gamma$  (Fig. 3d). The level of

neopterin then dropped in the following 24 h, indicating a decrease in oxidant production. Interferon- $\gamma$  stimulation of the PBMC caused a total neopterin rise that was larger than that seen with HMDM (Fig. 3e). In contrast, the neopterin rose immediately and stayed elevated for the whole 72 h, like the stimulated plaque (Fig. 3b).

### 3.4. Indirect stimulation of macrophages in cultured plaque with PMA

Both PHA and PMA stimulation of T cells has been shown to cause the release of interferon- $\gamma$  which is capable of inducing macrophages to produce 7,8-dihydroneopterin. A plaque obtained from a 65-year-old male non-smoker who was suffering from dysphasia and amaurosis fugax was sectioned (shown in Fig. 1), and after a 24 h washout period was stimulated with PMA. In the first three sections (1–3) of the plaque there was a substantial rise in total neopterin within 24 h, and the level continued to rise in the following 24 h period (Fig. 5a). Sections 4, 7, and 8 only showed a rise after the second dose of PMA. However, the overall mean change in total neopterin across the plaque was not significant due to the wide variation between sections ( $3.06 \pm 1.54$  nmol/g,  $p = 0.073$ ). The level of oxidation in the plaque measured by neopterin was low compared to the output of total neopterin (Fig. 5b c.f. Fig. 5a). The rise in mean neopterin over 72 h ( $4.78 \pm 1.99$  nmol/g) was significant ( $p = 0.037$ ).

### 3.5. Indirect stimulation of macrophages and PBMCs in cell culture with PMA

With HMDM cells, total neopterin significantly increased with the addition of PMA after both 24 and 48 h of stimulation (Fig. 5c). The PMA was given twice as it is likely to take longer than 24 h to reach maximal activation if the process is being driven from a gene transcription level. The PMA was removed for the last 24 h incubation and replaced with interferon- $\gamma$  in order to test whether indirect stimulation had been successful, which generated a small but significant increase. The same treatment with PBMC showed a similar trend of increasing total neopterin by the PMA, but twice the level seen with the interferon- $\gamma$  (Fig. 5e). The presence of the T cells appears to have greatly enhanced the generation of 7,8-dihydroneopterin from the monocytes.

The time course of 7,8-dihydroneopterin oxidation to neopterin with PMA-stimulated HMDM cells was very like that seen with interferon- $\gamma$ , with an initial delay of 24 h in the rise of neopterin levels (Fig. 5d). With PBMC, the presence of the PMA has abolished the delay in the oxidation of 7,8-dihydroneopterin, starting strongly after 24 h, but with a small decrease in the following 24 h (Fig. 5f). The replacement of the PMA with interferon- $\gamma$  in the HMDM cells showed a decrease in oxidation or neopterin formation of 34%, but with PBMC the decrease was not significant.

### 3.6. Indirect stimulation of plaque with PHA

Addition of PHA a plaque obtained from a 77-year-old male non-smoker who was suffering from dysarthria and TIAs caused an increase in both mean total neopterin (5.28 nmol/g,  $p < 0.0001$ ) and neopterin (2.95 nmol/g,  $p < 0.0001$ ) by 72 h (Fig. 6a and b). The addition of interferon- $\gamma$  for the final 24 h resulted in a further rise in both mean total neopterin (1.3 nmol/g,  $p < 0.0001$ ) and neopterin (1.0 nmol/g,  $p < 0.0001$ ).

### 3.7. Indirect stimulation of macrophages and PBMCs in cell culture with PHA

In tissue culture, addition of PHA to HMDM cells produced a significant increase in mean total neopterin at 72 h (162.8 nmol/g,  $p < 0.0001$ ) and a further rise with the introduction of interferon- $\gamma$  (92.85 nmol/g,  $p = 0.0021$ ), like that seen in the plaque. Neopterin also rose significantly in the first 72 h (130.1 nmol/g,  $p < 0.0001$ ),

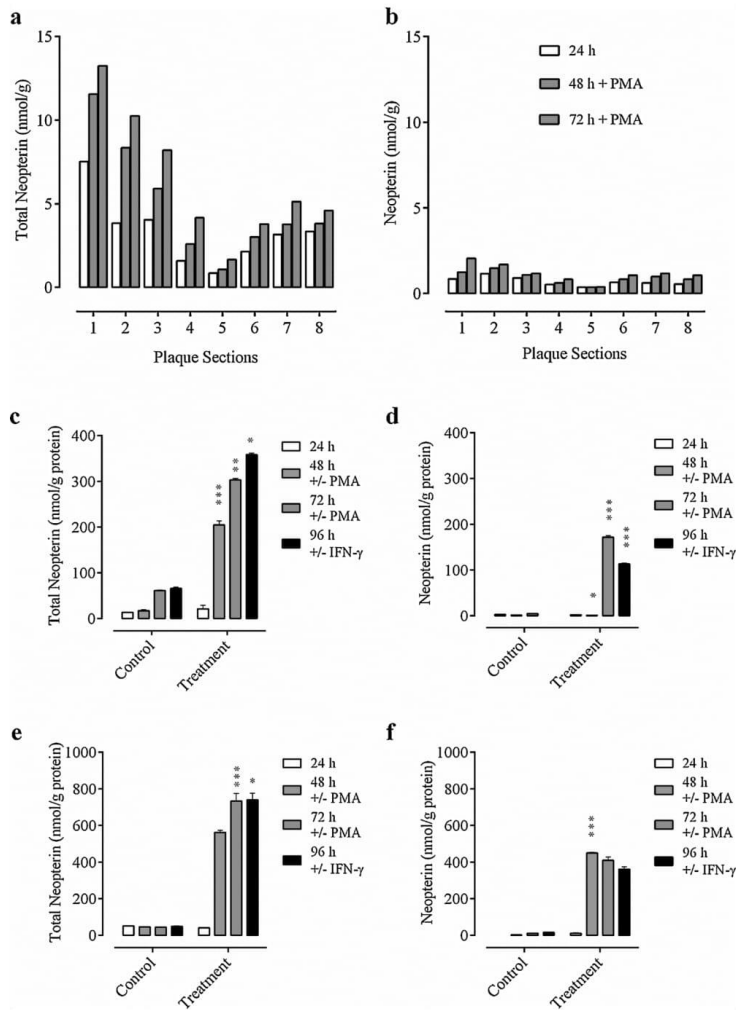


**Fig. 5.** Production of total neopterin and neopterin in media from plaque, macrophages, and PBMC culture stimulated with 5  $\mu$ M PMA. The plaque (a) and (b) and cells were treated with PMA for 2 d following an initial media-only day ( $N = 1$ ). The plaque was obtained from a 65-year-old male non-smoker who was suffering from dysphasia and amaurosis fugax. Stenosis of the artery was reported as 80–99%. In the HMDM (c) and (d) and PBMC (e) and (f) experiments ( $N = 3$ ), 500 U/mL of interferon- $\gamma$  was added on the final day. Error bars represent SEM. Significance is indicated as compared to the previous 24 h period: \* indicates  $p < 0.05$ ; \*\*,  $p < 0.01$ ; \*\*\*,  $p < 0.001$ .

however, unlike the plaque, neopterin fell upon stimulation with interferon- $\gamma$  ( $-73.71$  nmol/g,  $p < 0.0001$ ). In PBMCs both total neopterin and neopterin increased significantly by 72 h (20.86 nmol/g,  $p < 0.0001$  and 11.73 nmol/g,  $p = 0.005$  respectively). Addition of interferon- $\gamma$  caused a significant rise in total neopterin (31.74 nmol/g,  $p < 0.0001$ ) but not in neopterin.

The increase in total neopterin in both PBMC and some sections of the plaque tissue is suggestive of an interaction between T cells and macrophages within atherosclerotic plaque.

### 3.8. Plaque calcium quantification by spectral imaging

Examination of plaque tissue segments shows a variety of structural features (Fig. 1). We hypothesised that the measured output of total neopterin may vary from section to section due to the morphology of the tissue and the level of calcification. Because of the nature of the

tissue after several days of culture it was not possible to use traditional histology. Instead, to quantify the level of calcification, sections were imaged and calcium levels quantified by spectral photon-counting CT (SPCCT), a non-destructive high resolution X-ray imaging technique which provides quantitative histology-level images (Butler et al., 2008; Zainon et al., 2012).

Calcium content was inversely related to post-PMA treatment total neopterin values ( $R^2 = 0.91$ ) (Fig. 7a). Plaque sections with vastly differing weights (e.g. 0.166 g vs 0.082 g) but with very similar volumes of calcium (46 mm<sup>3</sup> vs 49 mm<sup>3</sup>) were activated to the same extent (4.2 nmol/g and 3.8 nmol/g total neopterin). Fig. 7b–e are material decomposition images of section 5 from the plaque in photographed in Fig. 1 (and analysed in Fig. 5a). These images taken at different planes through the plaque section, show many spotty calcium deposits and some lipid-rich areas. In comparison, section 7 from the same plaque, which had moderate levels of total neopterin production, is

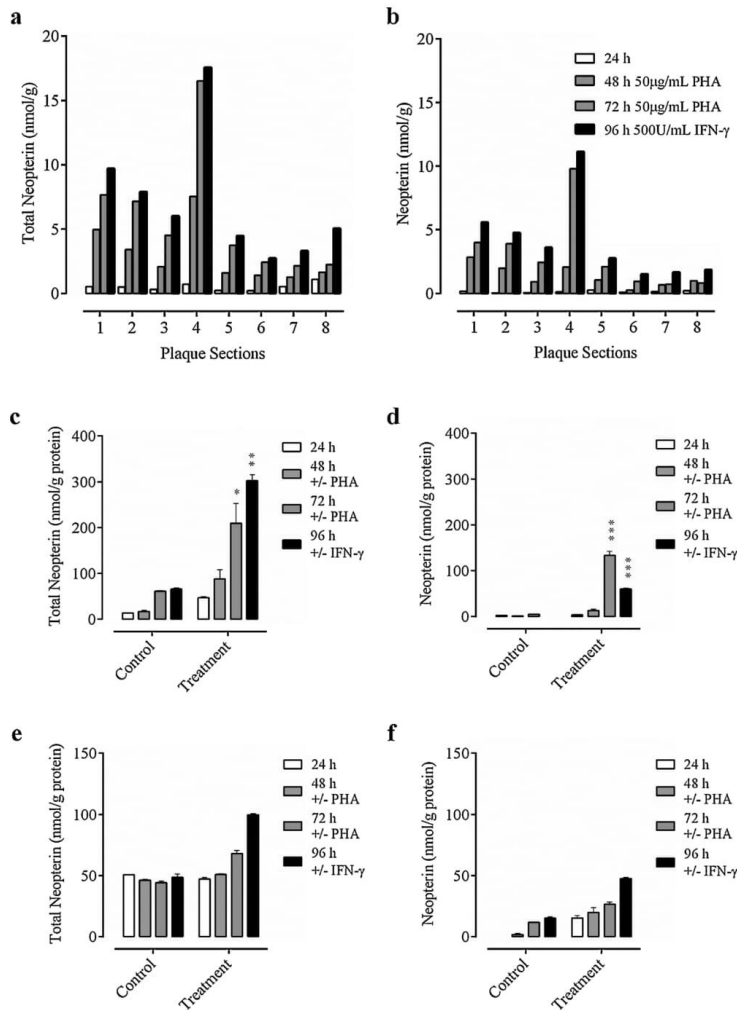


**Fig. 6.** Production of total neopterin and neopterin in media from plaque, macrophages, and PBMC culture stimulated with 50 ng/mL PHA. The plaque (a) and (b) was treated with PHA for 2 d following an initial media-only day, 500 U/mL of interferon- $\gamma$  was added on the final day (N-1). The plaque was obtained from a 77-year-old male non-smoker who was suffering from dysarthria and TIAs. Stenosis of the artery was reported as 80–95%. In the HMDM (c) and (d) and PBMC (e) and (f) experiments (N-3), cells were treated with PHA for 2 d following an initial media-only day and 500 U/mL of interferon- $\gamma$  was added on the final day. Error bars represent SEM. Significance is indicated as compared to the previous 24 h period: \* indicates  $p < 0.05$ ; \*\*,  $p < 0.01$ ; \*\*\*,  $p < 0.001$ .

predominantly composed of lipid-rich tissue (Fig. 7f).

#### 4. Discussion

We have shown that macrophages in live plaque tissues can be activated indirectly, possibly *via de novo* synthesis of interferon- $\gamma$  by Th-1 cells or directly through the addition of exogenous interferon- $\gamma$ . Comparisons to mono-layer tissue culture of either HMDMs or PBMCs demonstrate the effect of the complexity of plaque tissue on its biochemical profile. Live plaque tissue was more likely to respond immediately to stimuli than cells in culture, possibly due to differences in gene expression in the plaque tissue or the milieu of cells available.

Interferon- $\gamma$  stimulation of excised live plaque induced the activation of macrophages confirmed by a rise in total neopterin. This was accompanied by an increase in oxidant generation, which was measured as a rise in neopterin. As in our previous work (Jannale et al.,

2015), the response of each section of plaque tissue is highly variable and not related to its location along the length of the plaque. The macrophage activation was sustained even after the removal of interferon- $\gamma$  from the media. This phenomenon is consistent with other research that indicates interferon- $\gamma$  induces the expression of the enzyme GTPCH-I (Gesierich et al., 2003), which controls the rate limiting step in the production of 7,8-dihydroneopterin. Our results confirm that atherosclerotic plaque is a source of neopterin, particularly when macrophages are activated. Other studies have previously found that neopterin is increased after events such as stroke (Lin et al., 2012; Emsley et al., 2007), which is associated with macrophage activation (Chiba and Umegaki, 2013). Elevated serum neopterin is also a predictor of major adverse coronary events (Avanzas et al., 2005). Generation of neopterin from 7,8-dihydroneopterin is evidence of an increase in oxidative stress in the plaque tissue. This is likely due to interferon- $\gamma$  causing an increase the expression of gp91phox and

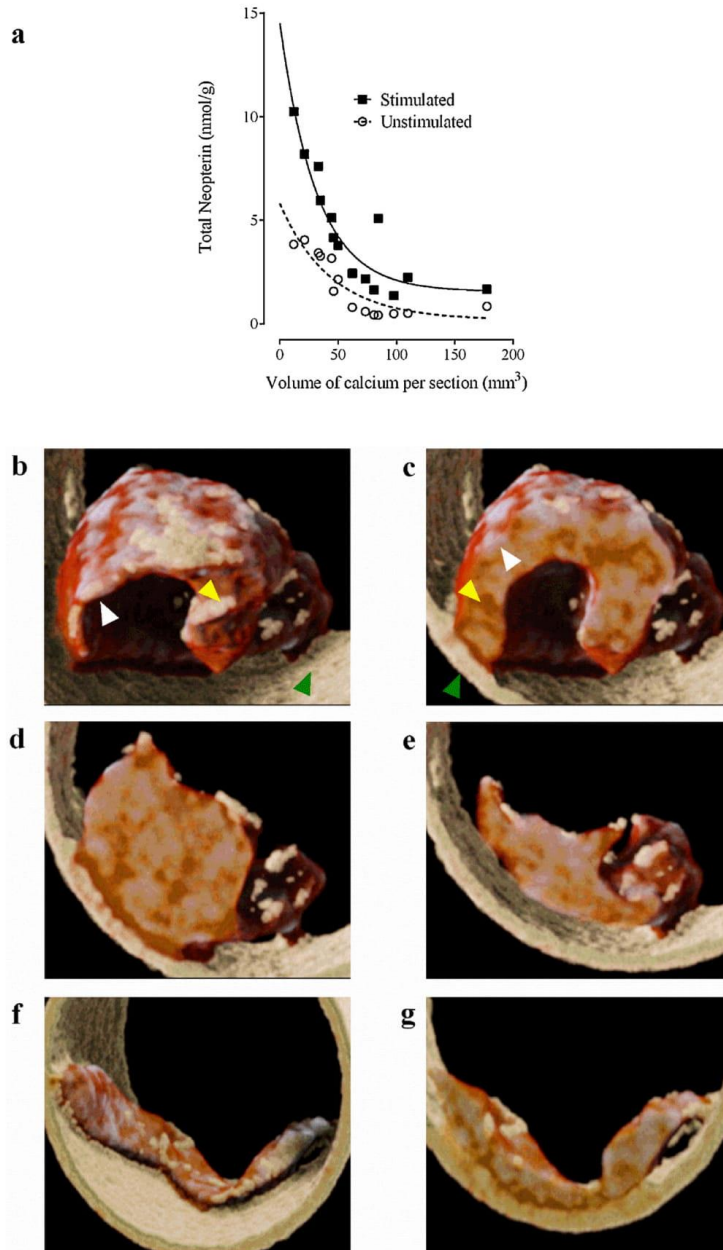


**Fig. 7.** SPCCT imaging of plaque tissue. Relationship between total neopterin production in plaque tissue and the volume of calcium present in each section using 14 sections from two PMA-treated plaques, prior to and after stimulation ( $N = 2$ ).  $R^2$  for the non-linear line of best fit was 0.76 for unstimulated plaque and 0.91 for stimulated. (b) – (g) Three-dimensional reconstructions of MARS spectral CT slices using material decomposition for water, lipid, and calcium. Sections 5 (b) – (e) and 7 (f) – (g) of the PMA-treated plaque were selected for examining morphological differences. Tissue samples were retrieved after being cultured and imaged using the MARS spectral scanner. In this slice-through view, (b) – (e) are images from plaque section 5, which are progressing away from the viewer moving along the Z-axis. White arrowheads show examples of calcification; lipid is in yellow. A green arrowhead indicates the polypropylene sample tube, which gives a lipid-like reading. (f) A view of the whole of section 7. (g) A cut-through image midway through section 7. (For interpretation of the references to colour in the figure text, the reader is referred to the web version of this article.)

p47phox which form the active NOX complex, generating superoxide (Ellison et al., 2015).

The activation of HMDMs by PMA and PHA was somewhat surprising as the generation of 7,8-dihydroneopterin and neopterin by HMDM cells alone has not been previously reported. PMA is known to

activate the NOX complex via protein kinase C activation (Matthews et al., 2016). Total neopterin in plaque tissue treated with PMA rose significantly over 72 h. Initial indications suggest that this is due to *de novo* synthesis of interferon- $\gamma$  by T cells within the plaque. It was surprising to find that PMA could cause a significant increase in the

production of 7,8-dihydroneopterin in a macrophage-only culture in the absence of interferon- $\gamma$  (Fig. 5c). *In vivo* labelling studies have shown that although interferon- $\gamma$  controls the expression of GTPCH-I, the activity of the enzyme is under post-translational control through phosphorylation (Hesslinger et al., 1998). PMA has been shown to cause hyperphosphorylation of GTPCH-I which induces a substantial rise in enzyme activity (Hesslinger et al., 1998).

Our results suggest that both *de novo* synthesis of interferon- $\gamma$  and phosphorylation of GTPCH-I may be occurring in the PMA treated plaque tissue. Oxidant production as measured by neopterin was much higher in the monolayer cultures (PBMC and HMDM) compared to the PMA-treated plaque tissue. Neopterin generation in the monolayer cultures was expected due to the PMA-induced activation of NOX. In the plaque, most of the 7,8-dihydroneopterin remained unoxidized suggesting that the treatment with PMA had elevated the antioxidant 7,8-dihydroneopterin such that it greatly exceeded any oxidant generation, or that the level of oxidant generation in the plaque was much lower than in tissue culture.

There is an inverse association between the amount of calcification and the macrophage-derived production of 7,8-dihydroneopterin and neopterin in advanced atherosclerotic plaque. Our finding suggests that plaque tissue with large volumes of calcium contributes less to the inflammatory burden than tissue with little calcification. From our results, it is not possible to distinguish whether the increase in macrophage activation in sections containing smaller volumes of calcium is due to a change in macrophage phenotype related to the presence of microcalcifications or if there is an exclusion of macrophages in highly calcified tissue which lowers the immune activation.

Macrophages present in *ex-vivo* carotid plaque samples can be stimulated either directly or indirectly via T cells. Macrophage behaviour in live plaque samples varies along the length of the plaque. Cell culture experiments, therefore, have limited use in modelling the inflammatory response within atherosclerotic plaque. In addition, we have found that the microenvironment of the plaque is associated with differences in macrophage activation, again highlighting the importance of using an *ex-vivo* system to investigate the role of macrophages in atherosclerosis.

#### Conflict of interest

A.B. is a director of MARS Bioimaging Ltd and N.A. is a shareholder. S.P.G. and H.P. are involved in the commercial promotion of the MARS spectral scanner, but have no financial holding in the company.

#### Funding

This work was partly funded through a project grant from the Heart Foundation of New Zealand. The MARS spectral scanner was developed through a project funded by Ministry of Business, Innovation and Employment (MBIE), New Zealand under contract number UOCX0805. Hannah Prebble was supported by a School of Biological Sciences PhD scholarship.

#### Acknowledgements

The authors would like to thank all members of the MARS scanner project, the Medipix2 and Medipix3 collaborations. We would like to thank our tissue donors and the vascular surgery teams for their assistance in collecting plaque tissue.

#### References

- Avanzas, P., Arroyo-Espiguero, R., Quiles, J., Roy, D., Kaski, J.C., 2005. Elevated serum neopterin predicts future adverse cardiac events in patients with chronic stable angina pectoris. *Eur. Heart J.* 26 (5), 457–463.
- Biesen, E.A.L., Wouters, K., 2017. Macrophage complexity in human atherosclerosis: opportunities for treatment? *Curr. Opin. Lipidol.* 28 (5), 419–426.
- Butler, A.P.H., Anderson, N.G., Tipples, R., Cook, N., Watts, R., Meyer, J., et al., 2008.

- Bio-medical X-ray imaging with spectroscopic pixel detectors. *Nucl. Instrum. Methods Phys. Res. Sect. A-Accel. Spectrom. Dect. Assoc. Equip.* 591 (1), 141–146.
- Chiba, T., Umegaki, K., 2013. Pivotal roles of monocytes/macrophages in stroke. *Mediat. Inflamm.* 10.
- De Rosa, S., Cirillo, P., Pacileo, M., Petrillo, G., D'Ascoli, G.L., Maresca, F., et al., 2011. Neopterin: from forgotten biomarker to leading actor in cardiovascular pathophysiology. *Curr. Vasc. Pharmacol.* 9 (2), 188–199.
- Elayalwar, S., Natarajan, S., Lakshminpathi, J., 2016. Serum Neopterin A novel biomarker in acute myocardial infarction. *J. Evol. Med. Dent. Sci.-Jemds* 5 (54), 3582–3585.
- Ellison, M.A., Thurman, G., Gearheart, C.M., Seewald, R.H., Porter, C.C., Ambruso, D.R., 2015. INF-gamma enhances nox2 activity by upregulating phox proteins when applied to differentiating PLB-985 cells but does not induce nox2 activity by itself. *PLoS One* 10 (8), 19.
- Emsley, H.C.A., Smith, C.J., Gavin, C.M., Georgiou, R.F., Vail, A., Barberan, E.M., et al., 2007. Clinical outcome following acute ischaemic stroke relates to both activation and autoregulatory inhibition of cytokine production. *BMC Neurol.* 7, 12.
- Flavall, E.A., Crone, E.M., Moore, G.A., Gieseg, S.P., 2008. Dissociation of neopterin and 7,8-dihydroneopterin from plasma components before HPLC analysis. *J. Chromatogr. B* 863 (1), 167–171.
- Gao, H., Long, Q., 2008. Effects of varied lipid core volume and fibrous cap thickness on stress distribution in carotid arterial plaques. *J. Biomech.* 41 (14), 3053–3059.
- Gesierich, A., Niroomand, F., Tiefenbacher, C.P., 2003. Role of human GTP cyclohydrolase I and its regulatory protein in tetrahydrobiopterin metabolism. *Basic Res. Cardiol.* 98 (2), 69–75.
- Gieseg, S.P., Whybrow, J., Glubb, D., Rait, C., 2001. Protection of U937 cells from free radical damage by the macrophage synthesized antioxidant 7,8-dihydroneopterin. *Free Radic. Res.* 35 (3), 311–318.
- Gieseg, S.P., Crone, E.M., Flavall, E.A., Amit, Z., 2008. Potential to inhibit growth of atherosclerotic plaque development through modulation of macrophage neopterin/7,8-dihydroneopterin synthesis. *Br. J. Pharmacol.* 153 (4), 627–635.
- Gostner, J.M., Raggel, E., Becker, K., Oberall, F., Schennach, H., Pease, J.E., et al., 2015. Bisphenol A suppresses Th1-type immune response in human peripheral blood mononuclear cells in vitro. *Immunol. Lett.* 168 (2), 285–292.
- Hesslinger, C., Kremmer, E., Hultner, L., Ueffing, M., Ziegler, I., 1998. Phosphorylation of GTP cyclohydrolase I and modulation of its activity in rodent mast cells – GTP cyclohydrolase I hyperphosphorylation is coupled to high affinity IgE receptor signaling and involves protein kinase C. *J. Biol. Chem.* 273 (34), 21616–21622.
- Howell, K.W., Meng, X.Z., Fullerton, D.A., Jin, C.H., Reece, T.B., 2011. Cleveland JC: toll-like receptor 4 mediates oxidized LDL-induced macrophage differentiation to foam cells. *J. Surg. Res.* 171 (1), E27–E31.
- Hsu, J.J., Lim, J., Tintut, Y., Demer, L.L., 2016. Cell-matrix mechanics and pattern formation in inflammatory cardiovascular calcification. *Heart* 102 (21), 1710–1715.
- Huber, C., Batchelor, J.R., Fuchs, D., Hausen, A., Lang, A., Niederwieser, D., et al., 1984. Immune-response associated production of neopterin – release from macrophages primarily under control of interferon-gamma. *J. Exp. Med.* 160 (1), 310–316.
- Janmale, T., Genet, R., Crone, E., Flavall, E., Firth, C., Pirker, J., et al., 2015. Neopterin and 7,8-dihydroneopterin are generated within atherosclerotic plaques. *Pteridines* 26 (3), 93–103.
- Jenny, M., Klieber, M., Zaknun, D., Schroecksnadel, S., Kurz, K., Ledochowski, M., et al., 2011. In vitro testing for anti-inflammatory properties of compounds employing peripheral blood mononuclear cells freshly isolated from healthy donors. *Inflamm. Res.* 60 (2), 127–135.
- Kavurma, M.M., Rayner, K.J., Karunakaran, D., 2017. The walking dead: macrophage inflammation and death in atherosclerosis. *Curr. Opin. Lipidol.* 28 (2), 91–98.
- Kong, Y.Z., Yu, X.Y., Tang, J.J., Ouyang, X.S., Huang, X.R., Fingerle-Rowson, G., et al., 2005. Macrophage migration inhibitory factor induces MMP-9 expression: implications for destabilization of human atherosclerotic plaques. *Atherosclerosis* 178 (1), 207–215.
- Lin, H.S., Tsai, T.H., Liu, C.F., Lu, C.H., Chang, W.N., Chen, S.F., et al., 2012. Serum level and prognostic value of neopterin in patients after ischemic stroke. *Clin. Biochem.* 45 (18), 1596–1601.
- Lindsay, A., Janmale, T., Draper, N., Gieseg, S.P., 2014. Measurement of changes in urinary neopterin and total neopterin in body builders using SCX HPLC. *Pteridines* 25 (2), 53–62.
- Lindsay, A., Othman, M.I., Prebble, H., Davies, S., Gieseg, S.P., 2016. Repetitive cryotherapy attenuates the in vitro and in vivo mononuclear cell activation response. *Exp. Physiol.* 101 (7), 851–865.
- Matthews, A.T., Lee, J.H., Borazjani, A., Mangum, L.C., Hou, X., Ross, M.K., 2016. Oxidative stress increases the biosynthesis of 2-arachidonoylglycerol: involvement of NADPH oxidase. *Am. J. Physiol.-Cell Physiol.* 311 (6), C960–C974.
- Otsuka, F., Kramer, M.C.A., Woudstra, P., Yahagi, K., Ladich, E., Finn, A.V., et al., 2015. Natural progression of atherosclerosis from pathologic intimal thickening to late fibroatheroma in human coronary arteries: a pathology study. *Atherosclerosis* 241 (2), 772–782.
- Owens, A.P., Mackman, N., 2012. Sources of tissue factor that contribute to thrombosis after rupture of an atherosclerotic plaque. *Thromb. Res.* 129, S30–S33.
- Psychogios, K., Stathopoulos, P., Takis, K., Vemmu, A., Manios, E., Spegoc, K., et al., 2015. The pathophysiological mechanism is an independent predictor of long-term outcome in stroke patients with large vessel atherosclerosis. *J. Stroke Cerebrovasc. Dis.* 24 (11), 2580–2587.
- Ray, K.K., Morrow, D.A., Sabatine, M.S., Shui, A., Rifai, N., Cannon, C.P., et al., 2007. Long-term prognostic value of neopterin a novel marker of monocyte activation in patients with acute coronary syndrome. *Circulation* 115 (24), 3071–3078.
- Schroecksnadel, S., Sucher, R., Kurz, K., Fuchs, D., Brandacher, G., 2011. Influence of immunosuppressive agents on tryptophan degradation and neopterin production in



- human peripheral blood mononuclear cells. *Transplant Immunol.* 25 (2–3), 119–123.
- Shchepetkina, A.A., Hock, B.D., Miller, A., Kennedy, M.A., Gieseg, S.P., 2017. Effect of 7,8-dihydroneopterin mediated CD36 down regulation and oxidant scavenging on oxidised low-density lipoprotein induced cell death in human macrophages. *Int. J. Biochem. Cell Biol.* 87, 27–33.
- Silvestre-Roig, C., de Winther, M.P., Weber, C., Daemen, M.J., Lutgens, E., Soehnlein, O., 2014. Atherosclerotic plaque destabilization: mechanisms, models, and therapeutic strategies. *Circul. Res.* 114 (1), 214–226.
- Soeki, T., Sata, M., 2016. Inflammatory biomarkers and atherosclerosis. *Int. Heart J.* 57 (2), 134–139.
- Srivastava, M.V.P., Bhasin, A., Chaudhry, R., Sharma, S., Subbaiah, V., Bhatia, R., et al., 2014. Novel inflammatory biomarkers and their correlation to chlamydia pneumoniae titres in acute ischemic stroke. *J. Stroke Cerebrovasc. Dis.* 23 (9), 2391–2396.
- Stary, H.C., Chandler, A.B., Dinsmore, R.E., Fuster, V., Glagov, S., Insull, W., et al., 1995. A definition of advanced types of atherosclerotic lesions and a histological classification of atherosclerosis. *Circulation* 92 (5), 1355–1374.
- Tabas, I., 2009. Macrophage apoptosis in atherosclerosis: consequences on plaque progression and the role of endoplasmic reticulum stress. *Antioxid. Redox Signal.* 11 (9), 2333–2339.
- Tang, C.Z., Zhang, Y.L., Wang, W.S., Li, W.G., Shi, J.P., 2016. Elevated serum levels of neopterin at admission predicts depression after acute ischemic stroke: a 6-month follow-up study. *Mol. Neurobiol.* 53 (5), 3194–3204.
- Tarkin, J.M., Dweck, M.R., Evans, N.R., Takx, R.A.P., Brown, A.J., Tawakol, A., et al., 2016. Imaging atherosclerosis. *Circul. Res.* 118 (4), 750–769.
- Vengen, I.T., Daleb, A.C., Wiseth, R., Midthjell, K., Videm, V., 2009. Neopterin predicts the risk for fatal ischemic heart disease in type 2 diabetes mellitus Long-term follow-up of the HUNT 1 study. *Atherosclerosis* 207 (1), 239–244.
- Wachter, H., Fuchs, D., Hausen, A., Reibnegger, G., Werner, E.R., 1989. Neopterin as marker for activation of cellular immunity: immunologic basis and clinical application. *Adv. Clin. Chem.* 27, 81–141.
- Wolf, D., Zirlik, A., Ley, K., 2015. Beyond vascular inflammation-recent advances in understanding atherosclerosis. *Cell. Mol. Life Sci.* 72 (20), 3853–3869.
- Zainon, R., Ronaldson, J.P., Janmale, T., Scott, N.J., Buckenham, T.M., Butler, A.P.H., et al., 2012. Spectral CT of carotid atherosclerotic plaque: comparison with histology. *Eur. Radiol.* 22 (12), 2581–2588.
- Zeng, X.W., Zhang, G.Q., Yang, B., Zhang, B., Zhang, L.P., Ni, Y., et al., 2016. Neopterin as a predictor of functional outcome and mortality in chinese patients with acute ischemic stroke. *Mol. Neurobiol.* 53 (6), 3939–3947.

# Appendix B

Plaque	Plaque	Collection	Info	Date	Num.	Age	Weight in kg	Smoker	Diabetic	sex	BP	Treated for HBP	Symptoms	stenois	%	Collection				Patient Medication
																Location	Appearance	Plaque	Dimensions	
13-Aug-15	112	82	M	145/98/80	no	no	no	no	yes	TIA right upper limb weakness	0-9-69% Left ICA	slight bifurcation, some calcification	0.8332	37mm long	Atorvastatin, Clopidogrel, Metoprolol.					
16-Aug-15	113	75	M	150/65	no	yes	yes	yes	yes	TIA acute expressive dysphasia	>50% Left carotid artery				Atorvastatin, Aspirin, Enalapril, Metformin, Metoprolol, Temazepam					
05-Oct-15	114	73	F	86.2	no	yes	yes	yes	yes	TIA/R and L leg weakness, preceded by headache 8-5% Right ICA?					? Aspirin, Benidrofumethiazide, Candesartan, Clopidogrel, Metformin, Pantoprazole					
19-Nov-15	116	83	M	150/70	no	no	no	no	yes	TIA Right arm symptoms (weakness) for 10-10-69% Left carotid	Bifurc present (just)				Aspirin 100mg, Atorvastatin 20mg, Dalargin 1 10mg bid, Fluoxetine 10mg, Metoprolol 17.5mg, Quinapril 20mg, Terazosin 10mg QD?					
14-Jan-16	119	70	M		no	yes	yes	yes	yes	TIA (right sided) 77% Of face, Expressive dysphasia 69% Left ICA, ECA					Aspirin, Atorvastatin, Clopidogrel, Insulin, Metoprolol, Omeprazole, Quinapril					
02-Mar-16	120	65	M	70	ex	no	no	no	no	Dysphasia (2-3 weeks ago), amaurosis fugax	0-9-99% Left ICA	Bifurc (slamp side arm) minimal calcif	0.67	21mm long, 10mm x Clopidogrel, Aspirin, Metoprolol, Cilazapril						
19-May-16	122	68	M	153/76	no	no	no	no	no	TIA left side weakness fully resolved	Right ICA	no bifurc	0.8826		Losartan, aspirin, carvedilol 25mg					
19-May-16	123	64	M		recent ex					Facial droop - slurred speech, MRI left watershed zone left ICA		bifurc present (just)	1.0566		Clopidogrel, Aspirin, Metoprolol, Cilazapril, Atorvastatin					
09-Jun-16	126	64	M	65	no	no	no	no	no	TIA: right arm sensory loss	0-6-69% Left ICA	bifurc present	0.8772	12mm long 10mm w dilucon, candesartan, clopidogrel, terazosin HCL, atorvastatin, paracetamol						
10-Jun-16	127	83	M							TIA: 3 hours of weakness of right hand	0-6-69% left carotid	bifurc present heavily calcified	0.9795	30mm x 15mm	aspirin, clopidogrel, candesartan, atorvastatin, metoprolol					
06-Jul-16	129	56	M	107	no	yes	yes	yes	yes	Amaurosis fugax x2	0-9-09% Right carotid	no bifurc small hard calc, thin tissue	0.524	25mm long 15 wide	candesartan, atenolol, aspirin, metformin					
13-Feb-17	131	75	F	60	no	no	no	no	yes	Stroke, Right MCA infarct thrombolysed on ac	right common at bifurc, one small branch, one larger, be		1.19	26mm long 60mm w centrize, losartan, atorvastatin, seretide, subatamol, venlafaxine						
07-Apr-17	134	69	F		yes	yes	yes	yes	yes	Stroke in right frontal lobe	0-6-69% Right ICA	no bifurc small hard calc, thin tissue	0.3259		metformin, clopidogrel, aspirin, Cholecalciferol, paracetamol, cilazapril HCL, Alopurinol, Atorabi					
05-Apr-17	135	81	m		no	no	no	no		stroke, previous L ICA, 2005	0-6-69%				aspirin, clopidogrel, ezetimibe, metoprolol, ipratropium, salbutamol, glicolon					
24-May-17	137	85	M		yes	yes	yes	yes	yes	TIA	0-8-09% Left carotid	bifurc present, not heavily calcified	1.0957	28mm long 10mm w waist, metoprolol, losartan, atorvastatin, ism, fuzamide, glaxizole						
13-Jul-17	138	84	F	200/90	yes	Stroke TIA	yes	Stroke TIA	yes	Stroke TIA	Right Carotid	bifurc present heavily calcified			nicotinic, clopidogrel, aspirin, atorvastatin, tyrosine, flucanazole inhibitor, demipridone					